FAILURE PREVENTION AND RESTORATION IN POWER SYSTEMS

FAILURE PREVENTION AND RESTORATION IN POWER SYSTEMS

Dissertation

Dissertation
for the purpose of obtaining the degree of doctor
at Delft University of Technology
by the authority of the Rector Magnificus, prof. dr. ir. T.H.J.J. van der Hagen,
chair of the Board for Doctorates
to be defended publicly on
Tuesday, 20 September 2022 at 15:00

by

Jianfeng Fu

Master of Engineering in Electrical Engineering,
Xi'an Jiaotong University, Xi'an, China,
born in Dalian, China.

This dissertation has been approved by the promotors.

Composition of the doctoral committee:

Rector Magnificus	chairman
Prof. dr. ir. B. De Schutter	Delft University of Technology, Promotor
Dr. ir. A. Núñez	Delft University of Technology, Co-promotor

Independent members:

Prof. dr. ir. Z. Lukszo	Delft University of Technology
Prof. dr. P. Palensky	Delft University of Technology
Prof. dr. ir. F. van Keulen	Delft University of Technology
Prof. dr. M. Dotoli	Polytechnic University of Bari
Prof. dr. C. Chen	Xi'an Jiaotong University

无曰已是
Seeking truth

CONTENTS

PREFACE

Time flies. In these four years, I saw different views, people from different nationalities, and different foods from my home country. At this moment, in Chinese zodiac, TU Delft has just spent its third sexagenary cycle and the forth sexagenary cycle is coming. Hope my university long live! Furthermore, I would like to express my sincere gratitude to the people who guided and supported me during my PhD period.

First, I would like to express my great gratitude to Prof. Bart De Schutter and Prof. Alfredo Núñez. It is very lucky to meet you and also my glory to be your student! Thank you very much for your constant trust, backing, and insight that help me to pursue the PhD degree. Currently, I still miss the days we spent on sharing interesting topics, discussing methods, and polishing works. It is also worthy of mentioning the free environment you provide to me, in which I can choose my own and favored research path.

Second, the same gratitude goes to Prof. Saeed Peyghami and Prof. Frede Blaabjerg for being the hosts of my research visit to Aalborg University. I finally visited Prof. Blaabjerg, who I had hoped to meet since I was a master student! Thanks very much for their help in sharing the frontiers of power electronics engineering and their valuable advice. I spent a very comfortable and peaceful journey at Aalborg University.

Dear Prof. Guobing Song, thank you for your guidance during my master period. Your kindness and supervision guide me to touch the gate of research for the first time. I miss Xi'an Jiaotong University and also the people there.

I would like to thank all the committee members, Dear Prof. Van Keulen, Prof. Peter Palensky, Prof. Chen Chen, Prof. Mariagrazia Dotoli, and Prof. Lukszo Zofia, for your time and efforts on commenting my draft thesis. The quality of this thesis is definitely improved by incorporating your comments.

To all my colleges in the Delft Center for Systems and Control, thank you all. Thanks my "brothers in academic" (fellow apprentices), Prof. Rudy Negenborn, Prof. Anahita Jamshidnejad, Luigi, Zhou, Maolong, Tomas, Shengling, Dingshan, Xiaoyu, and Kanghui, for helping me during my PhD period. I also want to say thanks to Abhimanyu, Jingwei, Ximan, Raja, Mattia, Zhixin, Luyao, Yun, and Tian.

I am also so grateful to my friends, Yu, Haodong, Zongbo, Na, Le, Zhe, Dai, and so on. Thanks for making my study and my life more colorful and joyful.

Finally, I owe special thanks to my parents. They have always been taking care of me, unconditionally loving me, and believing in me. Because of my parents, I never feel hopeless no matter what happens. Words are never sufficient to express my love and gratitude to my parents.

Jianfeng Fu
Delft, July 2022

SUMMARY

In typical power system operations, failures, e.g., caused by degradation, may result in service interruption and loss of power supply. Furthermore, low-occurrence-probability but high-impact extreme events, e.g., natural disasters and cyber-attacks, may also damage the power grid. This thesis aims to develop innovative strategies for handling these two kinds of failures in power grids. In particular, we develop preventive maintenance strategies, a pre-disaster electrical vehicle charging control strategy, an accurate fault location algorithm, and an unmanned aerial vehicles routing strategy for post-disaster distribution networks.

In the first part of this thesis, we develop failure prevention strategies for power grids. We propose a short-term condition-based preventive maintenance scheduling strategy that considers the supporting potential of distributed generators and batteries. Then a novel bidding mechanism for maintenance of generation units is proposed. In this mechanism, the generation companies (GENCOs) of the host independent system operator (ISO) can change their maintenance slots by purchasing supportive energy from the GENCOs of the neighbor ISOs and/or by paying penalty fees in case the energy transmitted from the host ISO to the neighbor ISOs is reduced for ensuring the reserved energy level in the host ISO. Consequently, more maintenance actions can be performed on the generation units so that the reliability of the transmission power network can be enhanced. Afterwards, a truthful maintenance platform is proposed for generation units in transmission power networks. By using the proposed platform for truthful condition-based maintenance of generation units, the GENCOs and manufacturers of the equipment can share their data in a trustworthy environment without worrying about tampered data or data breaches.

In the second part of this thesis, we propose a novel charging control strategy for pre-disaster evacuation situations. Compared with the charging strategies in the literature, we explicitly include two specific contributions. Firstly, compared with the load and charging demands prediction method for regular daily situations, a more accurate load and charging demands prediction method for pre-disaster situations is proposed based on human evacuation behaviour. Secondly, to ensure fairness, in the method to determine the charging schedule for the plugged-in electric vehicles (EVs), a higher priority is given to plugged-in EVs whose departure times are more heavily delayed. Then we propose a novel Aitken-distributed-model-predictive-control algorithm with fast convergence speeds to solve the charging optimal control problem for plugged-in EVs.

In the third part of this thesis, we propose an estimation method based on maximum likelihood estimation that can effectively reduce the uncertainty in the measurements when determining the transmission line parameters. In this way, the inspection distance for searching the fault location by the crews can be reduced. Besides, an unmanned aerial vehicle routing strategy integrating of monitoring roads and lines, and inspection of damages for post-disaster situations is proposed for distribution networks.

To adapt to unpredictable events, the UAV routing strategy is implemented in real time by adopting a receding horizon strategy. This routing strategy can facilitate to find the damages and potential dangers and also can provide the real-time traffic situation to the repair crews.

ACRONYMS

ARMA	Autoregressive moving average
ARIMA	Autoregressive integrated moving average
BB	Branch and bound
CBMGU	Condition-based maintenance of generation units
DA-DMPC	Dual-ascent-based distributed model predictive control
DFS	Depth first search
DMPC	Distributed model predictive control
EV	Electric vehicle
GENCO	Generation company
IBMM	Interchangeable bidding mechanism for maintenance
ISO	Independent system operator
MGU	Maintenance of generation units
MILP	Mixed-integer linear programming
MINLP	Mixed-integer non-linear programming
MIQP	Mixed-integer quadratic programming
MISOCP	Mixed-integer second order cone programming
MLE	Maximum likelihood estimation
NBMM	Non-interchangeable bidding mechanism for maintenance
PCC	Point of common coupling
PDF	Probability density function
PEV	Plug-in electric vehicle
PMU	Phasor measurement unit
PSO	Particle swarm optimization
RES	Renewable energy source

SOC   State of charge

T-CBMGU   Truthful condition-based maintenance of generation units platform

UAV   Unmanned aerial vehicle

UAVRS   Unmanned aerial vehicle routing strategy

1

INTRODUCTION

1.1. BACKGROUND AND SCOPE

1.1.1. BASIC COMPONENTS IN POWER SYSTEMS

Current power systems mainly include generation units, distributed generators, transformers, transmission lines, distribution networks, batteries, and loads, as shown in Figure 1.1. The electrical energy in power systems is generated from the generation units. Then, the transmission networks that include transmission lines deliver the generated energy from generation units to distribution networks. Afterward, distribution networks distribute the energy to the loads. Note that there can be distributed generators in the distribution networks. These distributed generators also can generate electrical energy but deliver the generated energy directly to the distribution network [90].

In power systems, the generation units are managed by the generation companies (GENCOs). One of the basic purposes of a GENCO is to earn benefits from energy generation. Furthermore, in power systems, there is another entity called the independent system operator (ISO). The ISO is a non-profit organization that manages the power systems in an area. It is responsible for scheduling the maintenance actions of the generation units in its area to ensure the reliability of the power systems in the given area.

In this thesis, failure prevention strategies of generation units and distribution networks are considered in Chapters 2 to 4. The GENCOs and ISOs are considered in failure prevention strategies of the generation units in Chapters 3 and 4. Moreover, the distribution network is considered in the charging strategy in Chapters 5. Furthermore, failure restoration strategies of the distribution and transmission networks are discussed in Chapters 6 and 7.

1.1.2. POWER SYSTEM RELIABILITY AND RESILIENCE

In general, power system reliability addresses service interruptions and power supply losses in power systems [141]. Service interruption occurs when e.g. scheduled maintenance actions are performed or a component breaks down, and may result in load loss.
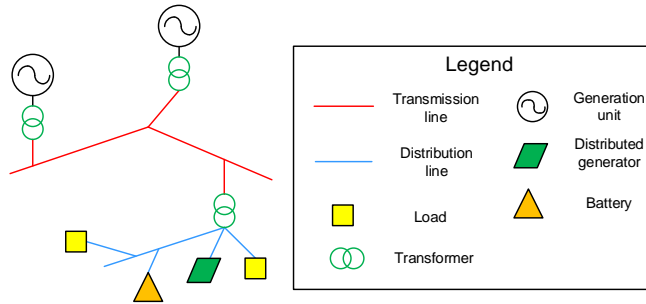
Figure 1.1: Basic components of power systems

Thus, power system reliability is an important performance criterion and highly influences the quality of service of the power system.

The resilience of the power system describes the fast restoration capacity after the power system has been impaired by e.g., extreme natural disasters [32] and cyberattacks [158]. Different from the reliability, resilience involves low-probability but high-influence events. A fast restoration process with less load loss reduces the influence of the outage on the quality of living and even on the basic requirements of the residents, e.g., as reported in the recent winter storm in Texas 2021 [60]. Power system resilience has received increased attention in recent decades because of the frequent occurrences of extreme natural disasters around the world.

1.1.3. POWER SYSTEM MAINTENANCE
To guarantee the power system reliability, maintenance actions should be performed on the components of the power systems. Maintenance actions reduce the failure rate of the components so as to prevent sudden failures that may result in large-scale outages or damage the other components. The components in power systems mainly include generation units, transformers, and transmission lines. Since without implementing a redundant design, performing maintenance actions usually results in the scheduled (i.e., non-sudden) shutdown of the components, scheduling the maintenance actions with the lowest costs is one of the major responsibilities of the power system operators. These costs involve the maintenance performance costs, load loss costs resulting from performing scheduled maintenance actions, penalty fees for shutting-down the components, and so on.

1.1.4. PRE-DISASTER EMERGENCY COUNTERMEASURES
The pre-disaster emergency situation is in the period before an extreme natural disaster occurs. During the pre-disaster situation, the residents may behave differently from their behavior in regular daily life. Thus, operation and control strategies for power systems should adapt to pre-disaster human behavior. For instance, in pre-disaster situations, the charging requirements of the owners of electric vehicles (EVs) may increase significantly. That is because the owners may intend to use their EVs to evacuate before the disaster. So, the load and charging demands in pre-disaster evacuation situations cannot

be accurately predicted by using the load and charging demands prediction methods for regular daily life. Consequently, it is important to develop a charging control strategy for pre-disaster evacuation situations.

1.1.5. POWER SYSTEM RESTORATION

After extreme natural disasters, the components in power systems may be damaged. To recover the power systems quickly, the power system operators require to first know where the damages are. For distribution networks, locating the damages via electrical fault signals only is very difficult. Thus, the inspections of damage via nonelectrical measures should be performed, e.g., by human crews or unmanned aerial vehicles (UAVs).

1.2. PROBLEM STATEMENT

1.2.1. POWER SYSTEM CONDITION-BASED MAINTENANCE SCHEDULING

Maintenance strategies can be mainly categorized into corrective and preventive maintenance strategies [71], [194], [207]. The corrective maintenance involves repairing the failures after they have occurred. Corrective maintenance is easy to implement, since there is no need to estimate the degradation conditions of the components. However, the sudden shutdowns caused by failures may result in large-scale outage or instability of the power system. Customers will be unhappy with sudden outages and other components in the power system may get influenced by the sudden shutdowns of some components. Preventive maintenance is to regularly perform maintenance actions on the equipment aiming at avoiding sudden failures. Thus, preventive maintenance should be developed for power systems.

Preventive maintenance can further be categorized into periodical maintenance [155] and condition-based maintenance [71]. In periodical maintenance, the maintenance actions are scheduled periodically according to the degradation curves of the components, e.g., bathtub curves. The degradation curves of the components can be provided by the producers via accelerated ageing tests and/or data/experience collected from the real-life environment. However, not all the components produced by the same producer have the same degradation curves. Moreover, the same components in different environments may have different degradation curves. Thus, periodical maintenance actions may be performed on components with low failure rates (e.g., as they are installed in an environment with slower degradation). On the other hand, periodical maintenance actions may be performed on components installed in an environment with faster degradation. Thus, the maintenance period design in periodical maintenance may result in over-maintenance in an environment with slower degradation and lack of maintenance in an environment with faster degradation. Therefore, this thesis focuses on condition-based preventive maintenance, which periodically estimates the degradation status of the components, and next determines whether the components should be maintained.

The first problem considered in this thesis involves how to develop a preventive maintenance scheduling strategy for distribution networks integrated with distributed generators (called active distribution networks). Currently, more and more distributed generators are integrated into the distribution network. Different from the traditional distribution networks, the distributed generators can provide some of the required en-

ergy during the outage caused by performing maintenance actions on the upstream components. Thus, this motivates us to develop a maintenance strategy for active distribution networks that takes into account the generation capabilities of distributed generators.

The second problem involves how to design an improved bidding mechanism for the maintenance of generation units in power systems. In deregulated power systems, the generation units are assets of the generation companies. The independent system operator manages the maintenance scheduling of the generation units by maximizing the overall profits of the GENCOs that the ISO manages while guaranteeing the power system reliability.However, maximizing the overall profits may conflict with the profits of individual GENCOs. Consequently, in deregulated environments, the GENCOs are allowed to change their scheduled maintenance time slots. In the literature, some authors, e.g., [67], [212] propose bidding mechanisms for maintenance of generation units. However, the question then arises whether it is possible to design an improved bidding mechanism by considering the inter-ISO power exchange, so that the GENCOs can gain more chances to change their scheduled maintenance time slots.

The third problem involves how blockchain technology can improve the state-of-the-art condition-based maintenance for maintenance of generation units in power systems. The maintenance scheduling of generation units mainly involves five processes, operational data acquisition, failure rate diagnosis/prognosis, maintenance scheduling, bidding for changing scheduled time slots, and performance of maintenance actions. Furthermore, blockchain technology is mainly characterized by the immutability of the stored data, distributed data storage, smart contracts [43]. Thus, one may wonder whether the features of the blockchain technology can improve the data trustworthiness and decision-making result transparency of the five processes for maintenance scheduling of generation units.

1.2.2. EV CHARGING CONTROL FOR PRE-DISASTER EVACUATIONS
The fourth problem addressed in this thesis involves EV charging strategies for pre-disaster evacuation situations. Since in pre-disaster situations residents may intend to evacuate to other safe places, the pre-disaster charging requirements may intensively increase. Predicting the charging loads for pre-disaster evacuation situations require studying human behaviors. Thus, the question arises how to predict the charging loads and how to design the charging control strategies to counter the intensive increased charging requirements.

1.2.3. DAMAGE LOCATION IN POST-DISASTER RESTORATION
The fifth problem involves fault location of faults on two-terminal high voltage transmission lines. In post-disaster restoration situation, a fast restoration requires an accurate fault location, so that the size of the regions for manual inspection can be shrunk. To locate the faults on the transmission line, parameters of the transmission line, e.g., impedance and conductance, should be estimated. However, the uncertainty of the measurement devices may influence the accuracy of parameter estimation. Thus, this motivates us to develop an accurate transmission line parameter estimation algorithm, so that the fault location can be more accurate.

1

For the fifth problem, we propose a fault location algorithm for transmission lines. The sixth problem considered in this PhD thesis involves using UAVs to inspect and monitor damages in distribution networks. Since after extreme natural disasters the distribution network may be damaged and potential dangers may occur, locating the damages and potential dangers can facilitate fast restoration of the distribution networks. However, in some situations, it is dangerous for human crews to perform inspection and monitoring tasks. Thus, it is important to investigate whether it is possible to use UAVs to inspect the damages and monitor the potential dangers of the distribution networks. Furthermore, the question arises whether the UAVs can also monitor the road situation so that the repair crews can select a non-blocked path to reach the damages and then fix the damages.

1.3. CONTRIBUTIONS

The contributions of the thesis are listed below:

1. We propose a short-term condition-based preventive maintenance scheduling strategy that considers the supporting potential of distributed generators and batteries. Aspects faced in practice are included, such as the uncertainties in decision making, different electricity prices in different locations, and different durations of maintenance actions. A depth-first search clustering method is proposed to simplify the topology into a smaller-scale but equivalent topology, resulting in a large reduction of the complexity of the distribution network topology and the computational burden. Furthermore, two optimization algorithms are considered: a branch-and-bound algorithm and a modified particle swarm optimization algorithm.

2. A novel bidding mechanism for maintenance of generation units is proposed. In this mechanism, the GENCOs of the host ISO can change their maintenance slots by purchasing supportive energy from the GENCOs of the neighbor ISOs, paying penalty fees in case the energy transmitted from the host ISO to the neighbor ISOs is reduced for ensuring the reserved energy level in the host ISO, or both. Afterwards, a non-linear mixed-integer bidding programming problem is formulated to include the load loss on the tie lines caused by inter-ISO energy exchange of supportive energy. A coordination algorithm based on genetic algorithms and particle swarm optimization is proposed to solve the formulated bidding programming problem. Then, three possible organization schemes, i.e., centralized, priority, and impromptu bidding schemes, for starting the bidding processes in a large power grid associated with multiple ISOs are discussed.

3. A truthful maintenance platform is proposed for generation units in power systems. By using the proposed platform for truthful condition-based maintenance of generation units platform, the stored data can be immutable, data sharing can be efficient and secure, and the decision making can be fair. Furthermore, maintenance scheduling problems are time-costly mixed-integer quadratic programming problems. Then, two novel dedicated valid inequalities based on technical/physical analysis and greedy-based heuristic initialization are proposed for accelerating the convergence speed of Benders decomposition for solving the formulated maintenance scheduling problems. Finally, a truthful condition-based maintenance of generation units platform is established and tested on the Go-Ethereal platform.

4. We propose a novel charging control strategy for pre-disaster evacuation situa-

1

tions. Compared with the charging strategies in the literature, we explicitly include two specific contributions. Firstly, compared with the load and charging demands prediction method for regular daily situations, a more accurate load and charging demands prediction method for pre-disaster situations is proposed based on human evacuation behavior. Secondly, to ensure fairness, in the method to determine the charging schedule for the plugged-in EVs, a higher priority is given to plugged-in EVs whose departure times are more heavily delayed. Then we propose a novel Aitken-DMPC algorithm to solve the plugged-in EVs for charging optimal control problem for fast convergence speeds.

5. We analyze the influence of the uncertainty in the measurements on the fault location algorithms for transmission lines based on a case study. Then, we model the uncertainty in the measurements of phasor measurement units based on the information supplied by the phasor measurement unit supplier or by a newly proposed method based on the confidence level and deviation bounds if the information on the distributions of the uncertainties is not available. Afterwards, we propose an estimation method based on maximum likelihood estimation that can effectively reduce the uncertainty in the measurements when determining the transmission line parameters.

6. To facilitate the post-disaster restoration process and to make the human crews work safely and efficiently, a UAV routing strategy integrating of monitoring roads and lines, and inspection of damages is proposed for distribution networks. To adapt to unpredictable events, the UAV routing strategy is implemented in real time by adopting a receding horizon strategy. Moreover, a two-layer decision-making architecture is adopted due to inconsistency between time scales of inspection and monitoring. In the first layer, a method to roughly route the traces of UAVs is proposed. In addition, in the second layer, a method is proposed to determine the routes of UAVs in detail.

1.4. ORGANIZATION AND CATEGORIZATION OF THE THESIS

This thesis consists of eight chapters whose organization and relationship are shown in Figure 1.2. Chapters 2 to 7 are a collection of published and submitted journal papers. In Chapter 2, based on [71], a short-term preventive maintenance scheduling method for distribution networks with distributed generators and batteries is presented. Chapter 3, based on [73], deals with a bidding mechanism for maintenance of generation units considering inter-ISO power exchange. Based on [74], a truthful platform for condition-based maintenance of generation units in power systems is presented in Chapter 4. Chapter 5, based on [72], proposes a real-time accelerated distributed charging control strategy for plugged-in EVs for pre-disaster evacuation situations. Chapter 6, based on [76], presents the influence of measurement uncertainty on parameter estimation and fault location for transmission lines. In Chapter 7, based on [75], a real-time UAV routing strategy for monitoring and inspection for post-disaster restoration of distribution networks is proposed. Chapter 8 concludes the whole thesis.

Apart from the organization figure, we also provide a structure figure to categorize the contents of the main chapters as shown in Figure 1.3. The arrows in Figure 1.3 refer to the categories the contents in the main chapters attribute to. The categories in this thesis include transmission network/distribution network, and blockchain/optimal planning & control/situation awareness.
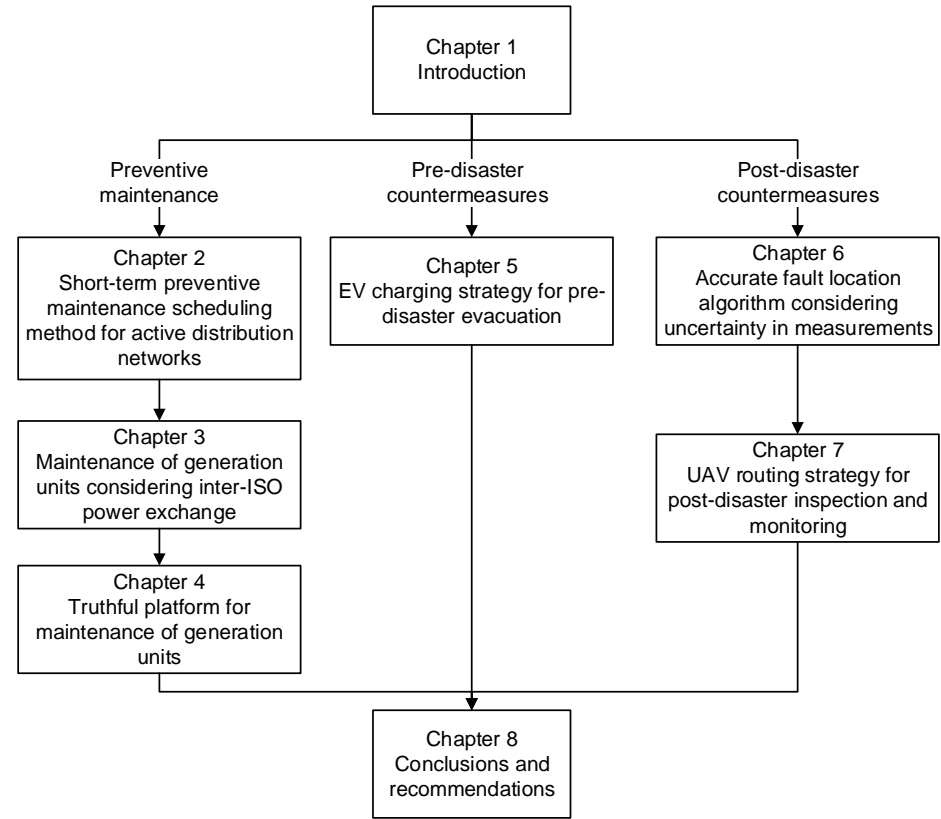
Figure 1.2: Outline of the thesis
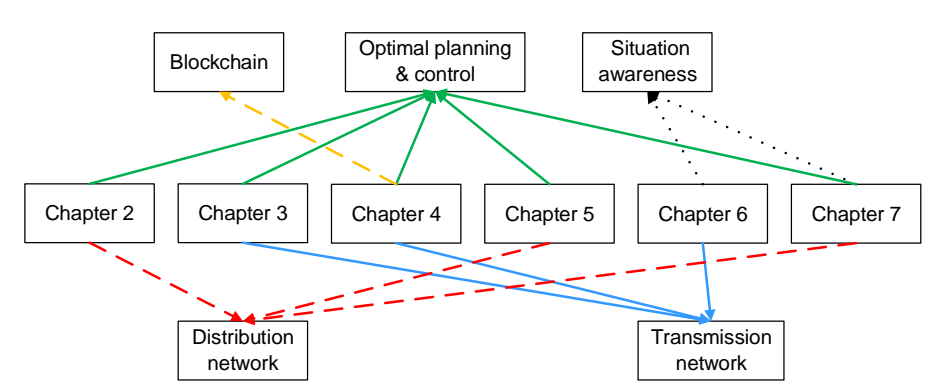
Figure 1.3: Categorization of the contents of the chapters

2

ACTIVE DISTRIBUTION NETWORK PREDICTIVE MAINTENANCE

2.1. INTRODUCTION

In 2016, 12% of the installed wind turbine capacity in Europe was older than 15 years, and this share will increase to 28% by 2020 [52]. These old wind turbines will soon reach the end of their designed service life, which is typically 20 years [246]. In addition, in today's power systems, commonly used XLPE cables are suffering from degradation, especially the water tree [237], [243]. Transformers, one of the critical assets in a power grid, are also suffering from degradation [5], [88]. Due to the deterioration of the components in the power system, the efficiency of generation and the reliability of the power system will be decreased, as the power system may suffer from faults or breakdowns. Thus, adequately scheduled maintenance actions are necessary to ensure the quality of the components and the efficiency and reliability of power generation and delivery.

Maintenance scheduling of power systems is mostly corrective or preventive [203]. Corrective maintenance is performed after failure of components [18], [138]. Preventive maintenance is performed before the failure of components [3], [26], [209]. It can result in significant budget savings compared to the corrective maintenance. For example, in [123], [159], [166], [178], the preventive maintenance actions are performed to avoid failures of generation units. Besides, in [11], [12], [35], [98] a new preventive maintenance concept "smart maintenance" has been proposed. Smart maintenance utilizes smart inspections based on big data analysis technologies, smart devices to collect the data, smart services, asset management, and other techniques to make preventive maintenance decisions. In particular, in [35], a review of the possible applications of big data on failure diagnosis, the internet of things on data collecting, and other technologies on smart maintenance can be found.

In preventive maintenance, the degradation conditions of the components can be

---

This chapter is based on [71].
The nomenclature of this chapter is at the end of this chapter.

2

evaluated based on different standards. For example, [8] analyzed the influence of factors such as power fluctuation, states of charge, and the charging/discharging rates on the life spans of the electric vehicle batteries. According to the factors, a charging plan was proposed to enlarge the life spans of electric vehicle batteries. In [10], the bathtub curve is used to measure the probability that a component will survive beyond an established time. A mathematical quantification model is presented to evaluate the degradation condition of the components by representing the bathtub curve as a Markov process. Then the degradation condition is used in the preventive maintenance of generation units. In [238], a reliability modeling method for systems composed by multiple components is proposed. The reliability indices of each component were used to derive the reliability of the whole system. In the standards such as the "Guide for condition evaluation of distribution network equipment", as shown in Chapter 7 of [168], a procedure to evaluate the condition scores of the components is described by evaluating the condition score of each sub-component individually and then summing them up with different weights.

Then, a cost-effective strategy [3] or a reliability-based strategy [2], [56], [232] can be used to determine a maintenance schedule. In the literature, different methods for preventive maintenance scheduling have been proposed [28], [144]. In [28], preventive maintenance is derived by considering the impact of increased short-circuit current flows on the failure rate. In [144], a cost-effective maintenance scheduling method with reliability constraints for overhead lines is proposed. Cost-based reliability indices are used for modeling. The methods in the literature for preventive maintenance scheduling in power systems minimize maintenance costs, maximize reliability, and also consider other factors, e.g., the influence of short-circuit currents on the failure rate [28] and the reliability [144]. In these *preventive* maintenance scheduling methods, the supporting power potential of DGs and batteries to reduce load loss cost was not explicitly considered. In [163], a preventive maintenance strategy considering the distributed generation in distribution networks is proposed. However, the islanding mode of the microgrids is not considered in the problem formulation. Thus, the supporting power potential of the DGs and batteries when microgrids are being islanded was not assessed. Then, the scheduled maintenance actions without considering the supporting power potential may result in more shed loads when these maintenance actions are preformed. Consequently, this chapter proposes a method characterized by considering the supporting power potential of the DGs and batteries in the maintenance scheduling of the distribution networks. Then, the maintenance actions can be scheduled in better time slots resulting in fewer shed loads.

In literature, *corrective* maintenance and system restoration methods have been proposed considering the supporting power potential of DGs, batteries and the reconfiguration [17], [18], [30], [45]. Although one of the objectives of these methods is to serve more loads using DGs and batteries, these methods are designed for scheduling the maintenance actions after the failures and damages have emerged, e.g., a flood or a hurricane. However, preventive maintenance methods are designed for scheduling the maintenance actions so as to prevent the failures by considering the trade-off between the degradation status of the components and the total maintenance cost including cost of load shedding and the cost of performing maintenance actions. Thus, corrective main-

tenance methods differ from preventive maintenance methods and they cannot be used for the short-term preventive maintenance scheduling directly.

When the number of nodes of the distribution network increases, the number of the variables increases and the computation burden is enlarged. In this chapter, a state-of-art depth-first-search (DFS) clustering method is proposed to simplify the topology of the network into a smaller-scale but still equivalent topology. Different zones in the distribution network are constructed according to the locations of the candidate maintenance actions. Grouping by zones results in a significant decrease of the number of nodes. In this way, the formulated preventive maintenance scheduling problem is simplified, and the computational burden is reduced.

Further, a scenario-based approach is proposed to allow the inclusion of stochasticities in the optimization problem while avoiding expensive computational efforts resulting from traditional robust approaches that require complete realizations of the stochasticities. Still, the scenario-based approach is more complicated than a deterministic solution (where no stochasticities are included), but it can be kept tractable according to the selected scenario generation method and scenario reduction method.

After that, two solvers are analyzed, branch-and-bound (BB) and particle swarm optimization (PSO). The BB solver can obtain the optimal solution but takes more computation time. While the PSO solver cannot obtain the optimal solution but can take less computation time. Interesting results using the PSO solver have been reported in the literature. For example, a PSO algorithm is used in [115] to minimize the overall cost, including investment, replacement, operation, and maintenance costs during the 20 years of a hybrid wind/photovoltaic generation system lifetime. A novel multi-objective PSO optimization algorithm is proposed in [24] to minimize three objective functions, namely the annualized cost of the system, loss of load expected, and loss of energy expected, when designing hybrid wind-solar generating microgrid systems. A multi-objective PSO algorithm is proposed in [22] to solve the optimal allocation problem for flexible alternating current transmission system devices. Besides, a new multi-objective optimization problem for the coordination of overcurrent relays in interconnected networks is presented in [23]. The problem is then solved by using multi-objective PSO and a fuzzy decision-making tool.

The main contributions of this chapter are:

- A short-term condition-based preventive maintenance scheduling method that considers the supporting potential of DGs and batteries is proposed.

- Aspects faced in practice are included, such as the uncertainties in decision making, different electricity prices in different locations, and different durations of maintenance actions. The problem is formulated as a stochastic mixed-integer non-linear programming problem and solved using a scenario-based approach.

- A DFS clustering method is proposed to simplify the topology into a smaller-scale but equivalent topology, resulting in a large reduction of the complexity of the distribution network topology and the computational burden.

- Two optimization algorithms are considered: BB and a modified PSO algorithm. The BB approach uses an exact reformulation of the mixed-integer non-linear pro-

2

gramming problem into a linear programming one. The BB solver always finds the optimal global solution; however, recasting the problem increases the number of optimization variables. The modified PSO algorithm directly solves the mixed-integer non-linear programming problem and allows managing the computational burden at the expense of performance.

The remainder of this chapter is organized as follows. Section 2.2 describes the issues of the preventive maintenance problem and the framework of the proposed method. Section 2.3 introduces the method to simplify the topology of the distribution network. Section 2.4 proposes a method to generate topological connectivity constraints so as to obtain explicit relationships between served loads by DGs and batteries and maintenance decision making variables. Section 2.5 formulates the maintenance scheduling problem, proposes a method to generate and reduce the number of scenarios, and then introduces the BB solver and proposes a specific PSO solver for this problem. Section 2.6 presents the results and analysis of a case study. Section 2.7 discusses the contributions and possible applications of the proposed method. Finally, in Section 2.8 conclusions and topics for future research are included.

2.2. PROBLEM DESCRIPTION AND PROPOSED FRAMEWORK

In this section, we will first describe the problems we face and intend to tackle. After that, we propose a framework for scheduling short-term preventive maintenance actions and give a brief introduction.

2.2.1. PROBLEM DESCRIPTION

Mid-term preventive maintenance scheduling is a basic component in asset management of distribution networks. It is a maintenance scheduling strategy with a larger time scale and a longer period than the short-term preventive maintenance scheduling. Thus, it is a rougher preventive maintenance decision-making strategy. In the mid-term preventive maintenance scheduling, the maintenance actions are determined based on the operation cost, load loss, and degradation of the components in a medium time scale, e.g., one month or several months. In this chapter, we assume that a mid-term maintenance scheduling method determines which maintenance actions should be performed one week in advance [203]. Then we propose a method to allocate these candidate maintenance actions within the days of a week. Now, we discuss two major problems for the design of preventive short-term maintenance scheduling considering the supporting energy from DGs and batteries.

PROBLEM 1

In the case of large-scale distribution networks, the number of variables to characterize the possible dynamics during maintenance in the maintenance scheduling problem can be huge. As such, a method to reduce redundant variables and to simplify the distribution network without losing crucial information is required. In this chapter, a clustering method is proposed to simply the network so as to reduce the number of variables in the maintenance scheduling problem.

(a) Maintenance in one spot   (b) Maintenance in four spots
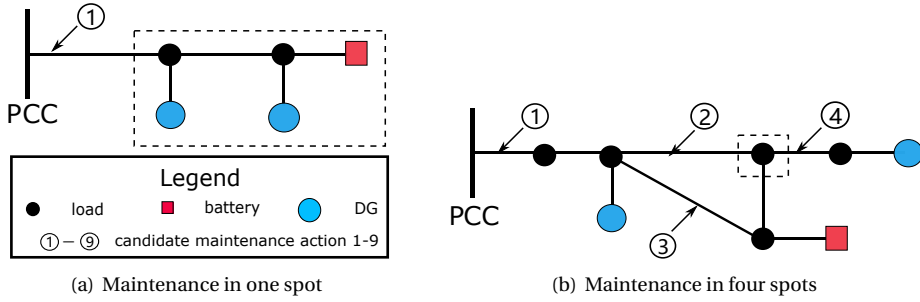
Figure 2.1: Distribution networks for illustrating Problem 2

PROBLEM 2

Figure 2.1 shows two networks to discuss another problem addressed in this chapter. The numbers in circles with an arrow indicate the locations where preventive maintenance actions are to be conducted and the numbers represent labels of maintenance actions. The blue circles represent DGs, while the red boxes represent batteries.

In practice, the isolation switches are applied to isolate the components, e.g., distribution lines, where maintenance actions are performed. Then, when performing the maintenance actions on the components, the connectivity will be changed.

In Figure 2.1(a), ① should be maintained when the DGs and the battery can support the loads as much as possible to reduce the load loss. The load loss is given by the power required by the loads minus the power provided by the DGs and the battery. Thus, the time slots to maintain ① when the minimum load loss happens can be estimated. However, when there are several maintenance actions and the network is more complex as shown in Figure 2.1(b), the load loss cannot be calculated easily because of the connectivities between loads, DGs and the battery determined by where and when maintenance actions are performed. Where and when maintenance actions are performed are decision making variables in the maintenance scheduling problem. For example, the served load in the dashed box of Figure 2.1(b) is determined by the sum of all the other connecting loads, DGs and the battery. Further, the connectivities are different for different combinations of maintenance actions, e.g., when maintenance is performed at ② or when ② and ③ are maintained simultaneously. Thus, another problem is to establish the relationships between load loss at each time step and maintenance action decision making variables for complex distribution networks.

2.2.2. PROPOSED FRAMEWORK

A framework for scheduling short-term preventive maintenance is proposed as shown in Figure 2.2.

In this framework, after obtaining the candidate maintenance actions from the mid-term maintenance scheduling method, a clustering method is applied to divide the network into zones according to the week-ahead candidate maintenance operations. Then, a sum of products method is proposed to represent the connectivity of the topology by maintenance decision making variables. The explicit expression of the relationship be-
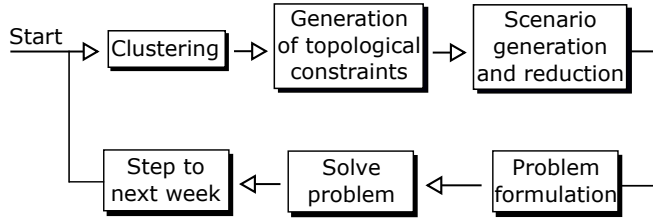
Figure 2.2: Flowchart of proposed method

tween maintenance decision making variables and load loss cost is then derived. After that, the scenarios used to describe the uncertainties in the programming problem will be generated by scenario generation and reduction methods. Then a stochastic MINLP problem is formulated and solved to determine the daily preventive maintenance schedule. The method determines the maintenance schedule by minimizing the maintenance cost including the performance cost, load loss cost, and the cost related to the degradation of the components based on a score index. We next introduce the three main parts of the proposed method including: clustering method, generation of topological connectivity constraints, and problem formulation associated with the scenario generation and reduction methods as well as two possible solvers.

2.3. CLUSTERING METHOD

Distribution networks consist of many components, e.g., paths, DGs, and batteries. Each of these components can be modeled to understand the dynamics of the network. However, when considering maintenance operations, usually not all the components have to be maintained. Thus, the detailed dynamics of each component might not be required for maintenance scheduling purposes, and methods can be used to reduce the complexity of the network. In this chapter, we define a zone as the maximal set of connected components such that no matter when and which candidate maintenance actions are performed, the connectivity in one zone will not change.

For illustration purposes, Figure 2.3 shows a distribution network with a coupled loop topology. There are five candidate maintenance actions, marked from ① to ⑤. In Figure 2.3(a), zone 1 contains one DG, one battery, and loads, while zone 2 contains loads; zone 3 contains one DG and zone 0 is a point of common coupling (PCC) zone that connects the outside system. From Figure 2.3(a), it can be seen that the connectivity between components within the five zones will not change when any of the candidate maintenance actions are being performed. The simplified representation of the distribution network in Figure 2.3(a) is shown in Figure 2.3(b).

In Figure 2.3(b), ① and ⑤ are inner maintenance actions of zone 1 whose scheduled execution time will not influence the connectivities of the components. From Figure 2.3(a) and Figure 2.3(b), it can be seen that components in Figure 2.3(a) are clustered into four zones in Figure 2.3(b). A zone can be seen as an integrated component, so the scale of the maintenance scheduling problem can be largely simplified.

As for a method to search the zones to simplify the network, the depth first search (DFS) method [20], [201], [206] is considered to find the largest connecting areas. To

(a) Illustration of zones division

(b) Final simplified topology

(c) Illustration of searching trees generations
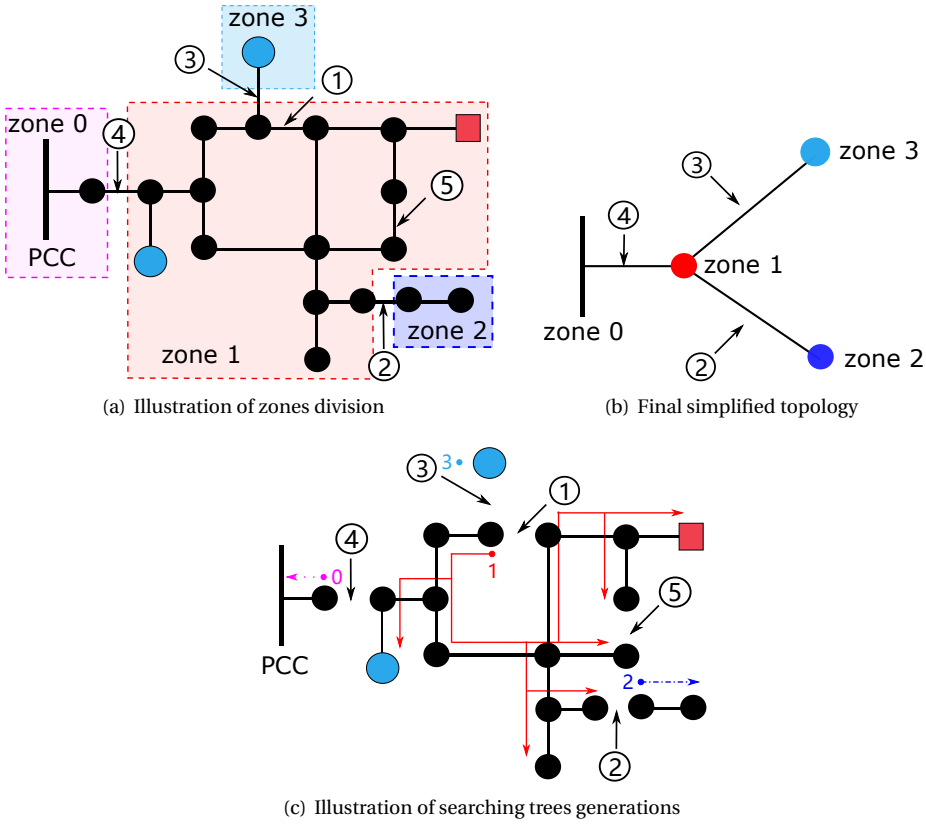
Figure 2.3: Illustrations of the proposed clustering mechanism

fit the DFS method in the maintenance clustering problem, each component is seen as a node, and the paths that do not need to be maintained are seen as connecting path, while the paths that need to be maintained are seen as break-points, as shown in Figure 2.3(c). Here we define a tree as a set of connected paths and nodes. The details of the steps of the DFS method are as follows:

1) Select as starting node one of the nodes that has not been visited by other trees. Start a new tree from this starting node.

2) Visit paths that come out of the most recently visited node p_0. Consider only paths going to un-visited nodes.

3) When all of p_0's paths have been visited, the search backtracks until it reaches an un-visited adjacent node. This process continues until all of the nodes that are reachable from the starting node have been visited. Then a largest connecting tree has been generated and the components on the tree originated from the starting point can be included in one zone.

4) If there are any un-visited nodes, select one of them as a new starting point and repeat the search from that node.

5) The algorithm repeats this entire process until it has visited every node. In this chapter, we define the zone that includes the PCC point as zone 0.

Different starting points selection sequences do not influence the simplified topology, because if from a node p_u there is a path that can reach another node p_v, this means that from p_v there must be a path can reach p_u. In Figure 2.3(c), the zone generation process is shown. The search trees for the cluster generations are marked with a purple line, red lines, a blue line, and a green line to represent zone 0 to zone 3 respectively. In addition, the starting nodes of these searching trees are marked as filled circles in respective colors.

2.4. GENERATION OF TOPOLOGICAL CONNECTIVITY CONSTRAINTS

The load loss cost mentioned in Section 2.2 is related to the gap between the power served to loads and the power required by the loads, such that for zone p:

$$P_{\text{loss},p}(t) = P_{\text{pred},p}(t) - P_p(t) \tag{2.1}$$

where $P_p(t)$ is determined by the connectivity between the loads and other loads, DGs, batteries, and the PCC based on power balance equation, such that:

$$\sum_{q=0}^{n_Z} \delta_{p,q}(t) P_p(t) = 0, \ \forall t \in \{1, ..., t_d\} \tag{2.2}$$

where the zone containing the PCC is zone 0. In (2.2), the binary variable $\delta_{p,q}(t)$ is introduced to describe the connectivity between zones. Define $\delta_{p,q}(t)$ equals 1 if zone p and zone q are connected in time slot t. The connectivity variables $\delta_{p,q}(t)$ are determined by the maintenance actions because these will generate break-points dynamically in the network. Next, we propose a method to express the connectivity between zones by the maintenance decision making variables.

We introduce the binary maintenance decision making variable $\Delta_{j,p,q}(t)$ to indicate whether the maintenance actions are performed or not. If the jth maintenance action is assigned to be performed on the path between zone p and zone q in time slot t, then $\Delta_{j,p,q}(t) = 1$; else $\Delta_{j,p,q}(t) = 0$.

Two points need to be clarified: Firstly, for the maintenance actions on DGs (or batteries), e.g. the DG in zone 3 of Figure 2.3(a), the DG in zone 3 will be shut down and disconnected from zone 1. Furthermore, performing maintenance actions on the connecting path between the DG in zone 3 and zone 1 will also cause the DG in zone 3 to be disconnected from zone 1. Thus, maintenance actions on DGs or batteries can be seen as maintenance actions on the connecting paths between these DGs or batteries and the other parts of the network. Secondly, if a maintenance action takes several hours, e.g. 4 hours, then the corresponding connectivity variable $\Delta_{j,p,q}(t)$ equals 1 for each of the 4 hours when the maintenance action is performed.
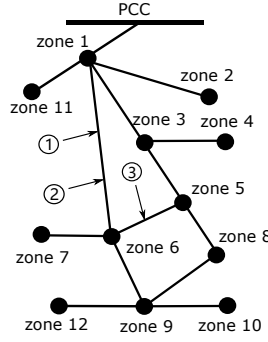
Figure 2.4: An example of a distribution network

After defining maintenance decision making variable $\Delta_{j,p,q}(t)$, firstly the connectivity status of zone p and its neighbor zone q can be derived as:

$$\delta_{p,q}(t) = \prod_{j=1}^{N_z}(1 - \Delta_{j,p,q}(t)),$$

$$\forall t \in \{1,...,t_\mathrm{d}\}, \forall p \in \{0,...,n_Z\}, q \in \Omega_p, j \in \Theta_{p,q} \tag{2.3}$$

Equation (2.3) represents that when maintenance actions are performed on the path between zone p and its neighbor zone q in time slot t, zone p and zone q will be disconnected. Secondly, by defining Ω_p^c as the set of the non-neighbor zones of p, for each pair of zones p and q' (with $p \neq q'$ and $q' \in \Omega_p^\mathrm{c}$), we determine all possible elementary (i.e. without circuits) paths $p \mapsto p_1 \mapsto p_2 \mapsto ... \mapsto p_{h-1} \mapsto q'$ from zone p to zone q', possibly including the PCC (with index 0) by using the paths searching approaches mentioned in, e.g. [142]. Let $(p, p_1, p_2, ..., p_{h-1}, q')$ represent an elementary path from p to q' and let $\mathcal{H}_{p,q'}$ be the set of all such paths, then we have:

$$\delta_{p,q'}(t) = \begin{cases} 0 & \sum\limits_{(p,...,q') \in \mathcal{H}_{p,q'}} \delta_{p,p}(t)\delta_{p,p_1}(t)...\delta_{p_{h-1},q'}(t) = 0 \\ 1 & \text{otherwise} \end{cases} \tag{2.4}$$

In this way, the relationship between the maintenance decision variables Δ and the connectivity variables δ can be derived. Apart from that, the connectivity status from zone p to its neighbor zone q or non-neighbor zone q' is the same as that from zone q' or zone q to zone p. In addition, the value for any $\delta_{p,p}$ is equal to 1 at any time because the status between a zone and itself is always connected. Thus, we have:

$$\delta_{p,q}(t) = \delta_{q,p}(t), \; \delta_{p,q'}(t) = \delta_{q',p}(t), \; \delta_{p,p}(t) = 1,$$

$$\forall t \in \{1,...,t_\mathrm{d}\}, \forall p \in \{0,...,n_Z\}, \forall q \in \Omega_p, \forall q' \in \Omega_p^\mathrm{c} \tag{2.5}$$

Figure 2.4 shows an example for illustration purposes. In Figure 2.4, we will derive $\delta_{1,8}(t)$ by using (2.3) to build the relationship between the connectivity status variable of zone 1 and zone 8 and the maintenance decision making variables. There are 3 paths

from zone 1 to zone 8, so $\mathcal{H}_{1,8} = \{(1,3,5,8),(1,6,5,8),(1,6,9,8)\}$. Thus, we can derive that:

$$\delta_{1,8}(t) = \begin{cases} 0 & \displaystyle\sum_{(p,...,q')\in\mathcal{H}_{1,8}} \delta_{p,p}(t)\delta_{p,p_1}(t)...\delta_{p_{h-1},q'}(t) = 0 \\ 1 & \text{otherwise} \end{cases} \tag{2.6}$$

as well as:

$$\begin{aligned}\delta_{1,6}(t) &= (1-\Delta_{1,1,6}(t))(1-\Delta_{2,1,6}(t)),\\ \delta_{5,6}(t) &= 1-\Delta_{1,5,6}(t), \forall t \in \{1,...,t_\mathrm{d}\},\end{aligned} \tag{2.7}$$

where $\Delta_{1,1,6}(t)$, $\Delta_{2,1,6}(t)$ and $\Delta_{1,5,6}(t)$ represent whether to perform maintenance actions ①, ② and ③ respectively in time slot t. Thus, in this way, the relationship between all the connectivity variables and maintenance decision-making variables can be built. The relationships can be used to generate the power balance functions. The generated power balance functions can dynamically represent the served powers to the zones using the maintenance decision variables (see Section 2.5.1).

2.5. SCHEDULING PROBLEM AND POSSIBLE SOLVERS
In this section, firstly the stochastic MINLP problem of the proposed short-term preventive maintenance method will be formulated. Secondly, the scenario generation and reduction methods will be illustrated. Thirdly, two possible solvers will be introduced.

2.5.1. PROBLEM FORMULATION
This subsection formulates the optimization problem for the proposed method. We search for a vector Δ that contains all the variables $\Delta_{j,p,q}(t)$, and that minimizes the following objective function:

$$\min_{\Delta} J = \mathbb{E}_\Phi[C_{\mathrm{loss},s} + C_{\mathrm{main}} - C_{\mathrm{deg}} + C_{\mathrm{soc},s}] \tag{2.8}$$

where $\mathbb{E}_\Phi$ represents the expected value for scenario set Φ. More specifically,

$$C_{\mathrm{loss},s} = \sum_{t=1}^{t_\mathrm{d}} \left(\sum_{p=1}^{n_\mathrm{Z}} \left(P_{\mathrm{pred},p,s}(t) - P_{p,s}(t) \right) C_{\mathrm{pril},p}(t) \right) \tag{2.9}$$

$$C_{\mathrm{main}} = \sum_{p=1}^{n_\mathrm{Z}} \sum_{q=p+1}^{n_\mathrm{Z}} \sum_{j\in\Theta_{p,q}} \frac{1}{\tau_{j,p,q}} \left(\sum_{t\in\mathcal{T}^\mathrm{D}} (1-\Delta_{j,p,q}(t))C_{j,p,q}^\mathrm{D} + \sum_{t\in\mathcal{T}^\mathrm{N}} (1-\Delta_{j,p,q}(t))C_{j,p,q}^\mathrm{N} \right) \tag{2.10}$$

In this chapter we assume that the working crews of day-time and night-time are different; so we do not consider maintenance actions that are partially performed during the day-time and partially during the night-time. Note that the result of summing the $(1-\Delta_{j,p,q}(t))$ values is $\tau_{j,p,q}$, so the result should be divided $\tau_{j,p,q}$ in order to avoid the maintenance cost $C_{j,p,q}$ being added multiple times. In addition,

$$C_{\mathrm{deg}} = \alpha \sum_{p=1}^{n_\mathrm{Z}} \sum_{q=p+1}^{n_\mathrm{Z}} \sum_{j\in\Theta_{p,q}} \frac{d_{j,p,q}}{\tau_{j,p,q}} \left(t_\mathrm{d} - \sum_{t=1}^{t_\mathrm{d}} (1-\Delta_{j,p,q}(t)) \right) \tag{2.11}$$

In (2.11), the deterioration stage $d_{j,p,q}$ can be identified by technicians based on standards (further discussed in Section 2.6.1).

It should be noticed that in the short-term preventive maintenance, the degradation condition of the components should also be included in the scheduling problem. That is because, if there are too many candidate maintenance actions to be performed in the current week, due to various uncertainties, limitations, and conditions, only a few time slots can be used for performing them. As not all candidate maintenance actions can be performed this week, the components more likely to become defective associated with a heavy degradation status should be maintained with a higher priority. Thus, the degradation status can help define a sort of priority to perform the maintenance actions in the short-term preventive maintenance when not all the maintenance actions can be performed. In our formulation, not only degradation but also other objectives such as costs are considered. Additionally, mid-term degradation evaluation is usually rougher, more uncertain, and dependent on a good degradation model. In the case of the degradation in the short-term, this can be more refined, for instance, if it relies on measurements conducted recently on the component. The short-term degradation factor will thus include the spatial behavior with the fact that at some locations, the degradation condition is different than in other locations. Regarding the temporal dimension, as the prediction is short-term, it is assumed that no huge changes in the dynamics of degradation are expected. If this is not the case for an application, reactive maintenance methodologies are to be considered. Furthermore,

$$C_{\text{soc},s} = \beta \sum_{b=1}^{N_b} \sum_{t=1}^{t_d} |S_{\text{bat},b,s}(t) - \sigma S_{\text{bat},b}^{\text{cap}}| \tag{2.12}$$

where $C_{\text{Soc},s}$ is defined to keep the SOC of all batteries of scenario s around a certain level σ, by adding penalties when the SOC is below or above this level, and the weight to assure the SOC to stay around the level σ is β.

Using the topological connectivity variables between two zones introduced in Section 2.4, now the power balance constraints can be derived:

$$\sum_{q=0}^{n_Z} \delta_{p,q}(t) P_{p,s}(t) = 0, \ \forall t \in \{1, ..., t_d\}, \ \forall p \in \{0, ..., n_Z\}, \ \forall s \in \Phi \tag{2.13}$$

The output power of one zone is the sum of all the output powers of all the loads, DGs, and batteries in this zone:

$$P_{p,s}(t) = \sum_{k=1}^{W_p} P_{p,k,s}(t), \ \forall t \in \{1, ..., t_d\}, \ \forall p \in \{1, ..., n_Z\}, \ \forall s \in \Phi \tag{2.14}$$

The power constraints of the components in the zones can be described as:

$$P_{p,k}^{\min}(t) \leq P_{p,k,s}(t) \leq P_{p,k}^{\max}(t), \ \forall t \in \{1, ..., t_d\},$$
$$\forall p \in \{1, ..., n_Z\}, \ \forall k \in \{1, ..., W_m\}, \ \forall s \in \Phi \tag{2.15}$$

2

The constraints on the maintenance costs are as follows:

$$\frac{1}{\tau_{j,p,q}} \sum_{p=1}^{n_Z} \sum_{q=p+1}^{n_Z} \sum_{j \in \Theta_{p,q}} \Delta_{j,p,q}(t) C_{j,p,q}^{D} \leq C_{set}^{day}(t), \ \forall t \in \mathcal{T}^{D},$$

$$\frac{1}{\tau_{j,p,q}} \sum_{p=1}^{n_Z} \sum_{q=p+1}^{n_Z} \sum_{j \in \Theta_{p,q}} \Delta_{j,p,q}(t) C_{j,p,q}^{N} \leq C_{set}^{night}(t), \ \forall t \in \mathcal{T}^{N} \tag{2.16}$$

To avoid that maintenance actions are performed more than once, the total maintenance duration for each maintenance action must be zero (i.e. maintenance will not be performed at all) or it should be equal to the duration $\tau_{j,p,q}$ (i.e. maintenance will be performed, but only once). So, the following constraint is added:

$$\sum_{t=1}^{t_d} \Delta_{j,p,q}(t) = \tau_{j,p,q} \vee \sum_{t=1}^{t_d} \Delta_{j,p,q}(t) = 0, \ \forall p, q \in \{1, ..., n_Z\}, \ \forall j \in \Theta_{p,q} \tag{2.17}$$

In order to keep the process of performing maintenance action continuous, we have the following constraint by assuming $\Delta_{j,p,q}(0) = 0$:

$$\sum_{t=1}^{t_d} |\Delta_{j,p,q}(t) - \Delta_{j,p,q}(t-1)| \leq 2, \ \forall p, q \in \{1, ..., n_Z\}, \ \forall j \in \Theta_{p,q} \tag{2.18}$$

which means that if a certain maintenance action will be performed, we can only start once (i.e. $\Delta_{j,p,q}(t-1) = 0$, $\Delta_{j,p,q}(t) = 1$) and only stop once (i.e. $\Delta_{j,p,q}(t-1) = 1$, $\Delta_{j,p,q}(t) = 0$). Furthermore, the SOC dynamic equations are:

$$S_{bat,b,s}(t) = \zeta_{leak} S_{bat,b,s}(t-1) + \zeta_{char} P_{bat,b,s}(t),$$

$$\forall t \in \{1, ..., t_d\}, \ \forall b \in \{1, ..., N_b\}, \ \forall s \in \Phi \tag{2.19}$$

The remaining capacity constraints are:

$$S_{bat,b}^{min} \leq S_{bat,b,s}(t) \leq S_{bat,b}^{max}, \ \forall t \in \{1, ..., t_d\}, \ \forall b \in \{1, ..., N_b\}, \ \forall s \in \Phi \tag{2.20}$$

2.5.2. SCENARIO GENERATION METHOD AND REDUCTION METHOD

In the short-term preventive maintenance problem, the uncertainties in the prediction of DG generated powers and load demands will affect the scheduling solutions. In this chapter, we include the uncertainties of the DG generations and load demands in the optimization problem as scenarios related to stochastic distributions [76]. The autoregressive moving average (ARMA) model is applied to generate a scenario tree [27]. However, the number of generated scenarios will increase with the number of prediction steps, and the computational efforts might become time-prohibitive. Thus, to reduce the computational burden, a fast forward selection scenario reduction method is applied.

A classic scenario tree is shown in Figure 2.5. In the figure, stages represent the prediction periods. For example, in this chapter, the weekly prediction horizon is 120 hours (24 hours per day and five workdays in one week), and each stage represents 4 hours. Then, there are 30 stages in the weekly prediction horizon. Stage 0 is the current time, so the value of the variables in stage 0 is known (deterministic). Then, to predict the value
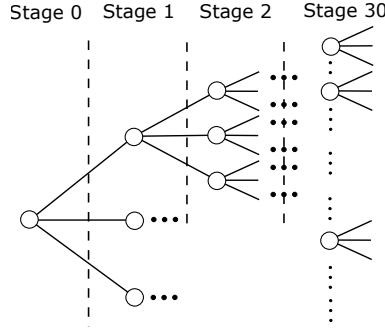
Figure 2.5: Scenario generation process and scenario tree

of stage 1, different scenarios are predicted and branched based on the value of stage 0. Iteratively, scenarios of each stage can be generated by the values of its related previous stage.

To generate the scenario tree of the wind speeds, solar radiations, and load demands, an ARMA model is used [235]. We define $X(k) = [X_L(k), X_W(k), X_P(k)]^T$ as the prediction error where $X_L(k)$, $X_D(k)$, and $X_P(k)$ are prediction errors of the load demand, the wind speeds, and solar radiations at stage k, respectively. Then, the vector $Y(k) = [Y_L(k), Y_W(k), Y_P(k)]^T$ includes the random Gaussian variables, where $Y_L(k)$, $Y_W(k)$, and $Y_P(k)$ are random Gaussian variables of the load demands, the wind speeds and solar radiations at stage k with standard deviations σ_L, σ_W and σ_P respectively. The general ARMA(p_g,q_g) model whose numbers of autoregressive terms and moving-average terms are p_g and q_g respectively, can be expressed as:

$$X(k) = \rho_0 + \sum_{m=1}^{p_g} \rho_m X(k-m) + Y(k) + \sum_{n=1}^{q_g} \varrho_n Y(k-n) \qquad (2.21)$$

where parameters ρ, σ_L, σ_W and σ_P of the Gaussian distributions can be obtained based on the historical data of the wind speeds, solar radiations, and load demands [106]. In order to branch the scenarios randomly, $Y(k)$ is sampled using the Monte-Carlo method. Then, each $X(k)$ obtained by each sampled $Y(k)$ is considered as one possible scenario at stage k.

The predictions of wind speeds, solar radiations, and demand loads are obtained by adding their averaged predicted profiles with their corresponding errors $X(k)$. The original prediction curves can be derived by data methods, e.g., regression analysis [106]. Then, the generation power of the wind turbines can be obtained by the equation below based on the wind speeds [77]:

$$p_{WT} = \begin{cases} 0, & v_w < v_{start} \\ \frac{1}{2}\rho A C_p v_w^3, & v_{start} \leq v_w \leq v_{wmax} \\ \frac{1}{2}\rho A C_p v_{wmax}^3, & v_{wmax} < v_w \leq v_{out} \\ 0, & v_w > v_{out} \end{cases} \qquad (2.22)$$

As for the PV panels, the generated powers can be obtained by [190]:

$$p_{PV} = I_{PV} S_{PV} \eta_{PV} \left(1 - \alpha_{PV}(T_{em} - T_{em}^{ref}) \right) \qquad (2.23)$$

A fixed number of scenarios per stage leads to many possible scenarios for the whole prediction horizon. For example, if ten scenarios are considered, at the 30 th stage of the scenario tree, there will be 10^{30} possible cases, which makes the scheduling problem unsolvable. Thus, we apply a fast forward selection method in [161] to reduce the number of generated scenarios. The goal is to reduce the original scenario set into a smaller one that still preserves characteristics of the original scenario set. In the fast forward selection method, at one particular stage, the preserved scenario set is generated based on minimizing the Kantorovich distances between the original scenario set distribution and the preserved scenario set distribution. The preserved scenarios are selected one by one until a maximum number of scenarios has been reached. Furthermore, the probability of one preserved scenario will be recomputed by summing its original probability and the probabilities of the deleted scenarios that are closest to this preserved scenario.

2.5.3. TWO POSSIBLE SOLVERS
In this chapter, we consider two solution strategies to solve the formulated MINLP problem. The BB solver can obtain the optimal solution, and the modified PSO solver may obtain a solution near the optimal solution but much faster than the BB solver [22]–[24], [115], [160].

BB SOLVER
The problem formulated in Section 2.5.1 can be transformed into an MILP problem. The 'or' logic in (2.17), the absolute value in (2.12) and (2.18), the products between binary variables in (2.3) and (2.4), can all be exactly recast into mixed-integer linear constraints as described in [29]. Thus, the optimization problem with objective function (2.8) and constraints (2.3) - (2.5), (2.9) - (2.20) can be categorized as an MILP problem. In the literature, various solvers are very useful for MILP problems. For instance, the BB solver can be used to obtain the optimal solution of the MILP problem.

PSO SOLVER
Using the PSO algorithm [22]–[24], [115], the optimization problem can be solved directly from its MINLP form. It is possible to directly handle non-linear constraints, e.g., the 'or' logic, the absolute values, or products between binary variables. That is because we just have to evaluate them when computing the objective function value and/or the constraint violations. Additionally, constraints can be converted into soft constraints via a penalty function. The PSO solver considers a population of candidate solutions (particles) and defines the dynamics of how these particles will move in the search space by updating their position and velocity. In the maintenance problem formulated in this chapter, it is difficult for randomly generated particles to satisfy the many included constraints. Thus, we propose a modified PSO algorithm such that the number of constraints is substantially reduced, making it more likely to obtain feasible solutions. The scheme of the modified PSO algorithm is shown in Figure 2.6.

Four main modifications are considered in the proposed PSO-based solution. The
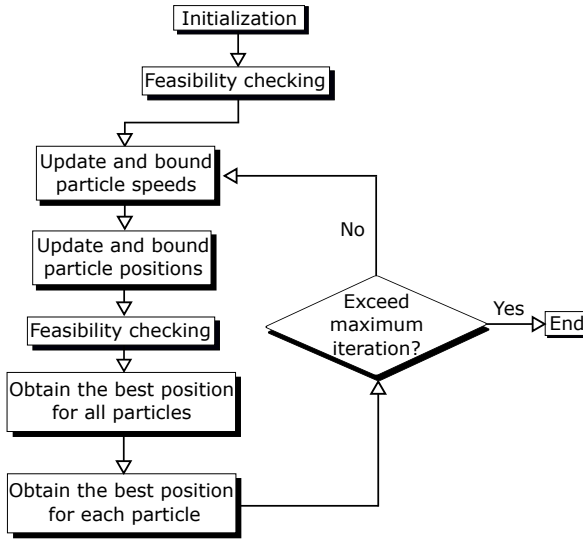
Figure 2.6: Modified PSO algorithm

first one is to deal with (2.17) and (2.18). These two constraints are hard to be satisfied when the binary decision-making variables $\Delta_{j,p,q}(t)$ are generated randomly. That is because for $\Delta_{j,p,q}(t)$ where $t \in \{1, ..., t_d\}$ we have 2^{t_d} combinations of $\Delta_{j,p,q}$, but only very a little number of them satisfy (2.17) and (2.18). Thus, instead of $\Delta_{j,p,q}(t)$, we consider the variable $\widetilde{\Delta}_{j,p,q}(t)$, $t \in \{0, ..., t_d\}$, which represents the starting time of the maintenance action. Only one component in $\widetilde{\Delta}_{j,p,q}(t)$ where $t \in \{1, ..., t_d\}$ will be equal to 1, and the others are set to 0. When we do not perform the maintenance action at any time slot, $\widetilde{\Delta}_{j,p,q}(0)$ will be set to 1, and other components are set to 0. For example, $\widetilde{\Delta}_{j,p,q}(5) = 1$ and $\widetilde{\Delta}_{j,p,q}(t) = 0$ for $t \in \{0, ..., t_d\} \setminus \{5\}$ represents a solution where the maintenance action $\Delta_{j,p,q}$ is performed starting at time slot 5. With $\widetilde{\Delta}_{j,p,q}$ and maintenance action durations $\tau_{j,p,q}$ is possible to calculate $\Delta_{j,p,q}$. For example, if $\widetilde{\Delta}_{j,p,q}(2) = 1$ and $\tau_{j,p,q} = 2$, then $\Delta_{j,p,q}$ is equal to 1 at $t = 2$, $\Delta_{j,p,q}(2) = 1$. As the duration is 2, then $\Delta_{j,p,q}$ is equal to 1 at $t = 3$, $\Delta_{j,p,q}(3) = 1$. Finally, $\Delta_{j,p,q} = 0$ for all other values of t. By using this transformation strategy, the number of combinations of $\Delta_{j,p,q}$ can be reduced from 2^{t_d} to $(t_d + 2 - \tau_{j,p,q})$, and constraints (2.17) and (2.18) can be easily satisfied by randomly generated variables.

The second modification is to obtain intermediate variables. For example, $\delta_{p,q}(t)$ can be obtained from $\Delta_{j,p,q}(t)$ using (2.3), (2.4), and (2.5). Variable $P_{p,s}(t)$ can be obtained from $P_{p,k,s}(t)$ via (2.14). Variable $S_{\text{bat},b,s}(t)$ can be obtained from $P_{\text{bat},b,s}(t)$. Then, constraints (2.3) - (2.5), (2.14), and (2.19) will be satisfied automatically, and the number of variables is further reduced.

The third modification is to set the boundaries of the particles by using some of the constraints. For instance, when generating the particle position of $P_{p,k,s}(t)$, (2.15) can limit the particle position of $P_{p,k,s}$ within its boundary. Then (2.15) can be removed from the feasibility checking process.

The fourth modification is that some of the equality constraints can be included in

the objective function via a penalty term weighted with considerable high value. Then these constraints can be removed from the feasibility checking process. Including the constraints (2.8) - (2.13) in the objective function results in the following:

$$J = \mathbb{E}_\Phi \left[C_{\text{loss},s} + C_{\text{main}} - C_{\text{deg}} + C_{\text{soc},s} + \varpi \cdot \sum_{p=0}^{n_Z} \left| \sum_{q=0}^{n_Z} \delta_{p,q}(t) P_{p,s}(t) \right| \right] \tag{2.24}$$

where $\varpi \gg 1$ is a very high positive number. Finally, only the inequality constraints (2.16) and (2.20) can be violated with the randomly generated particles, resulting in a reduced number of constraints in the feasibility checking process compared to the original problem.

As for updating the particle velocity and location iteration by iteration, the variables expressed by the particles are $\widetilde{\Delta}_{j,p,q}$ and $P_{p,k,s}$. First, feasibility check is conducted for each particle. For particles that do not lead to constraint violations, the velocities and positions of $P_{p,k,s}$ can be updated according to the basic PSO algorithm such that:

$$vP_{p,k,s}(h, g+1) = w_{\text{p}} \cdot vP_{p,k,s}(h,g) + c_{1\text{p}} \cdot \text{rand}() \cdot (P_{p,k,s}^{\text{lbest}}(h) - P_{p,k,s}(h,g)) +$$
$$c_{2\text{p}} \cdot \text{Rand}() \cdot (P_{p,k,s}^{\text{gbest}} - P_{p,k,s}(h,g)) \tag{2.25}$$

$$P_{p,k,s}(h, g+1) = P_{p,k,s}(h,g) + vP_{p,k,s}(h, g+1) \tag{2.26}$$

where rand() and Rand() are independent random variables, uniformly distributed between 0 and 1. Unfeasible particles are not updated, but they are also not removed from the population. In the next iteration, all particles are updated based on the feasible particles in the previous iteration. For the binary variable $\widetilde{\Delta}_{j,p,q}$, (2.25) and (2.26) cannot be applied as these are the equations of PSO for continuous variables. Thus, we use an integer/discrete strategy to update the velocity and position of $\widetilde{\Delta}_{j,p,q}$ in the next iteration directly, by introducing the 1-value index of $\widetilde{\Delta}_{j,p,q}$. By definition, among $\widetilde{\Delta}_{j,p,q}(t)$, $t \in \{0, ..., t_d\}$, there is only one value of t for which $\widetilde{\Delta}_{j,p,q}(t) = 1$, and we define t as the 1-value index. Then the updating steps of the 1-value index of $\widetilde{\Delta}_{j,p,q}$ for the next iteration are:

1. Firstly, the 1-value index of $\widetilde{\Delta}_{j,p,q}$ is a one dimensional representation of the particle position. Then we can obtain the velocity and position of the 1-value index in the next iteration using (2.25) and (2.26). The updated variables can then be real values.

2. Secondly, we separate the interval $[0, t_d + 2 - \tau_{j,p,q})$ into $t_d + 1 - \tau_{j,p,q}$ intervals $[k_1, k_2)$ where $k_1 \in \{0, ..., t_d + 1 - \tau_{j,p,q}\}$ and $k_2 = k_1 + 1$. If the position in the dimension of the 1-value index falls in interval $[k_1, k_2)$, then we assume the integer solution will be at the 1-value index k_1.

An example of the updating mechanism is shown in Figure 2.7. In Figure 2.7, at the current iteration, the 1-value index of $\widetilde{\Delta}_{j,p,q}(t)$ is 12, which represents that the particle position in the dimension of the 1-value index is 12. Just as an example, we assume that the current best 1-value index is 1, while the global best 1-value index is 3. Then the particle is updated according to (2.25)-(2.26). At the next iteration, this 1-value index
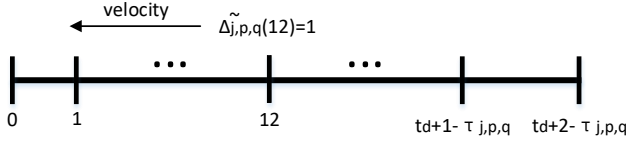
Figure 2.7: Update the 1-value index

moves to 7.83. So the position of the particle in the dimension of the 1-value index is 7. Until now, the 1-value index moves from $t = 12$ to $t = 7$. By doing this, we can update the 1-value index of $\widetilde{\Delta}_{j,p,q}$ and equivalently update $\Delta_{j,p,q}(t)$.

2.6. CASE STUDY

The test case considers a modified version of the IEEE 34-bus distribution network [102] as shown in Figure 2.8(a). Compared to the IEEE 34-bus network in [102], a path is added to generate a loop topology. Furthermore, two batteries and four DGs are added into the distribution network.

As for the candidate maintenance actions, five sets of candidate maintenance actions that have already been determined by the mid-term preventive maintenance scheduling are considered as five cases. In addition, in each case we consider scenarios with different generated powers of the DGs and different load demands that are generated by the scenario tree method and the scenario reduction method.

A comparison method that does not consider the the supporting ability of DGs and batteries in the preventive maintenance is designed to quantify the effectiveness of the proposed method. Both the proposed method and the comparison method will use the results from the clustering method, the topological constraints generation, and the scenarios generation and reduction.

Furthermore, after the comparison between the methods, the BB solver and PSO solver will be compared. Both solvers are implemented on Matlab R2020a.

2.6.1. SET-UP OF THE CASES

The case study networks marked with candidate maintenance actions of Case 1 - 5 are shown in Figure 2.8(a) and Figure 2.9, and the maintenance actions are indicated with an arrow pointing to the location where they are to be performed. The numbers surrounded by circles are the labels of the maintenance actions. Here we assume that the maintenance personnel only works from Monday to Friday, which means that t_d equals to 24×5. Because different sets of candidate maintenance actions cause different simplified network, here we only show the simplified networks of Case 1 after using the clustering method in Figure 2.8(b).

We assume that from the mid-term maintenance scheduling step we have obtained candidate maintenance actions as shown in Table 2.1, where "Performance duration" is the number of time slots (hours) required to perform these maintenance actions, the column of "Day-time cost" is the cost for performing the candidate maintenance action during the day-time (8:00-18:00) while the night-time (19:00-7:00) cost is shown in the

(a) Modified IEEE 34-bus network

(b) Zones obtained with the clustering method for Case 1
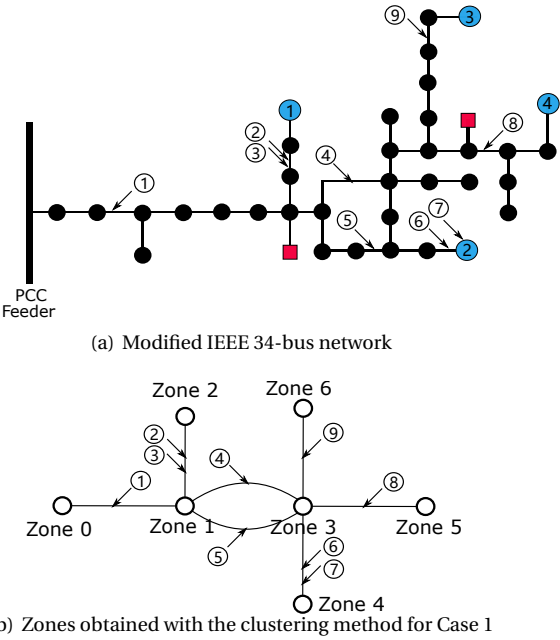
Figure 2.8: Distribution network of the case study and its simplification for Case 1

Table 2.1: Parameters of the candidate maintenance actions

Case	Candidate maintenance action	Performance duration (Hours)	Day-time cost ($/10 k)	Night-time cost ($/10 k)	Deterioration stage
1	①	1	1.82	2.22	34
	②	2	1.59	1.99	35
	③	3	2.76	3.36	41
	④	1	2.75	2.95	59
	⑤	1	1.91	2.11	81
	⑥	2	2.06	2.46	76
	⑦	1	2.71	2.91	62
	⑧	2	1.18	1.58	52
	⑨	3	1.46	2.06	52
2	①	2	1.11	2.02	45
	②	2	2.59	4.99	65
	③	3	1000	2.36	24
	④	3	2	3.95	81
	⑤	3	2.01	3.11	79
	⑥	2	1.76	2.54	63
	⑦	2	1.13	2.45	52
	⑧	2	1.38	2.76	48
3	①	1	1.11	4.02	36
	②	2	2	6.86	75
	③	3	1.4	1.76	64
	④	2	1.78	3.82	43
4	①	2	1.76	5.9	40
	②	2	1.89	8.2	73
5	①	2	1.76	5.9	40
	②	2	1.89	8.2	73

(a) Maintenance positions for Case 2

(b) Maintenance positions for Case 3

(c) Maintenance positions for Case 4

(d) Maintenance positions for Case 5
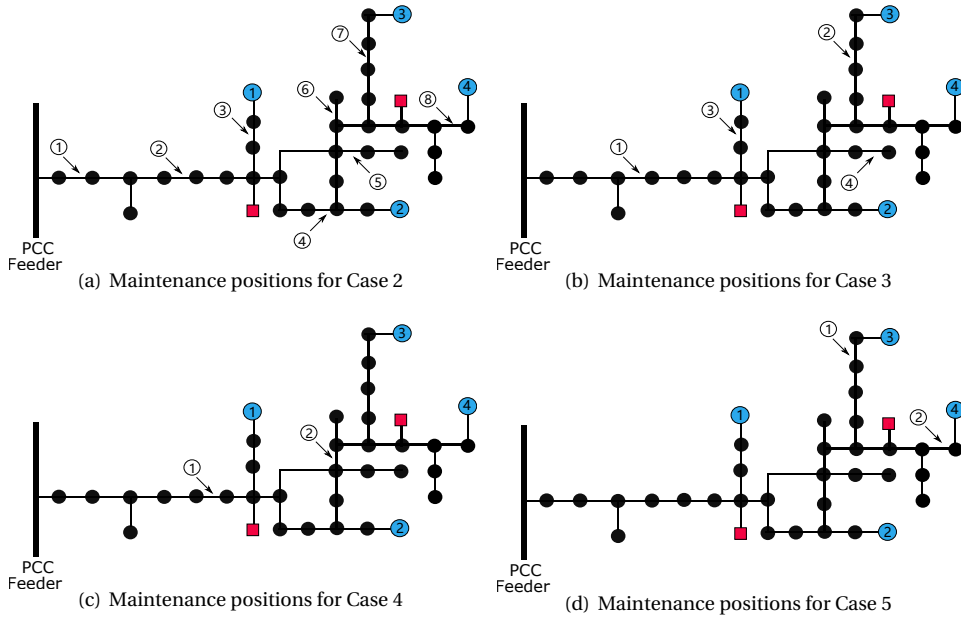
Figure 2.9: Distribution networks of Case 2 to Case 5

"Night-time cost" column. In Case 2, we consider a restriction that maintenance action 3 must be performed at night-time by giving the action a large day-time costs (1000 $/10 k). Other parameters, e.g. DGs and batteries parameters are the same as for Case 1. In addition, in all cases, we assume that after performing maintenance, the deterioration stage of the component will be zero (as good as new).

In Table 2.1, "Deterioration stage" is a score from 0 to 100 to represent the deterioration level of a component that this candidate maintenance action has to be performed on. The score for the deterioration stage can be evaluated based on standards, e.g., the ones of the State Grids for Chinese distribution network (Q/GDW 643-2011, Q/GDW 644-2011, and Q/GDW 645-2011). To evaluate the degradation status of a transmission line unit, the degradation statuses of the sub-components, e.g., conductors and tower structure, will be evaluated first by checking the temperature, broken strands, rustiness, etc., for conductors as well as toppling, and cracks, etc., for the tower structure. Then, the degradation status of each sub-component is multiplied by their weights and then be summed up as the degradation status of the whole transmission line unit [199].

Furthermore, for distribution networks, maintenance actions can be repair, replacement of the sub-components, or replacement of the component. According to different scoring results for the "deterioration stage", the most appropriate maintenance actions can be estimated by experts, by the manufacturer of the components, or by repair crews.

In addition, the rated generated powers of DG1, DG2, DG3, and DG4 are 100 kW, 150 kW, 200 kW, and 150 kW respectively; their composition details are shown in Table 2.2. We assume that these wind turbines and PV panels can operate in islanding mode.

Table 2.2: Composition of the DGs

DG	Wind turbine (kW)	PV panel (kW)	Controllable DGs (kW)
DG1	10	20	70
DG2	30	20	100
DG3	40	40	120
DG4	10	40	100

Table 2.3: Parameters of the batteries

Label	Capacity (kW.h)	Minimal/Maximal Capacity (kW.h)	Minimal/Minimal Power (kW)
1	300	45/270	-30/30
2	800	120/720	-80/80

This can be realized by planning controllable DGs, e.g., small hydro generators, which can support reference voltage and frequency when in islanding mode, and by installing small capacity batteries on the DC links of the wind turbines and PV panels as indicated in [133]. Furthermore, the parameters of the batteries are listed in Table 2.3 and the initial SOCs of the batteries are all 50%.

The load demand curves for the 10 scenarios are shown in Figure 2.10(a). The wind turbine generated power curves are shown in Figure 2.10(b). The PV panel generation curves are shown in Figure 2.10(c) and the load prices of the 34 buses are shown in Figure 2.10(d). In Figure 2.10(c), the power generated by the PV panels at night is 0 and during the day the generated power of the PV panels can slightly exceed their rated power [211]. In Figure 2.10(d), we adopt the electricity price data in the USA such that the industrial electricity, commercial electricity and residential electricity prices are 0.07 $, 0.1 $ and 0.13 $ per kW.h individually. Then the electricity prices of the 34 buses are the mixtures of these three different electricity prices.

The parameter α in (2.11) is set to be large enough to assume that all the maintenance actions obtained from the mid-term scheduling step are actually performed, e.g. $\alpha = 1$. Moreover, β and σ in (2.12) is set to 0.0001 and 0.5 individually to assure that the batteries can provide supporting energy to the shed loads as well as recover the SOC to the level σ when the SOC deviates from this level.

2.6.2. COMPARISON OF METHODS

The method used for comparison does not consider the supporting energy ability of the DGs and batteries. Thus, the corresponding optimization problem can be presented as:

$$\min_{\Delta'} J' = \mathbb{E}_\Phi[C'_{\text{loss},s} + C'_{\text{cost}} + C'_{\text{deg}}] \tag{2.27}$$

where the expressions of the terms are the same as (2.8)-(2.10). In constraints (2.13) and (2.14), the computation of the total output power of the zones omits the generation powers of the DGs and batteries in the zones, such that (2.14) we have:

$$P'_{p,s}(t) = \sum_{k=1}^{W'_m} P_{p,k,s}(t), \ \forall t \in \{1,...,t_{\text{d}}\}, \ \forall p \in \{0,...,n_{\text{Z}}\}, \ \forall s \in \Phi \tag{2.28}$$

(a) Scenarios load curves

(b) Scenarios wind turbine generated power curves

(c) Scenarios PV panel generated power curves

(d) The load prices of the 34 buses
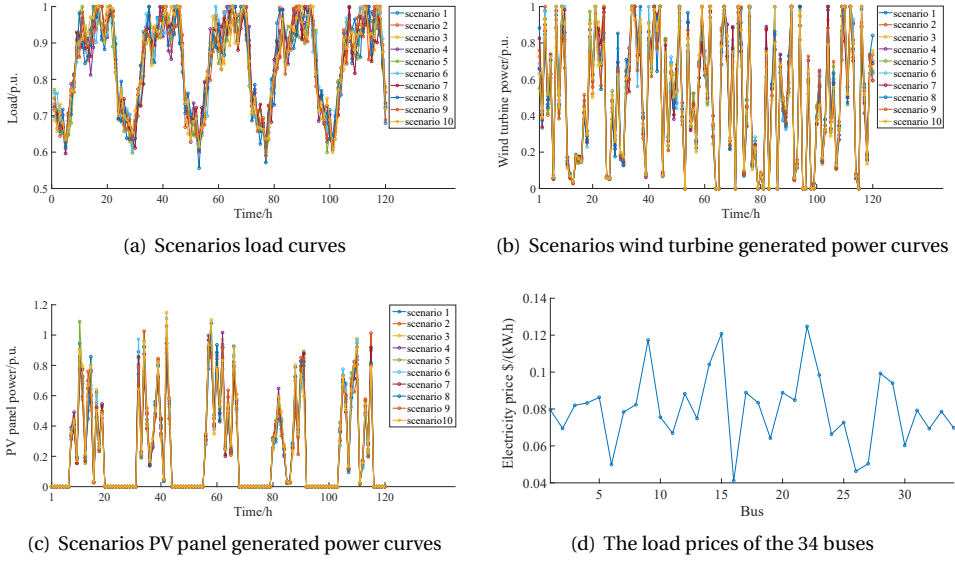
Figure 2.10: Scenarios curves and load price curves

Table 2.4: Modifications programming problem for comparison

Constraints or objective function	Modification
(2.3)-(2.5), (2.9)-(2.11), (2.13), (2.16)-(2.18)	No modification
(2.8), (2.14)-(2.15)	Delete terms related to DGs and batteries
(2.12), (2.19)-(2.20)	Not included

where W'_m is the total number of consuming components in zone p regardless of the powers of the DGs and the batteries, and $P'_{p,k,s}(t)$ is the power generated or consumed by the kth consuming component in zone p in time slot t of scenario s. In addition in (2.15), the power limitations on the components in the zones can be described as:

$$P_{p,k}^{\min}(t) \le P'_{p,k,s}(t) \le P_{p,k}^{\max}(t), \ \forall t \in \{1, ..., t_{\mathrm{d}}\},$$
$$\forall p \in \{1, ..., n_Z\}, \ \forall k \in \{1, ..., W'_m\} \ \forall s \in \Phi \tag{2.29}$$

As for (2.19)-(2.20), they are not included in the comparison model. The modifications of the programming problem for comparison are shown in Table 2.4.

In order to find the optimal solution, the BB solver is used for the proposed method and the comparison method. The simulation results are shown in Table 2.5 and Table 2.6. In Table 2.5, the details of the maintenance action performances are listed. In Table 2.6, the "Load loss costs for the proposed method" was calculated from the expectation of $C_{\mathrm{loss},s}$ in (2.8). The "Load loss costs for the comparison method" is the sum of the load loss costs in each zone while maintenance actions are performed.

When comparing between Case 4 and Case 5, although the durations of the mainte-

Table 2.5: Maintenance actions details of methods comparison

Case	Candidate maintenance action	Performance time slots of the proposed method	Performance time slots of the comparison method
1	①	72	74
	②	73 - 74	73 - 74
	③	33 - 35	105 - 107
	④	9	60
	⑤	18	87
	⑥	62 - 63	83 - 84
	⑦	13	81
	⑧	108 - 109	71 - 72
	⑨	72 - 74	71 - 73
2	①	105 - 106	57 - 58
	②	105 - 106	57 - 58
	③	72 - 74	72 - 74
	④	11 - 13	107 - 109
	⑤	84 - 86	36 - 38
	⑥	81 - 82	9 - 10
	⑦	83 - 84	12 - 13
	⑧	62 - 63	36 - 37
3	①	109	57
	②	107 - 108	58 - 59
	③	107 - 109	57 - 59
	④	73 - 74	73 - 74
4	①	108 - 109	57 - 58
	②	108 - 109	57 - 58
5	①	105 - 106	9-10
	②	105 - 106	57-58

Table 2.6: Load loss costs of method comparison

Case	Load loss costs for the proposed method ($)	Load loss costs for the comparison method ($)
1	124.8	167.87
2	454.18	533.65
3	200.49	215.13
4	227.98	247.14
5	0	0

nance actions are the same, the load loss costs are different. That is because in Case 4 maintenance actions are in the main paths, and performing these maintenance actions will cause a large amount of load loss. However in Case 5, performing maintenance actions will cause no load loss because DG3 and DG4 are sufficient to support the loads isolated from the PCC while maintenance actions are performed. So the more maintenance actions are on the main paths, the more load will be shed.

Furthermore, among the cases, the load loss costs of the proposed method are much lower than those obtained by the comparison method, with 35%, 17.5%, 7.3%, 8.4% load loss costs reductions in Case 1 to Case 4 individually. Thus, the proposed method can reduce the load loss costs effectively.

Table 2.7: Comparison between the PSO solver and the BB solver

Case	PSO solver					BB solver	
	Worst	Best	STD	AVR	Time	Cost	Time
1	248.85	130.79	33.4	174.89	4743	124.8	7563
2	646.99	489.89	66.89	570.31	725	454.18	1398
3	230.78	204.04	12.2	211.5	42.6	200.49	96
4	241.32	227.98	3.71	229	12.4	227.98	36
5	0	0	0	0	3	0	30

2.6.3. COMPARISON OF THE SOLVERS

In this subsection, the results of the comparison between the BB solver and the modified PSO solver will be presented and analyzed. After sensitivity analysis, we find the parameters associated with good performance are $\varpi = 500000$, $w_p = 0.9$, $c_{1p} = c_{2p} = 0.9$, and the velocity boundaries are ± 100. We study the influence of the number of particles and the number of iterations on the performance of the modified PSO solver, including the load loss costs and the CPU time. For each selected combination of the number of particles and the number of iterations, we run the PSO solver 10 times to obtain the average values of the load loss costs and the CPU time. The results are presented in Figure 2.11. Results of Case 5 are not included in Figure 2.11 because when the number of particles is 20 and the number of iterations is 20, the PSO can obtain the optimal solution in 3 s.

In Figure 2.11, in the parentheses are the number of iterations and the number of particles used to obtain the data point. From Figure 2.11, we can observe that when the combinations of the number of iterations and the number of particles are (500,30), (600,20), (200,20), (80,20), for Case 1 to 4 respectively, the increase of the number of iterations influences little on reducing the costs, but it results in a large increment of CPU time. We will use the combinations (500,30), (600,20), (200,20), (80,20), (20,20) for Case 1 to 5 respectively, to compare with the BB solver. The results of the comparison are in Table 2.7.

In Table 2.7, "Worst" and "Best" are the best and worst costs among ten runs separately. "STD" represents the standard deviation, and "AVR" the average of the costs. "Time" of the PSO solver is the average CPU time of the ten runs. It can be seen from Table 2.7 that the modified PSO solver obtains sub-optimal solutions that deviate from the optimal solution obtained by the BB solver with 40.14%, 25.57%, 5.49%, and 0.45%, and 0% for Cases 1 to 5, respectively. However, the modified PSO solver can largely reduce the computation time with 37.29%, 48.14%, 55.63%, 65.56%, and 90% for Cases 1 to 5, respectively. Besides, the relative standard deviations of the load loss costs with respect to 19.1%, 11.73%, 5.77%, 1.62%, and 0% for Cases 1 to 5, respectively.

According to the results, when the scale of the problem becomes larger, the sub-optimal solutions obtained by the PSO solver are characterized by larger differences from the optimal solution, but the computation time reduction is significant for all the cases. Also, the standard deviations for the PSO solver are not very large, except for Case 1. However, regarding the IEEE 34-bus distribution network associated with a small number of candidate maintenance actions, e.g., below 10, the computation time for BB
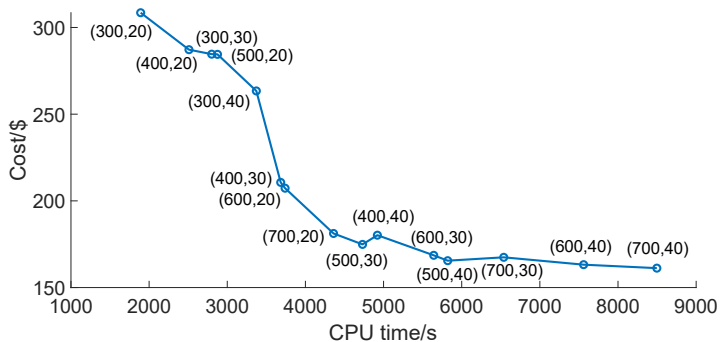
(a) PSO simulation results of Case 1
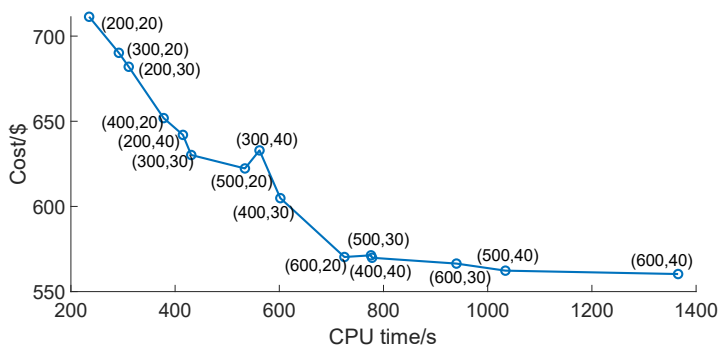
(b) PSO simulation results of Case 2
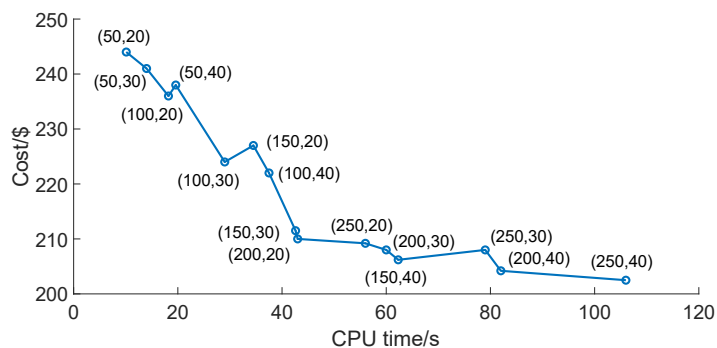
(c) PSO simulation results of Case 3
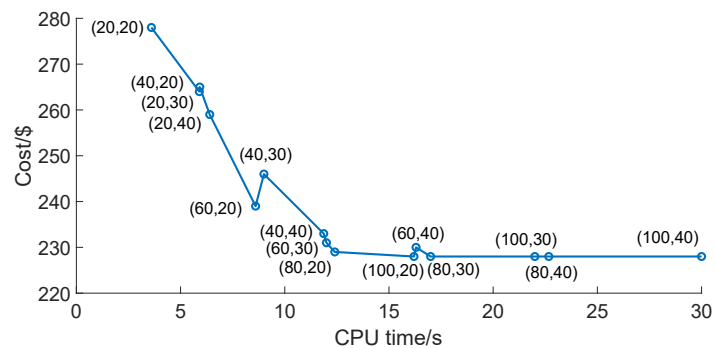
(d) PSO simulation results of Case 4

Figure 2.11: PSO simulation results

solver is acceptable. That is because, for weekly preventive maintenance scheduling, the decision-making time is sufficient. In this case study, the longest computing time is 7563 seconds. At the beginning of every week, the system operator can use 2-3 hours to solve the proposed short-term preventive maintenance scheduling problem using the BB solver. In this case, the BB solver is better than the PSO solver. In settings where less time is available for decision making, larger networks, and more maintenance activities, PSO will provide a sub-optimal solution within the time limitations.

2.7. Discussions

The proposed short-term preventive maintenance scheduling method is evaluated in five cases to schedule the maintenance actions to their optimal time slots. In these cases, different numbers of candidate maintenance actions with different locations, different durations, and different costs are considered. In all the cases, load losses can be caused when performing maintenance actions. The proposed method can reduce the load loss costs from 7.3% to 35% when the supporting power potential of the DGs and batteries is considered. The proposed short-term preventive maintenance method can be used by the power system operator to reduce the influence of the load shedding when performing maintenance actions.

Furthermore, a comparison between two different solvers is performed and the results are analyzed. The BB solver can obtain the optimal global solution, but the computation time is higher due to the number of equations and variables included when the exact reformulation of the original problem is constructed. With the modified PSO solver, sub-optimal solutions are obtained, but the computation time can be reduced. In addition, the evaluation of the cost function for each particle in PSO can be performed in a fully parallel way. That would make the computation time of PSO even more competitive. The power system operator should define the right trade-off between accuracy and computation time when selecting the right solver for the application. When the problem is solved for small-scale or medium-scale networks, e.g., the IEEE 34-bus network used in the case study, the computation time of the BB solver can be acceptable. However, when the topology of the distribution network is much more complex, and when there are many candidate maintenance actions, e.g., above ten candidate maintenance actions for the IEEE 34-bus network, the modified PSO might become a better choice.

In this study, the DGs can support energy to the loads, particularly when they are part of a dynamically formed microgrid functioning in islanding mode. An interesting further study would be to consider how to reduce the influence of the switching between the islanding mode and the connected mode on the power system stability. When the DGs are connected to the power systems by inverters, this will require to include aspects of power electronics, and for instance, to improve the performance of the controllers. This can be done by installing communication devices in the network, so that a synchronized or coordinated control can be realized. Other control frameworks proposed in the literature can be tested, such as the hierarchical droop-based control of [21].

In the case study settings of this chapter, we have assumed that there are controllable DGs and enough capacity batteries on the DC links of the wind turbines and PV panels. However, in some networks, this assumption might not hold. Then, additional constraints have to be included in the optimization problem. For instance, consider a

distribution network containing any number of loads, one DG whose zone label is d, one PCC whose zone label is 0, and one battery whose zone label is b. The actual generated power of the DG is $P_d(t)$, and the rated generated power of the DG is $P_{DG}(t)$. Then if we consider that the DGs can only operate when they are connected to the battery or PCC or both of them, the following additional constraint is required:

$$P_d(t) = P_{DG}(t)\Big(1 - (1 - \delta_{d,0}(t))(1 - \delta_{d,b}(t))\Big)$$

where $\delta_{d,0}(t)$ and $\delta_{d,b}(t)$ are the connecting statuses from the distributed generator to the PCC and to the battery at time step t. Then, if the distributed generator is neither connected to the PCC nor the battery, the value of $P_d(t)$ will be zero which means that no power is generated by the distributed generator.

In addition, the proposed approach is not limited to the use of the topological connectivity constraints to formulate the problem as shown in this chapter, but it can also consider constraints based on power balance rules or others.

2.8. CONCLUSIONS AND FUTURE WORK

This chapter has proposed a short-term preventive scheduling method for power systems to reduce the load loss costs when performing maintenance actions. The power supporting potential of DGs and batteries when performing maintenance actions in the distribution network can be systematically optimized with the proposed method. A DFS clustering method has been proposed to reduce the computational complexity of the short-term based scheduling problem. To be able to express the power balance equations in case of maintenance actions being performed, topological connectivity constraints are generated and used to define the corresponding maintenance action connectivity variables, which are then used to write down in the power balance equations. In addition, the scenarios generated by the scenario generation and reduction methods are considered to express the uncertainties of the generation powers of the DGs. The simulation results show the effectiveness and improvement of this method and its capacity to reduce the load loss costs during maintenance. In addition, for the IEEE 34-bus network with a small number of candidate maintenance actions, the BB solver is better than the PSO solver. As for the future work, the control strategy of the DGs, e.g., hierarchical droop-based control, will be considered so that the formed microgrids during maintenance can operate more in a more stable condition. Another topic of further research is the inclusion of transient stages in the formulation, particularly when the system switches from one configuration to another. Moreover, an approach based on Bayes theorem maybe be used for short-term preventive maintenance scheduling.

Nomenclature

b	Battery index
g	Iteration index in PSO
h	Particle index in PSO
j	Candidate maintenance action index
k	Generating or consuming component index
p, q, q'	Zone index
t	Time slot index
$\mathscr{T}^{\mathrm{D}}$	Set of day time slots
$\mathscr{T}^{\mathrm{N}}$	Set of night time slots
Ω_p	Set of neighbor zones of zone p
Ω_p^{c}	Set of non-neighbor zones of zone p
$\Theta_{p,q}$	Set of candidate maintenance actions on the path between zone p and its neighbor zone q
Φ	Set of scenarios
A	Sweep area of wind turbine blades
$c_{1\mathrm{p}}, c_{2\mathrm{p}}$	Acceleration constants of PSO
C_{p}	Tip speed ratio of wind turbines
$C_{\mathrm{pril},p}(t)$	Electricity price for zone p in time slot t
$C_{j,p,q}^{\mathrm{D}}, C_{j,p,q}^{\mathrm{N}}$	Day-time and night-time maintenance cost for action j between zone p and its neighbor zone q
$\mathrm{C}_{\mathrm{set}}^{\mathrm{day}}(t)$	Budget for performing day-time maintenance in time slot t
$\mathrm{C}_{\mathrm{set}}^{\mathrm{night}}(t)$	Budget for performing night-time maintenance in time slot t
$d_{j,p,q}$	Deterioration stage of the component where maintenance action j has to be performed on the path between zone p and zone q
n_{Z}	Total number of non-PCC zones after clustering
N_{b}	Number of batteries
$P_{\mathrm{pred},p,s}(t)$	Predicted load of zone p in time slot t when no maintenance actions are performed in time slot t for scenario s

S_{PV}	Area of PV panel
$S_{bat,b}^{min}$	Minimal battery capacity of battery b
$S_{bat,b}^{max}$	Maximal battery capacity of battery b
$S_{bat,b}^{cap}$	Capacity of battery b
t_d	Number of time slots in this maintenance scheduling period
T_{em}	Temperature of PV panel
T_{em}^{ref}	Reference temperature of PV panel
v_{out}	Cut-off wind speed
v_{start}	Start-up wind speed
v_{wmax}	Maximum wind speed
w_p	Inertia weight factor of PSO
W_p	Total number of generating, consuming and energy storage components in zone p
α	Weight coefficient of the deterioration cost
α_{PV}	Temperature coefficient
β	Weight coefficient to assure that SOC stays around the level σ
η_{PV}	PV panel conversion efficiency
ρ	Air density
σ	SOC penalty level
$\tau_{j,p,q}$	Duration of action j between zone p and its neighbor zone q
ϖ	Equality penalty weight in PSO
ζ_{leak}	Battery leakage coefficient
ζ_{char}	Battery charging efficiency
$C_{loss,s}$	Total cost of load losses for scenario s
C_{main}	Total cost of performing maintenance actions
C_{deg}	Cost related to the degradation of the components
$C_{soc,s}$	Penalty term for the SOC utilization of the batteries for scenario s
I_{PV}	Solar radiations

$P_{p,k,s}(t)$	Power generated or consumed by the kth generating, consuming, or energy storage component in zone p in time slot t for scenario s
$P_{\text{bat},b,s}(t)$	Power generated/consumed by battery b in time slot t for scenario s
$P_{\text{loss},p,s}(t)$	Load loss of the zone p in time slot t for scenario s
$P_{p,s}(t)$	Served load for zone p when maintenance actions are being performed in time slot t for scenario s
$S_{\text{bat},b,s}(t)$	SOC level of battery b at the end of time slot t for scenario s
v_w	Wind speed
$\delta_{p,q}(t)$	Connectivity between zone p and any other zone q in the distribution network in time slot t
$\Delta_{j,p,q}(t)$	Indicates whether the jth maintenance action on the path between the zone p and its neighbor zone q is performed in time slot t

3

MAINTENANCE OF GENERATION UNITS CONSIDERING INTER-ISO POWER EXCHANGE

3.1. INTRODUCTION

To ensure the reliability of a power system, keeping generation units in a good condition is one of the responsibilities of an independent system operator (ISO) [139], [147], [200]. In addition, the reserved energy should be above a certain level when some of the generation units are undergoing maintenance, so that the risks of large-scale load loss caused by a reserved energy shortage can be avoided. Thus, the maintenance schedules are required to be properly planned [108], [149], [169], [192]. The ISO manages the planning process of the maintenance considering the costs of maintenance actions for the generation units and the power system reliability. Maintenance scheduling is usually performed in a multi-time-scale manner and can consequently be categorized into long-term scheduling [61], [104], [148], mid-term scheduling [25], [222], and short-term scheduling [81], [173]. This chapter focuses on the design of a long-term maintenance scheduling framework.

Long-term maintenance of generation units (MGU) coordination frameworks that consider both the total benefits of the entire power system and the benefits of individual generation units are widely considered in the literature [50], [67], [82], [83], [134], [212]. For instance, a maintenance decision making model for generation companies (GENCOs) in an oligopolistic electricity market environment is proposed in [82]. The maintenance plans developed by GENCOs are reviewed and have to be approved by the ISO. In [50], a coordinating framework is introduced based on incentives/disincentives to balance the profits of producers and the reliability of the power system. In [83], the maintenance plan of generation units is scheduled considering N-1 examination for transmis-

---

This chapter is based on [73].
The nomenclature of this chapter is at the end of this chapter.

sion lines random failures. Then, the maintenance budget and power system reliability are balanced. In [134], random failures on transmission lines are considered in the maintenance scheduling of generation units. The uncertainty of the line failure is modeled via scenarios, and these scenarios are obtained randomly according to arbitrary failure rate functions. In [61], a risk-based model is proposed to schedule the preventive maintenance of generators by considering the stochastic wind energy. The model includes the risk of load loss and the desired level of risk. In [177], a multi-objective maintenance scheduling strategy for generation units in deregulated power systems is proposed. The objectives of GENCOs and the ISO are both considered in the strategy. Just as in the above literature, this chapter also focuses on designing a coordination framework to obtain a balanced trade-off between the overall power system benefit and the benefits of individual generation units.

In practice, some power systems operate in a deregulated environment, while others do not. In the case of the traditional regulated environment, the scheduling of the maintenance actions is managed by the power system operator. Then, the power producers are forced to perform maintenance actions according to the schedule defined by the operators [67]. In a deregulated environment, the GENCOs and the ISO are different entities. The role of the GENCOs is to supply energy to the power system with a major focus on obtaining profits. An important role of the ISO is to guarantee the reliability of the power system, considering the profits of the GENCOs. So, when the ISO manages the MGU processes, GENCOs schedule their maintenance actions by maximizing their profits and submitting them to the ISO. The ISO may reject some of the submitted schedules from the GENCOs to guarantee the reliability of the power system. Afterward, the GENCOs of the rejected schedules should reschedule their maintenance actions and then resubmit them. This process is iteratively implemented between the ISO and GENCOs until the reliability of the power system is guaranteed and the maintenance actions submitted by the GENCOs are all scheduled (if the reserve energy is sufficient) [212]. Other coordination strategies for deregulated environments have also been studied in the literature. For example, in [67], a competitive bidding mechanism after maintenance planning is proposed. The goal is to balance the benefits of the GENCOs by considering the system reliability and the health condition of the generating units. In [212], a framework is proposed in which first the ISO maximizes the reliability index of the whole power system by using a reliability-centered maintenance strategy. Then, GENCOs can bid for their preferred maintenance slots under the constraint of a given power system reliability index. Afterward, the ISO determines the bidding results.

This chapter considers coordinating the power system reliability and the profits of GENCOs via a bidding mechanism as proposed in [212]. The mechanism is implemented after an initial maintenance schedule is proposed. This initial schedule is usually based on global optimization of the ISO-wide profits of all the GENCOs. This solution (which may also be called a one-shot solution) might conflict with the individual profit of some GENCOs. Thus, the bidding mechanism allows GENCOs to have a platform where they can chase their profit. From the various strategies in the literature, this chapter selects the bidding mechanism because it will obtain maintenance schedules within less iterations and it is more straightforward. In this strategy, the ISO firstly determines the ISO-wide optimal MGU schedule. Then if the GENCOs are not satisfied with their scheduled

time slots, they can join in the bidding process to change their time slots. The ISO determines the biding result by maximizing the net benefit of the bids. Then the net benefit received by the host ISO (a non-profitable organization) is used to improve the power system operation and power quality. Thus, the net benefit received from the bidding process is also the social welfare. However, in [212], it is mentioned that, if after the bidding process the reliability goal of the power system cannot be reached, the ISO should seek other means, such as utilizing inter-regional power exchange, to ensure the reliability of the power system.

This chapter argues that it may be beneficial to include the inter-ISO power exchange in the bidding process for coordination directly, rather than after the bidding process. Thus, a novel bidding mechanism is proposed where the host ISO (the ISO who manages the planning process of MGU for its GENCOs is called the *host ISO* in this chapter) can start the bidding processes for MGU with the participation of the GENCOs of the host ISO and the GENCOs of the neighbor ISOs. The GENCOs of the host ISO can use their bid prices to buy supportive energy from the GENCOs of the neighbor ISOs of the host ISO, or to a pay penalty fee for reduction of the transmitted power from the host ISO to the neighbor ISO with respect to what has been stipulated in the inter-ISO power exchange contract. Then, the reserved energy level of the host ISO can be sustained when the generation units of the GENCOs that bid for their preferred time slots are undergoing maintenance. Moreover, buying supportive energy, reducing the transmitted power, or both buying supportive energy and reducing the transmitted power are influenced by to the direction and amount of the power flow on the tie line between the host ISO and its neighbor ISO. The direction and amount of this power flow can be contracted via the long-term inter-ISO power exchange transactions [165]. The host ISO determines the maintenance plans via bidding, by considering the reserved energy level of itself and of its neighbor ISOs, the tie line limitations (congestion), energy loss allocation during transmission, and so on. It should be mentioned that the neighbor ISOs cannot sell energy because they are non-profitable organizations [50], but they should monitor their own operation conditions, e.g., reserved energy levels, in the bidding process. The neighbor ISOs should prevent their GENCOs to over-support energy to the host ISO and as this could result in lack of reserved energy (i.e., a high marginal price) in the grids of the neighbor ISOs.

This proposed interchangeable bidding mechanism for maintenance (IBMM) has two distinguished advantages compared with bidding mechanisms that do not consider the direct participation of the GENCOs of the neighbor ISOs in the bidding process, namely helping the GENCOs to obtain their more preferred time slots, and improving the reliability of the power system. Later on in this chapter, these two advantages will be analyzed based on simulation results.

It will also be discussed how to organize the bidding processes for the situation in which there are multiple ISOs in a large grid. In particular, three organization schemes for starting the bidding processes will be discussed and analyzed: centralized bidding, priority bidding, and impromptu bidding.

The contributions of the current chapter are:

1) A novel bidding mechanism for maintenance of generation units is proposed. In this mechanism, the GENCOs of the host ISO can change their maintenance slots

via buying supportive energy from the GENCOs of the neighbor ISOs, paying penalty fees in case the energy transmitted from the host ISO to the neighbor ISOs is reduced for ensuring the reserved energy level in the host ISO, or both. The proposed interchangeable bidding mechanism in this chapter can help the GENCOs to obtain their preferred time slots, and more maintenance actions can be performed so that the reliability of the power system can be improved.

2) A non-linear mixed integer bidding programming problem is formulated to include the load loss on the tie lines caused by inter-ISO energy exchange of supportive energy transmission. The formulated problem is then recast into a second-order cone programming problem that can be solved efficiently by commercial software.

3) Three possible organization schemes for starting the bidding processes in a large power grid associated with multiple ISOs are discussed.

The outline of this chapter is as follows. Section 3.2 introduces three ways the GENCOs can use to ensure the reserved energy level of the host ISO, when they intend to change their scheduled maintenance time slots. More specifically, these proposed ways are based on inter-ISO energy transmission. In Section 3.3, the proposed bidding mechanism, the formulated bidding programming problem, and the details of recasting will be introduced. In Section 3.4, a case study is studied and the performance of the proposed bidding mechanism is analyzed via comparison. Discussions of three bidding organization schemes for large grids, implementation of the proposed bidding strategy, and a larger scheduling period of maintenance are provided in Section 3.5. Finally, Section 3.6 concludes the chapter.

3.2. Preliminaries

3.2.1. Illustration of the working principles via an example

To ensure fairness in a market environment, the GENCOs that are not satisfied with the first-stage MGU scheduling results will be given the opportunity to bid for their preferred time slots for maintenance of their generation units. However, when these GENCOs change the maintenance time slots for their generation units, the reserved energy may fall below the safety level, and consequently the power system of the host ISO may face a reliability problem. Thus, this chapter proposes to consider three possible cases, i.e., Cases 1 to 3, for the GENCOs of the host ISO for obtaining inter-ISO energy. As shown in Figure 3.1, a simple illustrative example is given below for an intuitive understanding of the reliability problem caused by changing the maintenance time slots and the three cases for obtaining the inter-ISO energy.

In the example of Figure 3.1, the host ISO manages the PJM 5-bus network [65], [129]. Generation units G1, G3, and G4 are satisfied with the first-stage MGU scheduling results, while generation unit G2 is not. The maintenance action of G2 takes one maintenance time slot, and G2 intends to change its scheduled maintenance slot to time slot k_{G2}. Furthermore, there are three neighbor ISOs of the host ISO. In time slot k_{G2}, the power flows are from neighbor ISO 1 to the host ISO, and from the host ISO to neighbor ISOs 2 and 3 in the long-term inter-ISO power exchange contract.
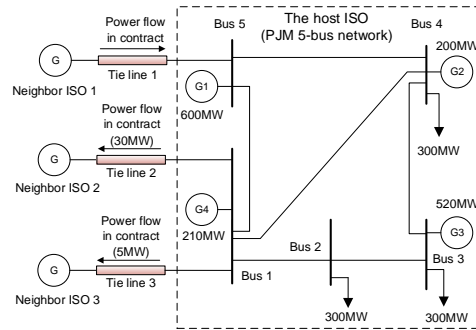
Figure 3.1: The power network topology of the example

In time slot k_{G2}, there is 80 MW of reserved energy in the PJM 5-bus network. Thus, if G2 intends to perform its maintenance action in time slot k_{G2}, there will be an energy gap of $200 - 80 = 120$ MW between the generated energy and the demand. The gap cannot be filled if the inter-ISO power exchange is not considered. Then, if the non-interchangeable bidding mechanism for maintenance (NBMM) is adopted, G2 cannot change its maintenance slot to k_{G2}. Using IBMM, the energy gap may be filled via the following three measures with the inter-ISO power exchange. First, neighbor ISO 1 can provide 80 MW supportive energy to the host ISO. Second, the power flow from the host ISO to neighbor ISO 2 can be reduced by 20 MW. Third, the power flow from the host ISO to neighbor ISO 3 can be reduced to 0 MW, and then the power flow turns inversely, and neighbor ISO 3 can provide 15 MW supportive energy to the host ISO. In this way, the 120 MW energy gap in time slot k_{G2} can be filled.

These three measures imply that G2 can change its maintenance time slot to k_{G2} via purchasing supportive energy from neighbor ISOs 1 and 3, and via paying the penalty fees for reducing the transmitted energy to neighbor ISOs 2 and 3. Additionally to the requirements of energy, G2 must consider its budget for changing its maintenance time slot and G2 will aim to change its maintenance time slot at the lowest costs. Thus, this chapter proposes a bidding mechanism, i.e., IBMM, that can help G2 purchase the cheapest supportive energy from the neighbor ISOs and pay the least penalty fees for reducing the transmitted energy.

3.2.2. CASES FOR OBTAINING INTER-ISO ENERGY

In the example in Chapter 3.2.1, the three measures can be generalized as three cases. These three cases are defined based on the long-term inter-ISO power exchange contract regarding the exchange of power between ISOs. In the long-term power exchange contract, the host ISO may transmit energy to support some of the neighbor ISOs and be supported by other neighbor ISOs.

Case 1 is with respect to the neighbor ISOs that transmit the energy to the host ISO in the long-term power exchange contract. In Case 1, the GENCOs of the host ISO can use their bid price to purchase the supportive energy generated by the GENCOs of these neighbor ISOs.

Case 2 is with respect to the neighbor ISOs that receive the energy from the host ISO

in the long-term power exchange contract. In Case 2, the host ISO can reduce the power transmitted to the neighbor ISOs w.r.t. the long-term inter-ISO power exchange contract, and use the bid prices of the GENCOs of the host ISO to pay the penalty fee for repurchase.

Finally, Case 3 is also with respect to the neighbor ISOs that receive the energy from the host ISO in the long-term power exchange contract. In Case 3, the host ISO reduces the power transmitted to the neighbor ISOs to zero but still it is not enough to fill the shortage of reserved energy; so then the GENCOs of the host ISO need to purchase the supportive energy from the GENCOs of the neighbor ISOs. Thus, the bid price of the GENCOs of the host ISO should be used to pay the penalty fee, and also to buy the supportive energy from the GENCOs of the neighbor ISOs.

In Cases 1 and 3, if the supportive energy is so expensive that the GENCOs in the host ISO cannot afford it, the GENCOs in the host ISO cannot change their time slots via purchasing supportive energy to fill the energy gap when they are under maintenance. Furthermore, in Cases 2 and 3, if the inter-ISO power exchange is not allowed for some neighbor ISOs, the penalty fee can be set to a very large value. Moreover, the amount of purchased supportive energy should be constrained by the capacity of the tie lines to avoid congestion. The cases will then be mathematically modeled in the bidding problem in Section 3.3.2.

3.3. Bidding mechanism for the host ISO

In this section, how the proposed IBMM is implemented for the host ISO is firstly introduced. Then the bidding programming problem is formulated.

3.3.1. IBMM bidding mechanism

When the host ISO decides to start a bidding process, it gathers the GENCOs who are not satisfied with the scheduling results, and the GENCOs who intend to sell energy in the neighbor ISOs to participate in the bidding process. A flowchart of the proposed bidding process is shown in Figure 3.2. The process consists of the following steps:

1) After obtaining the ISO-wide optimal scheduling results, the host ISO conveys the first-stage scheduling results and the amount of reserved energy at each time slot to its GENCOs.

2) GENCOs of the *host ISO* choose to fix their scheduled time slots by not participating in the bidding process or to change their scheduled time slots by participating in the bidding process. If there are no GENCOs that intend to participate, the bidding process ends.

3) The host ISO calculates the reserved energy by taking the time slots fixed by the GENCOs in Step 2) into account. For example,if in time slot 1, the total generation capacity of the generation units is 1 MW, while the maintenance actions of the generation units with a total generation capacity of 0.4 MW are fixed by the GENCOs, then the reserved energy in time slot 1 is 0.6 MW. Then the ISO updates the reserved energy and the updated reserved energy is conveyed to the GENCOs of the neighbor ISOs.
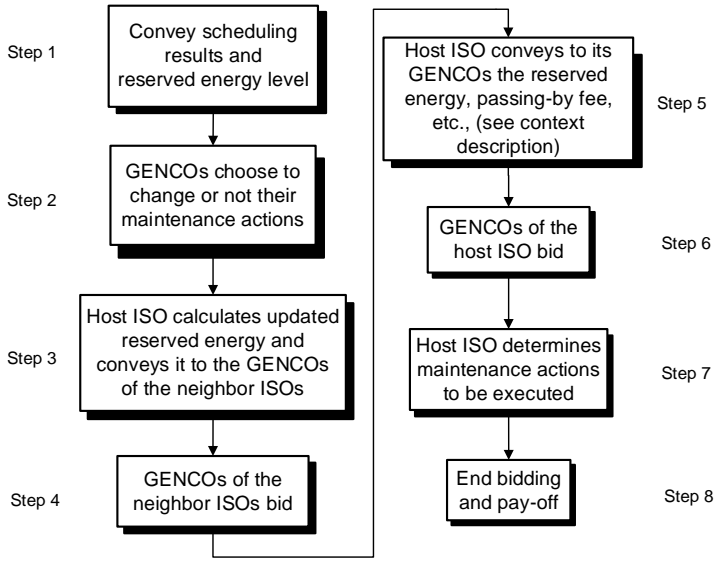
Figure 3.2: Flowchart for the bidding process

4) The GENCOs of the neighbor ISOs submit the price and amount of the energy they can deliver for each time slot.

5) Then the host ISO conveys the reserved energy level, passing-by fee for inter-ISO power transmission, the maximum amount and penalty fee for reducing transmitted energy on the tie line, and the amounts of available supportive energies from the GENCOs of the neighbor ISOs with their prices to the GENCOs of the *host ISO*.

6) The GENCOs of the host ISO will bid according to the cost to purchase supportive energy, the penalty fee to reduce transmitted energy, the benefits they can obtain by changing the maintenance schedule, among other factors. To obtain the bid price for the GENCOs of the host ISO, a method such as the multi-objective programming approach of [177] can be used. This chapter assumes that the bid price have been determined. The total bid price for a maintenance action that occupies multiple time slots is the sum of the prices of these time slots.

7) The host ISO decides which maintenance actions should be performed by maximizing the total social welfare. The corresponding optimization problem will be explained in Section 3.3.2.

8) End the bidding process and pay-off.

3.3.2. DECISION MAKING MODEL FOR THE HOST ISO

In Step 7) of the bidding process, the host ISO will determine which maintenance actions should be performed. The objective of the bidding process is to maximize the total social

welfare. The social welfare obtained from the bidding process can be calculated as:

$$B = \max_{\Delta,\delta,q,q_{\text{loss}},q_{\text{H}},p^{\text{re}}} \sum_{i\in\mathscr{I}}\sum_{k\in\mathscr{K}} \Delta(i,k)\Big(G_{\text{g}}^{\text{bid}}(i,k) -$$

$$\sum_{m\in\mathscr{M}}\sum_{n\in\mathscr{N}_m} (q(m,n,i,k) + q_{\text{loss}}(m,n,i,k))\cdot G_{\text{neigh}}^{\text{bid}}(m,n,k)$$

$$-\sum_{m\in\mathscr{M}}\sum_{n\in\mathscr{N}_m} (q(m,n,i,k) + q_{\text{loss}}(m,n,i,k))\cdot C_{\text{Tr}}(m) - \sum_{m\in\mathscr{M}} p^{\text{re}}(m,i,k)\cdot C_{\text{pen}}(m,k)\Big) \quad (3.1)$$

In (3.1), the first term involves the bid prices of the GENCOs; the second term involves the price for the GENCOs to purchase supportive energy from the neighbor ISOs; the third term corresponds to the price for paying the passing-by fees on the tie lines; and the forth term is the penalty fee for reducing the energy transmitted from the host ISO to the neighbor ISOs. Then, the total additional energy $q_{\text{loss}}^{\text{total}}(m,k)$ that should be generated by the GENCOs of neighbor ISO m in time slot k is formulated as:

$$q_{\text{loss}}^{\text{total}}(m,k) = q_{\text{loss}}^{\text{ref,out}}(m,k) \text{ if } k\in\mathscr{K}_m^{\text{out}},$$

$$q_{\text{loss}}^{\text{total}}(m,k) = 0 \text{ if } k\in\mathscr{K}_m^{\text{in}} \text{ and } \delta(m,k) = 1,$$

$$q_{\text{loss}}^{\text{total}}(m,k) = q_{\text{loss}}^{\text{ref,in}}(m,k) \text{ if } k\in\mathscr{K}_m^{\text{in}} \text{ and } \delta(m,k) = 0,$$

$$\text{where } q_{\text{loss}}^{\text{ref,out}}(m,k) = \left(\Big(P_{\text{Tr}}(m,k) + \sum_{i\in\mathscr{I}}\sum_{n\in\mathscr{N}_m} q(m,n,i,k)\Big)^2 - P_{\text{Tr}}^2(m,k)\right)R_m/U_m^2$$

$$\text{and } q_{\text{loss}}^{\text{ref,in}}(m,k) = \Big(\sum_{i\in\mathscr{I}}\sum_{n\in\mathscr{N}_m} q(m,n,i,k)\Big)^2 \cdot R_m/U_m^2, \forall m\in\mathscr{M}, \forall k\in\mathscr{K} \quad (3.2)$$

where $\delta(m,k)$ is the case indicator, i.e. $\delta(m,k) = 1$ represents that the reduced transmission power from the host ISO to ISO m on the tie line at time slot k is smaller than the transmission power in the inter-ISO power exchange contract, while otherwise $\delta(m,k) = 0$; $P_{\text{Tr}}(m,k)$ is the transmission power on the tie line between the host ISO and ISO m in time slot k that has been stipulated in the inter-ISO long-term energy transactions contract. As mentioned in Section 3.2, three cases are included in (3.2). Case 1 corresponds to purchasing supportive energy, Case 2 corresponds to reduce the transmitted power, and Case 3 corresponds to do both. In (3.2), in Case 2, by reducing the transmitted energy from the host ISO to the neighbor ISO, the energy loss is reduced. Then, the GENCOs of the neighbor ISO do not need to generate additional energy to compensate the additional energy loss, so $q_{\text{loss}}^{\text{total}}(m,k) = 0$.

Then, after adopting the loss allocation method as proposed in [137], $q_{\text{loss}}(m,n,i,k)$ can be obtained by:

$$q_{\text{loss}}(m,n,i,k) = q_{\text{loss}}^{\text{total}}(m,k)\cdot \frac{q(m,n,i,k)}{\sum_{i\in\mathscr{I}}\sum_{n\in\mathscr{N}_m} q(m,n,i,k)}$$

$$\forall m\in\mathscr{M}, \forall n\in\mathscr{N}_m, \forall i\in\mathscr{I}, \forall k\in\mathscr{K} \quad (3.3)$$

The reduced energy for each case can be described as:

$$\sum_{i\in\mathscr{I}} p^{\text{re}}(m,i,k) = 0, \text{ if } k\in\mathscr{K}_m^{\text{out}} \quad (3.4a)$$

$$\sum_{i \in \mathscr{I}} p^{\mathrm{re}}(m, i, k) < | P_{\mathrm{Tr}}(m, k) |, \text{ if } k \in \mathscr{K}_m^{\mathrm{in}} \text{ and } \delta(m, k) = 1 \tag{3.4b}$$

$$\sum_{i \in \mathscr{I}} p^{\mathrm{re}}(m, i, k) = | P_{\mathrm{Tr}}(m, k) |, \text{ if } k \in \mathscr{K}_m^{\mathrm{in}} \text{ and } \delta(m, k) = 0 \tag{3.4c}$$

The purchased supportive energy for each case can be described as:

$$q(m, n, i, k) \geq 0, \text{ if } k \in \mathscr{K}_m^{\mathrm{out}} \tag{3.5a}$$

$$q(m, n, i, k) = 0, \text{ if } k \in \mathscr{K}_m^{\mathrm{in}} \text{ and } \delta(m, k) = 1 \tag{3.5b}$$

$$q(m, n, i, k) \geq 0, \text{ if } k \in \mathscr{K}_m^{\mathrm{in}} \text{ and } \delta(m, k) = 0 \tag{3.5c}$$
$$\forall m \in \mathscr{M}, \forall n \in \mathscr{N}_m, i \in \mathscr{I}$$

The amount of energy obtained from the reserved energy cannot be negative:

$$q_{\mathrm{H}}(i, k) \geq 0, \forall m \in \mathscr{M}, \forall n \in \mathscr{N}_m, \forall i \in \mathscr{I}, \forall k \in \mathscr{K} \tag{3.6}$$

The constraints for balancing the amounts of energy are:

$$\Delta(i, k) P_{\mathrm{G}, i} = q_{\mathrm{H}}(i, k) + \sum_{m \in \mathscr{M}} \sum_{n \in \mathscr{N}_m} q(m, n, i, k) + \sum_{m \in \mathscr{M}} p^{\mathrm{re}}(m, i, k), \forall i \in \mathscr{I}, \forall k \in \mathscr{K} \tag{3.7}$$

Constraint (3.7) assures that, when $\Delta(i, k) = 0$, then $q_{\mathrm{H}}(i, k)$, $q(m, n, i, k)$ and $p^{\mathrm{re}}(m, i, k)$ are all zero (no reserved energy occupied, no supportive energy purchased, and no reduced transmitted power). The bid maintenance actions can only be performed once:

$$\sum_{k \in \mathscr{K}} \Delta(i, k) = 0 \text{ or } \sum_{k \in \mathscr{K}} \Delta(i, k) = \tau_i, \forall i \in \mathscr{I} \tag{3.8}$$

The constraints to consecutively perform maintenance actions are:

$$\sum_{k \in \mathscr{K}} | \Delta(i, k) - \Delta(i, k - 1) | \leq 2, \forall i \in \mathscr{I} \tag{3.9}$$

where $\Delta(i, 0) = 0$, $i \in \mathscr{I}$. The reserved energy obtained from the host ISO by generation units cannot exceed the maximum reserved energy $q_{\mathrm{H}}^{\max}(k)$ at each time slot k, while the available energy (constrained by the transmission line capacity limitation) obtained by the generation units from neighbor ISO m cannot exceed the available energy $q_{\mathrm{Tr}}^{\max}(m, k)$ that neighbor ISO m can deliver at each time slot k:

$$\sum_{i \in \mathscr{I}} q_{\mathrm{H}}(i, k) \leq q_{\mathrm{H}}^{\max}(k),$$
$$\sum_{n \in \mathscr{N}_m} \sum_{i \in \mathscr{I}} (q(m, n, i, k) + q_{\mathrm{loss}}(m, n, i, k)) \leq q_{\mathrm{Tr}}^{\max}(m, k), \tag{3.10}$$
$$\forall i \in \mathscr{I}, \forall m \in \mathscr{M}, \forall n \in \mathscr{N}_m, \forall k \in \mathscr{K}$$

Furthermore, the constraint regarding the reserved energy levels for the neighbor ISO is:

$$\sum_{i \in \mathscr{I}} \sum_{n \in \mathscr{N}_m} (q(m, n, i, k) + q_{\mathrm{loss}}(m, n, i, k)) \leq q_{\mathrm{N}}^{\max}(m, k), \forall m \in \mathscr{M}, \forall k \in \mathscr{K} \tag{3.11}$$

The supportive energy $q_{\text{G}}^{\max}(m, n, k)$ of GENCO n of ISO m in time slot k should be limited by the maximum supportive energy bid in Step 4):

$$\sum_{i \in \mathscr{I}} q(m, n, i, k) + q_{\text{loss}}(m, n, i, k) \leq q_{\text{G}}^{\max}(m, n, k), \forall m \in \mathscr{M}, n \in \mathscr{N}_m, k \in \mathscr{K} \qquad (3.12)$$

The bidding programming problem (1)-(12) is a mixed-integer non-linear programming problem.

3.3.3. RECASTING THE NONLINEAR PROGRAMMING PROBLEM

Since constraints (2)-(4), (8), and (9) are in mixed-integer non-linear constraints, the problem (1)-(12) is difficult to solve. Therefore, this subsection introduces a method to recast the constraints (2)-(4), (8), and (9) into tractable mixed-integer linear or mixed-integer second-order cone forms. First, regarding (2) and (3), we substitute (2) into (3), such that:

$$q_{\text{loss}}(m, n, i, k) = \left(\sum_{i \in \mathscr{I}} \sum_{n \in \mathscr{N}_m} q(m, n, i, k) + 2P_{\text{Tr}}(m, k) \right) \cdot R_m / U_m^2 \cdot q(m, n, i, k), \text{ if } k \in \mathscr{K}_m^{\text{out}},$$

$$q_{\text{loss}}(m, n, i, k) = 0 \text{ if } k \in \mathscr{K}_m^{\text{in}} \text{ and } \delta(m, k) = 1,$$

$$q_{\text{loss}}(m, n, i, k) = \sum_{i \in \mathscr{I}} \sum_{n \in \mathscr{N}_m} q(m, n, i, k) \cdot R_m / U_m^2 \cdot q(m, n, i, k),$$

$$\text{if } k \in \mathscr{K}_m^{\text{in}} \text{ and } \delta(m, k) = 0 \qquad (13)$$

Then (13) can be refined into:

$$q_{\text{loss}}(m, n, i, k) = \left(\sum_{i \in \mathscr{I}} \sum_{n \in \mathscr{N}_m} q(m, n, i, k) + 2P_{\text{Tr}}(m, k) \right) \cdot R_m / U_m^2 \cdot q(m, n, i, k), \text{ if } k \in \mathscr{K}_m^{\text{out}},$$

$$q_{\text{loss}}(m, n, i, k) = \left(1 - \delta(m, k) \right) \cdot \sum_{i \in \mathscr{I}} \sum_{n \in \mathscr{N}_m} q(m, n, i, k) \cdot R_m / U_m^2 \cdot q(m, n, i, k), \text{ if } k \in \mathscr{K}_m^{\text{in}} \qquad (14)$$

By using the method in [29], (14) can be recast into a mixed-integer second-order cone constraint, such that:

$$q_{\text{loss}}(m, n, i, k) = \left(\sum_{i \in \mathscr{I}} \sum_{n \in \mathscr{N}_m} q(m, n, i, k) + 2P_{\text{Tr}}(m, k) \right) \cdot R_m / U_m^2 \cdot q(m, n, i, k), \text{ if } k \in \mathscr{K}_m^{\text{out}},$$

$$q_{\text{loss}}(m, n, i, k) = \sum_{i \in \mathscr{I}} \sum_{n \in \mathscr{N}_m} q(m, n, i, k) \cdot R_m / U_m^2 \cdot q(m, n, i, k) - Q(m, n, i, k), \text{ if } k \in \mathscr{K}_m^{\text{in}},$$

$$Q(m, n, i, k) \leq M \cdot \delta(m, k),$$

$$Q(m, n, i, k) \geq -M \cdot \delta(m, k),$$

$$Q(m, n, i, k) \leq \sum_{i \in \mathscr{I}} \sum_{n \in \mathscr{N}_m} q(m, n, i, k) \cdot R_m / U_m^2 \cdot q(m, n, i, k) + M \cdot (1 - \delta(m, k)),$$

$$Q(m, n, i, k) \geq \sum_{i \in \mathscr{I}} \sum_{n \in \mathscr{N}_m} q(m, n, i, k) \cdot R_m / U_m^2 \cdot q(m, n, i, k) - M \cdot (1 - \delta(m, k)) \qquad (15)$$

Second, (4) can be refined into:

$$\sum_{i \in \mathscr{I}} p^{\text{re}}(m, i, k) = 0, \text{ if } k \in \mathscr{K}_m^{\text{out}} \qquad (16a)$$

$$\left(1 - \delta(m,k)\right) \cdot \mid P_{\text{Tr}}(m,k) \mid \leq \sum_{i \in \mathscr{I}} p^{\text{re}}(m,i,k) \leq \mid P_{\text{Tr}}(m,k) \mid -\delta(m,k) \cdot \epsilon, \text{ if } k \in \mathscr{K}_m^{\text{in}} \qquad (16b)$$

where ϵ is a very small positive value. Then (16a) is a linear constraint and (16b) is a mixed-integer linear constraint.

Third, (5) can be refined into:

$$q(m,n,i,k) \geq 0, \text{ if } k \in \mathscr{K}_m^{\text{out}} \qquad (17a)$$

$$0 \leq q(m,n,i,k) \leq \left(1 - \delta(m,k)\right) \cdot M, \text{ if } k \in \mathscr{K}_m^{\text{in}} \qquad (17b)$$

where M is a very large positive value. Then (17b) is a mixed-integer linear constraint.

The absolute value and "or" logic in constraints (8) and (9), respectively, can be recast into mixed-integer linear constraints by using the method in [29]. Consequently, the bidding programming problem (1)-(12) can be recast into an MISOCP problem that can be solved by the branch-and-bound algorithm in commercial software, e.g., Gurobi.

3.4. CASE STUDY

To illustrate the performance of the proposed bidding strategies, in this case, the IEEE 118-bus system that is an approximation of the American Electric Power system in the U.S. Midwest is considered. The data of this system are given in [103]. The IBMM will be simulated with a scheduling period of 13 weeks (time slots) for the host ISO. The simulation results will be compared with those of the non-interchangeable bidding mechanism for maintenance (NBMM), where NBMM does not consider the supportive energy from the neighbor ISOs nor the reduction of transmitted energy. In detail, NBMM is the programming problem by fixing $q(m,n_m,i,k)$ and $p^{\text{re}}(m,i,k)$ to zero in the IBMM problem.

3.4.1. PARAMETERS AND SEETINGS

This case study analyzes five scenarios, denoted as Scenario A to Scenario E. One host ISO is considered in all the scenarios, and five generation units intend to change their maintenance schedule via bidding. According to the topology of the IEEE 118-bus system, all the generation units are connected. So these five generation units are connected. Furthermore, there are two neighbor ISOs of the host ISO, and in each neighbor ISO, three GENCOs intend to provide the supportive energy. Table 3.1 shows the parameters of the GENCOs of the host ISO. Table 3.2 indicates the capacity for supportive energy of the GENCOs of the neighbor ISOs. In all five scenarios, the same parameters as in Tables I and II are considered.

The reserved energies of the host ISO for Scenarios A to C are the same, see Figure 3.3. For different scenarios, the bid price to change maintenance schedule and the bid price for supportive energy are different, as shown in Figure 3.4. Note that in Scenario D, the bid prices of the GENCOs of the host ISO are twice those of Scenario A, while other parameters are the same. In Scenario E, the bid prices for supportive energy are twice those of Scenario C, while other parameters are the same. Scenarios D and E are formulated to have conclusions regarding the influences of bid prices of the GENCOs of the host ISO and those of the supportive energy on the bidding results.

This chapter uses Gurobi to solve the MISOCP bidding optimization problems. For the given case study, the globally optimal solutions of the bidding optimization problems can be obtained within 10 minutes.

Table 3.1: GENERATION UNIT PARAMETERS

Maintenance action	Maintenance duration (week)	Generation unit capacity (GW·h/week)
1	3	20.4
2	2	16.8
3	2	16.8
4	2	20.4
5	1	16.8

Table 3.2: GENCOS IN NEIGHBOR ISOs

	GENCO1 (GW·h/week)	GENCO2 (GW·h/week)	GENCO3 (GW·h/week)
Neighbor ISO 1	10.8	8.8	10.4
Neighbor ISO 2	12.8	9.8	16.8
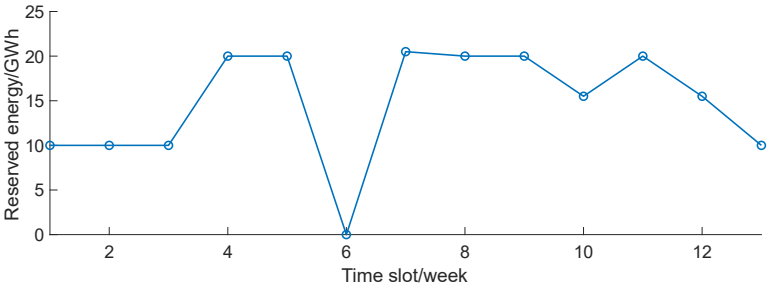
Figure 3.3: The reserved energy for Scenarios A to C

3.4.2. COMPARISON BETWEEN IBMM AND NBMM

Table 3.3: AMOUNT OF PURCHASED ENERGY FOR SCENARIOS A TO E

Scenario	From	To	Time slot	Purchased energy (GW·h)	Paid price (k$)
A	G 2 of ISO 1	G 4	4	0.4	36
	G 2 of ISO 2	G 4	5	0.4	32
	G 1 of ISO 1	G 2	12	1.3	133.9
B	G 3 of ISO 2	G 5	10	1.3	156
C	G 1 of ISO 2	G 2	2	6.8	544
	G 3 of ISO 1	G 2	3	3.8	380
	G 3 of ISO 1	G 4	9	0.4	36
	G 3 of ISO 2	G 1	10	4.9	563.5
	G 3 of ISO 1	G 1	11	0.4	40.4
	G 3 of ISO 2	G 1	12	2.9	298.7
D	G 2 of ISO 2	G 3	3	6.8	612
	G 1 of ISO 2	G 2	10	1.3	136.5
	G 3 of ISO 1	G 1	11	0.4	40.4
	G 1 of ISO 1	G 1	12	4.9	504.7
	G 1 of ISO 1	G 1	13	10.4	1029.6
E	-	-	-	-	-
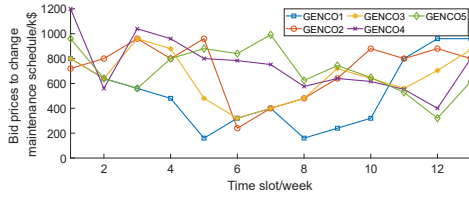
(a) Bid price to change maintenance schedule for Scenario A
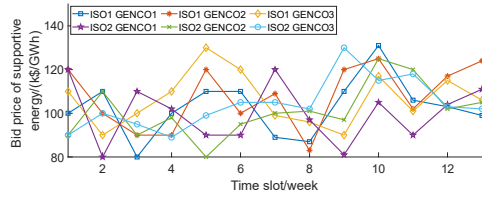
(b) Bid price for supportive energy for Scenario A
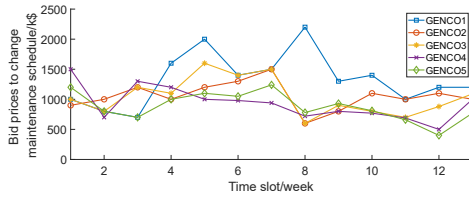
(c) Bid price to change maintenance schedule for Scenario B
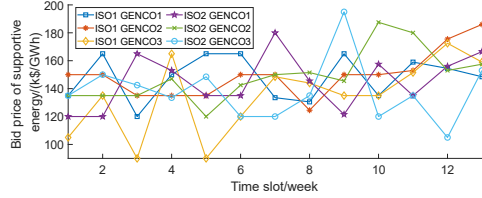
(d) Bid price for supportive energy for Scenario B
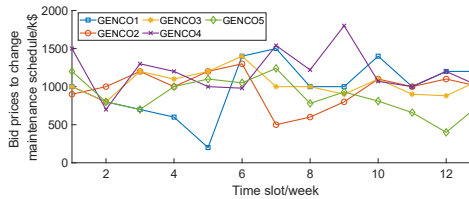
(e) Bid price to change maintenance schedule for Scenario C
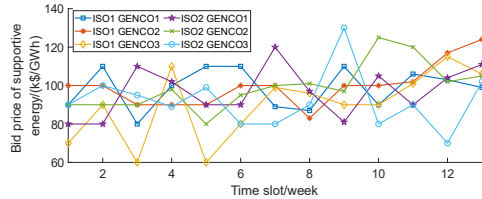
(f) Bid price for supportive energy for Scenario C

Figure 3.4: The bid prices for Scenarios A to C

	1	2	3	4	5	6	7	8	9	10	11	12	13
GENCO1													
GENCO2				■									
GENCO3								■	■				
GENCO4													
GENCO5							■						

(a) Bidding result with NBMM for Scenarios A to E

	1	2	3	4	5	6	7	8	9	10	11	12	13
GENCO1													
GENCO2											■	■	
GENCO3									■	■			
GENCO4				■	■								
GENCO5							■						

(b) Bidding result with IBMM for Scenario A

	1	2	3	4	5	6	7	8	9	10	11	12	13
GENCO1							■	■	■				
GENCO2											■	■	
GENCO3				■	■								
GENCO4													
GENCO5										■			

(c) Bidding result with IBMM for Scenario B

	1	2	3	4	5	6	7	8	9	10	11	12	13
GENCO1											■	■	
GENCO2		■	■										
GENCO3				■	■								
GENCO4							■	■					
GENCO5						■							

(d) Bidding result with IBMM for Scenario C

	1	2	3	4	5	6	7	8	9	10	11	12	13
GENCO1											■	■	■
GENCO2									■				
GENCO3			■	■									
GENCO4						■	■						
GENCO5				■									

(e) Bidding result with IBMM for Scenario D

|	1	2	3	4	5	6	7	8	9	10	11	12	13
GENCO1											■	■	
GENCO2													
GENCO3				■	■								
GENCO4								■	■				
GENCO5							■						

(f) Bidding result with IBMM for Scenario E

Figure 3.5: The comparison between IBMM and NBMM

Table 3.4: AMOUNT OF REDUCED ENERGY FOR SCENARIOS A TO E

Scenario	From	Time slot	Reduced energy (GW·h)
A	ISO 2	8	0.4
A	ISO 2	9	0.4
A	ISO 2	12	1.3
B	ISO 2	8	0.4
B	ISO 2	9	0.4
B	ISO 2	12	1.3
C	ISO 1	3	3
C	ISO 2	8	0.4
C	ISO 2	12	2
D	ISO 1	8	0.4
E	ISO 1	8	0.4
E	ISO 2	9	0.4
E	ISO 2	10	4.9
E	ISO 2	11	0.4
E	ISO 1	12	2.9
E	ISO 2	12	2

Comparative results between IBMM and NBMM for Scenarios A to E are shown in Figure 3.5. For Scenarios A to E with NBMM, the bidding results are the same and shown in Figure 3.5(a). Table 3.3 lists the amount of supportive energy purchased by the GENCOs in the host ISO and the prices for trade-off the supportive energy. In Table 3.3, "G x of ISO y" represents the GENCO x of ISO y, and "G z" represents GENCO z of the host ISO. For Case E, as shown in Table 3.3, no supportive energy is purchased. Table 3.4 lists the amount of reduced energy transmitted from the host ISO to the neighbor ISO for Scenarios A to E.

IBMM suggests for Scenarios A to E to perform 4, 4, 5, 5, and 4 maintenance actions respectively, see Figure 3.5. NBMM suggests only 3 maintenance actions for Scenarios A to E. With IBMM, the time slots in which the maintenance actions will be performed are different from those of NBMM. Furthermore, in Table 3.3, it can be observed that the GENCOs of the host ISO purchase the supportive energy and pay the penalty fee for reducing the transmission energy to the neighbor ISOs. Thus, more maintenance actions can be performed with IBMM, and as a consequence, an improvement of the reliability of the power system is obtained.

From Scenario A and Scenario D, see Figure 3.5, when the bid prices of the GENCOs of the host ISO increase, more maintenance actions can be performed. For example, in Scenario D, the maintenance action bid by GENCO 1 in the host ISO can be performed from time slots 11 to 13, while in Scenario A the maintenance action cannot be performed. Besides, as observed from Table 3.3, more supportive energy is purchased, especially from time slots 11 to 13. Thus, the increase of the bid prices of the GENCOs of the host ISO can be leveraged to purchase more supportive energy so that more maintenance actions can be performed.

When comparing Scenario C with Scenario E, it can be observed that maintenance action bid by GENCO 2 of the host ISO can no longer be performed in Scenario E, as in that scenario, the bid prices for supportive energy are larger than the penalty fees for reducing transmitted energy. Thus, the GENCOs of the host ISO pay more penalty fees for

reducing the transmitted energy instead of purchasing supportive energy. The increase of the bid prices of the supportive energy may result in fewer maintenance actions to be performed.

According to the analysis, the first advantage of using IBMM is that more generation units can be maintained, and consequently, the reliability of the power system can be improved. The second advantage of IBMM is that the GENCOs of the host ISO can obtain their preferred time slots by purchasing the supportive energy from the GENCOs of the neighbor ISOs participating in the bidding process and paying the penalty fee for reducing the transmitted energy to the neighbor ISOs. Furthermore, both the bid prices of the GENCOs of the host ISO and the bid prices for the supportive energy can influence the bidding results.

3.5. Discussions

3.5.1. Bidding organization schemes for large grids

In the proposed bidding mechanism, the ISOs should periodically start bidding processes as the host ISO to determine the maintenance schedule of their GENCOs considering the participation of the GENCOs of their neighbor ISOs. For a grid with multiple ISOs, the organization of the bidding processes, e.g., when an ISO can be the host ISO, should be explained. Thus, this chapter proposes that the bidding processes can be organized, e.g., in a centralized way or a distributed way. For the distributed ways, this chapter discusses two possible organization schemes. The first one is to determine a priority of being the host ISO for ISOs in this large grid. In the second one, any ISO who intends to schedule the MGU actions, can be the host ISO at any time if it intends so. Thus, one centralized and two distributed schemes to organize the bidding processes for a grid with multiple ISOs will be considered and analyzed in this chapter, called centralized bidding, priority bidding, and impromptu bidding respectively.

Centralized bidding

In a centralized bidding process, all the GENCOs of all the ISOs participate in one process. The centralized bidding processes will be started periodically, e.g., once every half year. Then the GENCOs of the ISOs who intend to determine their MGU actions will participate. There are three basic requirements for implementing the centralized bidding. First, the ISOs in the centralized bidding should be interconnected. Second, the power exchange between the ISOs has been allowed by the ISOs. Third, there will be an organization trusted by the ISOs and GENCOs to host the centralized bidding.

In the centralized bidding, the decision making problem formulated is different from the problem (3.1)-(3.12) in Section 3.3.2, because the set of maintenance actions is the union of the sets of maintenance actions of all the GENCOs of all the ISOs participating in the centralized bidding process, and supportive energy suppliers are all the GENCOs of all the ISOs. In the centralized bidding process, all the GENCOs of all the ISOs in the grid can participate, while for priority bidding and impromptu bidding, only the neighbor ISOs can participate. Therefore, the centralized market environment is the most competitive among the three bidding organization schemes considered in this chapter. However, there are two major drawbacks of centralized bidding.

Firstly, when delivering supportive energy among two non-neighbor ISOs, the energy

must be delivered through other ISOs. The delivery of the supportive energy may face more strict tie line conditions for transmission. Thus, the capacities of all the tie lines on the path between the supporting ISO and the receiving ISO should be considered. As a result, the transmission process will face more constraints; hence, the centralized bidding will be less practical.

Secondly, if the number of GENCOs in the grid is large, there will be computational complexity issues. Indeed if all the GENCOs of all the ISOs join the centralized bidding process to purchase or sell energy, the large computational complexity for solving the bidding programming problem for a large number of ISO participants is a drawback of the centralized bidding.

PRIORITY BIDDING

Another way to organize the bidding processes for a grid with multiple ISOs is the priority bidding. In each bidding process only one ISO can be the host ISO. The host ISO will gather the GENCOs of the neighbor ISOs with the host ISO and start the bidding process, and then it is the turn for another ISO to be the host ISO. There is one basic requirement for implementing the priority bidding, i.e., the power exchange between the host ISO and the neighbor ISOs has been allowed by the ISOs.

In priority bidding, the host ISO solves (3.1)-(3.12) when it starts a bidding process. The priority of being the host ISO can be determined by negotiation among the ISOs, e.g., the ISOs agree to be the *host ISO* in turn. Being the host ISO in turn implies that, e.g., when there are two connected ISOs in one grid, and in the current period, ISO 1 is the host ISO firstly, and then, at the next period, ISO 2 will be the host ISO firstly. If there are no GENCOs of the neighbor ISO that participate in the bidding process, the host ISO will start the bidding process without participation of GENCOs of the neighbor ISOs. In this scenario, during the bidding process, no supportive energy will be purchased.

In priority bidding, the delivery between two non-neighbor ISOs is avoided. Furthermore, if only the GENCOs of the neighbors ISOs are considered, the number of GENCOs can be kept relatively low and thus the computational complexity for solving the bidding problems will be limited. The disadvantage of priority bidding is its reduced competitiveness compared with centralized bidding. The definition of fairness of the ranking method can also be challenging.

IMPROMPTU BIDDING

Impromptu bidding is another way to organize the bidding process. Any ISO can be the host ISO at any time if it intends so, by gathering the GENCOs of its neighbor ISOs to participate in the bidding process. If there are multiple ISOs that intend to be the host ISO at the same time, the ISO who first claims its intention of being the host ISO will be the host ISO. Then after that ISO has finished its bidding process, other ISOs can announce their intention to be the host ISO and so on. If there is no GENCOs of the neighbor ISOs that participates in the bidding process, the host ISO will start the bidding process only with its GENCOs, and during the bidding process, no supportive energy will be purchased. There is one basic requirement for implementing the impromptu bidding, i.e., the power exchange between the host ISO and the neighbor ISOs has been allowed by the ISOs.

In impromptu bidding, the ISOs can get rid of both the drawbacks of the centralized

bidding. Besides, the starting times of the bidding processes are more flexible than with priority bidding. In impromptu bidding, the host ISO solves (3.1)-(3.12) when it starts a bidding process.

In impromptu bidding, whether the GENCOs of the neighbor ISOs can join the bidding is determined by the network conditions of the neighbor ISOs. It is not required that all the neighbor ISOs of the host ISO should join the bidding and supply their energy; so they can choose to join or not.

Remark 1 *Although three different schemes to organize the bidding process have been discussed, these three schemes face a same "synchronization" problem. In this chapter, ISOs in the bidding process are "synchronous" when they have the same beginning time of the scheduling and the same scheduling period. Consider a grid with two asynchronous ISOs where ISO 1 determines its maintenance schedule for a period of two months from April, while the ISO 2 determines its schedule for a period of four months from April. When ISO 2 determines its maintenance schedule from April to August, the GENCOs of ISO 1 only can sell its supportive energy to ISO 2 from April to June, but the GENCOs of ISO 2 can sell its supportive energy to ISO 1 from April to August. Thus, the GENCOs of ISO 2 (with the longer scheduling period) can sell more supportive energy, but the GENCOs of ISO 2 obtain less supportive energy from the GENCOs of ISO 1, and for ISO 1, the reverse holds. So this trade-off should be considered in designing maintenance scheduling periods for ISOs.*

3.5.2. Implementation of the proposed bidding strategy

Since different ISOs in different countries may have different power market mechanisms, the bidding mechanism proposed in this chapter may not be applicable in some of the deregulated power systems, e.g., in situations where the ISOs do not interconnect to other ISOs.

For deregulated power systems interconnecting with other ISOs, the reserved energy of the neighbor ISOs decreases when the GENCOs of the neighbor ISOs support the energy to the host ISO. Consequently, the marginal price of the neighbor ISO may increase. Thus, it is crucial to analyze the influence on the marginal price and to set regulation mechanisms to the amount of supportive energy the GENCOs of the neighbor ISO can bid. This can be implemented, for instance, via a threshold that defines the maximum support energy that a GENCO can provide, as included in (3.12) with the parameter $q_{\mathrm{G}}^{\max}(m, n, k)$.

Furthermore, the bidding problem formulated in this chapter includes the case when the reduction of the energy transmitted from the host ISO to some neighbor ISOs is not allowed. In that case, the parameter $C_{\mathrm{pen}}(m, k)$ can be set equal to a huge value. Additionally, the case when the bid prices of the supportive energy are too high is also considered in the proposed formulation. In that case, the bid prices of the GENCOs of the host ISO are not sufficient for paying the prices of the supportive energy, so the GENCOs of the host ISO may not choose to change their scheduled time slots. The GENCOs of the host ISO should follow the ISO-wide optimal scheduling results.

3.5.3. Discussion of a larger scheduling period of maintenance

The case study of this chapter sets the scheduling period (i.e., the period over which the maintenance actions are scheduled) as 13 weeks. If the scheduling period is set to

a larger value, the number of the time slots to be considered will increase. The interchangeable bidding mechanism (IBMM) proposed in this chapter can handle the longer period of maintenance by increasing the cardinality of set $\mathcal{K}$ in the formulated bidding problem Section 3.3.2.

However, a too-long scheduling period will increase the uncertainty in the predictions of failure rates, which means that in practice, the risk of sudden failure occurring during the scheduling period may increase. Thus, in practice, the scheduling period should not be set too long.

Furthermore, a longer scheduling period implies that the GENCOs of the host ISO and the GENCOs of the neighbor ISOs should predict their bids for a longer period. However, the profits for a long period are more difficult to predict. Thus, the participants of the bidding may not welcome a longer scheduling period.

3.6. CONCLUSIONS AND FUTURE WORK

This chapter has proposed a novel bidding mechanism for maintenance of generation units in transmission power systems. In this mechanism, the GENCOs of the host ISO can bid to change their scheduled maintenance actions and to achieve their own benefits. The GENCOs can use their bid price to purchase supportive energy from the GENCOs of the neighbor ISOs, to pay the penalty fee caused by reducing the energy transmitted from the host ISO to the neighbor ISOs w.r.t. the long-term power exchange transactions, or both. Besides, three possible schemes, including centralized bidding, priority bidding, and the impromptu bidding, to organize the bidding processes in a grid associated with multiple ISOs have been discussed. As indicated by the simulations for a case study, this interchangeable bidding mechanism for maintenance implies that the GENCOs can obtain their preferred time slots, and more maintenance actions can be performed so that the reliability of the power system can be improved. The results imply that the inter-ISO power exchange will give more flexibility to the GENCOs for maintaining their generation units and improve the reliability of the power systems.

As for future work, the proposed bidding strategy will be tested on larger-scale and real-life cases. Three proposed bidding organization schemes for large grids will be compared with the existing bidding schemes for scheduling the maintenance actions of the generation units. Furthermore, to avoid the scenario that the GENCOs of the neighbor ISOs raise their bid prices for supportive energy to any high level, a truthful bidding mechanism (Vickrey-Clarke-Groves mechanism), can be developed.

3

NOMENCLATURE

i	Maintenance action index
k	Time slot index
m	Neighbor ISO index
n	GENCO index in neighbor ISOs
$\mathscr{I}$	Set of maintenance actions in the bidding process
$\mathscr{K}$	Set of time slots in the bidding process
$\mathscr{M}$	Set of neighbor ISOs that join the bidding process
$\mathscr{N}_m$	Set of GENCOs that intend to sell their supportive energy in neighbor ISO m
$\mathscr{K}_m^{\text{in}}$	Set of time slots when the power flow in the contract of inter-ISO power exchange goes from the host ISO to neighbor ISO m
$\mathscr{K}_m^{\text{out}}$	Set of time slots when the power flow in the contract of inter-ISO power exchange goes from neighbor ISO m to the host ISO
$C_{\text{Tr}}(m)$	Energy passing-by fee for one unit of transmitted energy from neighbor ISO m to the host ISO
$C_{\text{pen}}(m, k)$	Penalty for reducing one unit of energy transmitted to neighbor ISO m in time slot k with respect to what has been stipulated in the inter-ISO power exchange contract
$G_{\text{g}}^{\text{bid}}(i, k)$	Bid price of maintenance action i in time slot k
$G_{\text{neigh}}^{\text{bid}}(m, n, k)$	Bid price of GENCO n of neighbor ISO m in time slot k
$P_{\text{G},i}$	Capacity of generation unit i
$P_{\text{Tr}}(m, k)$	Transmission power in the power exchange contract on the tie line between the host ISO and neighbor ISO m in time slot k
R_m	Resistance on the tie line between the host ISO and ISO m
U_m	Terminal voltage at the host ISO side terminal of the tie line between the host ISO and ISO m
$q_{\text{G}}^{\text{max}}(m, n, k)$	Maximum supportive energy of GENCO n of neighbor ISO m in time slot k
$q_{\text{H}}^{\text{max}}(k)$	Maximum available reserved energy of the host ISO in time slot k
$q_{\text{N}}^{\text{max}}(m, k)$	Maximum reserved energy for neighbor ISO m in time slot k

$q_{\text{Tr}}^{\max}(m,k)$	Maximum energy that neighbor ISO m can transmit in time slot k
ϵ	A very small positive value
M	A very large positive value
τ_i	Duration of maintenance action i
$p^{\text{re}}(m,i,k)$	Reduced transmitted energy from the host ISO to neighbor ISO m with respect to what has been stipulated in the inter-ISO power exchange contract for performing maintenance action i in time slot k
$q(m,n,i,k)$	Amount of energy purchased from GENCO n of the neighbor ISO m in time slot k for performing maintenance action i
$q_{\text{H}}(i,k)$	Amount of reserved energy of the host ISO that maintenance action i occupies in time slot k
$q_{\text{loss}}(m,n,i,k)$	Additional energy that GENCO n of neighbor ISO m needs to generate to compensate the energy losses when transmitting supportive energy to the host ISO for performing maintenance action i in time slot k
$q_{\text{loss}}^{\text{total}}(m,k)$	Total additional energy to be generated for compensating the energy losses when transmitting supportive energy from neighbor ISO m to the host ISO in time slot k
$q_{\text{loss}}^{\text{ref,out}}(m,k)$	Additional energy generated by the GENCOs of ISO m in time slot k for Case 1 (see Section 3.2 for details).
$q_{\text{loss}}^{\text{ref,in}}(m,k)$	Additional energy generated by the GENCOs of ISO m in time slot k for Case 3 (see Section 3.2 for details).
$Q(m,n,i,k)$	Auxiliary variable.
$\delta_{m,k}$	Case indicator. Equals 1 if Case 2 occurs (see Section 3.2 for details). Equals 0 if Case 3 occurs (see Section 3.2 for details).
$\Delta(i,k)$	Equals 1 if the maintenance action i is performed in time slot k, and 0 otherwise

4

TRUTHFUL PLATFORM FOR MAINTENANCE OF GENERATION UNITS

4.1. INTRODUCTION

Maintenance is a necessary measure for ensuring the reliability of power systems [71], [205]. A maintenance decision-making strategy based on the evaluation of the condition of the components is called condition-based maintenance. Mainly, condition-based maintenance of power systems can be categorized as short-term when determining the maintenance schedule for the upcoming days or weeks, mid-term for the upcoming several weeks or months, and long-term for the upcoming several months or years [11]. The scope of this chapter is long-term condition-based maintenance of generation units.

In deregulated power transmission networks, the generation companies, equipment manufacturers, transmission companies, and the independent system operators (ISOs) may be different entities. Sometimes these entities have to share their data for cooperative tasks. These tasks are essential for operating the transmission network safely and economically, e.g., condition-based maintenance of generation units (CBMGU). However, since the shared data for cooperative tasks may be tampered with, other entities may receive tampered data that may influence the final outcomes of the cooperative tasks. Thus, to make the entities trust the shared data in the CBMGU tasks, data security should be ensured as the most basic requirement for the cooperative tasks. Consequently, this chapter proposes a truthful maintenance platform for CBMGU to ensure data security among all the processes of CBMGU.

Generally, long-term state-of-the-art CBMGU mainly encompasses five processes: acquisition of operational data, failure rate diagnosis/prognosis, maintenance schedul-

---

This chapter is based on [74].

Table 4.1: Comparison between state-of-the-art CBMGU and the proposed T-CBMGU

Processes	state-of-the-art CBMGU	Proposed T-CBMGU
1. Acquisition of operational data 2. Failure rate diagnosis/prognosis 3. Performance of maintenance actions	1. Stored data can be tampered with 2. Stored data may be lost or deleted. 3. Sharing data with low efficiency. 4. Responsibility cannot be easily backtracked.	1. Stored data are immutable and trustworthy. 2. Loss of stored data is unlikely. 3. Sharing data with efficiency. 4. Responsibility can be easily backtracked.
1. Scheduling of maintenance actions 2. Bidding to change scheduled time slots	1. ISOs schedule the maintenance actions. 2. Actions that compromise fairness may occur. 3. Inefficient decision making processes due to manual work.	1. Decisions making via smart contract. 2. No actions that compromise the fairness. 3. Less manual work.

ing, bidding to change the scheduled time slots[1], and performance of the maintenance actions. All five processes of state-of-the-art CBMGU have been widely studied in the literature [64], [67], [97], [148], [157], [174], [212], [228].

Among the five processes of state-of-the-art CBMGU, three processes are related to data storage and sharing, i.e., the acquisition of operational data, the failure rate diagnosis/prognosis, and the performance of maintenance actions. In these three processes, the collected operational data, the failure rate diagnosis/prognosis results, and the maintenance action performance logs are recorded in the data storage center. However, using a data storage center may face these drawbacks. First, the data can be tampered with by hackers or personnel of the data storage center. Furthermore, the stored data may be lost or physically eliminated. Tampered and lost data can influence the diagnosis/prognosis results and the trained learning-based failure rate prediction model. Second, the identity verification process for data sharing is characterized by a low efficiency, especially due to manual verification. Third, since the data can be tampered with and lost, the data are hard to backtrack, as is the responsibility of, e.g., the maintenance implementer.

The other two processes among the five relate to decision making, i.e., scheduling of maintenance actions and bidding to change scheduled time slots. The decision making processes are managed by the ISOs. In the power system maintenance literature and in industry, these ISOs are assumed to be trusted. However, it cannot be guaranteed that ISOs can schedule maintenance actions and hold the bidding processes totally fairly. GENCOs may manipulate the fairness of the bidding processes by, e.g., bribes and blackmails, and tamper with the bidding prices of other GENCOs to obtain benefits. Moreover, it is time-costly for a human team to, e.g., manually verify the identity of the GENCOs, especially when many GENCOs are involved.

Table 4.1 presents the drawbacks of state-of-the-art CBMGU. In this chapter, a truthful CBMGU platform (T-CBMGU) based on blockchain is proposed to tackle these drawbacks. A blockchain is a chain of blocks that are linked via cryptography [136]. A block contains the data to be stored and hash points for encryption. Important features of blockchains include immutable data, no centralized authority, and traceable data [43].

T-CBMGU has three *main* advantages over state-of-the-art CBMGU. First, since data are stored on the nodes (participants) of the blockchain without referring to a data storage center, it is difficult to tamper with the stored data [112]. If the data on one node are tampered with, other nodes can verify the tampered data. Consequently, the stored data

---

[1]While some authors do not consider such a rescheduling process, the current chapter does include a rescheduling step, just as [67], [212].

in the blocks of the blockchain are immutable. Second, data sharing can be more efficient since time-consuming processes, such as, identity verification, can be performed automatically. Furthermore, because of the immutability of the data and asymmetric cryptography, data sharing is secure. Third, the scheduling and bidding processes can be implemented by smart contracts without involving a third party [184], [229]. The smart contract is designed by the participants of the blockchain to automatically drive decision making processes. Thus, actions that compromise fairness can be avoided.

Moreover, the maintenance scheduling problem is an MIQP problem that is time-costly to solve. In the literature, Benders decomposition is widely leveraged for solving mixed-integer programming problems, especially when after fixing the integer variables, the remaining problem is convex [91]. In the literature, to tackle the slow convergence of Benders decomposition, acceleration methods, e.g., valid inequalities [172], approximation (e.g., rounding [156], relaxation induction [213], and outer approximation [9]) have been studied. Among them, valid inequalities can efficiently accelerate the convergence process of Benders decomposition. Valid inequalities are usually designed for specified problems based on technical/physical analysis of the given problem. Regarding the use of valid inequalities in the maintenance scheduling of generation units, a methodology is proposed in [172] for hydrogenerators. The proposed valid inequalities are tailored for hydrogenerators. Thus, this chapter proposes two valid inequalities tailored for accelerating Benders decomposition for CBMGU in power systems.

The contributions of the current chapter are:

- A truthful maintenance platform is proposed for generation units in power systems. By using the proposed T-CBMGU platform, the stored data can be immutable, the data sharing can be efficient and secure, and the decision-making can be fair (see Table 4.1 for details).

- Maintenance scheduling problems are time-costly MIQP problems. Thus, two novel dedicated valid inequalities based on technical/physical analysis and greedy-based heuristic initialization are proposed for accelerating the convergence speed of Benders decomposition.

The remainder of this chapter is organized as follows. Section 4.2 reviews the literature on the relevant topics of this chapter and also briefly introduces blockchain. Section 4.3 explains the processes of state-of-the-art CBMGU. Section 4.4 describes the T-CBMGU platform. Section 4.5 explains the blockchain implementation in the T-CBMGU platform. In Section 4.6, a Benders decomposition algorithm with valid inequalities is proposed. In Section 4.7, a case study based on the IEEE 300-bus system is presented to show the importance of the proposed T-CBMGU by comparing its performance with that of state-of-the-art CBMGU that is affected by fairness manipulations and tampered data. Finally, in Section 4.8, conclusions are presented and further research is discussed.

4.2. RELATED WORK AND INTRODUCTION OF BLOCKCHAIN

4.2.1. RELATED WORK

In the literature, blockchain technology has been widely applied in various fields, e.g., truthful market design [15], [226]. For example, in [62], Ethereum, a blockchain platform

is leveraged in a decentralized power market. The prosumers can trade energy peer-to-peer conveniently via the smart contract of Ethereum without involving a third party. In [181], a secure blockchain-based platform is designed for educational credential evaluation. The academic credentials are generated, verified, and validated via this platform. In [36], blockchain is applied to sharing medical service records between different clinical jobs. In [152], an edge computing platform is designed for decentralized household air quality monitoring devices for ensuring data security. In [132], a blockchain-based radio access network is proposed for truthful network management and authentication. In [193], the resources require for leveraging blockchain in decentralized local energy markets are studied. In [221], a transaction platform for the energy storage market is proposed. By using blockchain technology, the platform can be secure and transparent.

However, there are only a few articles in the literature on leveraging blockchain in the maintenance industry. For example, in [42], a knowledge-sharing platform is designed based on blockchain for maintaining a honing machine system with multiple components. The degradation knowledge of the components can then be shared securely. In [7], blockchain is applied to formulate an aircraft maintenance logbook that cannot be tampered with or destroyed. In [1], blockchain is applied to the maintenance of rolling stock, and the truthfulness of the business logic and data is enhanced. All these articles in the literature use blockchain in maintenance for truthful data storing and sharing. However, the use of blockchain in CBMGU has not yet been studied. Moreover, truthful data storage and sharing are not sufficient for CBMGU since CBMGU also involves decision-making processes in which actions that compromise fairness, e.g., fairness manipulation, may occur. Thus, in this chapter, to address the drawbacks of state-of-the-art CBMGU, the T-CBMGU platform is proposed and designed for all five CBMGU processes.

Moreover, the maintenance scheduling problem is an MIQP problem that is time-costly to solve. In the literature, Benders decomposition is widely leveraged for solving mixed-integer programming problems, especially when after fixing the integer variables, the remaining problem is convex [91]. In the literature, to tackle the slow convergence of Benders decomposition, acceleration methods, e.g., valid inequalities [172], approximation (e.g., rounding [156], relaxation induction [213], and outer approximation [9]) have been studied. Among them, valid inequalities can efficiently accelerate the convergence process of Benders decomposition. Valid inequalities are usually designed for specified problems based on technical/physical analysis of the given problem. Regarding the use of valid inequalities in the maintenance scheduling of generation units, a methodology is proposed in [172] for hydrogenerators. The proposed valid inequalities are tailored for hydrogenerators. Thus, this chapter proposes two valid inequalities tailored for accelerating Benders decomposition for CBMGU in power systems.

4.2.2. INTRODUCTION TO BLOCKCHAINS

A blockchain is a chain of blocks linked in series. Once a block is formulated, each block stores a certain amount of data and then is linked to the blockchain [53].

A peer-to-peer network is a simple type of network where servers are able to communicate with one another and share what is on or attached to their server with other users [14]. The formulated blockchain is stored distributively by all the servers in the peer-
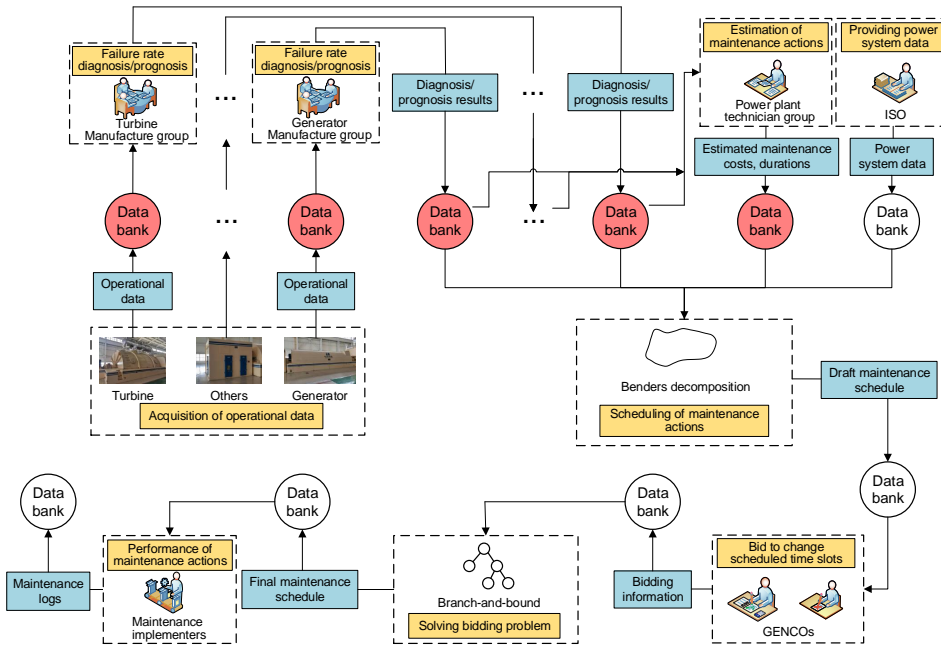
Figure 4.1: Work processes of the state-of-the-art CBMGU platform for one time step

to-peer networks. If some of the servers in the network cannot work, the data stored in the blocks is still secure. Furthermore, these servers are called nodes that provide the space for storage and computing power for formulating the blocks. If an entity intends to tamper with the data stored in the blocks, it must control more than half of the nodes in the network. However, gaining control of more than half of the nodes in the network is nearly impossible. Thus, it is almost impossible to tamper with the data stored in the blocks.

In summary, compared with traditional ways to store digital data, blockchain mainly has two advantages. First, the data stored in blocks are difficult to tamper with. Second, the data are stored distributively in the peer-to-peer network. Thus, the data stored in the blocks are trustworthy.

4.3. State-of-the-art CBMGU platform

The work processes of state-of-the-art CBMGU are shown in Figure 4.1. In Figure 4.1, the labels in yellow boxes identify the processes; the labels in blue boxes indicate the categories of data that are stored in the data banks; and the arrows represent the input or output directions of the data flows. Regarding the data banks used to store the data, the data banks in red represent the stored data that are related to one generation unit. Maintenance of generation units usually involves multiple generation units. However, for simplification, data banks for other generation units in CBMGU are not included in

Figure 4.1.

CBMGU is implemented periodically, and each period of which the length is several months for long-term CBMGU corresponds to a time step. Regarding maintenance scheduling, this chapter adopts a receding horizon mechanism. Maintenance scheduling is performed for one prediction horizon that always includes multiple time steps, but only the maintenance actions of the scheduling results for the first time step are performed; subsequently, one proceeds to the next time step. The duration of maintenance actions of generation units is expressed in time slots of the long-term CBMGU (i.e., weeks). In Figure 4.1, only the work processes for one time step are shown since in other time steps, the work processes repeat.

In Figure 4.1, five processes are shown, i.e., acquisition of operational data, failure rate diagnosis/prognosis, maintenance scheduling, bidding to change the scheduled time slots, and performance of the maintenance actions.

In the first two processes, operational data of the components, e.g., generators and turbines, are collected by sensors to obtain the failure rates and to train the failure rate prediction models of the components [64], [97], [228]. For example, operational data are collected by sensors and sent to a central data hub [228]. Afterwards, the failure rate is predicted based on the data in the central data hub and Bayesian learning. In [64], a sensor-driven method and a Bayesian model are applied to predict the remaining life of generators in microgrids. In [97], operational data and historical data are leveraged to train predictive degradation models for wind turbines using random forest and decision tree algorithms.

In the third process, the maintenance actions are scheduled by a centralized organization, i.e., an independent system operators (ISO). The ISO aims at maximizing the generation benefits and/or minimizing the maintenance costs for all generation units it manages while ensuring power system reliability [148], [174].

In the fourth process, since the scheduled maintenance actions in the third process (overall optimal schedule) may conflict with the individual benefit of the owners of generation units, i.e., generation companies (GENCOs), a bidding process for GENCOs to change their scheduled time slots is managed by the ISO [67], [212].

In the fifth process, the maintenance logs, the material consumption situation, and the implementer information, among other information, are recorded for management and to keep the know-how in the company [157].

In these processes of state-of-the-art CBMGU, the data may be recorded on the paper lists, digital lists, or other data formats in data banks. The data banks may be managed by some of the entities involved in the maintenance processes, e.g., the ISO, or data storage companies. Since the data stored in data banks may be tampered with by cyber or physical attacks, the stored data may not be trustworthy. In addition, since the decision-making processes, i.e., maintenance scheduling and bidding to change the scheduled time slots, are implemented by the ISOs, the results of the decision-making processes may be influenced by, e.g., fairness manipulation, etc. Thus, the decision-making results also may not be trustworthy.
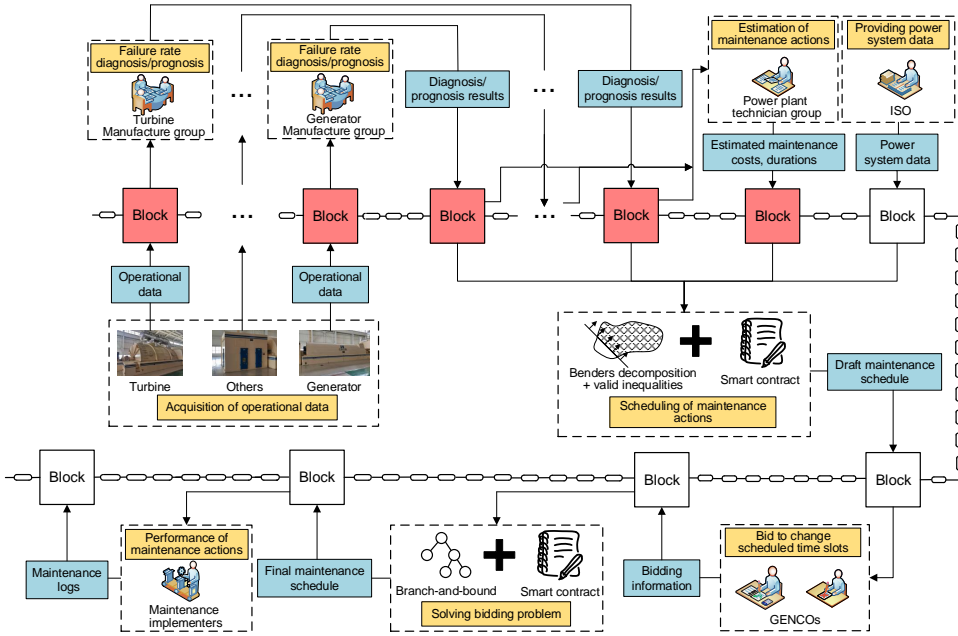
Figure 4.2: Work processes of the T-CBMGU platform for one time step

4.4. T-CBMGU PLATFORM

To make the stored data and the results of decision-making processes trustworthy, we propose a blockchain-based T-CBMGU. The work processes of the proposed T-CBMGU platform for one time step are illustrated in Figure 4.2.

In Figure 4.2, at the beginning of the period corresponding to a given time step, the operational data are collected by the sensors on the components of generation units, e.g., exciters and turbines. For each component of each generation unit, a block for storing the operating data of this component is built and validated in the blockchain.

After that, the operational data in the blockchain block for each component of each generation unit are extracted by the corresponding manufacturing expert groups who provide or manufacture the component. The manufacturing expert groups may belong to the providers and/or the manufacturers of the components of the generation units. They use their knowledge, numerical models, and/or trained data-driven models to evaluate the failure rates of the components. Then, the block of the diagnosis/prognosis results for each component is built and validated.

Afterwards, the power plant technician groups estimate the maintenance costs and the maintenance durations according to the data extracted from the blocks of operational data and failure rate diagnosis/prognosis results. The estimation of the maintenance costs is based on, e.g., the replacement costs of the components, the costs for performing maintenance actions, and the outsourcing fee (if applicable). The estimation of the maintenance duration is based on, e.g., the arrangement and the internal structure

of the generation units.

The block of the power system data is built by ISOs, including the load, the reserved energy level, the electricity prices, and the breakdown penalty fee.

The maintenance actions will be scheduled to minimize the overall maintenance cost and to maximize the overall benefits for all the generation units. Additionally, the scheduling problems include data extracted from previously built blocks, such as the failure rate diagnosis/prognosis data, the evaluation data of maintenance costs and durations, and the power system data as parameters. Since this chapter formulates *maintenance scheduling problem* as an MIQP problem, a Benders decomposition algorithm with acceleration techniques is proposed for solving the problems more efficiently. The smart contract, rather than ISOs, implements this process automatically. Afterwards, the determined optimal maintenance schedule is stored in one block.

Then, the GENCOs extract the optimal maintenance plan from the block. According to scheduled time slots for performing maintenance actions, if the GENCOs are not satisfied with their scheduled maintenance actions, they can join in the bidding process to change their scheduled time slots. The GENCOs who intend to join the bidding process should provide their bidding information, including the time slots in which they intend to maintain their generation units and the bidding price the GENCOs intend to pay for changing their scheduled time slots. Then, each GENCO builds a block to store the bidding information (in Figure 4.1, the blocks of GENCOs are integrated as one block for saving space).

By extracting the bidding information, the final schedule for performing maintenance actions is determined with the objective of maximizing the total amount of money bid by the GENCOs. Then the ISOs will use the money to improve, e.g., the reliability of the power system [212]. The formulated *bidding problems* are mixed-integer linear programming problems that can be solved efficiently by using the branch-and-bound solvers. Similar to maintenance scheduling, bidding to change scheduled time slots is also implemented automatically via the smart contract. Then, the final maintenance schedule is stored in one block.

Finally, by extracting the final schedule, the maintenance implementer perform maintenance actions on their corresponding generation units according to the final schedule. While performing the maintenance actions, the maintenance logs are recorded, including the materials that are used, information on the implementer, on-the-spot measurements such as video and photos, and information on new components for replacement. Then, blocks are built to store the maintenance logs.

4.5. IMPLEMENTATION OF BLOCKCHAIN

A blockchain can be fully public or permission-based [111]. Since the data stored in the blocks of T-CBMGU, e.g., failure rates of generation units, can be considered sensitive information, a permission-based blockchain is preferred.

In the T-CBMGU platform, the participants include the GENCOs, the providers or manufacturers of the components, the power plant technician groups, the ISO, and the maintenance implementers. When a new GENCO is founded or an existing GENCO goes bankrupt, the ISO should verify the identity of the new GENCO for participation or eliminate the bankrupted GENCO from the list of participants in the T-CBMGU platform.

In Figure 4.1, the participants extract the data from the built blocks. After completing their individual tasks (e.g., failure rate diagnosis/prognosis), they build new blocks to store their obtained results. The steps for building a block are as follows:

Step I In one process, the participant authenticates and decrypts the block(s) that store the data that are required by the participant (see Remark 2). Then, the participant extracts the data and starts its tasks, e.g., diagnosis.

Step II The participant packages the data that it intends to store in the block, which are usually the results of tasks obtained in Step I, via a hash function. Then, it builds a block and encrypts the block.

Step III The built block is broadcast to all the participants.

Step IV All the participants validate the block by reaching consensus with, e.g., the proof-of-work.

Step V The validated block is linked to the blockchain and stored distributively.

Remark 2 *Encryption/decryption and authentication can be done by asymmetric cryptography. In asymmetric cryptography, two kinds of keys, i.e., a public key and a private key, are used for encryption/decryption and authentication. The public key is published to all the participants, while the private key is kept only by the participant itself.*

Regarding encryption/decryption, when e.g., the owner of a generation unit intends to store the operational data of a component into a block, the owner encrypts the block using the public key of the manufacturing expert group, and the manufacturing expert group can decrypt the block using its private key to extract the operating data of the component. By doing so, except for the owner of the generation unit and the manufacturing expert group of the component, other participants cannot decrypt the block to extract the operational data of the component. Hence, data privacy is guaranteed.

To determine whether, e.g., the extracted data truly originate from the corresponding generation unit, authentication can also be implemented by asymmetric cryptography. The owner of the generation unit signs on the block with stored operational data by using its private key. Then, the manufacturer expert group can authenticate the signature by using the public key of the owner of the generation unit.

4.6. MAINTENANCE SCHEDULING PROBLEM AND BENDERS DE-COMPOSITION WITH VALID INEQUALITIES

In T-CBMGU, two decision making problems are solved, i.e., *maintenance scheduling problem* and *bidding problem*. The formulated maintenance scheduling problems in this chapter are defined for generation units but not for the components of the distribution networks, as done in Chapter 2. Furthermore, the formulated maintenance scheduling problems in this chapter are the same as the ones in Chapter 3. However, the formulated bidding problems in this chapter differ from those in Chapter 3 since, in the current chapter, the inter-ISO power exchange is not considered in the bidding problems.

This section focuses on the formulation and solution process of the maintenance scheduling problem. The formulation of the bidding problem is discussed in [212]. Bidding problems are mixed-integer-linear programming problems that can be solved efficiently by commercial solvers, e.g., CPLEX.

4.6.1. PROBLEM FORMULATION FOR MAINTENANCE SCHEDULING

The objective of maintenance scheduling is to minimize the overall costs and to maximize the overall benefits of the generation units. Consequently, the objective function is:

$$
\min_{\delta_{g,k}, \Delta_{g,k}, \sigma_{g,k}, \varsigma_g, P^G_{g,k}} \sum_{g \in \mathcal{G}} \sum_{k \in \mathcal{K}} c^m_g \delta_{g,k} / \tau_g + \sum_{g \in \mathcal{G}} p_g c^p_g (1 - \sum_{k \in \mathcal{K}} \delta_{g,k} / \tau_g) + \sum_{g \in \mathcal{G}} \sum_{k \in \mathcal{K}} \left(\sigma_{g,k} c^{st}_{g,k} + \right.
$$
$$
\left. \Delta_{g,k} \left(c^g_{2,g} (P^G_{g,k})^2 + c^g_{1,g} P^G_{g,k} + c^g_{0,g} - c^e P^G_{g,k} \right) \right)
$$

$$(4.1a)$$

where $\mathcal{G}$ is the set of generation units, $\mathcal{K}$ is the set of time slots in one prediction window, $\delta_{g,k}$ equals 1 if the maintenance action on generation unit g is performed in time slot k and equals 0 otherwise, c^m_g is the maintenance cost for generation unit g, τ_g is the maintenance duration for generation unit g, p_g is the failure rate of generation unit g. In this chapter, the health condition of the generation units is described by a failure rate. In (4.1a), c^p_g is the penalty fee of a failure on generation unit g, $\sigma_{g,k}$ equals 1 if generation unit g starts up in time slot k and equals 0 otherwise, ς_g equals to 1 if generation unit g is maintained, $c^{st}_{g,k}$ is the start-up cost for generation unit g in time slot k, $\Delta_{g,k}$ equals 1 if generation unit g is connected to the grid in time slot k and equals 0 otherwise, $c^g_{2,g}$, $c^g_{1,g}$ and $c^g_{0,g}$ are the coefficients of the power generation cost of generation unit g, c^e is the electricity price for generating power, and $P^G_{g,k}$ is the power generated by generation unit g in time slot k. The first two terms in (4.1a) express that if a maintenance action is performed on one generation unit, the generation unit is recovered, and the failure rate of the generation unit becomes zero. The terms in (4.1a) represent the overall maintenance costs of the generation units, the penalty fees for failures, and the balance of the start-up costs, generation costs, and generation benefits. The constraints are:

$$1 - \delta_{g,k} \geq \Delta_{g,k}, \forall g \in \mathcal{G}, \forall k \in \mathcal{K} \tag{4.1b}$$

$$\Delta_{g,k} P^{G-}_g \leq P^G_{g,k} \leq \Delta_{g,k} P^{G+}_g, \forall g \in \mathcal{G}, \forall k \in \mathcal{K} \tag{4.1c}$$

$$\sigma_{g,k} \geq \Delta_{g,k} - \Delta_{g,k-1}, \forall g \in \mathcal{G}, \forall k \in \mathcal{K} \tag{4.1d}$$

$$\sum_{k \in \mathcal{K}} \delta_{g,k} = \varsigma_g \tau_g, \forall g \in \mathcal{G} \tag{4.1e}$$

$$\sum_{k \in \mathcal{K}} |\delta_{g,k} - \delta_{g,k-1}| \leq 2, \forall g \in \mathcal{G} \tag{4.1f}$$

$$P^D_k = \sum_{g \in \mathcal{G}} \Delta_{g,k} P^G_{g,k}, \forall k \in \mathcal{K} \tag{4.1g}$$

$$\sum_{g \in \mathcal{G}} \Delta_{g,k} P^{G+}_g \geq P^D_k + r^+, \forall k \in \mathcal{K} \tag{4.1h}$$

$$\delta_{g,k} \in \{0,1\}, \Delta_{g,k} \in \{0,1\}, \sigma_{g,k} \in \{0,1\},$$
$$\varsigma_g \in \{0,1\}, P^G_{g,k} \geq 0, \forall g \in \mathcal{G}, \forall k \in \mathcal{K} \tag{4.1i}$$

where (4.1b) indicates that if generation unit g is in maintenance, it cannot be connected to the grid. Constraint (4.1c) limits the power generated by the generation units, where
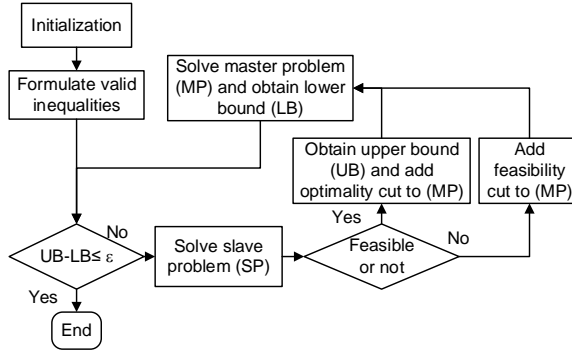
Figure 4.3: Benders decomposition solving process

$P_g^{\mathrm{G}-}$ and $P_g^{\mathrm{G}+}$ are the upper and lower bounds of the power generated by generation unit g. Constraint (4.1d) guarantees that when a previously disconnected generation unit is connected to the grid again, then there is a start-up action. Constraint (4.1e) represents that in each generation unit g the sum of time slots used for maintenance equals 0 if the maintenance action will not be performed (binary variable $\varsigma_g = 0$); otherwise, it equals the duration of the maintenance action of generation unit g ($\varsigma_g = 1$). Constraint (4.1f) represents that the maintenance actions should be performed consecutively, where $\delta_{g,0} = 0$. Constraint (4.1g) expresses the power balance of the power system, where P_k^{D} is the predicted load demand in time slot k. Constraint (4.1h) is the constraint for the reserved energy, where r^+ is the reserved energy level.

The maintenance scheduling problem (4.1) can be formulated into an MIQP problem by using the approach of [71][2]. To solve the formulated MIQP problem efficiently, in Section 4.6.3, two valid inequalities are proposed to accelerate the Benders decomposition solver.

4.6.2. SOLUTION PROCESS BASED ON BENDERS DECOMPOSITION

For a mixed-integer programming problem, Benders decomposition separates the integer variables and continuous variables and solve a master problem and a slave problem separately. The solution process of Benders decomposition with the proposed valid inequalities is shown in Figure 4.3. If the slave problem is feasible, an upper bound for the whole problem is obtained, and an extra constraint, called optimality cut is added to the master problem. If the slave problem is infeasible, an extra constraint, called feasibility cut is added to the master problem. Then, the master problem is solved to obtain the values of the fixed variables for the next iteration, and a lower bound is obtained. The termination condition involves the convergence of the upper and lower bounds. The general form of problem (4.1) is expressed as:

---

[2]Regarding (4.1a), since $\Delta_{g,k}(P_{g,k}^{\mathrm{G}})^2 = (\Delta_{g,k}P_{g,k}^{\mathrm{G}})^2 = \psi_{g,k}^2$, where $\psi_{g,k}$ is a continuous auxiliary variable, the objective function is in quadratic form.

Figure 4.4: Illustration of initialization mechanism
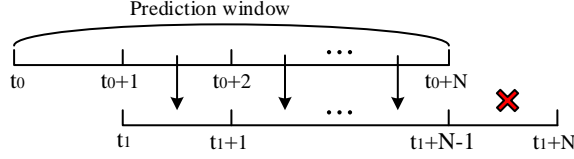
$$\min_{x\in(\mathbb{R}^+)^{n_x},y\in\{0,1\}^{n_y}} x^{\mathrm{T}}Hx + f_1^{\mathrm{T}}x + f_2^{\mathrm{T}}y \tag{P}$$
$$\text{s.t. } Ax + By \le b$$

In (P), since the continuous variable $P_{g,k}^{\mathrm{G}}$ and the continuous auxiliary variables $\psi_{g,k}$ are non-negative, the continuous vector $x = [P_{g,k}^{\mathrm{G}}, \psi_{g,k}]_{g\in\mathcal{G},k\in\mathcal{K}}^{\mathrm{T}}$ is a vector of non-negative real variables, where n_x is the length of x. Besides, $y = [\delta_{g,k}, \Delta_{g,k}, \sigma_{g,k}, \varsigma_g]_{g\in\mathcal{G},k\in\mathcal{K}}^{\mathrm{T}}$ is a vector of binary variables, where n_y is the length y. For a fixed y, we can define the slave problem (SP):

$$\min_{x\in(\mathbb{R}^+)^{n_x}} x^{\mathrm{T}}Hx + f_1^{\mathrm{T}}x + f_2^{\mathrm{T}}\overline{y} \tag{SP}$$
$$\text{s.t. } Ax \le b - B\overline{y}$$

where $\overline{y}$ is the fixed y that is determined by the initialization or the solution of the master problem of the last iteration. Since (SP) is a quadratic programming problem, the solving process can be driven by, e.g., interior-point-convex algorithm, so as to verify feasibility judgment and to return the Lagrangian multipliers (if (SP) is feasible). If (SP) is feasible, the obtained Lagrangian multiplier is defined as λ_m, where m is the current number of obtained optimality cuts. If (SP) is infeasible, an extreme ray μ_n is generated via a Phase I algorithm, e.g., the one in [70], where n is the current number of obtained feasibility cuts. Then, the master problem (MP) is:

$$\min_{y\in\{0,1\}^{n_y},\eta} \eta$$
$$\text{s.t. } \eta \ge \lambda_i(b - By) + f_2^{\mathrm{T}}y,\ i \in \{1...m\}, \tag{4.1}$$
$$0 \ge \mu_j(b - By),\ j \in \{1...n\},$$
$$\text{with (VI}-1)\text{ and (VI}-2)$$

where η is an intermediate continuous variable; (VI-1) and (VI-2) are the proposed valid inequalities, which are linear constraints and which will be further explained in Section 4.6.3. Problem (MP) is a mixed-integer linear programming problem that can be solved by, e.g., branch-and-bound algorithm.

4.6.3. Formulation of valid inequalities
1) VI-1: Since a receding horizon mechanism is adopted, the maintenance scheduling results of the previous time step can be used to formulate (VI-1) for the problem of the current time step. In Figure 4.4, the initialization mechanism for dynamic scheduling problems with a receding horizon mechanism is illustrated. Figure 4.4 assumes that a

prediction window includes N time slots, where N is an integer. At the current time step, the maintenance decisions of the previous problem whose prediction window is from $t_0 + 1$ to $t_0 + N$ can be used as the initial solution from t_1 to $t_1 + N - 1$ of the current problem whose prediction window is from t_1 to $t_1 + N$. Without loss of feasibility, no maintenance actions are performed from $t_1 + N - 1$ to $t_1 + N$ to formulate the initial solution.

However, this initial solution may not be feasible if the *currently predicted* loads from t_1 to $t_1 + N - 1$ differ from the *previously predicted* loads from $t_0 + 1$ to $t_0 + N$. Thus, two scenarios are discussed.

First, if the currently predictive loads for the scheduling problem from t_1 to $t_1 + N - 1$ are no larger than the previously predicted loads for the problem from $t_0 + 1$ to $t_0 + N$, the integer variables of the maintenance plan (δ, Δ, and σ) can be initialized as before. Then, the initial maintenance plan is substituted into (SP), and (SP) is solved to obtain P^G, and λ_0.

Second, if some of the currently predicted loads are larger than the previously predicted loads, some of the scheduled maintenance actions of the problem of the last time step cannot be performed to guarantee the reserved energy level (constraint (4.1h)). To determine which maintenance actions cannot be performed, a greedy-based process is proposed:

Step 1 Define $\mathscr{P}$ as the set of time slots in which the scheduled results of the previous time step do not satisfy the reserved energy level. Rank the time slot $p \in \mathscr{P}$ from the largest reserved energy gaps (i.e., $\sum_{g \in \mathscr{G}} \Delta_{g,p} \, P_g^{G+} \text{-} P_p^D + r^+$) to the smallest.

Step 2 Select the first element $p \in \mathscr{P}$, i.e., the time slot p with the largest reserved spinning energy gaps.

Step 3 Define $\mathscr{M}_p$ as the set of maintenance actions for p in the scheduled result of the previous problem. Then rank the elements of $\mathscr{M}_p$, according to $p_g c_g^p - c_g^m$, where $g \in \mathscr{M}_p$. Subsequently, keep removing the first entry in the ranked set $\mathscr{M}_p$ until (4.1h) is satisfied for p. Then remove p from $\mathscr{P}$.

Step 4 Repeat **Step 2** and **Step 3** until $\mathscr{P} = \emptyset$.

Step 5 Obtain δ according to the remaining maintenance actions. Let $\Delta_{g,k} = 1 - \delta_{g,k}$. Then, $\sigma_{g,k} = \Delta_{g,k} - \Delta_{g,k-1}$. Afterwards, substitute the obtained δ, Δ, and σ into (SP), and solve (SP) to obtain P^G and λ_0. End the process.

After obtaining P^G and λ_0 according to the applicable two scenarios, (VI-1) can be expressed as:

$$\eta \geq \lambda_0 (b - By) + f_2^T y \qquad \text{(VI-1)}$$

2) VI-2: The second valid inequality is formulated by considering the maintenance cost and the benefits. The second valid inequality is only applicable if the currently predicted loads from t_1 to $t_1 + N - 1$ are no larger than the previously predicted loads from $t_0 + 1$ to $t_0 + N$. If generation unit g' is maintained from time slots k' to k'', then $\delta_{g',k} = 1$ and $\Delta_{g',k} = 0$, for $k \in \{k', ..., k''\}$. Therefore, the cost from k' to k'' includes only the maintenance cost c_g^m. In comparison, if generation unit g is not maintained from k' to k'', the cost from k' to k'' includes $p_g c_g^p$ and the balance containing the start-up costs, the power generation costs, and the benefits. The balance can always be smaller than 0 since if the balance (costs minus benefits) is larger than 0, disconnecting generation unit g (i.e., setting $\Delta_{g',k} = 0$) will cause the balance to equal 0. Thus, if the penalty fee is smaller than
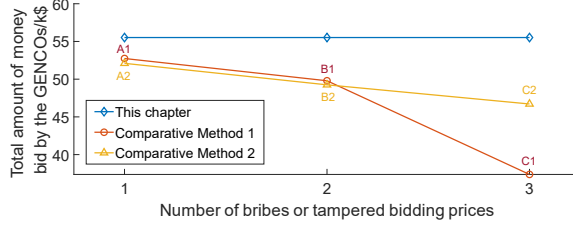
Figure 4.5: Comparison between T-CBMGU and state-of-the-art CBMGU platforms with fairness manipulation or tampered data

the maintenance cost (i.e., $p_g c_g^{\mathrm{p}} < c_g^{\mathrm{m}}$), the generation unit must not be maintained:

$$\delta_{g,k}(p_g c_g^{\mathrm{p}} - c_g^{\mathrm{m}}) \geq 0, \, \forall g \in \mathcal{G}, \, \forall k \in \mathcal{K} \tag{VI-2}$$

4.7. CASE STUDY
In this case study, the IEEE-300 bus system with 69 generation units and 195 loads is investigated [4]. The simulation of T-CBMGU is based on Go-Ethereum, which is implemented on the GoLand platform. Two comparative studies are performed in this section. The first comparison is between the proposed T-CBMGU and state-of-the-art CBMGU. The second comparison is between the proposed Benders decomposition solver and the other three solvers.

4.7.1. COMPARISON BETWEEN THE PROPOSED T-CBMGU AND STATE-OF-THE-ART CBMGU
Since data banks of state-of-the-art CBMGU may not be truthful, the data tampering and fairness manipulation may occur. To compare the proposed T-CBMGU platform with the state-of-the-art CBMGU platform, data tampering and fairness manipulation (i.e., bribes in this case study) are simulated in the bidding to change scheduled time slots with 7 GENCOs. On the state-of-the-art CBMGU platform, three cases (A1, B1, C1) with 1 to 3 bribes are simulated. In case A1, the briber with the highest bribe price fixes its preferred time slots. In case B1, based on the fixed time slots of the first briber, the briber with second-highest bribe price fixes its preferred time slots. Case C1 is similar, but with 3 bribes. After each bribe occurs, the bidding problem is solved for feasibility checking (satisfaction of the reserved energy requirement). If feasible, then the next briber fixes its preferred time slots. If not, the briber should select other time slots to fix. Furthermore, three cases with 1 to 3 tampered bidding prices are simulated (A2, B2, C2). The hacker tampers with 1 to 3 bidding prices of others whose bidding prices are larger than those of his employer. The *bidding problems* (mixed-integer linear programming problems) are solved by CPLEX to obtain globally optimal solutions.

In the simulation of T-CBMGU, Figure 4.5 compares the T-CBMGU and the state-of-the-art CBMGU platforms, where fairness manipulation and tampering data may occur when solving *bidding problems*. In Figure 4.5, comparative method 1 refers to simulations with bribes and comparative method 2 refers to simulations with tampered data.

Table 4.2: Number of conflicts between currently predicted and previously predicted loads

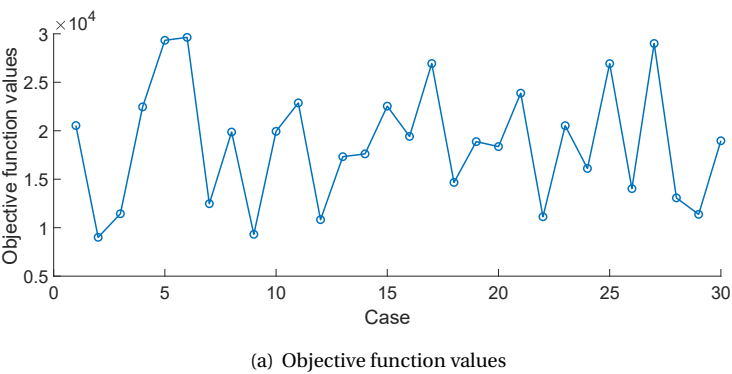| Case	11	12	13	14	15	16	17	18	19	20	21	22	23	24	25	26	27	28	29	30
Number of conflicts	12	21	27	14	19	21	15	8	25	10	21	15	7	12	8	15	21	10	21	20

From Figure 4.5, it is observed that as the numbers of bribes and tampered bidding prices increase, social welfare (i.e., total amount of money bid by the GENCOs) decreases. In cases A1, B1, and C1, social welfare decreases by 5%, 10.32%, and 32.69%, respectively, compared to T-CBMGU. In cases A2, B2, and C2, social welfare decreases by 6.16%, 11.29%, and 15.87%, respectively. Thus, T-CBMGU can avoid fairness manipulation and data tampering to obtain higher social welfare.

4.7.2. COMPARISON BETWEEN THE PROPOSED BENDERS DECOMPOSITION AND OTHER SOLVERS

Regarding the *maintenance scheduling problems* the performance of the proposed Benders decomposition solver (BD+VIs) is evaluated by comparing it with three other *global* optimization solvers for MIQP problems. The three compared solvers include a branch-and-bound solver with *filter* sequential quadratic programming (BB+SQP) [69], a branch-and-bound solver with BQPD (BB+BQPD) [68], and a custom Benders decomposition solver [172]. Among them, BB+SQP and BB+BQPD are implemented by the Tomlab toolbox in MATLAB, while BD and the proposed BD+VIs are implemented by self-written coding scripts in MATLAB.

Moreover, to demonstrate the effectiveness of the proposed solver, 30 cases with various maintenance actions (maintenance costs and maintenance durations) and failure rates are tested. In each case, the valid inequalities are obtained using the scheduling result of the last time step according to Section 4.6.3. The length of one prediction window, one time step, and one time slot are 52, 13, and 1 week, respectively. To test the effectiveness of the valid inequalities under various initialization cases, 30 cases are simulated in total with different situations of conflicts between currently and previously predicted loads. From Cases 1 to 10, the currently predicted loads are the same as the previously predicted loads. In the next 10 cases, in some time slots, the currently predicted loads are smaller than the previously predicted loads, and in the other time slots, the currently predicted loads and the previously predicted loads are the same. Finally, in some of the time slots in the last 10 cases, the currently predicted loads are larger than the previously predicted loads, and in other time slots, the currently predicted loads and the previously predicted loads are the same. As presented in Table 4.2, in Cases 11-20, the number of conflicts represents the number of time slots in which the currently predicted loads are smaller than the previously predicted loads. In Cases 21-30, the number of conflicts represents the number of time slots in which the currently predicted loads are larger than the previously predicted loads.

In Figure 4.6(a), the objective function values of 30 cases of the *maintenance scheduling problem* are shown, while Figure 4.6(b) presents the maintenance scheduling results of 69 generation units in Case 1. In Figure 4.6(a), the horizontal axis and vertical axis represent the objective function values in (4.1a) and cases respectively. In Figure 4.6(b),

(a) Objective function values

(b) Maintenance scheduling result of Case 1

Figure 4.6: Simulation results for the network.

the maintenance scheduling results of 69 generation units in Case 1 are shown. It can be observed that the maintenance actions are scattered over the whole prediction window,
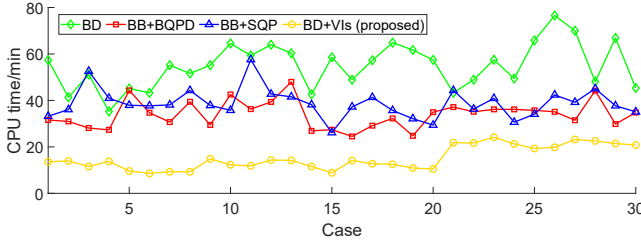
Figure 4.7: Comparison of the CPU times with various solvers

and not all the generation units required to be maintained.

Furthermore, since the solvers, i.e., BB+SQP, BB+BQPD, BD, and BD+VIs, can converge to the globally optimal solution, this chapter compares the CPU times between the solvers, as shown in Figure 4.7. The average CPU times for 30 cases for the BB+SQP, BB+BQPD, BD, and BD+VIs solvers are 54.9 min, 33.9 min, 38.7 min, and 15.1 min, respectively. Thus, the solving speed of BD is lower than those of BB+SQP and BB+BQPD, while the solving speeds of BB+SQP and BB+BQPD are nearly the same. The BD+VIs solver is the fastest among all the solvers that are compared in this chapter. More specifically, BD+VIs reduces computation times by nearly 50% compared with BB+SQP and BB+BQPD. Furthermore, the computing time of BD+VIs is 27.5% that of BD on average. Thus, our proposed VIs can efficiently reduce the computation time, especially compared with BD without adding the proposed valid inequalities.

Moreover, for BD+VIs, the average CPU times of the first, second, and third 10 sets of cases are 11.6 min, 12.1 min, and 21.6 min, respectively. Regarding the first and second sets of 10 cases, the CPU times are nearly the same, while for the third set of 10 cases, the CPU times increase. This phenomenon shows that the effectiveness of the valid inequalities is determined by whether the currently predicted loads are larger than the previously predicted loads, i.e., the effectiveness of the proposed valid inequalities decreases when the "larger than" scenario occurs.

4.8. CONCLUSIONS AND FUTURE WORK

This chapter has proposed a truthful platform for the maintenance of generation units. Compared with state-of-the-art maintenance platforms, the major advantage of the proposed truthful maintenance platform is that it provides a truthful environment for data storage, data sharing, and decision making. Furthermore, since the solving speeds of maintenance scheduling problems (MIQP problems) are low, an accelerated Benders decomposition algorithm is proposed by using two specially designed valid inequalities. The simulation results shows that the proposed T-CBMGU platform can obtain more social welfare by avoiding actions that compromise fairness, e.g., fairness manipulation and data tampering, compared with state-of-the-art CBMGU. Furthermore, the results demonstrate a faster solving speed of the proposed BD+VIs solver compared with three other solvers on maintenance scheduling problems. Finally, the solving speed reduction, w.r.t., the other solvers, of the proposed BD+VIs solver is large for the cases that

the currently predicted loads are no larger than the previously predicted loads, while the solving speed reduction decreases when the currently predicted loads are larger than the previously predicted loads. However, the BD+VIs is still the fastest solver among the four compared in this chapter.

Future work will focus on exploring additional potentials of blockchains in the maintenance of infrastructure. Moreover, the concept of truthful maintenance will be expanded further.

4

EV CHARGING STRATEGY FOR PRE-DISASTER EVACUATION

5.1. INTRODUCTION

In recent years, the share of electrified means of transportation has risen [135], [146], [216]. Specifically, higher demands for electric vehicles have increased the need for the development of new smart infrastructure. In [33], it was reported that electric vehicles are in motion approximately 4% of their life span. Thus, for approximately 96% of their time, plug-in electric vehicles (PEVs)[1] at charging stations can be used to participate in control of the consumption and generation of energy. The charging of PEVs can be scheduled to consume the redundant generated energy from renewable energy sources (RESs) in distributed energy systems [6], [84], [95], [105], [223]. Thus, the PEVs in charging stations integrated with the energy system can play a significant role in the optimal control of distribution networks via efficient charging control strategies [162], [185], [208], [220], [236].

In [231], a strategy to reduce the number of overstay PEVs is proposed to increase the utilization of charging stations. A strategic planning problem is solved, including an interchange mechanism that allows the automatic release of fully charged PEVs to enable uncharged PEVs to start their charging process earlier. A novel fuzzy-inference-based response strategy for maximizing the benefits of the aggregators and the consumers was presented in [86]. In [130], traffic flows that are simulated via a microscopic traffic flow model are considered while determining the real-time EV charging strategy. In [128], the PEV charging problem is formulated as a contained Markov decision process, and then it is solved by a deep reinforcement learning method. In [215], a two-stage PEV charging strategy to minimize charging cost is formulated as a generalized Nash game. The solutions should satisfy both congestion and renewable energy utility constraints.

This chapter is based on [72].

The nomenclature of this chapter is at the end of this chapter.

[1] The term "PEV" in this chapter refers to purely electric vehicles rather the fuel-electric hybrid vehicles.

In [87], [233], water-filling algorithms are adopted in PEV charging with limited charging powers of the charging stations. However, the charging problems in [87], [233] do not consider the operational constraints of the distribution network, e.g., bus voltage bounds and maximum transmission capacity of the lines. In general, the charging control strategies of PEVs in the literature are formulated as optimization problems that aim at maximizing benefits while minimizing operational costs.

However, to the best of our knowledge, PEV charging control strategies under pre-disaster situations (e.g., typhoons, snowstorms, heavy rain) have not yet been studied in the literature. Since optional evacuation is usually suggested, this chapter does not focus on the obligated evacuation scenario. Furthermore, this chapter focuses on the urgent emergency pre-disaster situations for residential areas where the warnings of evacuation are announced less than about two days before the landfall of the disasters. For example, the warnings of Hurricane Ida in 2021, were announced by the State of Louisiana on 28th August, while the landfall of the hurricane is on 29th August [121].

Actually, the pre-disaster load profile and the intended departure times of the PEVs will drastically deviate from the daily profiles, as illustrated in Figure 5.1 (see the case study in Section 5.6 for background and details). In Figure 5.1, a disaster is expected to happen at 0 a.m., and the disaster warning is broadcast 24 hours before. Since this chapter assumes a non-obligatory evacuation scenario (as for Hurricane Ivan in 2004), some residents may evacuate in pre-disaster situations [224]. Once the residents have evacuated, they do not create high load demand anymore (but may keep, e.g., fridges and freezers). The load demands of the evacuated residents will reduce significantly after the evacuation of those residents compared with the loads in the daily situation. Thus, in general, in pre-disaster situations, the load will decrease because of the residents that have left the disaster-prone areas (see, e.g., the load profile in Figure 5.1). The pre-disaster load profile will still experience fluctuations according to the daily profile because not all residents may choose to leave before the disaster, and those residents will still use their electrical appliances. In pre-disaster situations, the prediction of the load demands using the load prediction methods for daily situations will make it hard to capture the correct load demands. As mentioned in [34], an accurate estimate of the residential load is vital for the charging strategy to avoid grid congestion and load shortage. Thus, in this chapter, we propose a load prediction method for pre-disaster evacuation situations based on human evacuation behavior. The proposed load prediction method is then included in the PEV charging strategy for pre-disaster evacuation situations.

Regarding the times PEV owners intend to depart, an example is shown in Figure 5.1. When the occurrence time of the disaster approaches, the number of PEV owners intending to depart decreases mainly because the remaining number of PEVs in the disaster-prone area is decreasing. Moreover, in pre-disaster situations, compared to the daily patterns, more PEVs owners may intend to depart for evacuation in an emergency after the warning has been broadcast. The charging demands for the PEVs are thus more concentrated in time in pre-disaster situations, resulting in a shortage of charging power for some of the PEVs. This shortage will in general not happen in daily situations because the charging demands are distributed more evenly over the day for daily situations. Then the shortage of charging power results in unmet demands of PEVs whose departures are thus delayed. In the literature, unmet demands of PEVs are mainly studied in the con-
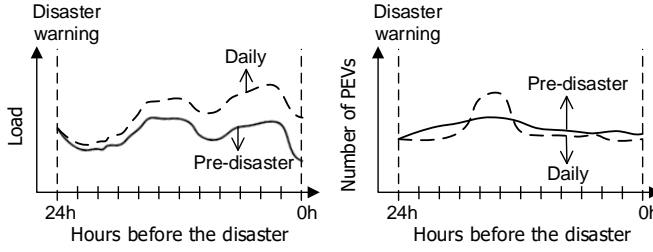
Figure 5.1: The evolution of the energy demand and the number of PEVs for daily situations and pre-disaster situations

text of charging station placement and design [34], [59], [100], rather than in the context of charging control strategies. Consequently, in the charging control strategy (for daily situations), the unmet departure demands of PEVs are mainly not considered because charging stations are designed to satisfy the departure demands for daily situations. In pre-disaster situations, with potential charging power shortage, it is important to also include fairness in the objective function. Here fairness means that the delays in charging will be equalized among all PEVs owners. Thus, in our proposed charging strategy, we give a higher weight for charging for the PEVs whose charging processes have been delayed a lot. Then, the number of PEV holders whose charging processes have been heavily delayed can be reduced.

To reduce the bandwidth of the communication system, to improve the scalability, and to increase the robustness of the controller, distributed control strategies for charging stations in distribution networks are often adopted in the literature [175], [182], [239], [241], [244]. Consequently, in some distribution networks with charging stations, the installed hardware, e.g., communication systems, will be geared towards distributed charging control strategies. In pre-disaster situations, the charging control strategy should also be implemented on the same hardware system as daily situations. Thus, this chapter focuses on the charging control strategy based on distributed charging control.

In [241], the charging strategy for the distributed model predictive control (DMPC) problem is formulated as a game. The converged solution of the game is given by the Nash equilibrium point. In [244], a distributed scheduling strategy for PEV charging is proposed based on $\epsilon-$Nash equilibrium and Lyapunov optimization. In [182], Lagrangian relaxation is applied to formulate the charging strategy planning problem in a distributed manner. In [239], different charging modes, i.e., slow charging, fast charging, and battery swapping are considered in PEV charging planning. A distributed neurodynamic algorithm is proposed to solve the formulated planning problem. In [175], day-ahead charging price is considered in distributed PEV charging planning. The problem is formulated as a Stackelberg game, where the charging station is treated as the leader and the owners of PEVs are treated as followers. In the chapters [175], [182], [239], [241], [244], DMPC is adopted because it can avoid short-sighted solutions by using a predictive model and a receding horizon mechanism.

Furthermore, as mentioned in [120], [124], [220], [225], [241], in real-time PEV charging strategy design, the computation time is vital. This chapter uses the insight that

the widely used dual-ascent-based distributed computing structure in [153] is actually a fixed-point iteration process, i.e., $x^{(k+1)} = d(x^{(k)})$, where the vector $x^{(k)}$ refers to the vector of multipliers and inter-connecting variables for iteration k and $d(\cdot)$ represents the iteration operator for DA-DMPC. Then we propose to use the Aitken method, a fixed-point acceleration method, to accelerate the convergence speed of the DMPC solving process. Note that, leveraging the Aitken method to accelerate DA-DMPC has not yet been proposed in the literature.

The contributions of this chapter are the following:

1 We propose a novel charging control strategy for pre-disaster evacuation situations. A load and charging demand prediction method for pre-disaster situations is proposed. This load and charging demand prediction method considers the prediction of human evacuation behavior. To the best of our knowledge, pre-disaster human evacuation behavior has not yet been explicitly included in the PEV charging control strategies in the literature.

2 In pre-disaster situations, with potential charging power shortages, it is important to also include fairness in the objective function. Here fairness means that the delays in charging will be equalized among all PEVs owners. To ensure fairness, we give a higher weight for charging for the PEVs whose charging processes have been delayed significantly. Then, the number of PEV holders whose charging is heavily delayed can be reduced.

3 We propose a novel Aitken-DMPC algorithm to solve the PEV charging optimal control problem with faster convergence speeds than the widely used DA-DMPC algorithm from the literature. Specifically, different from DA-DMPC, the updates of the multipliers and interconnecting variables are implemented by the Aitken iteration mechanism, rather the dual ascent iteration mechanism. To the best of our knowledge, this combination of the Aitken iteration mechanism and DMPC has not yet been proposed in the literature.

This chapter is organized as follows. Section 5.2 describes the methodology of the proposed charging control strategy. Section 5.3 explains the behavior of the residents in pre-disaster evacuation situations. Section 5.4 predicts the profiles (loads and generation powers) via human behavior analysis and autoregressive integrated moving average (ARIMA) model, and then formulates the scenario-based charging control problem for the whole system. Section 5.5 formulates the problems that must be solved for each subsystem in the DMPC setting and describes the process of the proposed Aitken-DMPC algorithm. In Section 5.6, a case study based on the IEEE 13-bus distribution network is presented. Finally, in Section 5.7, conclusions and further research are discussed.

5.2. PROBLEM STATEMENT AND DMPC APPROACH
5.2.1. CHARGING CONTROL STRATEGY FOR PEVS
In Figure 5.2, a distribution network is shown. For convenience, in this chapter, the whole distribution network is called the micro-grid, and the part encompassing the yellow area is called the main grid (of the micro-grid). Besides, the outside power system
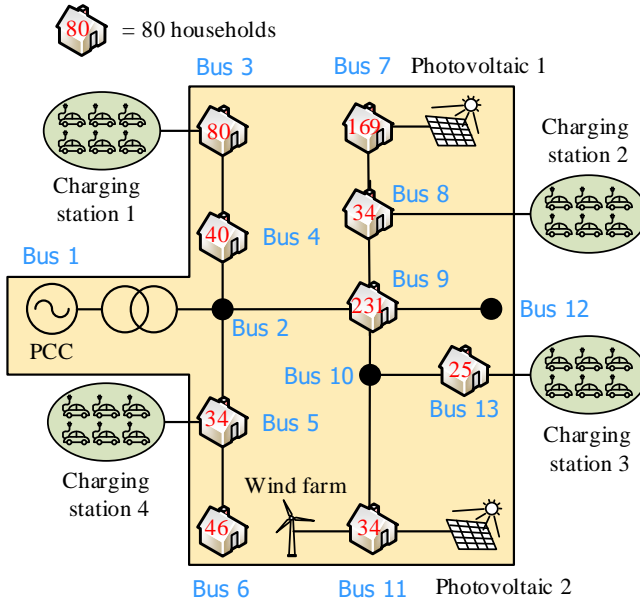
Figure 5.2: IEEE 13-bus network integrated with four charging stations

connected to the PCC points of the micro-grid is called the macro-grid. In this chapter, real-time MPC-based control is proposed to implement charging control of a micro-grid, as shown in Figure 5.3. At each time step, e.g., 15 min, three actions are performed: collecting the real-time data at the current time instant, predicting the profiles over a prediction window (always including multiple time steps in one prediction window), and solving the charging problem over a prediction window. Afterward, the plan of the first time step is implemented and the MPC process starts all over again in the next time step (receding horizon strategy).

For the real-time data collection part, the data for evacuation behavior prediction, the data for the micro-grid, and the data for the weather are collected (see details in Section 5.5.2 step 1)). These data can be used to predict the load profile for the following time steps in one prediction window, the evacuation profile (e.g., the preferred departure times for residents), and the RES profile (e.g., generation powers). Note that the evacuation profile also influences the load profile since the loads of the evacuated residents are largely reduced. In order to predict an accurate load profile in pre-disaster situations, as proposed in this chapter, human behavior on evacuation is also included (see Section 5.3 for details).

For the planning part, the target for the charging control is to reduce the energy delivered from the outside grid to the micro-grid, to increase the energy transmitted to the outside grid to earn benefits and to meet the departure demands of the PEV owners. The PEV owners should already indicate their departure time when they plug their EV into the charging station. This departure time demand includes two parts: the departure times to evacuate for residents who choose to evacuate and the departure times
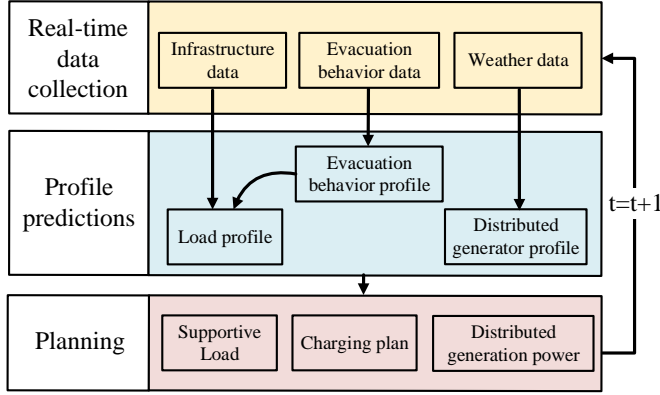
Figure 5.3: The MPC implementation process of this chapter

for residents who choose to stay. In pre-disaster situations, the departure demands cannot always be satisfied in the same way as in daily situations. For example, for upcoming heavy disasters, residents may hurry to evacuate and set departure times earlier than the daily departure time, and unmet departure demands may emerge because of a shortage of charging power. To tackle the cases with the unmet departure demands fairly for all of the PEVs, a weight value is introduced to penalize long delayed departure times in the objective function. More specifically, when an unmet departure demand occurs for a PEV, in the planning problem of the next time step, the weight of this PEV will be increased, so that its priority to be charged increases if a shortage of charging power occurs. Furthermore, in this chapter, we adopt a scenario-based approach. The uncertainty of the evacuated residents, and the solar and wind generation powers are considered in composing the scenarios, and $\mathscr{S}$ is the combined set of scenarios.

5.2.2. MECHANISM OF DMPC
The MPC charging control strategy should be implemented in a distributed manner to reduce the required bandwidth of the communication system, to improve the scalability, and to increase the robustness of the controller (see also Section 5.1). In this DMPC approach, a mechanism is implemented to coordinate the charging plans of different charging stations. For example, considering Figure 5.2, the micro-grid can be divided into 5 areas (the main grid and 4 charging stations). Then, each area will correspond to a single agent that solves a local optimization problem for that area. Then, the proposed Aitken-DMPC algorithm coordinates the interconnecting variables of the agents to obtain the optimal solution for the whole micro-grid.

5.3. PRE-DISASTER EVACUATION BEHAVIOR
The state-of-the-art modelling method for resident evacuation behavior follows three main steps [164], namely, the determination of whether or not to participate in the evacuation and the departure time for the evacuation, the destination choice, and the route choice. Among these three steps, the destination choice and the route choice are mostly

related to the traffic network rather than to the charging process. PEV owners can set their required charging energy based on their destination and route choice. Thus, in this chapter, we include the required charging energy given by the owners in our model, but their destination and route choices are not included.

For the determination of whether to depart and when to depart, the residents make decisions according to the following factors [13], [164]:

1) Socio-demographic characteristics, e.g., age, gender, and education level.

2) Spatio-temporal disaster characteristics, e.g., the intensity, location and speed of the disaster (hurricane, mud-rock flow, flood).

3) Living characteristics, e.g., affordability of the living house and the amount of stored food and necessaries.

4) Traffic conditions, e.g., traffic network congestion condition and travel distance for evacuation.

5) Psycho-social characteristics, e.g., whether neighbours have been evacuated and whether residents want to stay at their home to protect their property.

Then, the binary logit models for the residents determining to evacuate are given by [179]:

$$p_{n,i,t,s}^{\mathrm{r}} = \frac{1}{1 + e^{-\beta_t Y_{n,i,t,s}^{\mathrm{T}}}}, \forall n \in \mathcal{N}_{i,t,s}, \forall i \in \mathcal{I}, \forall t \in \mathcal{T}, \forall s \in \mathcal{S} \tag{5.1}$$

where $\mathcal{T} = \{t_0, t_0+1, ..., t_0+T_{\mathrm{D}}\}$ is the set of time steps in the prediction window (t_0 is the starting time step for MPC, T_{D} is the length of prediction window for MPC). Parameter vector $Y_{n,i,t,s}$ includes the four quantified factors mentioned above as parameters (socio-demographic, spatio-temporal, living-traffic, and psycho-social factors) and β_t is the coefficients of the parameters. Furthermore, β_t can be obtained by firstly collecting data via, e.g., census, questionnaires, and then processing the collected data via, e.g., logistic regression [195], probit regression [13].

Define $\mathcal{N}_{i,t,s}'$ as the set of residents on bus i who evacuate at time step t for scenario s. In this chapter, $\mathcal{N}_{i,t,s}'$ is obtained by the Monte Carlo method. More specifically, for scenario s, resident n on bus i, and time step t, a random number $r_{n,i,t,s}^{\mathrm{MC}}$ sampled from a uniform distribution U(0,1) is compared with $p_{n,i,t,s}^{\mathrm{r}}$. If $r_{n,i,t,s}^{\mathrm{MC}} \leq p_{n,i,t,s}^{\mathrm{r}}$, resident n on bus i will evacuate at time step t for scenario s and resident n on bus i will be included in the set $\mathcal{N}_{i,t,s}'$; otherwise, resident n on bus i will not evacuate at time step t for scenario s and will be included in set $\mathcal{N}_{i,t+1,s}$.

5.4. CENTRALIZED PRE-DISASTER PEV CHARGING PROBLEM

5.4.1. PREDICTION OF THE PROFILES

As shown in Figure 5.3, before formulating and solving the PEV charging optimization problem, the load profile, evacuation behavior profile, PEV profile, and RES profile should

be predicted for a prediction horizon based on the real-time data collected from the current time step. These profiles will be treated as the parameters in the optimization problem and are predicted before solving the optimization problem. Firstly, the load profile can be presented as:

$$P_{i,t,s}^{\text{L0}} = \sum_{n \in \mathcal{N}_{i,t,s}} P_{n,i,t,s}^{\text{Lbase}}, \forall i \in \mathcal{I}, \forall t \in \mathcal{T}, \forall s \in \mathcal{S} \tag{5.2}$$

Since ARIMA model is widely applied in the residential load prediction [37], the scenarios for the residential load $P_{n,i,t,s}^{\text{Lbase}}$ are generated by the ARIMA model. Then, the RES profile can be expressed as:

$$P_{i,t,s}^{\text{WT0}} = f^{\text{WT}}(v_{i,t,s}^{\text{w}}), P_{i,t,s}^{\text{PV0}} = f^{\text{PV}}(I_{i,t,s}^{\text{PV}}), \forall i \in \mathcal{I}, \forall t \in \mathcal{T}, \forall s \in \mathcal{S} \tag{5.3}$$

where $f^{\text{WT}}(\cdot)$ and $f^{\text{PV}}(\cdot)$ are the generation power prediction functions of wind farms and photovoltaic farms as introduced in [71]. In particular, the generation power predictions are obtained by the wind speed prediction results for wind farms and the solar radiations prediction results for photovoltaic farms. Furthermore in (5.3), $v_{i,t,s}^{\text{w}}$ and $I_{i,t,s}^{\text{PV}}$ can be predicted by the widely used ARIMA model [71].

5.4.2. PROBLEM FORMULATION

The objective function of the PEV charging problem for the whole micro-grid is:

$$J = \min_{\Phi} \mathbb{E}_{\mathcal{S}} \left(\sum_{t \in \mathcal{T}} (c_2 P_{1,2,t,s}^2 + c_1 P_{1,2,t,s}) - \gamma \sum_{m \in \mathcal{M}} \sum_{t \in \mathcal{T}_m} (\rho_m + 1) \left(\frac{w_{m,t}}{S_m^{\text{B}}} - \sigma_m \right) \right) \tag{5.4a}$$

where $\mathbb{E}_{\mathcal{S}}$ represents the expected value over all the scenarios in $\mathcal{S}$, $\mathcal{T}_m = \{t_m^{\text{d}}, t_m^{\text{d}} + 1, ..., t_0 + T_{\text{D}}\}$ is the subset of time steps in the prediction window after the departure time step of PEV m, $P_{1,2,t,s}$ is the active power flow fed by the macro-grid at time step t for scenario s, c_2 and c_1 are coefficients for the energy generation cost for thermal generators in macro-grid as shown in [241]. By introducing ρ_m, the most delayed PEVs can be prioritized for charging so as to ensure fairness. Moreover, σ_m is the state of charge (SOC) level in percentage[2] of fully charged that is set by the owner of PEV m. Then, the first term in (5.4a) represents the trade-off between the micro-grid and the macro-grid, while the second term weighted by γ represents the penalty of the unmet departure demands of the PEV owners. Then, the constraints w.r.t. the micro-grid connection are expressed

---

[2]In this chapter, to assure fairness among diverse PEVs with different battery capacities, the percentage is applied.

as:

$$\sum_{j \in \mathscr{I}_i} P_{j,i,t,s} + P_{i,t,s}^{\mathrm{WT}} + P_{i,t,s}^{\mathrm{PV}} = P_{i,t,s}^{\mathrm{L}} + P_{i,t}^{\mathrm{CH}} \tag{5.4b}$$

$$\sum_{j \in \mathscr{I}_i} Q_{j,i,t,s} - Q_{i,t,s}^{\mathrm{L}} = 0 \tag{5.4c}$$

$$P_{i,j,t,s} = -P_{j,i,t,s}, \, Q_{i,j,t,s} = -Q_{j,i,t,s} \tag{5.4d}$$

$$V_{i,t,s} - V_{j,t,s} = (P_{i,j,t,s} \, R_{i,j} + Q_{i,j,t,s} \, X_{i,j}) / V^{\mathrm{ref}} \tag{5.4e}$$

$$0 \le P_{i,t,s}^{\mathrm{WT}} \le P_{i,t,s}^{\mathrm{WT0}}, \, 0 \le P_{i,t,s}^{\mathrm{PV}} \le P_{i,t,s}^{\mathrm{PV0}} \tag{5.4f}$$

$$\alpha P_{i,t,s}^{\mathrm{L0}} \le P_{i,t,s}^{\mathrm{L}} \le P_{i,t,s}^{\mathrm{L0}}, \, Q_{i,t,s}^{\mathrm{L-}} \le Q_{i,t,s}^{\mathrm{L}} \le Q_{i,t,s}^{\mathrm{L+}} \tag{5.4g}$$

$$(1 - \eta) V^{\mathrm{ref}} \le V_{i,t,s} \le (1 + \eta) V^{\mathrm{ref}} \tag{5.4h}$$

$$\forall i \in \mathscr{I}, \, \forall j \in \mathscr{I}_i, \, t \in \mathscr{T}, \, s \in \mathscr{S}$$

where (5.4b)[3] and (5.4c) represent the power balance and the reactive power balance on bus i at time step t for scenario s. Constraint (5.4d) expresses that the active (or reactive) power flow from bus i to bus j is the reverse of that from bus j to bus i. Constraint (5.4e) calculates the voltage drop between bus i and bus j at time step t for scenario s [18]. Constraints (5.4f)-(5.4g) reflect the maximum and minimum bounds on the active powers of wind farms, photovoltaic farms, and active/reactive power of loads. Constraint (5.4h) describes the voltage bounds, where η is the tolerance level of the voltage deviation (e.g., 0.05).

The PEV charging and charging station constraints can be expressed by:

$$w_{m,t+1} = w_{m,t} + P_{m,t}^{\mathrm{c}}, \, \forall t \in \mathscr{T}', \tag{5.4i}$$

$$\sum_{m \in \mathscr{M}_i} P_{m,t}^{\mathrm{c}} = P_{i,t}^{\mathrm{CH}}, \, \forall i \in \mathscr{I}, \, t \in \mathscr{T} \tag{5.4j}$$

$$P_i^{\mathrm{CH-}} \le P_{i,t}^{\mathrm{CH}} \le P_i^{\mathrm{CH+}}, \, \forall i \in \mathscr{I}, \, t \in \mathscr{T}, \tag{5.4k}$$

$$P_m^{\mathrm{c-}} \le P_{m,t}^{\mathrm{c}} \le P_m^{\mathrm{c+}}, \, m \in \mathscr{M}_i, \, t \in \mathscr{T}, \tag{5.4l}$$

$$w_{m,t} / S_m^{\mathrm{B}} \le \sigma_m, \, m \in \mathscr{M}_i, \, i \in \mathscr{I}, \, t \in \mathscr{T} \tag{5.4m}$$

where constraint (5.4i) derives the SOC status, where the initial SOC is collected from the real-time data collection. Constraint (5.4j) describes the balance between the charging powers of the PEVs and the charging station power. Constraint (5.4k) represents the bounds on the charging power of each charging station. Constraint (5.4l) reflects the charging speed for PEVs in the charging station on bus i. Constraint (5.4m) expresses the SOC bounds.

The vector of the variables considered in (5.4) is $\Phi = [P_{j,i,t,s}, \, P_{i,t,s}^{\mathrm{WT}}, \, P_{i,t,s}^{\mathrm{PV}}, \, P_{i,t,s}^{\mathrm{L}}, \, P_{i,t}^{\mathrm{CH}},$ $Q_{j,i,t,s}, \, Q_{i,t,s}^{\mathrm{L}}, \, V_{i,t,s}, \, w_{m,t}, \, P_{m,t}^{\mathrm{c}}]_{i \in \mathscr{I}, m \in \mathscr{M}_i, j \in \mathscr{I}_i, t \in \mathscr{T}, s \in \mathscr{S}}^{\mathrm{T}}$. From (5.4), it can be observed that the centralized pre-disaster PEV charging problem is a convex quadratic programming problem. For such a problem, efficient algorithms are available, e.g., active-set algorithm [217] or interior point method [85].

---

[3]In (5.4b), $P_{i,t}^{\mathrm{CH}}$ is the total charging power of charging station i, the decision variables are the charging powers of PEVs in charging station i, and they cannot be stochastic. Thus their sum, i.e., $P_{i,t}^{\mathrm{CH}}$, cannot be stochastic.

5.5. DISTRIBUTED PRE-DISASTER PEV CHARGING PROBLEM AND THE AITKEN-DMPC ALGORITHM

5.5.1. DMPC MECHANISM AND PROBLEM FORMULATION

As illustrated in Figure 5.2, the whole micro-grid is divided into several subsystems, namely subsystems for the charging stations (in green) and one subsystem for the main grid (in yellow). Each charging station subsystem agent determines the subsystem-wide optimal charging plans and the main grid subsystem agent determines the optimal power flow in the main grid in parallel. Then, the DMPC approach interconnects the optimal plans for the subsystems to obtain the optimal plan for the whole micro-grid.

Next, the optimization problems solved by subsystem agents are formalized and it is explained how the optimal plans for the subsystems are coordinated to obtain an optimal charging plan for the whole micro-grid. Figure 5.4 shows the system topology after the division into subsystems, and where all the charging stations are connected to the main grid (marked as subsystem 1). In Figure 5.4, the interconnecting variable considered by the agent of subsystem 1 (main grid) is $\widetilde{P}_{i,1}$ (active power from subsystem i to subsystem 1), while the interconnecting variables considered by the agent of subsystem i is $\widetilde{P}_{1,i}$ (active power from subsystem 1 to subsystem i). The aim of the coordination approach of DMPC is to iteratively make the pairs of interconnecting variables, i.e., $\widetilde{P}_{i,1}$ and $-\widetilde{P}_{1,i}$, converge to an optimal value iteration by iteration. In each iteration, the main grid determines $\widetilde{P}_{i,1}$ by receiving the value of $\widetilde{P}_{1,i}$ from the charging station i via communication. Then, it transmits the interconnecting variables that have been determined to the charging station i for use in the next iteration. Next, the charging station i agent determines $\widetilde{P}_{1,i}$ based on the value of $\widetilde{P}_{i,1}$ received from the main grid agent via communication. Then, it transmits the interconnecting variables that were determined to the main grid agent for use in the next iteration[4].

Since the convergence speed of the ordinary Lagrangian decomposition algorithms is slow [126], the augmented-Lagrangian DMPC is applied in this chapter. To further accelerate the convergence speed of the iteration process of augmented-Lagrangian DMPC, the Aitken-DMPC is proposed. Below, the subsystem problems to be considered in iteration k for the main grid and the charging stations are formulated. Then the iteration process will be explained in Section 5.5.2.

CHARGING STATION PROBLEM

For the charging station on bus i (also marked along with subsystem i), the objective function that the agent will consider for iteration k is:

$$\min_{\Omega_{1,i}^{(k)}} J_{\text{local},i}^{(k)} + \sum_{t \in \mathcal{T}} J_{\text{inter},i,t}^{(k)},$$

$$\text{with} \quad J_{\text{local},i}^{(k)} = -\gamma \cdot \sum_{m \in \mathcal{M}_i} \sum_{t \in \mathcal{T}_m} \rho_m (w_{m,t}^{(k)}/S_m^{\text{B}} - \sigma_m), \tag{5.5a}$$

$$J_{\text{inter},i,t}^{(k)} = \widetilde{\lambda}_{1,i,t}^{(k)} \cdot \widetilde{P}_{1,i,t}^{(k)} + \frac{\gamma_{\text{c}}}{2}\left(-\widetilde{P}_{i,1,t}^{(k-1)} - \widetilde{P}_{1,i,t}^{(k)}\right)^2 + \frac{\gamma_{\text{b}} - \gamma_{\text{c}}}{2}\left(\widetilde{P}_{1,i,t}^{(k)} - \widetilde{P}_{1,i,t}^{(k-1)}\right)^2$$

---

[4]Recall that agent 1 (i.e., the main grid agent) can communicate with all charging station agents, but that the charging station agents cannot communicate with each other, because there are no connections between the charging stations (see also Figure 5.2).
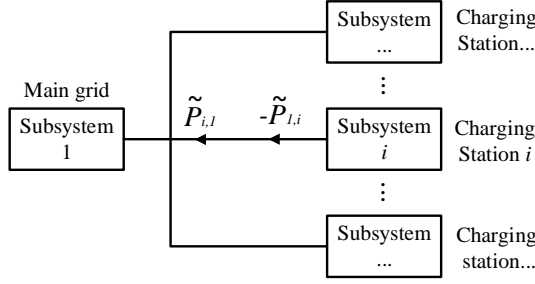
Figure 5.4: Illustration of subsystems and interconnecting variables

where the vector of variables for iteration k considered is $\Omega_{1,i}^{(k)}=[\widetilde{P}_{1,i,t}^{(k)}, w_{m,t}^{(k)}, P_{m,t}^{\mathrm{c},(k)}]_{m\in\mathcal{M}_i, t\in\mathcal{T}}^{\mathrm{T}}$.
To represent the communication between the subsystems, $J_{\mathrm{inter},i,t}^{(k)}$ is the augmented-Lagrangian term with quadratic terms for subsystem i at time step t for iteration k, where $\widetilde{\lambda}_{1,i,t}^{(k)}$ is the Lagrangian multiplier for the interconnecting constraints, $\widetilde{P}_{i,1,t}^{(k-1)}$ and $\widetilde{P}_{1,i,t}^{(k-1)}$ are obtained from the previous iteration, and γ_{b} and γ_{c} are coefficients. Then, the constraints of the charging station on bus i are:

$$\sum_{m\in\mathcal{M}_i} P_{m,t}^{\mathrm{c},(k)} = \widetilde{P}_{1,i,t}^{(k)}, \; P_i^{\mathrm{CH}-} \leq \widetilde{P}_{1,i,t}^{(k)} \leq P_i^{\mathrm{CH}+}, \forall i \in \mathcal{I}, \, t \in \mathcal{T}, \tag{5.5b}$$

$$\text{with } (5.5\text{c}) - (5.5\text{e})$$

where (5.5c)-(5.5e) are similar as (5.4i), (5.4l), and (5.4m). The charging station problems are convex quadratic programming problems.

MAIN GRID PROBLEM

The objective function of the main grid problem (subsystem 1) for iteration k also includes the local terms and the interconnecting terms, which can be represented as:

$$\min_{\Theta^{(k)}} J_{\mathrm{local},1}^{(k)} + \sum_{i\in\mathcal{I}'} \sum_{t\in\mathcal{T}} J_{\mathrm{inter},1,i,t}^{(k)},$$

$$\text{with} \quad J_{\mathrm{local},1}^{(k)} = \mathbb{E}_{\mathcal{S}}\Big(\sum_{t\in\mathcal{T}} c_t \, P_{1,2,t,s} \Big), \tag{5.6a}$$

$$J_{\mathrm{inter},1,i,t}^{(k)} = \widetilde{\lambda}_{i,1,t}^{(k)} \cdot \widetilde{P}_{i,1,t}^{(k)} + \frac{\gamma_{\mathrm{c}}}{2}(-\widetilde{P}_{1,i,t}^{(k-1)} - \widetilde{P}_{i,1,t}^{(k)})^2 + \frac{\gamma_{\mathrm{b}} - \gamma_{\mathrm{c}}}{2}(\widetilde{P}_{i,1,t}^{(k)} - \widetilde{P}_{i,1,t}^{(k-1)})^2$$

where the vector of variables of the optimization problem is $\Theta^{(k)}=[\widetilde{P}_{i,1,t}^{(k)}, P_{j,i,t,s}^{(k)}, P_{i,t,s}^{\mathrm{WT},(k)},$ $P_{i,t,s}^{\mathrm{PV},(k)}, P_{i,t,s}^{\mathrm{L},(k)}, Q_{j,i,t,s}^{(k)}, Q_{i,t,s}^{\mathrm{L},(k)}, V_{i,t,s}^{(k)}]_{i\in\mathcal{I}, j\in\mathcal{I}_i, t\in\mathcal{T}, s\in\mathcal{S}}^{\mathrm{T}}$. The constraints of the problem that will be solved by the main grid agent are:

$$\sum_{j\in\mathcal{I}_i} P_{j,i,t,s}^{(k)} + P_{i,t,s}^{\mathrm{WT},(k)} + P_{i,t,s}^{\mathrm{PV},(k)} = P_{i,t,s}^{\mathrm{L},(k)} - \widetilde{P}_{\mathrm{in},i1,t}^{(k)}, \; \forall i \in \mathcal{I}, \forall j \in \mathcal{I}_i, \, t \in \mathcal{T}, \, s \in \mathcal{S} \tag{5.6b}$$

$$\text{with } (5.6\text{c}) - (5.6\text{h})$$

where (5.6c)-(5.6h) are similar as (5.4c)-(5.4h). The main grid problem is a convex quadratic programming problem.

5.5.2. AITKEN-DMPC ALGORITHM

The process for the main grid agent and the charging station agents to solve their optimization problem at time step t_0 for one prediction window is designed as follows:

Step 1): At time step t_0, each agent collects the real-time data of its own main grid or charging station. For the charging station on bus i, the real-time data includes the set $\mathscr{M}_i$ of PEVs at the charging station on bus i, the set departure time t_m^{d}, the number of delayed time steps ρ_m, and the SOC level w_{m,t_0} for each PEV $m \in \mathscr{M}_i$. For the main grid, the real-time data includes the evacuation decision-making factors (i.e. socio-demographic characteristics, spatio-temporal disaster characteristics, living characteristics, traffic conditions, and psycho-social characteristics), the wind speeds and the solar radiation, the set $\mathscr{N}_{i,t_0,s}$ of residents remaining in the micro-grid for all $s \in \mathscr{S}$, and the present load $P_{i,t_0,s}^{\mathrm{L0}}$ for all $s \in \mathscr{S}$. Then, the agents of the main grid and the charging stations predict the profiles via (5.1)-(5.3).

Step 2): Set the iteration counter k to 1. Initialize the Lagrangian multipliers ($\widetilde{\lambda}_{i,1,t}^{(0)}$ and $\widetilde{\lambda}_{1,i,t}^{(0)}$), $\widetilde{P}_{i,1,t}^{(0)}$ and $\widetilde{P}_{1,i,t}^{(0)}$ as random non-zero values.

Step 3): After receiving $\widetilde{\lambda}_{1,i,t}^{(k)}$, $\widetilde{\lambda}_{i,1,t}^{(k)}$, $\widetilde{P}_{i,1,t}^{(k)}$, and $\widetilde{P}_{1,i,t}^{(k)}$ from the initialization or the previous iteration, the first step in the Aitken algorithm is implemented as:

$$
\begin{aligned}
\hat{\lambda}_{1,i,t}^{(k+1)} &= \widetilde{\lambda}_{1,i,t}^{(k)} + \gamma_{\mathrm{c}}(\hat{P}_{1,i,t}^{(k+1)} + \hat{P}_{i,1,t}^{(k+1)}) \\
\hat{\lambda}_{i,1,t}^{(k+1)} &= \widetilde{\lambda}_{i,1,t}^{(k)} + \gamma_{\mathrm{c}}(\hat{P}_{i,1,t}^{(k+1)} + \hat{P}_{1,i,t}^{(k+1)})
\end{aligned}
\tag{5.7a}
$$

where $\hat{P}_{1,i,t}^{(k+1)}$ and $\hat{P}_{i,1,t}^{(k+1)}$ are obtained by solving problems (5.5) and (5.6) using $\widetilde{\lambda}_{1,i,t}^{(k)}$, $\widetilde{\lambda}_{i,1,t}^{(k)}$, $\widetilde{P}_{i,1,t}^{(k)}$, and $\widetilde{P}_{1,i,t}^{(k)}$.

Step 4): After receiving $\hat{\lambda}_{1,i,t}^{(k+1)}$, $\hat{\lambda}_{i,1,t}^{(k+1)}$, $\hat{P}_{1,i,t}^{(k+1)}$, and $\hat{P}_{i,1,t}^{(k+1)}$ from the first step in Aitken acceleration, the second step in Aitken acceleration is implemented as:

$$
\begin{aligned}
\overline{\lambda}_{1,i,t}^{(k+1)} &= \hat{\lambda}_{1,i,t}^{(k+1)} + \gamma_{\mathrm{c}}(\overline{P}_{1,i,t}^{(k+1)} + \overline{P}_{i,1,t}^{(k+1)}) \\
\overline{\lambda}_{i,1,t}^{(k+1)} &= \hat{\lambda}_{i,1,t}^{(k+1)} + \gamma_{\mathrm{c}}(\overline{P}_{i,1,t}^{(k+1)} + \overline{P}_{1,i,t}^{(k+1)})
\end{aligned}
\tag{5.7b}
$$

where $\overline{P}_{1,i,t}^{(k+1)}$ and $\overline{P}_{i,1,t}^{(k+1)}$ are obtained by solving problems (5.5) and (5.6) using $\hat{\lambda}_{1,i,t}^{(k+1)}$, $\hat{\lambda}_{i,1,t}^{(k+1)}$, $\hat{P}_{1,i,t}^{(k+1)}$, $\hat{P}_{i,1,t}^{(k+1)}$.

Step 5): Then, the Lagrangian multipliers and the interconnecting variables are updated for the next iteration:

$$
\widetilde{\lambda}_{1,i,t}^{(k+1)} = \overline{\lambda}_{1,i,t}^{(k+1)} - \frac{(\overline{\lambda}_{1,i,t}^{(k+1)} - \hat{\lambda}_{1,i,t}^{(k+1)})^2}{\overline{\lambda}_{1,i,t}^{(k+1)} - 2 \cdot \hat{\lambda}_{1,i,t}^{(k+1)} + \widetilde{\lambda}_{1,i,t}^{(k)}}, \quad
\widetilde{\lambda}_{i,1,t}^{(k+1)} = \overline{\lambda}_{i,1,t}^{(k+1)} - \frac{(\overline{\lambda}_{i,1,t}^{(k+1)} - \hat{\lambda}_{i,1,t}^{(k+1)})^2}{\overline{\lambda}_{i,1,t}^{(k+1)} - 2 \cdot \hat{\lambda}_{i,1,t}^{(k+1)} + \widetilde{\lambda}_{i,1,t}^{(k)}}
$$

$$
\widetilde{P}_{1,i,t}^{(k+1)} = \overline{P}_{1,i,t}^{(k+1)} - \frac{(\overline{P}_{1,i,t}^{(k+1)} - \hat{P}_{1,i,t}^{(k+1)})^2}{\overline{P}_{1,i,t}^{(k+1)} - 2 \cdot \hat{P}_{1,i,t}^{(k+1)} + \widetilde{P}_{1,i,t}^{(k)}}, \quad
\widetilde{P}_{i,1,t}^{(k+1)} = \overline{P}_{i,1,t}^{(k+1)} - \frac{(\overline{P}_{i,1,t}^{(k+1)} - \hat{P}_{i,1,t}^{(k+1)})^2}{\overline{P}_{i,1,t}^{(k+1)} - 2 \cdot \hat{P}_{i,1,t}^{(k+1)} + \widetilde{P}_{i,1,t}^{(k)}}
\tag{5.7c}
$$

Step 6): Let $k \leftarrow k+1$ and repeat Steps 3) to 5) until one of the following termination conditions is met:

$$
\max\left\{ \mid \widetilde{\lambda}_{1,i,t}^{(k+1)} - \widetilde{\lambda}_{1,i,t}^{(k)} \mid_{i \in \mathscr{I}', t \in \mathscr{T}}, \mid \widetilde{\lambda}_{i,1,t}^{(k+1)} - \widetilde{\lambda}_{i,1,t}^{(k)} \mid_{i \in \mathscr{I}', t \in \mathscr{T}} \right\} \le \epsilon
\tag{5.8}
$$

where ϵ is a small positive value.

Remark 3 *In (5.7c), when the Lagrangian multipliers and the interconnecting variables converge to the optimal solution, the denominators may approximate to zero. If the value of the denominator in (5.7c) is small, we get very large multipliers, which causes numerical issues. These numerical issues may disrupt the iteration processes. Since the bounds on multipliers can ruin the convergence according to the simulation results, in the revised version of our chapter, we propose a method to avoid the emergence of very large values without using bounds on multipliers.*

If the absolute value of the denominator in (5.7c), i.e., $|\overline{\lambda}_{1,i,t}^{(k+1)} - 2 \cdot \hat{\lambda}_{1,i,t}^{(k+1)} + \widetilde{\lambda}_{1,i,t}^{(k)}|$, is smaller than a threshold value, the Lagrangian multiplier or the interconnecting variable at the left-hand-side of this equation is set equal to the value of the last iteration. For example, if $|\overline{\lambda}_{1,i,t}^{(k+1)} - 2 \cdot \hat{\lambda}_{1,i,t}^{(k+1)} + \widetilde{\lambda}_{1,i,t}^{(k)}| \leq \varphi$, then $\widetilde{\lambda}_{1,i,t}^{(k+1)}$ takes the value of the last iteration, i.e., $\widetilde{\lambda}_{1,i,t}^{(k)}$.

5.6. Case study

5.6.1. Settings and parameters

The case study involves the modified IEEE-13 bus micro-grid in Figure 5.2. Different from the IEEE-13 bus network used in [180], four charging stations, two photovoltaic farms and a small-scale wind farm are added to create a micro-grid integrated with heterogeneous renewable energy sources. The rated powers of photovoltaic farm 1, photovoltaic farm 2 and the wind farm are 200 kW, 250 kW, and 200 kW respectively. Furthermore, there are 693 households in total (marked in Figure 5.2) and each household consumes 5 kW on average. The vehicle occupation rate is 84.2% and the electrical vehicle rate among the vehicles is 30% (i.e., 175 PEVs in this case study). There are three types of PEVs, marked as PEV1, PEV2, and PEV3, whose battery capacities are 8 kWh, 18 kWh, 48 kWh, with maximum charging powers of 1.6 kW, 3.6 kW, and 9.6 kW, corresponding to 20%, 60%, and 20% of the total number of PEVs respectively. The maximum charging SOC is 90% while the minimum charging SOC is 20%. The number of charging piles and the maximum charging powers for charging stations are 20/52/73/30 and 35/60/80/25 kW respectively, which are *sufficient* for meeting the *daily* departure demands.

The tested disaster is the Ivan hurricane that occurred in Alabama, the USA in September 2004. Ivan made landfall in Alabama at 2 a.m. on September 16, 2004, and the warning was broadcast 30 h before the landfall (i.e. 9 p.m. on September 14, 2004). The data for evacuation decision-making factors are collected from [179] and are used in (5.1). The data collected from [179] are the real data during the Ivan hurricane in September 2004. The time step for the charging control procedure is 15 min and one prediction window is 12 hours.

Furthermore, the proposed Aitken-DMPC algorithm is compared with the DA-DMPC algorithm on the convergence speed. Note that, as mentioned in Section 5.5.1, the charging planning problems are convex quadratic programming problem. According to the simulation results, both the Aitken-DMPC and the DA-DMPC algorithms always converge to the optimal solution. Thus, the optimality of Aitken-DMPC versus DA-DMPC
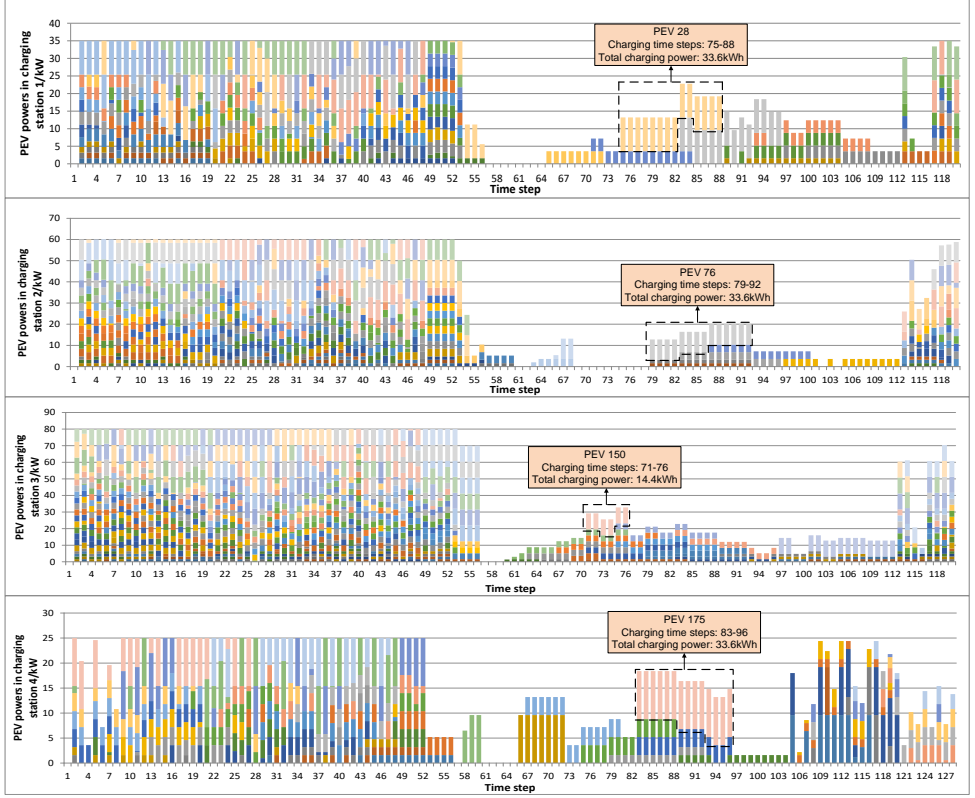
Figure 5.5: Charging power results for four charging stations (Bars with different colors represent different PEVs.)

is not compared and shown further here. The process of the DA-DMPC algorithm will only implement Step 3), instead of Steps 3) to 5) as in the process of the Aikten-DMPC algorithm, and it takes $\hat{\lambda}_{1,i,t}^{(k+1)}$, $\hat{\lambda}_{i,1,t}^{(k+1)}$, $\widetilde{P}_{i,1,t}^{(k)}$, and $\widetilde{P}_{1,i,t}^{(k)}$ as the inputs of the next iteration until the termination condition (5.8) is satisfied[5]. All of the simulations are performed on the MATLAB 2020a platform with a Core i5-8250U CPU @1.60 GHz and 8 GB RAM. The quadratic programming problems are solved by the "interior-point-convex" algorithm implemented by the "quadprog" function in Matlab. The values of the coefficients are $\gamma = 10000$, $\alpha = 0.8$, $\eta = 0.05$, $\sigma_m = 0.9$, $\gamma_b = 5$, $\gamma_c = 2$, $\varphi = 100$, $\epsilon_1 = 0.1$, and $\epsilon_2 = 10^{-6}$.

5.6.2. PREDICTION AND CHARGING RESULTS

The results of the charging powers at the four charging stations obtained with the proposed Aitken-DMPC algorithm are shown in Figure 5.5. In Figure 5.5, the horizontal axis represents the number of time steps (15 min) after the broadcast disaster warning. Bars with different colors in Figure 5.5 represent different PEVs. From Figure 5.5, it can be

---

[5] The detailed process of the DA-DMPC algorithm can also be found in [182] and [154].

(a) Load process

(b) Number of set departure times for each time step
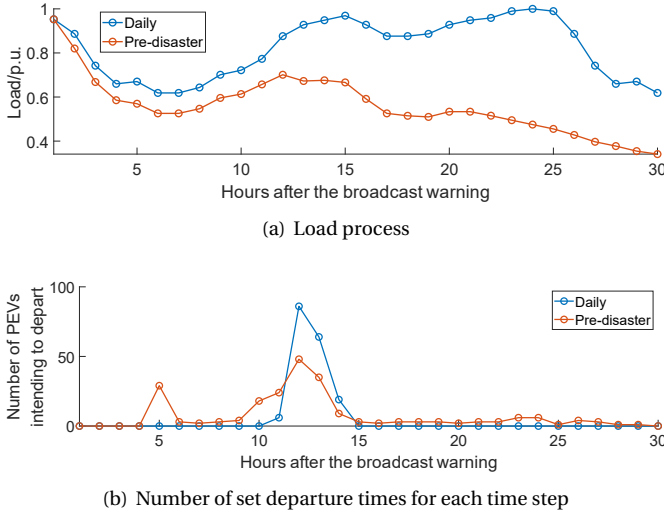
Figure 5.6: Load profile and the number of set departure times
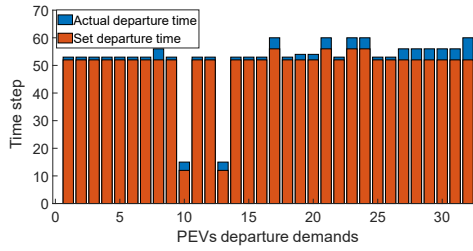
Figure 5.7: Departure demands of PEVs

observed that most charging actions of the PEVs occur during the night hours (8 p.m.-8 a.m.), while a small number of charging actions occur during the daytime. That is mainly because, during the daytime, some residents leave their residential areas to go to work using their EVs. In addition, our charging control strategy is for charging stations in residential areas. Thus, there will be lower charging demands in residential areas during the daytime, and consequently, the charging power levels will be lower. During the night time, i.e., time steps 112-118, after the residents have arrived home, the charging powers of the residential areas will increase. Thus, the charging powers during the night time are higher than those in the daytime. Furthermore, it can also be observed that there are more charging actions for the first night from time step 1 to time step 48 (9 p.m. on September 14 to 8 a.m. on September 15) than those for the second night from time steps 96 to time step 120 (9 p.m. on September 15 to 2 a.m. on September 16), resulting from the PEV owners leaving for evacuation. Furthermore, in time steps 10 to 52, the charging powers of four charging stations reach their charging capacities. This shows that the charging demands in this period are no less than the charging capacities of the
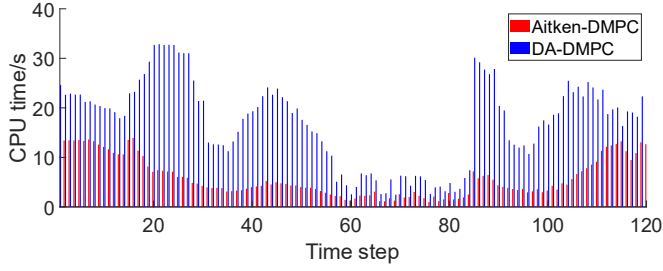
Figure 5.8: CPU times of the Aitken-DMPC algorithm and the DA-DMPC algorithm

charging stations. However, in other time steps, the charging capacities of the charging stations can cover the charging demands.

In Figure 5.6(a), the load profile for the whole pre-disaster process from the broadcast warning on is shown (30 hours). It can be observed that the pre-disaster load profile is distinguished from the daily profile especially when more households evacuate from the micro-grid. In this case, when Ivan landfall occurs, the number of the remaining households is approximately 40% of the number of households in the daily case. Furthermore, the gaps between the load profiles of the daily and pre-disaster situations enlarge over time. These two observations show that considering the human behavior in the load prediction for pre-disaster evacuation situations is necessary. Figure 5.6(b) shows the numbers of PEVs intending to depart in the pre-disaster period. From Figure 5.6(b), it can be observed that in pre-disaster cases, the PEV owners will set different departure times than in their daily cases. A small group of PEV owners intend to depart for evacuation during the early mid-night as observed by the first peak in Figure 5.6(b). This first peak results from the fact that at least 5 hours is required for the PEVs to be fully charged. Furthermore, a few of the PEV owners intend to depart for evacuation in the late-midnight, and then another group of PEV owners intend to depart early in the morning both for evacuation and daily activities. Although in the daily case, the departure demands can be satisfied, in pre-disaster cases, the unmet departure demands emerge as a result of that difference.

Moreover, Figure 5.7 shows the unmet departure demands of the PEVs that cannot depart at their set departure time for the proposed Aitken-DMPC algorithm. From Figure 5.7, it can be observed that, due to the different departure demands for the evacuation situations with the daily situations, the unmet departure demands emerge even though the power settings of the charging stations are sufficient for the daily situations. In Figure 5.7, there is a total of 32 PEVs delayed for departure (departures for both evacuation and daily use), and the more urgently the PEV's departure is (e.g., for PEVs 10 and 13), the earlier they get charged. Furthermore, no PEV is critically delayed. Thus, the proposed charging strategy for pre-disaster evacuation situations is fair for PEV owners.

5.6.3. COMPARISON OF THE ALGORITHMS

Since both the Aitken-DMPC and the DA-DMPC algorithms can converge to the optimal solution, in this subsection, we only compare the convergence speed between Aitken-
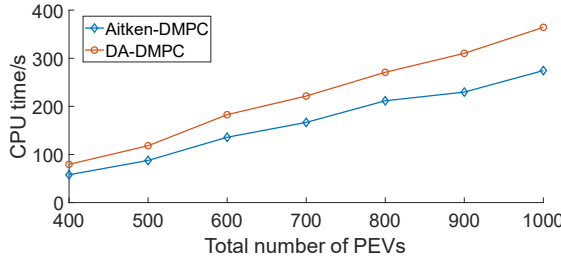
Figure 5.9: Comparison of the CPU times of the large-scale cases

DMPC and DA-DMPC. Simulating 30 h represents 120 time steps in total. For all the 120 simulations, the comparisons of the CPU times between the Aitken-DMPC algorithm and the DA-DMPC algorithm are shown in Figure 5.8. Note that, since the charging problems of time steps 57-84 involve several PEVs, the planning problems at these time steps are solved faster than at other time steps. Furthermore, the optimal solutions of the subsystem problems are determined by the interior-point-convex method via MATLAB (with default settings of the function "quadprog").

From Figure 5.8, it can be observed that in all the simulations, the Aitken-DMPC algorithm is faster than the DA-DMPC algorithm. The average CPU time gap in percentage between the Aitken-DMPC algorithm and the DA-DMPC algorithm is -63.89% in 120 simulations. Note that the CPU time gap in percentage of one simulation is obtained as the CPU time of Aitken-DMPC minus the CPU time of DA-DMPC and divided by the CPU time of DA-DMPC. Thus, the proposed Aitken-DMPC algorithm is more efficient for solving the charging problems than the DA-DMPC algorithm.

5.6.4. LARGE-SCALE CASES FOR ALGORITHM COMPARISON

Apart from the small-scale cases, the larger-scale cases are also tested to further study the performance of our proposed Aitken-DMPC. In the larger-scale cases, we still use the network in Figure 5.2, but the total PEV numbers are increased from 400 to 1000. These PEVs in the larger-scale cases are averagely distributed to the four charging stations. More specifically, the numbers of PEVs in charging stations are 100 to 250 for large-scale cases with 400 to 1000 PEVs in total. The values of the parameters S^B, P^{CH+}, and t^d in the larger-scale cases are equal to their values of the small-scale cases multiplying a number selected randomly from uniform random distributions ranged 0 to 2. Both Aitken-DMPC and DA-DMPC converge to the optimal solution for all cases. The simulation results of the CPU times for larger-scale cases are shown in Figure 5.9.

In Figure 5.9, the CPU time reduction ratios for Aitken-DMPC are 27.29%, 25.86%, 25.67%, 24.73%, 21.86%, 25.97%, and 24.66% respectively for cases with 400 to 1000 PEVs. So in these larger-scale cases, Aitken-DMPC still converges faster to the optimal solution than DA-DMPC. Furthermore, it can be observed that the gaps between the CPU times of Aitken-DMPC and DA-DMPC majorly increase with the total number of PEVs. This observation indicates that, in this case study, the CPU time reductions of the proposed Aitken-DMPC algorithm is more significant for optimization problems with larger scales.

5.7. CONCLUSIONS AND FUTURE WORK

This chapter has proposed a PEV charging strategy for pre-disaster evacuation situations and a novel acceleration Aitken-DMPC algorithm to solve the formulated charging problems. The proposed PEV charging control strategy can handle charging planning for pre-disaster evacuation situations by accounting for human evacuation behavior, and it can handle the unmet departure demands of the PEVs fairly by adding a penalty mechanism in the formulated charging planning problem. For the proposed Aitken-DMPC algorithm, according to the simulation results, the CPU times of the proposed Aitken-DMPC algorithm are shorter than those of the widely used DA-DMPC algorithm. Furthermore, the average CPU time reduction ratio for Aitken-DMPC with respect to DA-DMPC is -63.89%.

Future work will involve modeling the behavior of residents who decide not to evacuate, e.g., what activities they may do and when, and what the resulting load profiles will be. Then, the places the evacuated residents would go to, and the charging for the evacuating EVs from other areas will also be considered in the PEV charging problem. The load profile will be generated via the combined method of the simulation-based and learning-based methods. Furthermore, the current approach will be extended to also include charging control at workplaces for pre-disaster situations. In addition, the theoretical investigation of the convergence properties of Aitken-DMPC will be explored.

5.A. APPENDIX I: CONVERGENCE OF THE PROPOSED AITKEN-DMPC

In the current literature, the theoretical proof of the convergence of the DA-DMPC algorithm (for a system with more than two sub-systems) to the global optimal solution is still an open problem [44], [118], [154]. Since a residential distributed network mostly has more than one charging station, the PEV charging strategy involves more than two sub-systems (one distributed network and at least one charging station). Thus, at present, there are no theoretical guarantees for the convergence of DA-DMPC for general charging control problems whose parameters can be selected as arbitrary real values. In case our proposed Aitken-DMPC is based on DA-DMPC, the theoretical guarantees for the convergence of Aitken-DMPC for general charging control problems whose parameters can be selected as arbitrary real values. In literature, one then may resort to numerical experiments to give an impression of convergence properties for the DMPC algorithms for a system with more than two sub-systems. In this context, from the simulations results of hundreds of runs for both the small-scale cases (Section 5.6.2 and Section 5.6.3) and the larger-scale cases (Section 5.6.4), we saw that both DA-DMPC and Aitken-DMPC always converged to the global optimal solutions.

5.B. APPENDIX II: CONVERGENCE AND γ_b AND γ_c

To check whether $\gamma_b \geq 2\gamma_c$ is also a proper setting in the case of this chapter, we have tested several combinations of γ_b and γ_c on the charging problem at time step 1. The
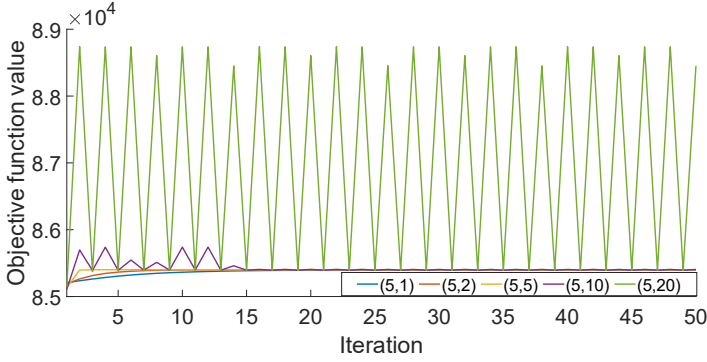
Figure 5.10: Coefficients γ_b and γ_c and convergence ("(x,y)" represents $\gamma_b = x$ and $\gamma_c = y$)
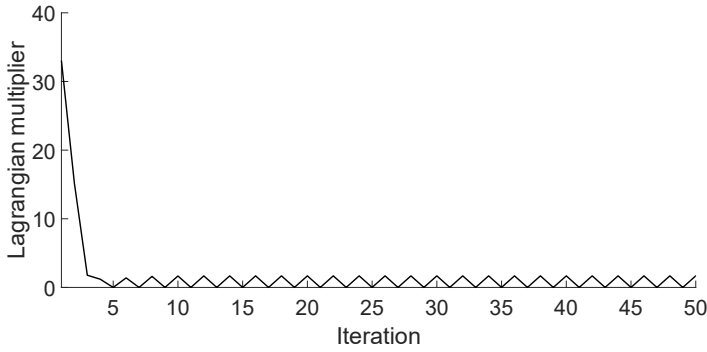
Figure 5.11: Lagrangian multiplier of subsystem 4 at time step 14 with $\gamma_b = 5$ and $\gamma_c = 5$

results are shown in Figure 5.10.

In Figure 5.10, "(x,y)" represents $\gamma_b = x$ and $\gamma_c = y$. Five different combinations of γ_b and γ_c are tested. It can be observed from Figure 5.10 that when the ratio between γ_b and γ_c increases, the curves converge to the global optimal value with less fluctuations. In the case that $\gamma_b = 5$ and $\gamma_c = 20$, the curve does not converge to the global optimal value. Furthermore, the curve of the case $\gamma_b = 5$ and $\gamma_c = 10$ also has large fluctuations and the objective function value does not converge to the optimal solution. Regarding the situation with $\gamma_b = 5$ and $\gamma_c = 5$, although the objective function value converges to the optimal solution, the Lagrangian multipliers do not. The Lagrangian multiplier of subsystem 4 at time step 14 with $\gamma_b = 5$ and $\gamma_c = 5$ is shown in Figure 5.11. In Figure 5.11, the Lagrangian multiplier does converge in 50 iterations, although the objective function value converges. Thus, in our case, we still adopt the empirical guideline to select γ_b and γ_c such that $\gamma_b \geq 2\gamma_c$, e.g., $\gamma_b = 5$ and $\gamma_c = 2$.

5.C. APPENDIX III: CONSIDERATION OF HOUSEHOLD BATTER-IES

In some situations, the residents who do not intend to evacuate may choose to charge their household batteries. Thus, the total charging demand of the household battery and the PEVs thus may increase. Consequently, the shortage of charging power will increase. Thus, considering the charging power of the household battery will further stress the need for an accurate charging demand prediction as proposed in this chapter. It is easy to include this effect by modifying the constraints and the objective function of the main grid. The objective function can be changed into:

$$
J = \min_{\Phi} \mathbb{E}_{\mathscr{S}} \Bigg(\sum_{t \in \mathscr{T}} (c_2 P_{1,2,t,s}^2 + c_1 P_{1,2,t,s}) - \gamma \sum_{m \in \mathscr{M}} \sum_{t \in \mathscr{T}_m^r} (\rho_m + 1) \Big(\frac{w_{m,t}}{S_m^B} - \sigma_m \Big) +
$$
$$
\gamma' \sum_{i \in \mathscr{I}} \sum_{h \in \mathscr{H}_i} (w_{i,h,t_0+T_D}^H - w_{i,h}^{H0}) \Bigg) \tag{5.9a}
$$

where $\mathscr{H}_i$ is the set of household batteries on bus i, $w_{i,h,t_0+T_D}^H$ is the state of charge of battery h on bus i at time step $t_0 + T_D$ (the last time step of the prediction horizon), $w_{i,h}^{H0}$ is the state of charge when household battery h on bus i is fully charged. Furthermore, two new constraints should be added:

$$
w_{i,h,t-1}^H + P_{i,h,t}^H = w_{i,h,t}^H, \ \forall i \in \mathscr{I}, h \in \mathscr{H}_i, t \in \mathscr{T} \tag{5.9n}
$$

$$
\sum_{h \in \mathscr{H}_i} P_{i,h,t}^H + P_{i,t,s}^L = P_{i,t,s}^{TL}, \ i \in \mathscr{I}, t \in \mathscr{T}, s \in \mathscr{S} \tag{5.9o}
$$

where $w_{i,h,0}^H$ is the initial state of charge of the battery h on bus i, $P_{i,h,t}^H$ is the charging power of battery h on bus i at time step t, $P_{i,t,s}^{TL}$ is the total load power (including the household use and the household battery charging) of bus i at time step t for scenario s. Then constraint (5.9b) should also be modified:

$$
\sum_{j \in \mathscr{Z}_i} P_{j,i,t,s} + P_{i,t,s}^{WT} + P_{i,t,s}^{PV} = P_{i,t,s}^{TL} + P_{i,t}^{CH}, \ \forall i \in \mathscr{I}, h \in \mathscr{H}_i, t \in \mathscr{T}, s \in \mathscr{S} \tag{5.9b}
$$

Finally, (5.9a) to (5.9o) constitute the new problem considering the effect of charging household batteries, where (5.9c) to (5.9m) are the same with (5.4c) to (5.4m). This newly formulated problem is still a quadratic programming problem.

Nomenclature

i	Bus index
j	Neighbor bus index
m	PEV index
n	Resident index
s	Scenario index
t	Time step index
$\mathcal{I}$	Set of buses
$\mathcal{M}$	Set of residents
$\mathcal{M}_i$	Set of residents on bus i
$\mathcal{N}_{i,t,s}$	Set of residents on bus i at time step t for scenario s
$\mathcal{S}$	Set of scenarios
$\mathcal{T}$	Set of time steps
$\mathcal{T}_m$	Subset of time steps in the prediction window after the set departure time step of PEV m
$\mathcal{I}_i$	Set of neighbor buses of bus i
Φ	Set of variables
c_2, c_1	Energy generation cost coefficients for thermal generators
$I_{i,t,s}^{\mathrm{PV}}$	Solar radiation of the photovoltaic farm on bus i at time step t for scenario s
$p_{n,i,t,s}^{\mathrm{r}}$	Probability resident n on bus i will evacuate at time step t for scenario s
$P_m^{\mathrm{c-}}, P_m^{\mathrm{c+}}$	Minimum and maximum charging powers of PEV m
$P_i^{\mathrm{CH-}}, P_i^{\mathrm{CH+}}$	Minimum and maximum charging powers of the charging station on bus i
$P_{i,t,s}^{\mathrm{L0}}$	Total rated load on bus i at time step t for scenario s
$P_{n,i,t,s}^{\mathrm{Lbase}}$	Load of resident n on bus i at time step t for scenario s
$P_{i,t,s}^{\mathrm{WT0}}$	Maximum generation powers of the wind farm on bus i at time step t for scenario s

$P_{i,t,s}^{\mathrm{PV0}}$	Maximum generation powers of the photovoltaic farm on bus i at time step t for scenario s
$Q_{i,t,s}^{\mathrm{L-}}$, $Q_{i,t,s}^{\mathrm{L+}}$	Minimum and maximum reactive powers for loads on bus i at time step t for scenario s
$R_{i,j}$	Resistant of transmission line between bus i and j
S_m^{B}	Maximum capacity of the battery in PEV m
t_0	Starting time step of the prediction window
t_m^{d}	Departure time of PEV m set by its owner
T_{D}	Number of time steps in one prediction window
$v_{i,t,s}^{\mathrm{w}}$	Wind speed of the wind farm on bus i at time step t for scenario s
V^{ref}	Reference voltage
$X_{i,j}$	Reactance of transmission line between bus i and j
$Y_{n,i,t,s}$	Parameter vector for resident n on bus i at time step t for scenario s
α	Demand response tolerance level
β_t	Parameter vector of coefficients at time step t
η	Tolerance level of voltage deviation
γ	Weight of penalty of the unmet departure demands
ρ_m	Number of delayed time steps for PEV m caused by unmet departure demands
σ_m	State of charge level in percentage of fully charged that is set by the owner of PEV m
J	Objective function value
$P_{i,j,t,s}$	Active power flow from bus i to bus j at time step t for scenario s
$P_{m,t}^{\mathrm{c}}$	Charging power of PEV m at time step t
$P_{i,t}^{\mathrm{CH}}$	Active power of the charging station on bus i at time step t
$P_{i,t,s}^{\mathrm{L}}$	Active power of the load on bus i at time step t for scenario s
$P_{i,t,s}^{\mathrm{PV}}$	Active power of the photovoltaic farm on bus i at time step t for scenario s
$P_{i,t,s}^{\mathrm{WT}}$	Active power of the wind farm on bus i at time step t for scenario s

$Q_{i,j,t,s}$	Reactive power flow from bus i to bus j at time step t for scenario s
$Q^{\text{L}}_{i,t,s}$	Reactive power of the load on bus i at time step t for scenario s
$V_{i,t,s}$	Voltage on bus i at time step t for scenario s
$w_{m,t}$	Actual stored energy in PEV m at time step t

5

6

ACCURATE FAULT LOCATION ALGORITHM CONSIDERING UNCERTAINTY IN MEASUREMENTS

6.1. INTRODUCTION

Fault location algorithms for transmission lines are used to locate the fault after a fault along the transmission line has occurred and they are operated by protection relay devices [39], [46], [101], [191]. After that, the maintenance team of the transmission line operator searches the area near the located spot that is calculated by fault location algorithms to find out where exactly the fault is, and then performs maintenance actions to resolve the fault. For a given transmission line, a large deviation between the exact fault location and the evaluated fault location may emerge when the evaluated location is derived from an inaccurate fault location algorithm. This deviation will enlarge the search burden, searching costs, and the unavailability period of the faulty transmission line. For example, for a 300 km long transmission line lying beneath the continental shelf in a sea area, a 1% deviation in the location will give rise to a ±3 km gap between the exact fault location and the evaluated fault location and searching such a large area in the sea is extremely costly. Thus, the accuracy of the fault location algorithm is very relevant for the reduction of the costs in power system maintenance [58], [202].

At present, in the literature on fault location algorithms, factors related the inaccuracy of the fault location algorithms are discussed and analyzed as follows:

Firstly, the generation of the DC offset and harmonics during the fault transient stage by the faults results in inaccuracy of the voltage and current phasor calculations and thus inaccuracy of the fault location algorithms [16], [114], [125], [183], [189], [197]. These factors are usually considered as additional signals added to the fundamental signals. Thus, the solution approach to address this factor is mainly related to signal transformations (or filters). For example, the paper [189] proposes a new application of Park's

---

This chapter is based on [76].

transformation to calculate fundamental components among the sampled voltages and currents that are distorted by the DC offset and harmonics. The authors of [197] propose a method for phasor calculation of the fundamental component by obtaining the DC amplitude from the Hilbert transform and the fault current signals within 20 ms. The paper [16] proposes a method for removing the exponential component among the electrical signals in the transient stage to evaluate the fundamental frequency phasor.

Secondly, noise and disturbances caused by the external environment also result in inaccuracy of fault location algorithms [55], [122]. This factor is usually addressed by robust filters or transformations. For example, the paper [55] proposes an approach for the protection of parallel transmission lines by using the S-transform that is an extension of the wavelet transform. The test results show the robustness of the proposed algorithm by adding significant noise to the simulated voltage and current. In [122] a pattern recognition approach with a new S-transform method is proposed by using different types of techniques, e.g. frequency scaling, to reduce the computational cost and to remove redundant information. The simulation results show the robustness of the proposed algorithm in an environment with significant noise.

It can be concluded that the influences of the DC offset and harmonics during the transient stages on the fault location algorithms can be reduced in a systematic way by using a patched algorithm, and that the influence of some noises and disturbances can be reduced by designing a more robust algorithm. Apart from these factors, the fault location algorithms are also influenced by inaccuracies regarding the values of the transmission line parameters. For example, a transmission line might be put into practice in summer and the parameters are measured and recorded before its putting into use. Then under a fault occurs in winter, the fault location results are no longer accurate when the parameters recorded in summer are used. In addition, the inaccuracies of the parameters may also result from different humidity and temperature circumstances. However, these factors can be addressed by the increasing popularization of phasor measurement units (PMUs) that are installed at the terminal(s) of the transmission line. Installed PMUs can measure the transmission line parameters continuously by using the voltage and current phasors collected and calculated from the instruments and the computing unit inside the PMUs [31], [110], [167]. However, the uncertainty in PMU measurements emerges during the calculation of the phasors, which will lead to inaccuracies of the calculated transmission line parameters. For example, papers [19], [143], [171], [187] reveal the uncertainty phenomena and mechanisms during the transmission line measurement by PMUs. In paper [171] the systematic errors in the measurements are assumed to be constant values when calculating the transmission line parameters. However, [19], [140], [143], [187] reveal that the error between the exact value and the measured value cannot be properly evaluated nor corrected because of the multitude of influential factors, e.g. humidity, temperature, and load level on top of the systematic errors; the authors of [19], [140], [143], [187] recommend to use the uncertainty to describe the possibility distribution of the error in the measurements. In [19], [187], the bounds of the uncertainties in the measurements are analyzed and calculated for ensuring the reliability of protection relay algorithms. However, these bounds cannot be applied in fault location algorithms because the bounds will lead to conservative results. In addition, [196], [230] have analyzed the influence of all the uncertainties of the transmission
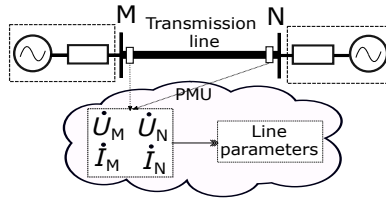
Figure 6.1: Mechanism for estimations of line parameters

line parameters on fault location algorithms, but they do not model the uncertainty in the measurement specifically nor do they propose a method to calculate and reduce the influence due to the uncertainties in the measurements of PMUs on transmission line parameters.

Thus, it can be concluded from the literature a lot of work still needs to be done on the analysis of the influence of the uncertainty in the measurements on the behavior of fault location algorithms. Further, the uncertainty in the measurements should be addressed properly. Both topics will be addressed in this chapter. Thus, the contribution of the chapter can be summarized as follows: firstly, we analyze the influence of the uncertainty in the measurements on the fault location algorithms based on a case study; secondly, we model the uncertainty in the measurements of PMUs based on the information supplied by the PMU supplier, or by a newly proposed method based on the confidence level and deviation bounds if the information on the distributions of the uncertainties is not available; thirdly, we propose an estimation method based on maximum likelihood estimation (MLE) that can effectively reduce the uncertainty in the measurements when determining the transmission line parameters.

The chapter is organized as follows: In Section 6.2, the modeling method for the uncertainty in the transmission line parameter measurements is introduced. In Section 6.3, a method is proposed to obtain the distributions of the uncertainties based on the data provided by the device supplier or by using big data methods. In Section 6.4, a method is given to reduce the influence of the uncertainty in the measurements. In Section 6.5, a case study is presented to show and analyze the influence of the uncertainty in the measurements on the two-terminal positive sequence network fault location algorithm as well as the effectiveness of the proposed method. In Section 6.6 conclusions are drawn and some topics for future work are discussed.

6.2. TRANSMISSION LINE PARAMETERS CALCULATION MODEL WITH UNCERTAINTIES

The transmission line parameters measurement process is shown in Figure 6.1. In Figure 6.1, the voltage and current phasors from the M and N terminals of the line are marked as $\dot{U}_M$, $\dot{U}_N$, $\dot{I}_M$, and $\dot{I}_N$. The phasors collected from the PMUs at the two terminals will be used to calculate the transmission line parameters. In the view of the single phase of the transmission line [109], [198], the telegrapher's equation of the voltage and current phasor from both two terminals can be described as:

$$\begin{cases} \dot{U}_M = \dot{U}_N \cosh(\gamma D) - \dot{I}_N z_c \sinh(\gamma D) \\ \dot{I}_M = \dot{U}_N \sinh(\gamma D)/z_c - \dot{I}_N \cosh(\gamma D) \end{cases} \tag{6.1}$$

where γ is the propagation constant of the transmission line, and z_c is the characteristic impedance of the transmission line, and D is the length of the transmission line. According to (6.1), γ and z_c can be obtained as:

$$\begin{cases} \gamma = \dfrac{1}{D} \cosh^{-1} \dfrac{\dot{U}_M \dot{I}_M - \dot{U}_N \dot{I}_N}{\dot{U}_N \dot{I}_M - \dot{U}_M \dot{I}_N} \\ z_c = \sqrt{(\dot{U}_M^2 - \dot{U}_N^2)/(\dot{I}_M^2 - \dot{I}_N^2)} \end{cases} \tag{6.2}$$

Thus, the transmission line parameters of the positive sequence network can be derived as [96], [210], [242]:

$$\begin{cases} z_1 = \gamma z_c = r_1 + i x_1 \\ y_1 = \gamma/z_c = i b_1 \end{cases} \tag{6.3}$$

where z_1 and y_1 are respectively the positive sequence impedance and admittance of the unit length; r_1, x_1, and b_1 are the positive sequence resistance, reactance, and conductance; and i represents the unit imaginary number. It should be mentioned that because the value of the susceptance is rather small, the susceptance is neglected mostly in fault location algorithms for transmission lines. Thus, we do not consider the susceptance. Thus, z_1 and y_1 can be obtained based on (6.2) and (6.3), such that

$$\begin{cases} z_1 = r_1 + i x_1 = \gamma z_c \\ y_1 = i b_1 = \gamma/z_c \\ \gamma = \dfrac{1}{D} \cosh^{-1} \left(\dfrac{U_M I_M \angle(\theta_M + \phi_M) - U_N I_N \angle(\theta_N + \phi_N)}{U_N I_M \angle(\theta_N + \phi_M) - U_M I_N \angle(\theta_M + \phi_N)} \right) \\ z_c = \sqrt{\dfrac{(U_M)^2 \angle(2\theta_M) - (U_N)^2 \angle(2\theta_N)}{(I_M)^2 \angle(2\phi_M) - (I_N)^2 \angle(2\phi_N)}} \end{cases} \tag{6.4}$$

However, the error between the exact value and measured value should be considered in order to obtain more accurate parameter estimations. In addition, this error cannot be evaluated properly and corrected because of its complex influential factors, e.g. the humidity, temperature, and load. According to the guide to express the uncertainty in the measurements that is published by the joint working group of the International Electrotechnical Commission, the International Organization for Standardization, etc.[63], the uncertainty in the measurements can be used to describe the distribution of the error deviations where the error in the measurements is seen as a stochastic variable.

Thus, if we define the voltage or current phasor at the M or N terminal as the combination of the amplitudes and angles, the collected value vectors from the PMUs can be expressed as $X_{collect}^{amp} = [U_M^c \quad U_N^c \quad I_M^c \quad I_N^c]^T$ and $X_{collect}^{ang} = [\theta_M^c \quad \theta_N^c \quad \phi_M^c \quad \phi_N^c]^T$ where U^c and θ^c are respectively the voltage amplitude and angle of collected voltage phasors at the M and N terminals, and where I^c and ϕ^c are the current amplitude and angle of collected current phasors at the M and N terminals. Furthermore, the true

Table 6.1: Maximum uncertainty in measurements

Voltage amplitude (%)	Current amplitude (%)	Voltage angle (degree)	Current angle (degree)
1	1	0.667	1

value vector of the actual phasors can be expressed as $X_{\text{true}}^{\text{amp}} = [U_{\text{M}}^{\text{t}} \quad U_{\text{N}}^{\text{t}} \quad I_{\text{M}}^{\text{t}} \quad I_{\text{N}}^{\text{t}}]^{\text{T}}$ and $X_{\text{true}}^{\text{ang}} = [\theta_{\text{M}}^{\text{t}} \quad \theta_{\text{N}}^{\text{t}} \quad \phi_{\text{M}}^{\text{t}} \quad \phi_{\text{N}}^{\text{t}}]^{\text{T}}$ where U^{t} and θ^{t} are respectively the voltage amplitude and angle of true voltage phasors at the M and N terminals, and where I^{t} and ϕ^{t} are the current amplitude and angle of true current phasors at the M and N terminals. Then we define two 4-dimensional vectors $e^{\text{amp}} = [e_{\text{MU}} \quad e_{\text{NU}} \quad e_{\text{MI}} \quad e_{\text{NI}}]^{\text{T}}$ as the errors between $X_{\text{collect}}^{\text{amp}}$ and $X_{\text{true}}^{\text{amp}}$, and $e^{\text{ang}} = [e_{\text{M}\theta} \quad e_{\text{N}\theta} \quad e_{\text{M}\phi} \quad e_{\text{N}\phi}]^{\text{T}}$ as the errors between $X_{\text{collect}}^{\text{ang}}$ and $X_{\text{true}}^{\text{ang}}$, such that:

$$X_{\text{collect}}^{\text{amp}} = X_{\text{true}}^{\text{amp}} \odot (1_{4 \times 1} + e^{\text{amp}})$$
$$X_{\text{collect}}^{\text{ang}} = X_{\text{true}}^{\text{ang}} + e^{\text{ang}}$$

(6.5)

where $1_{4 \times 1}$ is the unit vector of four rows and the symbol $\odot$ represents the Hadamard product.

6.3. MODEL THE UNCERTAINTIES IN THE MEASUREMENTS

To model the uncertainty in the measurements, the amplitude error e^{amp} and angle error e^{ang} are considered as stochastic variables subject to specific distributions. These specific distributions of errors can be given by the supplier of the PMU or by big data algorithms, e.g. [186]. In the worst case that no distributions of errors are available, the maximum bound of the uncertainty in the measurements of the PMU will usually be known [41], [145] and the normal distribution will be recommended to model the distribution of errors as indicated in the guide to express the uncertainty in the measurements. For instance, assuming that no information about the distributions of the errors is available, however the maximum uncertainty in the measurements of one certain PMU using the 1S accuracy class current and voltage transformers is given, as listed in Table 6.1[41]. Based on the character of the standard deviation in the normal distribution, the maximum uncertainty boundaries can be approximately seen as end points of the confidence interval between $\mu \pm 3\sigma$ (the error has 99.7% possibility to lie in this interval) where μ and σ are the expectation and standard deviation of the normal distribution, and as a result, the distribution of error can be obtained. Define f_e^{amp} and f_e^{ang} as the probability density function (PDF) of e^{amp} and e^{ang} individually where $f_e^{\text{amp}} = [f_{e_{\text{MU}}}^{\text{amp}} \quad f_{e_{\text{NU}}}^{\text{amp}} \quad f_{e_{\text{MI}}}^{\text{amp}} \quad f_{e_{\text{NI}}}^{\text{amp}}]^{\text{T}}$ and $f_e^{\text{ang}} = [f_{e_{\text{MU}}}^{\text{ang}} \quad f_{e_{\text{NU}}}^{\text{ang}} \quad f_{e_{\text{MI}}}^{\text{ang}} \quad f_{e_{\text{NI}}}^{\text{ang}}]^{\text{T}}$.

6.4. REDUCE THE UNCERTAINTY IN MEASUREMENTS

In order to evaluate the true values defined as $\hat{X}_{\text{true}}^{\text{amp}}$ and $\hat{X}_{\text{true}}^{\text{ang}}$ by using the collected values and PDFs of e^{amp} and e^{ang}, theoretically both the MLE method and the method of moments can be used. However, considering the case that all the errors are subject to the normal distribution, the expectation and variance of $X_{\text{collect}}^{\text{amp}}$ are both related to the

parameter $\hat{X}_{\text{true}}^{\text{ang}}$ that is required to be estimated. Simply using the least squares method (for the first moment) to estimate the parameter $\hat{X}_{\text{true}}^{\text{ang}}$ will lead to a loss of accuracy because of neglecting the variance of $X_{\text{collect}}^{\text{ang}}$. Thus, the MLE method is a better method to address the estimation problem. Therefore, we introduce the MLE method to estimate undetermined parameters as follows:

DERIVE PDFS

According to the PDFs of e^{amp} and e^{ang} as well as (6.5), the PDFs f_e^{amp} and f_e^{ang} of $X_{\text{collect}}^{\text{amp}}$ and $X_{\text{collect}}^{\text{ang}}$ can be obtained such that:

$$
\begin{aligned}
f_{x^{\text{amp}}}(X_{\text{collect}}^{\text{amp}}) &= f_{x^{\text{amp}}}(X_{\text{true}}^{\text{amp}} \circ (I_{8\times1} + e^{\text{amp}})) \\
f_{x^{\text{ang}}}(X_{\text{collect}}^{\text{ang}}) &= f_{x^{\text{ang}}}(X_{\text{true}}^{\text{ang}} + e^{\text{ang}})
\end{aligned}
\tag{6.6}
$$

where $X_{\text{true}}^{\text{amp}}$ and $X_{\text{true}}^{\text{ang}}$ are values required to be evaluated.

MLE

According to (6.6) and using the sampling points $X_{\text{collect}}^{\text{amp}}(t_0-n)$ to $X_{\text{collect}}^{\text{amp}}(t_0)$ and $X_{\text{collect}}^{\text{ang}}(t_0-n)$ to $X_{\text{collect}}^{\text{ang}}(t_0)$, the maximum likelihood functions can be expressed as:

$$
\begin{aligned}
L(\hat{X}_{\text{true}}^{\text{amp}}) &= \sup_{X_{\text{true}}^{\text{amp}}} \prod_{k=1}^{n} p(X_{\text{collect}}^{\text{amp}} \mid X_{\text{true}}^{\text{amp}}(k)) \\
L(\hat{X}_{\text{true}}^{\text{ang}}) &= \sup_{X_{\text{true}}^{\text{ang}}} \prod_{k=1}^{n} p(X_{\text{collect}}^{\text{ang}} \mid X_{\text{true}}^{\text{ang}}(k))
\end{aligned}
\tag{6.7}
$$

where $L(\cdot)$ is the MLE function and $p(X_{\text{collect}}^{\text{amp}} \mid X_{\text{true}}^{\text{amp}}(k))$ is the probability of $X_{\text{collect}}^{\text{amp}}(k)$ that can be expressed by the parameter $X_{\text{true}}^{\text{amp}}$. Because the distributions of e^{amp} and e^{ang} will be influenced by environmental factors, e.g. humidity, temperature, load level, and so on, the distributions may vary during long time periods [127]. Thus in (6.7), a large n value is not recommended and the value of n can be set to a number of sampling points during which the environmental factors have little influence on the distribution e.g., the number of points in a time period of 0.5 s [117]. According to (6.7), the best estimated values $\hat{X}_{\text{true}}^{\text{amp}}$ and $\hat{X}_{\text{true}}^{\text{ang}}$ can be obtained. Then, substituting the estimated results obtained from (6.7) into (6.4), the estimations of parameters of the transmission line can be obtained as follows:

$$
\begin{cases}
\hat{z}_1 = \hat{r}_1 + \mathrm{i}\hat{x}_1 = \hat{\gamma}\hat{z}_{\text{c}} \\
\hat{y}_1 = \mathrm{i}\hat{b}_1 = \hat{\gamma}/\hat{z}_{\text{c}} \\
\hat{\gamma} = \dfrac{1}{D}\cosh^{-1}\left(\dfrac{\hat{U}_{\text{M}}^{\text{t}}\hat{I}_{\text{M}}^{\text{t}}\angle(\hat{\theta}_{\text{M}}^{\text{t}} + \hat{\phi}_{\text{M}}^{\text{t}}) - \hat{U}_{\text{N}}^{\text{t}}\hat{I}_{\text{N}}^{\text{t}}\angle(\hat{\theta}_{\text{N}}^{\text{t}} + \hat{\phi}_{\text{N}}^{\text{t}})}{\hat{U}_{\text{N}}^{\text{t}}\hat{I}_{\text{M}}^{\text{t}}\angle(\hat{\theta}_{\text{N}}^{\text{t}} + \hat{\phi}_{\text{M}}^{\text{t}}) - \hat{U}_{\text{M}}^{\text{t}}\hat{I}_{\text{N}}^{\text{t}}\angle(\hat{\theta}_{\text{M}}^{\text{t}} + \hat{\phi}_{\text{N}}^{\text{t}})}\right) \\
\hat{z}_{\text{c}} = \sqrt{\dfrac{(\hat{U}_{\text{M}}^{\text{t}})^2\angle(2\hat{\theta}_{\text{M}}^{\text{t}}) - (\hat{U}_{\text{N}}^{\text{t}})^2\angle(2\hat{\theta}_{\text{N}}^{\text{t}})}{(\hat{I}_{\text{M}}^{\text{t}})^2\angle(2\hat{\phi}_{\text{M}}^{\text{t}}) - (\hat{I}_{\text{N}}^{\text{t}})^2\angle(2\hat{\phi}_{\text{N}}^{\text{t}})}}
\end{cases}
\tag{6.8}
$$

By solving (6.8), the estimated values $\hat{z}_1$ and $\hat{y}_1$ can be obtained. In addition, these estimated values will largely reduce the uncertainty in the measurements. In Section 6.4,

Table 6.2: Transmission line parameters

Sequence	Resistance (Ω/km)	Inductance (H/km)	Capacitance (F/km)
Positive	0.0386	$1.02846 \cdot 10^{-3}$	$11.575 \cdot 10^{-9}$
Zero	0.2955	$3.377 \cdot 10^{-3}$	$7.2 \cdot 10^{-9}$

Table 6.3: Parameters of the sources

Terminal	Voltage (kV)	Angle (degree)	Impedance (Ω)
M	400	30	$0.1014 + i8.0133$
N	400	0	$1.128 + i16.0391$

the parameters evaluation will be illustrated specifically based on a practical transmission line model and the uncertainties in measurements subject to normal distributions.

After obtaining the estimated parameters of the transmission line, we can use following equation and measured phasors after a fault occurs to obtain the fault location L:

$$L = \frac{\dot{U}_{M1} - \dot{U}_{N1} + D(\hat{r}_1 + i\hat{x}_1)\dot{I}'_{N1}}{D(\hat{r}_1 + i\hat{x}_1)(\dot{I}'_{M1} + \dot{I}'_{N1})} \tag{6.9}$$

The nomenclature, illustration, and derivation can be found in the appendix.

6.5. CASE STUDY

In the first subsection of this section, a simulation case study will be presented to show the influence of the uncertainty in the measurements on the fault location algorithm and the effectiveness of the proposed uncertainty reduction method. In addition, the influence of the uncertainty in the measurements on the parameter evaluation and the positive sequence impedance fault location method will be analyzed. In the second subsection of this section, the effectiveness of the proposed MLE method will be illustrated.

6.5.1. BACKGROUND SET-UP

The transmission line used in this case study is a 500 km long transmission line whose standard fundamental frequency is 50 Hz and its topology is shown in Figure 6.1[219]. The parameters of this transmission line are listed in Table 6.2. The parameters of the sources at the M terminal and the N terminal are listed in Table 6.3 where the "Voltage" and "Current" represent the line-to-line voltage and current respectively. The PMUs compute the current and voltage phasors 50 times per second. The number of samples n in (6.7) is 25 [117] where during a period of 0.5 second, environmental factors have little influence on the distributions of the uncertainties in the measurements. In addition, the distributions of the uncertainties in the measurements are assumed to be normal distributions whose parameters are listed in Table 6.4 where the unit of the angle error is "rad".

Table 6.4: Parameters of the uncertainty distributions

Distributions	Expectation	Standard Deviation
e_{MU}	0.0001	$5 \cdot 10^{-3}$
e_{NU}	0	$5 \cdot 10^{-3}$
e_{MI}	0.0003	$5 \cdot 10^{-3}$
e_{NI}	0	$5 \cdot 10^{-3}$
$e_{\text{M}\theta}$	0.001 rad	$5.8 \cdot 10^{-3}$
$e_{\text{N}\theta}$	0 rad	$5.8 \cdot 10^{-3}$
$e_{\text{M}\phi}$	0.001 rad	$8.7 \cdot 10^{-3}$
$e_{\text{N}\phi}$	0 rad	$8.7 \cdot 10^{-3}$

Table 6.5: Voltage and current phasors

Phasor	Amplitude (kV or kA)	Angle (degree)
U_{M}^{t}	188.4414	28.02
U_{N}^{t}	186.7095	3.8564
I_{M}^{t}	0.8131	28.6925
I_{N}^{t}	0.7931	-165.7

6

6.5.2. INFLUENCE OF UNCERTAINTY IN MEASUREMENTS ON FAULT LOCA-TION

During the normal operation status (no faults occurring), the true value of the voltage and current phasors at the M and N terminals simulated by MATLAB/Simulink are listed in Table 6.5. After adding the uncertainties, which are subject to the normal distributions whose parameters are shown in Table 6.4, to the measurements of the phasors, the phasors are distorted as seen in Figure 6.2.

In Figure 6.2, the red line represents the exact value and the circles represent values distorted by the uncertainty in the measurements. In all the sub-figures of Figure 6.2, 20 scenarios of the uncertainty are generated by a Monte-Carlo method based on the distributions whose parameters are shown in Table 6.4. In Figure 6.2, it can be seen that both the amplitudes and the angles are distorted slightly, within quite small intervals that are no larger than 2% in the amplitudes and not larger than 0.04/rad in the angles. After substituting the distorted values into (6.4), the transmission line parameters can be evaluated as shown in Figure 6.3.

In Figure 6.3, the positive sequence transmission line parameters distorted by the uncertainty in the measurements are indicated by circles and the exact positive sequence transmission line parameters are indicated by red plusses. All these points are computed using the voltage and current phasors obtained from Figure 6.2. According to Figure 6.3, it can be seen that the variations of the transmission line parameters are large (16% for the impedance and 8% for the admittance). From Figure 6.2 and Figure 6.3, it can be concluded that even slight distortions in the measurements caused by the uncertainty in the measurements can result in large distortions in calculated transmission line parameters. Then according to (6.9), the gaps between the fault location calculated by exact

(a) Distorted phasor amplitudes

(b) Distorted phasor angles
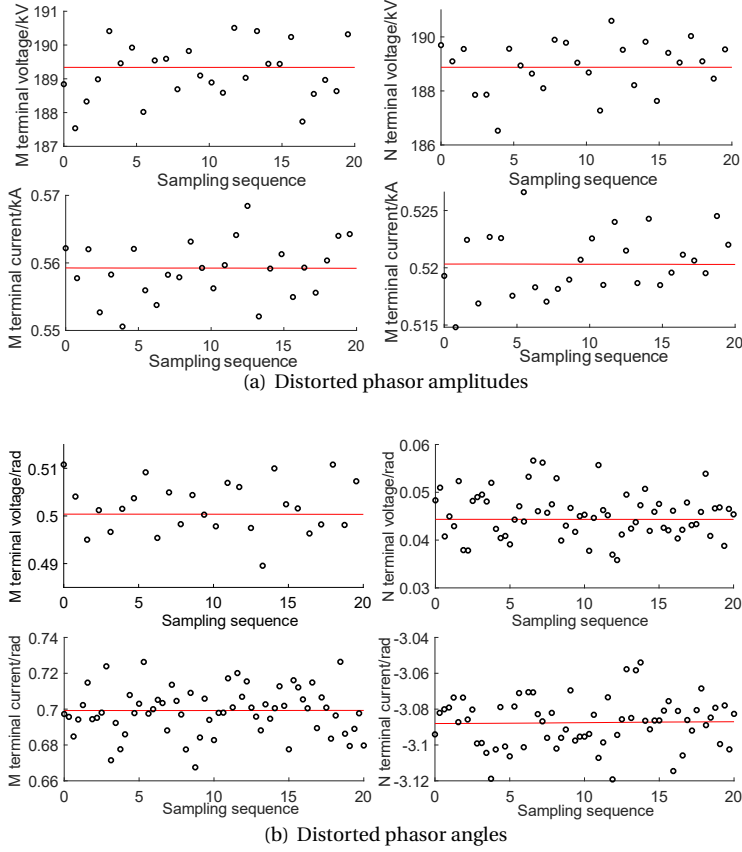
Figure 6.2: Distorted phasors

transmission line parameters and calculated by the distorted transmission line parame-
ters are listed in Table 6.6.

In practical operation of a transmission line, the fault can occur anywhere along the
line, while different fault locations may cause different fault characters. Thus, different
fault locations are usually considered when evaluating and examining the performance
of a fault location algorithm. These fault location cases are usually dispersed along the
line. Thus, in Table 6.6, we have selected 5 fault locations and the distances between
these 5 fault locations; the M terminal are set to 50 km, 125 km, 250 km, 375 km, 450 km
respectively. In addition, by considering 5 different fault locations, we also intend to ex-
amine whether our proposed MLE method is effective for all fault locations, and whether
the fault location gaps between the exact value and the calculated value are influenced
by the different fault locations. Note that the gaps listed in Table 6.6 are all relative val-
ues, so not absolute values. Thus, a positive or negative value represents whether the
distance between the calculated fault location and the M terminal is larger than or less

(a) Distorted positive sequence impedance

(b) Distorted positive sequence admittance
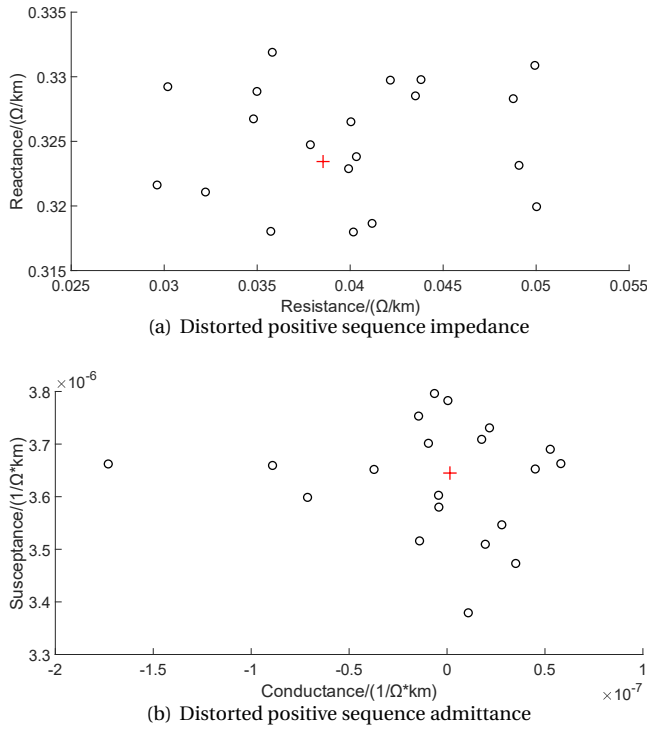
Figure 6.3: Distorted positive sequence transmission line parameters

than the distance between the exact fault location and the M terminal.

In Table 6.6, it can be seen that the gaps are large and even sometimes the gap is larger than 1 km, which cannot be ignored in the practical fault maintenance. A gap larger than 1 km will actually result in an additional 2 km search work by the maintenance personnel, which means a large additional cost. In addition from the comparison between the columns of Table 6.6, it can also be observed that the variance of gaps for the fault at 125 km is smaller than at any other location. That is because during the fault location calculation (see (6.9)), the variance of the gaps is transmitted from the uncertainty in the measurements to the fault location result. Thus, the variance of the gaps changes following the changes in the parameters in (6.9), including the measured voltage and current values after a fault has occurred. It can be seen that the variances of the gaps for different fault locations are different because different fault locations lead to different measured voltages and currents after a fault has occurred. Moreover, because the different values of fault resistances also result in different voltage and current values after a fault has occurred, it can be inferred that the fault resistance also influences the variance of the gap.

Table 6.6: Fault location gaps considering the uncertainty in the measurements

Scenario	Fault location (km)				
	50 km	125 km	250 km	375 km	450 km
1	0.100	0.221	-0.187	-0.053	-0.318
2	-0.060	-0.125	-0.051	0.088	-0.366
3	-0.168	-0.032	0.178	0.890	0.002
4	0.327	-0.160	-0.036	-0.033	-1.161
5	-0.166	-0.005	0.049	-0.644	0.500
6	-0.271	0.241	0.014	0.449	0.910
7	0.333	0.112	-0.243	-0.214	0.724
8	-0.225	-0.140	-0.198	-0.201	0.035
9	0.446	0.023	0.144	0.081	0.564
10	0.325	0.062	0.042	0.026	0.944
11	0.048	0.067	-0.044	-0.026	0.023
12	-0.01	0.131	-0.095	-0.017	-0.253
13	0.104	-0.045	0.167	-0.023	-0.120
14	0.306	-0.052	0.146	-0.265	0.796
15	0.034	0.115	-0.054	-0.831	0.025
16	0.197	0.069	-0.337	-0.102	0.265
17	-0.184	0.044	0.089	0.885	0.957
18	0.270	0.012	0.328	0.097	0.065
19	0.146	0.138	-0.228	0.318	-0.404
20	0.113	0.157	0.203	0.067	0.980

6

6.5.3. SIMULATION RESULTS OF THE PROPOSED METHOD

As illustrated above, the influence of the uncertainty in the measurements on the positive sequence impedance fault location method cannot be neglected. Thus, this subsection is designed to show the effectiveness of the proposed method in reducing the uncertainty in the measurements.

Firstly the PDFs of e^{amp} and e^{ang} are normal distributions that can be expressed by $\hat{X}_{\mathrm{true}}^{\mathrm{amp}}$ and $\hat{X}_{\mathrm{true}}^{\mathrm{ang}}$ which are required to be estimated. Then according to the PDFs of e^{amp} and e^{ang} and (6.5), the distributions of $X_{\mathrm{collect}}^{\mathrm{amp}}$ and $X_{\mathrm{collect}}^{\mathrm{ang}}$ can be expressed using $\hat{X}_{\mathrm{true}}^{\mathrm{amp}}$ and $\hat{X}_{\mathrm{true}}^{\mathrm{ang}}$, such that: $X_{\mathrm{collect}}^{\mathrm{amp}} \sim N\left(\hat{X}_{\mathrm{true}}^{\mathrm{amp}}(1 + \mu_{e^{\mathrm{mag}}}), (\hat{X}_{\mathrm{true}}^{\mathrm{amp}} \sigma_{e^{\mathrm{mag}}})^2\right)$ and $X_{\mathrm{collect}}^{\mathrm{ang}} \sim N\left(\hat{X}_{\mathrm{true}}^{\mathrm{ang}}(1 + \mu_{e^{\mathrm{ang}}}), (\hat{X}_{\mathrm{true}}^{\mathrm{ang}} \sigma_{e^{\mathrm{ang}}})^2\right)$, where the PDFs of $X_{\mathrm{collect}}^{\mathrm{amp}}$ and $X_{\mathrm{collect}}^{\mathrm{ang}}$ are respectively $f_{x^{\mathrm{mag}}}$ and $f_{x^{\mathrm{ang}}}$ as defined in (6.6). Then, based on the PDFs, the parameters can be evaluated by substituting the sampled data into (6.7). The results of parameter estimations using MLE are shown in Figure 6.4.

More specifically, Figure 6.4 shows 20 scenarios of the uncertainty in the measurements. The red plus represents transmission line parameters obtained from the exact voltage and current phasors and the circles represent parameters obtained from 25 sampled points under the uncertainty in the measurements by using the MLE method to reduce the uncertainty. It can be observed that the distortions of the resistance, reactance, and susceptance are respectively 0.67%, 0.05%, and 0.015%. Note that the value of the conductance is very small so that the distortion of the conductance can be neglected. Comparing the results of Figure 6.3 and Figure 6.4, the uncertainty in the measurements can be largely reduced by using the MLE method in estimating the transmission line pa-
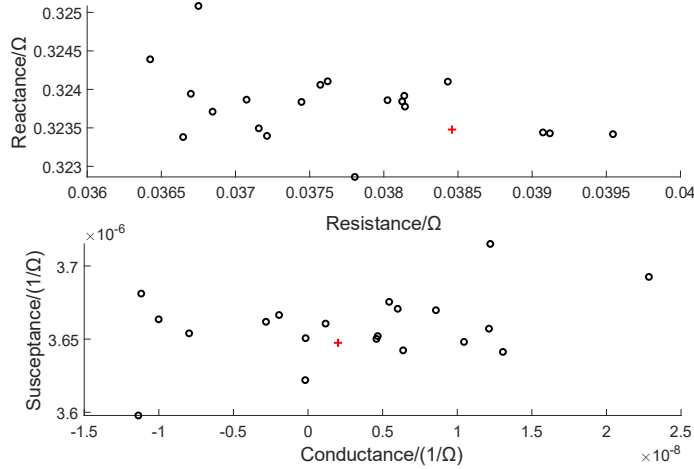
Figure 6.4: Estimated transmssion line parameters using MLE

Table 6.7: Fault location gaps by using the MLE method

Scenario	Fault location (km)				
	50 km	125 km	250 km	375 km	450 km
1	-0.0038	0.011	0.0048	-0.0530	-0.0495
2	-0.0083	-0.0193	-0.0124	-0.0571	-0.0400
3	0.0179	0.0066	-0.0007	0.0213	0.0585
4	0.0385	-0.0036	-0.0125	-0.1095	0.0917
5	-0.0340	-0.0015	-0.0525	-0.0114	-0.0499
6	0.0438	0.0205	0.0143	0.0055	0.0720
7	0.0233	0.0054	-0.0014	0.0082	-0.0068
8	0.0212	0.0019	-0.0079	-0.0516	0.1116
9	0.0035	-0.0125	-0.0229	-0.0119	0.0200
10	0.0270	0.0118	0.0029	0.0012	0.0216
11	0.0125	-0.0267	-0.0062	0.0604	-0.0377
12	0.0515	0.0235	0.0140	0.0053	0.0770
13	0.0011	-0.0041	-0.0166	-0.0131	-0.0712
14	-0.0033	0.0151	-0.0194	0.0082	-0.0051
15	0.0268	0.0094	-0.0097	-0.0203	0.0458
16	0.0568	-0.0115	0.0013	-0.0274	0.0777
17	-0.0057	-0.0125	-0.0117	-0.0438	0.0423
18	0.0390	0.0118	0.0146	0.0130	-0.0269
19	0.0404	-0.0069	-0.0132	0.0371	-0.0005
20	0.0033	0.0073	-0.0172	0.0959	-0.0277

rameters. Furthermore, gaps between the fault location results using exact transmission line parameters and the results using distorted parameters but addressed by the MLE method are shown in Table 6.7.

By comparing Table 6.6 with Table 6.7, different from the analysis results of the Table 6.6, the gaps no longer influenced by the measured terminal voltage and current phasors after a fault has occurred. It can also be observed that the gaps are largely reduced. Thus,

the MLE method is suitable and effective to reduce the uncertainty in the measurements when the distributions of the measurement errors are known.

6.6. CONCLUSIONS AND FUTURE WORK

This chapter has analyzed the influence of uncertainty in the measurements on the transmission line parameter estimations, which in its turn influence the results of the fault location methods. In this analysis, we have used the classic two-terminal positive sequence network fault location algorithm as an example. We have adopted the maximum likelihood estimation (MLE) method to reduce the uncertainty in the measurements by using the distribution of the uncertainty. Simulation results show that even if the uncertainty in the measurements only causes a slight distortion in the measurements of less than 2%, the distortions on transmission line parameter calculations can be even larger than 10%. In addition, the gap between the calculated fault location and the exact fault location is sometimes larger than 1 km for a 500 km transmission line. Thus, the influence of the uncertainty in the measurements cannot be neglected. By using the proposed MLE method, both the distortion of the transmission line parameters and the gap between the calculated fault location and the exact fault location are at least 10 times lower than when the proposed MLE method is not used. Thus, the proposed MLE method is suitable and effective to handle the uncertainty in the measurements.

Future work could investigate how to obtain more accurate stochastic distributions of phasor errors by using big data methods. Bayesian inference might be an effective way to derive the error distributions by considering the different environmental factors that influence the errors in the measurements.

6.A. APPENDIX: FAULT LOCATION ALGORITHM

According to the mechanisms used in fault location algorithms, the fault location algorithms can be categorized into 2 main categories: fault analysis algorithms [151] and traveling-wave-based algorithms [54]. The basic idea of the fault location algorithms is to model the transmission lines as electrical circuits. These electrical circuits contain e.g., impedances, capacitors, power sources, a ground, and so on. Then, the fault location signals, e.g., the fault current or voltage, are derived based on the electrical circuit. In contrary, the basic idea of the traveling-wave-based algorithms is to model the transmission lines by partial differential equations. The fault location signals, e.g., fault current traveling waves and voltages, along the transmission lines can be derived by the partial differential equations of the traveling waves. Both the fault analysis algorithms and traveling-wave-based algorithms are influenced by inaccurately measured transmission line parameters.

In this chapter we consider a typical fault analysis algorithm based on the two terminal positive sequence impedance [113], which is widely applied for the transmission lines in China, because its performance is independent from source impedance variations, fault types, fault resistances, and fault distances. In electrical engineering, the transmission lines can be represented by the pi model [188] for the study of electrical characteristics, e.g., the currents passing through the transmission lines and the terminal voltages of the transmission lines, as shown in Figure. 6.5. Based on the pi model, to
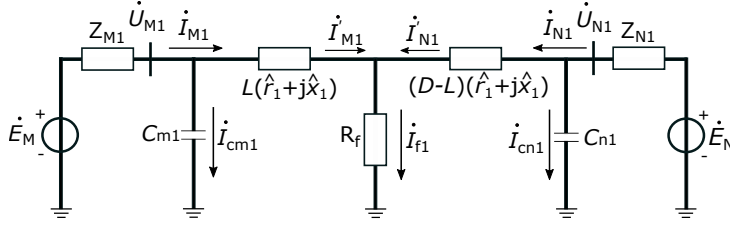
6

Figure 6.5: Positive sequence network of the transmission line

analyze three-phase transmission lines easily, a mathematical tool named symmetrical
components is proposed to model the current, voltage, and impedance of the transmis-
sion lines. Then a transmission line can be decomposed into a positive sequence net-
work, a negative sequence network, and a zero sequence network of the transmission
line by symmetrical components. A detailed explanation of the symmetrical compo-
nents can be found in [176].

In Figure 6.5, the pi model of the transmission line [176], the positive sequence net-
work of the transmission line when a fault has occurred along the line can be explained
using Figure 6.5.

In Figure 6.5, the fault occurs at the location that is L km away from the M termi-
nal where the length of the whole transmission line is D km. Note that in Figure 6.5 all
the impedance and conductance parameters are positive values. In detail, Z_{M1}, Z_{N1},
$C_{m1} = \mathrm{i}D\hat{b}_1/2$, $C_{n1} = \mathrm{i}D\hat{b}_1/2$, $L(\hat{r}_1 + \mathrm{i}\hat{x}_1)$, $(D - L)(\hat{r}_1 + \mathrm{i}\hat{x}_1)$ and R_f are respectively the M
terminal equivalent impedance, N terminal equivalent impedance, shunt capacitance
between the fault location and the M terminal, shunt capacitance between the fault
location and the N terminal, impedance between fault location and the M terminal,
impedance between fault location and the N terminal, and the fault resistance. In ad-
dition, $\hat{r}_1$, $\hat{x}_1$, and $\hat{b}_1$ are evaluated transmission line parameters that can be obtained
by (6.8). Note that all the phasors in Figure 6.5 are fault components of the positive se-
quence network by extracting the fault components from the positive symmetrical com-
ponents [80]. In detail, $\dot{E}_M$, $\dot{U}_{M1}$, $\dot{I}_{M1}$, $\dot{I}_{cm1}$ and $\dot{I}'_{M1}$ are respectively the voltage of the M
terminal source, voltage at M terminal, current at M terminal, current of shunt capac-
itance of the M terminal side and current from the M terminal injecting into the fault
point. The phasors for the N terminal are defined similarly. Furthermore, $\dot{I}_{f1}$ is the cur-
rent flowing through the fault resistance. Then the Kirchhoff's law functions concerning
the fault location can be formulated as follows:

$$\dot{U}_{M1} = L(\hat{r}_1 + \mathrm{i}\hat{x}_1)\dot{I}_{M1} + \dot{U}_{f1}, \tag{6.10a}$$

$$\dot{U}_{N1} = (D - L)(\hat{r}_1 + \mathrm{i}\hat{x}_1)\dot{I}_{N1} + \dot{U}_{f1}, \tag{6.10b}$$

$$\dot{I}_{cm1} = \mathrm{i}D\hat{b}_1\dot{U}_{M1}/2, \tag{6.10c}$$

$$\dot{I}_{cn1} = \mathrm{i}D\hat{b}_1\dot{U}_{N1}/2, \tag{6.10d}$$

$$\dot{I}'_{M1} = \dot{I}_{M1} - \dot{I}_{cm1}, \tag{6.10e}$$

$$\dot{I}'_{N1} = \dot{I}_{N1} - \dot{I}_{cn1} \tag{6.10f}$$

where ω is the angular velocity of the AC current. From (6.10), we can derive the final fault location:

$$L = \frac{\dot{U}_{M1} - \dot{U}_{N1} + D(\hat{r}_1 + i\hat{x}_1)\dot{I}'_{N1}}{D(\hat{r}_1 + i\hat{x}_1)(\dot{I}'_{M1} + \dot{I}'_{N1})} \tag{6.11}$$

After substituting (6.10c)-(6.10f) into (6.11), the fault location L can be expressed using the measured phasors $\dot{U}_{M1}$, $\dot{I}_{M1}$, $\dot{U}_{N1}$ and $\dot{I}_{N1}$ that are collected after a fault has occurred. In practice, the expression of the fault location has fluctuations during an electromagnetic transient stage. Thus, a criterion should be used to derive the fault location result, such that: if the gap between the L value at time step t_0 and that at the next time step $t_0 + 1$ is less than a threshold τ, then the fault location at time t_0 is L.

6

7

UAV ROUTING STRATEGY FOR POST-DISASTER INSPECTION AND MONITORING

7.1. INTRODUCTION

Disasters, e.g., hurricanes, floods, and earthquakes, can damage components of distribution networks. To reduce the impact of the disasters on distribution networks, a variety of post-disaster countermeasures have been proposed in the literature [32], [79], [214].

Before implementing countermeasures, a clear assessment of types of damages, their locations, statuses and causes can facilitate and improve the performance of the repair crews. Thus, post-disaster inspection should be carried out in a fast manner, so as to significantly improve the reliability and resilience of the power system. UAVs can inspect the status of the components that are difficult to reach in a safe or efficient way, e.g., in case of blocked roads due to floods or mudslides. In this way, the human repair crews can work more safely and efficiently. For instance, in [131], a multi-UAV routing strategy is proposed to start post-disaster inspection as quick as possible. A two-stage optimization problem is formulated to firstly determine the starting locations of the UAVs by minimizing setup cost and to secondly determine the inspection routes by minimizing the completion time of inspection. In [57], a fault inspection strategy for UAVs is proposed, where the UAVs establish the information exchange network themselves in areas with telecommunication network coverage. Hoang *et al.* [92] present a strategy for surface inspection using UAVs. The Internet of Things is utilized as the communication network and a particle swarm optimization algorithm is proposed to route the UAVs. Zheng *et al.* [240] propose a cooperative strategy for transmission line inspections involving UAV schedules and human-team schedules.

This chapter is based on [75].

119

Different from the inspection tasks performed by hovering above the damages, monitoring tasks are performed by fast passing along the transmission lines and roads as shown in the blue trajectories (monitoring) and red trajectory (inspection) in Figure 7.1. In this chapter, UAVs are used for monitoring networks after disasters with two purposes. Firstly, because of some potential dangers and early-stage damages, the components might still be working but with a risk of becoming damaged soon, e.g., leaning but still working towers. By monitoring the transmission lines, potential dangers and early-stage damages can be found. Additionally, fixed non-movable sensors might have become damaged and usually these are not able to cover the whole distribution network. Thus, this chapter considers using UAVs to frequently monitor the whole distribution network after the disaster. Secondly, the repair crews require to know the real-time condition of road infrastructure, so as to select the best routes to reach damaged components during restoration. Thus, using UAVs to monitor the road infrastructure after the disaster is also considered in this chapter to prevent repair crews from using routes that are dangerous or not accessible.

In literature, monitoring routing strategies have been proposed for other applications [48], [51], [89], [93], [94], [99], [119], [218], [245]. For instance, in [89], [119], [218], routing strategies for monitoring of transmission lines are studied. However, these papers focus on how the UAVs can examine the transmission lines from different locations of a particular tower, but not on how to determine the optimal monitoring routes for the whole network. In [245], a UAV monitoring scheme is developed targeting energy efficiency for transmission lines. In [51], [94], UAV monitoring routing strategies for road traffic are proposed. Other applications include wildlife rescue, surveillance, and offshore wind farm monitoring [48], [93], [99].

In current strategies, inspection and monitoring are not integrated nor coordinated. Therefore, this chapter focuses on an integrated and coordinated UAVRS that combines the inspection routing and the monitoring routing. Note that our proposed UAVRS only determines the routes to damages required to be inspected, the detailed routes for how to inspect the damages and manipulate the UAVs, e.g., how to hover, are not considered; the total inspection times for damages are considered instead. Furthermore, the UAV routing strategy should be implemented in real time. That is because during the restoration process, some unpredictable events may happen. New damages may emerge because of, e.g., a subsequent earthquake. Besides, some of the components could already have been inspected by human repair crews, which implies that they do no need to be inspected anymore by UAVs. Furthermore, the position of a UAV might deviate from the originally planned route because of, e.g., a blast of heavy wind, flying speed changes, or communication with the UAVs being temporally disrupted during restoration. Thus, the routes of UAVs should be adapted to these unpredictable events in real time.

To obtain the optimal routes for UAVs, there are a lot of decision-making strategies in literature. For instance, branch-and-bound solvers [170], evolutionary optimization algorithms [47], [78], and meta-heuristic algorithms for multi-objective programming [49] are adopted to solve the UAV routing problems. However, these strategies cannot be applied for multi-time-scale programming as they may easily become intractable for large problem. In order to get a computationally tractable approach, we consider a control architecture with 3 layers: layer 1 gives the results of mode allocation, inspection,

and rough monitoring; layer 2 gives the trajectory of the detailed monitoring; and layer 3 takes care of the manipulation of the UAVs, e.g., flight control and trajectory tracking. However, layer 3 has been widely studied in the literature [66], [234], therefore we do not consider layer 3 in detail in this chapter.

The contributions of the current chapter are as follows:

- To facilitate the restoration process and to make the human crews work safely and efficiently, a UAV routing strategy integrating of monitoring roads and lines, and inspection of damages is proposed for distribution networks.

- To adapt to unpredictable events, the UAV routing strategy is implemented in real time by adopting a receding horizon strategy.

- A two-layer decision-making architecture is adopted due to inconsistency between time scales of inspection and monitoring. The architecture proposes to use a bi-level programming problem in the first layer to make the problem tractable.

The chapter is organized as follows. Section 7.2 describes the UAVRS problem and explains the proposed two-layer real-time UAVRS architecture. In Section 7.3, the bi-level programming problem of the first layer is described. Then in Section 7.4, the monitoring problem solved by the second layer is formulated. Section 7.5 analyzes a case study based on a real-life distribution network to evaluate the proposed UAVRS. Section 7.6 concludes the chapter.

7.2. Problem description and two-layer UAVRS

7.2.1. Problem description

After disasters, aggravating situations such as damages (e.g., insulator flashover), potential dangers (e.g. mudslides, floods near the poles), and early-stage damages (e.g. severely tilted but still working poles) may occur in distribution networks, and aggravating situations such as heavily damaged roads and congestion may occur in road traffic networks as shown in Figure 7.1. Thus, the problem of real-time UAVRS for post-disaster restoration is to determine the UAV routes to provide more and real-time information of the distribution network and of the road traffic network, so as to help restore the distribution networks. The UAVs collect real-time information, e.g., pictures and videos, via the camera installed on UAVs and then send them to the control center of the distribution network to make the human crews aware of the real-time situation of the distribution network. Regarding the routing of the UAVs, the control center solves the routing problem and obtains the control sequences for UAVs. Then, the UAVs implement the control sequences and finish the inspection and monitoring tasks. Note that this problem is dynamic. Thus, a predictive decision-making approach with a moving prediction window is proposed to avoid having a short-sighted real-time strategy. In such an approach, the prediction window contains several decision steps. Optimal decisions are obtained for one prediction horizon window, but only the decisions determined for the first step are implemented. At the next time step, the whole optimization over a shifted prediction window is performed again in the next step with updated information.

According to the categories of the events and the charging requirements of UAVs,
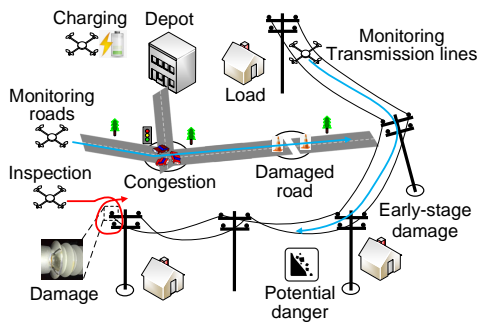
Figure 7.1: Illustration of the restoration problem and the modes of the UAVs

Table 7.1: Proposed two-layer architecture for real-time UAVRS

Layers	Network model	Time scale	Formulated problem	Obtained results
First layer	Graph	Inspection time step (e.g., 5 min)	Top level of bi-level programming	Mode allocation
			Bottom level of bi-level programming	Inspection routes
				Rough monitoring routes
Second layer	Hexagons	Monitoring time step (e.g., 30 s)	Mixed-integer programming	Detailed monitoring routes

in this chapter, three UAV operation modes are defined: monitoring mode, inspection mode, and charging mode. Possible trajectories for these three modes are illustrated in Figure 7.1. For the monitoring mode (blue trajectories in Figure 7.1), the UAVs fly along the transmission lines and the road infrastructure. By monitoring the distribution network, UAVs will detect potential dangers, early-stage damages, and damages that cannot be monitored by fixed sensors. By monitoring the road infrastructure, UAVs will update repair crews about the road traffic conditions in order to guide the repair crews to reach the damages. For the inspection mode (red trajectory in Figure 7.1), the UAVs visit located damages to provide more information that facilitates the repair crews in judging the type of damage, and in selecting the required spare components and the required repair materials. In this mode, UAVs fly from their current position to the located damages directly and then stay a while to inspect them carefully by hovering. In the charging mode, UAVs return to the nearest depots before their batteries are depleted.

7.2.2. TWO-LAYER ARCHITECTURE FOR REAL-TIME UAVRS

In the charging mode, the UAVs are recalled back to the nearest depot (considering detours for avoiding obstacles). Then the UAVs in the charging mode do not need to be routed. Next, the models for the monitoring mode and the inspection mode are explained.

For monitoring routing, as shown in Figure 7.2.1, the radius R of the monitoring footprints of UAVs is determined by the cameras installed on the UAVs and the flying height of the UAVs. Thus, when the type of UAVs and their equipment are given, R is also known. Since this chapter focuses on route planning, the radius of the footprints of the UAVs for

monitoring is assumed to be the same for all UAVs. According to R, the distribution network and the road traffic network are divided into hexagons that are inscribed-hexagons of the footprints, so that the kinematic behavior of the UAVs can be modeled. Then the monitoring process can be seen as the movement from the center of one hexagon to the center of one of the six neighbor hexagons (6 options for moving directions) to monitor the lines/roads inside the hexagons as shown in the flight trajectory in Figure 7.2.1. For concerns about small obstacles (including no-fly areas and buildings) in monitoring, the UAVs avoid obstacles to monitor by passing through the centers of nearby hexagons that do not contain obstacles as shown in Figure 7.2.4. Besides, the time taken for one movement from the center of one hexagon to the center of a neighbor hexagon is defined as the monitoring time step (e.g., for R=173 m and UAV speed 0.6 km/min, a monitoring time step takes 30 s), which is the basic time unit for monitoring.

In the inspection mode, the inspection routes are planned based on the graph without dividing into hexagons as shown in Figure 7.2.2. The UAVs travel from their current positions to damages directly, and they do not need to travel along the lines/roads (seen as the straight flight trajectory in Figure 7.2.2). Note that our proposed real-time UAVRS only determines the routes to damages required to be inspected; the detailed movements at the manipulation layer for inspecting the damages, e.g., how to hover, are not considered; the total inspection times for damages are considered instead. For concerns about obstacles in inspection, the UAVs make a detour on the travel to avoid the obstacles on the way to the damages as shown in Figure 7.2.5. The flights to remote damages may take tens of minutes, and the duration of inspections take several or tens of minutes in practical distribution networks. Thus, the basic time unit for inspection is several minutes, which is defined as the inspection time step.

In general, the length of the monitoring time step (e.g., 30 s) is not comparable to that of the inspection time step (e.g., 5 min in Section 7.5) in practice. Thus, the real-time UAVRS has an inherent multi-time-scale characteristic. In order to coordinate the time scales of monitoring and inspection problems and to reduce the computational complexity, we use a two-layer architecture as described in Table 7.1. In the first layer, the mode allocation, the inspection routes, and the rough monitoring routes are determined with the inspection time step as basic time unit, where a graph is used to model the problem. For tractability, a bi-level linear programming problem [150] is proposed to formulate the first-layer programming problem. More specifically, in the bi-level programming problem, if the results of the top-level problem (mode allocation results) are fixed, the inspection and rough monitoring programming problems at the bottom level can be separated and solved as two individual programming problems. If we would formulate the first-layer problem in a single-level problem, the scale of this problem will be very large. Furthermore, the inspection programming problem and the rough programming problem can then no longer be separated and be solved individually. This is why a bi-level approach is adopted. For the bi-level programming problem, the inspection process has been explained earlier in this subsection, as is also shown in Figure 7.2.2 and Figure 7.2.5. The rough monitoring process can be described as the UAVs traveling along the transmission lines and roads as shown in Figure 7.2.3 and Figure 7.2.6 to obtain rewards by finishing monitoring tasks, where a monitoring task corresponds to the monitoring of one transmission line or one road. In the rough monitoring problem, two
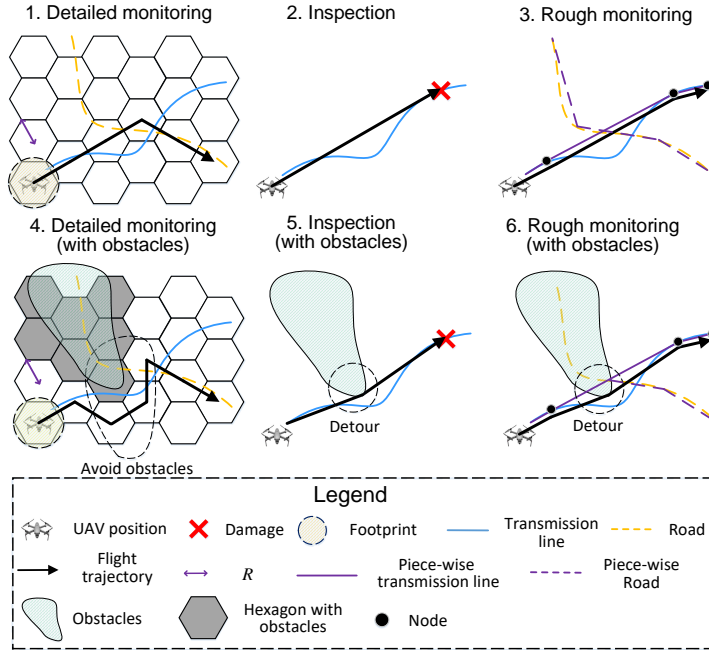
Figure 7.2: Difference of monitoring and inspection and obstacle concerns

7

assumptions are made: firstly, the winding parts and branches of transmission lines and roads are approximated, by considering a sequence of straight lines using some intermediate points as shown in Figure 7.2.3 and Figure 7.2.6. Secondly, every UAV monitors a transmission line or a road starting from one terminal node to another without turning around until another terminal node is reached. We believe that these two assumptions make sense, because on one hand, the rough monitoring does not need an exact model, as we still have a subsequent detailed monitoring problem (see below). On the other hand, we can let the piece-wise curve approximate the real graph of the lines and nodes arbitrarily well by considering more straight pieces (at the cost of increased computation time). In Section 7.3, we will formulate the first-layer problem and discuss how to solve it.

Then in the second layer, a more detailed monitoring problem with the monitoring time step as basic time unit and a hexagonal grid is proposed to determine the detailed monitoring routes. The detailed monitoring problem takes care of feasibility by tracking the rough monitoring routes as closely as possible given the exact layout of the distribution network, including obstacles. The detailed monitoring process is explained earlier in this subsection as shown in Figure 7.2.1 and Figure 7.2.4. In Section 7.4, we will formulate the second-layer problem.

7.3. BI-LEVEL PROGRAMMING PROBLEM FORMULATION

7.3.1. OBJECTIVE FUNCTION

Considering that the inspection processes may take a longer period than one inspection time step, it is assumed that the UAVs in inspecting tasks cannot be interrupted, except when their energy levels are below their thresholds. In addition, in one inspection time step, only one mode can be allocated for each UAV. The mode allocation problem is formulated as follows:

$$\min_{\delta} \min_{y_1, y_2} (R_{\mathrm{I}}(\delta, y_1) + \gamma R_{\mathrm{M}}(\delta, y_2)) \tag{7.1}$$

$$\text{s.t.} \quad \sum_{m \in \mathcal{M}} \delta_{n,m} = 1, \forall n \in \mathcal{N} \tag{7.2}$$

$$\delta_{n,3} E_n \leq E_{\mathrm{set},n}, (1 - \delta_{n,3}) E_{\mathrm{set},n} \leq E_n, \forall n \in \mathcal{N} \tag{7.3}$$

$$y_1 \in \Phi_1(\delta), y_2 \in \Phi_2(\delta) \tag{7.4}$$

where $\delta_{n,m}$ equals 1 if UAV n is allocated to mode m, $\gamma \geq 0$ is a weight coefficient indicating the relative importance of monitoring with respect to inspection, $R_{\mathrm{I}}(\cdot)$ and $R_{\mathrm{M}}(\cdot)$ are the extra cost of inspection and the total monitoring reward respectively (see below for details), $\mathcal{N}$ represents the set of UAVs, $\mathcal{M} = \{1, 2, 3\}$ is the set of modes (the monitoring mode, inspection mode, and charging mode corresponding to mode 1, 2, and 3 respectively), y_1 and y_2 are the vectors of variables of monitoring and inspection respectively that will be defined in Sections 3.2 and 3.3. Constraint (7.2) indicates that one UAV only can be allocated to one mode. Constraint (7.3) forces that when E_n, the energy of UAV n, is lower than the threshold value $E_{\mathrm{set},n}$, UAV n should be allocated to the charging mode ($m = 3$). In (7.4), $\Phi_1(\delta)$ and $\Phi_2(\delta)$ define the feasibility sets of variable vectors y_1 and y_2 in the monitoring mode routing problem and the inspection mode routing problem respectively.

7.3.2. ROUGH MONITORING ROUTING PROBLEM

In this section, a stochastic rough monitoring routing problem is formulated. The load profiles and the monitoring times of the transmission lines and roads are considered as stochastic parameters with a scenario-based approach. The set of scenarios $\mathcal{S}$ is defined by the stochastic distribution of the loads obtained by the autoregressive moving average approach [71] and the distribution of the monitoring times obtained by discrete Gaussian distributions [227].

Then the rough monitoring routing problem can be formulated by maximizing the rewards obtained in one prediction horizon. The rewards for monitoring a transmission line or a road can be calculated according to their importance. The reward $r_{i,j,s}$ of monitoring from node i to j at the current inspection time step of scenario s is calculated by:

$$r_{i,j,s} = r_{i,j,s}^{\mathrm{T}} + r_{i,j}^{\mathrm{R}}, \forall i \in \mathcal{I}, \forall j \in \mathcal{I}_i^{\mathrm{N}}, \forall s \in \mathcal{S} \tag{7.5}$$

where $\mathcal{I}$ is the set of nodes, $\mathcal{I}_i^{\mathrm{N}}$ is the set of neighbor nodes connected to node i via transmission lines or roads, $r_{i,j,s}^{\mathrm{T}}$ and $r_{i,j}^{\mathrm{R}}$ are the rewards of monitoring the transmission line and the road between nodes i and j respectively. If there is no transmission line or

no roads between nodes i and j, correspondingly $r^{\mathrm{T}}_{i,j,s} = 0$ or $r^{\mathrm{R}}_{i,j} = 0$. Otherwise, $r^{\mathrm{T}}_{i,j,s}$ and $r^{\mathrm{R}}_{i,j}$ can be calculated by:

$$
\begin{aligned}
r^{\mathrm{T}}_{i,j,s} &= \zeta^{\mathrm{T}}_{i,j} \, r^{\mathrm{T}}_{i,j,\min} + (1 - \zeta^{\mathrm{T}}_{i,j}) \, r^{\mathrm{T}-}_{i,j,s} \, e^{P_{i,j,s}}, \\
r^{\mathrm{R}}_{i,j} &= \zeta^{\mathrm{R}}_{i,j} \, r^{\mathrm{R}}_{i,j,\min} + (1 - \zeta^{\mathrm{R}}_{i,j}) \, r^{\mathrm{R}-}_{i,j} \, e^{Q_{i,j}}, \\
&\forall i \in \mathscr{I}, \forall j \in \mathscr{I}^{\mathrm{N}}_i \, \forall s \in \mathscr{S}
\end{aligned}
\tag{7.6}
$$

where $\zeta^{\mathrm{T}}_{i,j}$ or $\zeta^{\mathrm{R}}_{i,j}$ equals 1 if the transmission line or the road from terminal i to j has been monitored at the previous inspection time step, else it equals 0. In (7.6), $r^{\mathrm{T}}_{i,j,\min}$ and $r^{\mathrm{R}}_{i,j,\min}$ are the minimum rewards for the transmission line and road between nodes i and j, $r^{\mathrm{T}-}_{i,j,s}$ is the reward of monitoring the transmission line between nodes i and j at the previous inspection time step for scenario s, $r^{\mathrm{R}-}_{i,j}$ is the rewards of monitoring the road between nodes i and j at the previous inspection time step, $P_{i,j,s}$ is the downstream power load of the transmission line from node i to j at the current inspection time step of scenario s, $Q_{i,j}$ is the importance of road from node i to j at the current inspection time step, which is determined by whether the repair crews intend to pass by this road to reach the damages or not. The repair crews can propose one or several preferred routes to reach a given damage before they depart. Then, UAVs can monitor their preferred routes with a priority so that the real-time situation of the roads can be provided to the repair crews. The objective function of the rough monitoring routing problem is defined as:

$$
R_{\mathrm{M}}(\cdot) = -\mathbb{E}_{\mathscr{S}} \left(\sum_{i \in \mathscr{I}} \sum_{j \in \mathscr{I}} \delta_{n,1} \, z_{i,j} \, r_{i,j,s} \right)
\tag{7.7}
$$

where $\mathbb{E}_{\mathscr{S}}$ represents the expectation over all the scenarios in set $\mathscr{S}$, and the binary variable $z_{i,j}$ indicates if the set of UAVs have monitored from node i to j at the current time step:

$$
z_{i,j} = \begin{cases} 1 & \text{if } \sum_{n \in \mathscr{N}} \delta_{n,1} \Delta^{\mathrm{M}}_{n,i,j} \geq 1 \\ 0 & \text{otherwise} \end{cases} \quad \forall i \in \mathscr{I}, \forall j \in \mathscr{I}
\tag{7.8}
$$

where $\Delta^{\mathrm{M}}_{n,i,j}$ is the variable indicating whether UAV n travels from node i to j or not.

When UAV n is allocated to the rough monitoring mode (i.e. $\delta_{n,1} = 1$), it starts from its starting point, while if it is not allocated, there is no constraint for the starting point of UAV n. So:

$$
(\delta_{n,1} - 1) \, M_{\mathrm{big}} \leq \sum_{i \in \mathscr{I}} \Delta^{\mathrm{M}}_{n,\varrho_n,i} - 1 \leq (1 - \delta_{n,1}) \, M_{\mathrm{big}}, \forall n \in \mathscr{N}
\tag{7.9}
$$

where ϱ_n is the starting point of UAV n, M_{big} is an extremely large positive constant. The UAVs allocated to the rough monitoring mode are not supposed to remain stationary at one node i:

$$
(\delta_{n,1} - 1) \, M_{\mathrm{big}} \leq \Delta^{\mathrm{M}}_{n,i,i} \leq (1 - \delta_{n,1}) \, M_{\mathrm{big}}, \forall n \in \mathscr{N}, \forall i \in \mathscr{I}
\tag{7.10}
$$

The time constraints for UAVs are:

$$
\begin{aligned}
(\delta_{n,1} \Delta^{\mathrm{M}}_{n,i,j} - 1) \, M_{\mathrm{big}} &\leq T^{\mathrm{M}}_{n,j,s} - T^{\mathrm{M}}_{n,i,s} - \tau^{\mathrm{M}}_{i,j,s} \leq \\
(1 - \delta_{n,1} \Delta^{\mathrm{M}}_{n,i,j}) \, M_{\mathrm{big}}, &\forall n \in \mathscr{N}, \forall i \in \mathscr{I}', \forall j \in \mathscr{I}, \forall s \in \mathscr{S}
\end{aligned}
\tag{7.11}
$$

where $\mathscr{I}' = \mathscr{I} \cup \{\varrho_n\}$, $T_{n,i,s}^{\mathrm{M}}$ is the time instant at which UAV n reaches node i in scenario s, $\tau_{i,j,s}^{\mathrm{M}}$ is the travel time from node i to j for scenario s. Note that the travel time should consider the detouring time for obstacles. Furthermore, if node i and j are not connected and i is not the starting point, $\tau_{i,j,s}^{\mathrm{M}}$ is an extremely large positive value for all the scenarios. For $i = \varrho_n$, $\tau_{\varrho_n,j,s}^{\mathrm{M}}$ equals the travel time from the starting point to node j for scenario s. For the starting point ϱ_n of UAV n, $T_{n,\varrho_n,s}^{\mathrm{M}} = 0$. When UAV n departs from node i, it must have arrived at node i:

$$\sum_{j \in \mathscr{I}} \delta_{n,1} \, \Delta_{n,i,j}^{\mathrm{M}} \le \sum_{j \in \mathscr{I}'} \delta_{n,1} \, \Delta_{n,j,i}^{\mathrm{M}}, \, \forall n \in \mathscr{N}, \, \forall i \in \mathscr{I} \tag{7.12}$$

The monitoring process for all UAVs cannot exceed the prediction horizon:

$$0 \le T_{n,i,s}^{\mathrm{M}} \le T_{\mathrm{D}}, \, \forall n \in \mathscr{N}, \, i \in \mathscr{I}, \, \forall s \in \mathscr{S} \tag{7.13}$$

Then the feasibility set can be defined by constraints (7.5)-(7.13), and the optimization vector is $y_1 = [\Delta_{n,i,j}^{M}, T_{n,j,s}^{\mathrm{M}}]_{n \in \mathscr{N}, i \in \mathscr{I}', j \in \mathscr{I}, s \in \mathscr{S}}^{\mathrm{T}}$.

7.3.3. INSPECTION ROUTING PROBLEM

In this subsection, a stochastic inspection routing problem is formulated. The inspection time, the traveling time, and the load loss cost are stochastic variables included in the problem via scenarios. When formulating the inspection routing problem, a target time for each inspection is considered. If the earliest UAV reaches one component later than the target time for inspection, an extra cost of inspection will be added to penalize this delay. In this chapter, the extra cost of inspection is defined to be equal to the load loss costs from the target time to the earliest arrival time of UAVs. If the UAVs do not reach the component in one prediction horizon, the extra cost of inspection equals the load loss costs from the target time to the end of the prediction horizon. Furthermore, at the next inspection time step, the target time for components not yet reached in the previous inspection time step will be a negative value to capture that their inspection is delayed from the previous inspection time step(s). In addition, the absolute value of this negative value equals the time between the starting time of the current inspection time step and the target time of this component.

Furthermore, the space-varying characteristics of the load loss costs should be considered, such that damages in different locations will lead to different load loss costs, e.g., some damages can lead to large outages while others only influence small loads. Then, the extra cost of inspection is:

$$R_{\mathrm{I}}(\cdot) = \mathbb{E}_{\mathscr{S}'}\Big(\sum_{q \in \mathscr{P}} \sum_{n \in \mathscr{N}} \delta_{n,2}\Big(\sum_{p \in \mathscr{P}'_n} (\Delta_{n,p,q}^{\mathrm{I}} \cdot \max\{(T_{n,q,s'}^{\mathrm{I}} -$$
$$w_q) \cdot C_{q,s'}, 0\}) + \max\{(1 - \sum_{p \in \mathscr{P}'_n} \Delta_{n,p,q}^{\mathrm{I}}), 0\} \cdot T_{\mathrm{D}} \cdot C_{q,s'}\Big)\Big) \tag{7.14}$$

where $\mathscr{P}$ is the set of components that have to be inspected, $\mathscr{P}'_n = \mathscr{P} \cup \{\varrho_n\}$, $\mathscr{S}'$ is the set of scenarios in inspection routing problem. At the beginning of each inspection time

step, some UAVs have finished monitoring or inspection, or are flying through the distribution network or road infrastructure, or are in the depots charging their batteries, so the starting points of UAVs will be different. In (7.14), the extra costs of inspections is separated into two terms. The first term is the total inspection cost. If time instant of scenario s', $T^I_{n,q,s'}$ at which UAV n finishes inspecting component q is later than target time w_q, there will be an additional cost of inspection. If not, the extra cost of inspection will be zero. The second term is the total non-inspection cost when components were not inspected in one prediction horizon. In (7.14), the load loss cost for damaged component q of scenario s' is $C_{q,s'}$ per unit time, $\Delta^I_{n,p,q}$ is the variable indicating whether UAV n travels from damaged component or starting point p to damaged component q.

When UAV n is allocated to the inspection mode ($\delta_{n,2} = 1$), it starts from its starting point, while if not allocated, there is no constraint for the starting point of UAV n, such that:

$$(\delta_{n,2} - 1) M_{\text{big}} \le \sum_{q \in \mathscr{P}} \Delta^I_{n,\varrho_n,q} - 1 \le (1 - \delta_{n,2}) M_{\text{big}}, \forall n \in \mathscr{N} \tag{7.15}$$

The UAVs allocated to the inspection mode are not supposed to remain stationary at one location p:

$$(\delta_{n,2} - 1) M_{\text{big}} \le \Delta^I_{n,p,p} \le (1 - \delta_{n,2}) M_{\text{big}}, \forall n \in \mathscr{N}, \forall p \in \mathscr{P} \tag{7.16}$$

To simplify the expression of the following constraints, intermediate variables are introduced:

$$x_{n,p,q} = \delta_{n,2} \Delta^I_{n,p,q} \forall n \in \mathscr{N}, \forall p, q \in \mathscr{P}'_n \tag{7.17}$$

The time constraints for UAVs are:

$$(x_{n,p,q} - 1) M_{\text{big}} \le T^I_{n,q,s'} - T^I_{n,p,s'} - \tau^I_{p,q,s'} - \sigma_{q,s'} \le$$
$$(1 - x_{n,p,q}) M_{\text{big}}, \forall n \in \mathscr{N}, \forall p \in \mathscr{P}'_n, \forall q \in \mathscr{P}, \forall s' \in \mathscr{S}', \tag{7.18}$$

where $\tau^I_{p,q,s'}$ and $\sigma_{q,s'}$ are the travel time from component p to q and the inspection time for component q of scenario s' respectively. Notice that, the travel time should consider the detouring time for obstacles. Besides, for the starting point ϱ_n of UAV n, $T^I_{n,\varrho_n,s'} = 0$ and $\sigma_{\varrho_n,s'} = 0$ are defined for all $s' \in \mathscr{S}'$. Each component can only be reached once and the UAVs can only depart once from each component:

$$\sum_{n \in \mathscr{N}} \sum_{p \in \mathscr{P}'_n} x_{n,p,q} \le 1, \forall q \in \mathscr{P}, \sum_{n \in \mathscr{N}} \sum_{q \in \mathscr{P}} x_{n,p,q} \le 1, \forall p \in \mathscr{P} \tag{7.19}$$

When UAV n departs from component p, it must have arrived at component p:

$$\sum_{q \in \mathscr{P}} x_{n,p,q} \le \sum_{q \in \mathscr{P}'_n} x_{n,q,p}, \forall n \in \mathscr{N}, \forall p \in \mathscr{P} \tag{7.20}$$

The beginning time of inspections for all the UAVs cannot exceed the prediction horizon:

$$0 \le T^I_{n,p,s'} \le T_D, \forall n \in \mathscr{N}, p \in \mathscr{P}'_n, \forall s' \in \mathscr{S}' \tag{7.21}$$

Then the feasibility set can be defined by constraints (7.14)-(7.21), and the optimization vector is $y_2 = [\Delta^I_{n,p,q}, T^I_{n,p,s'}]^T_{n \in \mathscr{N}, p \in \mathscr{P}'_n, q \in \mathscr{P}, s' \in \mathscr{S}'}$.

7.3.4. Solution approach

To reduce the computational burden and to avoid conservative solutions, a chance-constrained method is used to transform the stochastic constraints into deterministic constraints [194]. Then, the mixed-integer linear bi-level programming problem can be solved by a branch-and-bound computing structure [150]. This branch-and-bound computing structure solves the bi-level programming problem by generating the feasible subsets of the solution set in the top-level problem. Then, it solves the bottom-level problem by substituting these feasible subsets into the bottom-level problem. After that, the solutions of the bottom-level problems associated with the subsets will be obtained and compared to find the optimal solution of the top-level problem via the branch-and-bound algorithm.

Four kinds of bi-level solvers are studied and compared in this chapter, including Matlab+CPLEX solver, Matlab+Intlinprog solver[1], Matlab+GA (genetic algorithm) solver, and Matlab+Greedy (greedy algorithm) solver. All these solvers use a branch-and-bound computing structure that can be implemented in Matlab at the top level of the bi-level programming problem, while the difference of these solvers lies in the solvers for the bottom-level mixed-integer linear programming problem. CPLEX and Intlinprog bottom-level solvers can be implemented by the functions "cplexmilp" and "intlinprog" respectively. Here we explain the mechanism of the GA and Greedy algorithms applied in this chapter.

The GA algorithm has been implemented in Matlab M files for convenience. Furthermore, as can be seen in Section 7.3.2 and Section 7.3.3, when the mode allocation results are fixed by the top-level branch-and-bound solver, the inspection and the rough monitoring problems are two individual problems. Then, the inspection programming problem and the rough monitoring programming problem at the bottom level can be solved separately by using the mechanism for the multiple traveling salesman problem presented in [40]. In detail, the inspection problem is to route UAVs from their starting points to the locations of the damages, and the rough monitoring problem is to route UAVs from nodes to the locations of the damages. Thus, they are both essentially multiple traveling salesman problems.

For the greedy algorithm, the strategy for inspection is as follows: for each inspection time step, first we select the damage that is most urgently required to be inspected, but has not yet been inspected. Then we select the nearest UAV to inspect that damage. Then repeat this process until all UAVs are allocated or all damages are allocated to be inspected. Furthermore, the strategy for rough monitoring is such that: for each inspection time step, we select the line/road with the highest monitoring reward, and select the nearest UAV to monitor it. Then we repeat this process until all UAVs are allocated or all lines/roads are allocated to be monitored.

7.4. Detailed monitoring problem

After mode allocation and determining the inspection routes and the rough monitoring routes, the detailed monitoring routing problem is formulated and solved. At each

---

[1] Because CPLEX is implemented in object code whereas GA and the greedy algorithm implemented in Matlab, to have a fair comparison with the MILP solvers, we also use the MILP solver implemented in Matlab i.e. Intlinprog.

monitoring time step, the positions of the UAVs are updated as:

$$\chi_n(\phi+1) = \chi_n(\phi) + l \cdot \begin{bmatrix} \cos(\theta_n(\phi)) \\ \sin(\theta_n(\phi)) \end{bmatrix}, \forall n \in \mathcal{N}', \forall \phi \in \Phi' \tag{7.22}$$

where $\chi_n(\phi)$ is the geographical position of UAV n at monitoring time step ϕ, and $\chi_n(0)$ is the initial position of UAV n. The variable $\theta_n(\phi)$ represents the moving direction of UAV n at monitoring time step ϕ where $\theta_n(\phi) \in \Theta = \{ \frac{\pi}{6}, \frac{\pi}{2}, \frac{5\pi}{6}, \frac{7\pi}{6}, \frac{3\pi}{2}, \frac{11\pi}{6} \}$, Φ' is the set of monitoring time steps in the one prediction horizon but excluding the last monitoring time step, and $\mathcal{N}'$ is the set of UAVs that are working in monitoring mode. To use the UAVs more efficiently in one inspection time step, once UAVs finish their charging and inspection tasks, at the remaining monitoring time steps of the current inspection time step, they can be put into the set $\mathcal{N}'$ and used to perform monitoring tasks until the beginning of the next inspection time step. For example, consider that there are 5 monitoring time steps in one inspection time step. When a UAV finishes inspection or charging at the third monitoring time step, then for the remaining two monitoring time steps, this UAV will be allocated to monitoring tasks by solving the detailed monitoring routing problem.

Considering that one inspection time step includes multiple monitoring time steps, solving a programming problem for one inspection time step is time consuming. Thus, a predictive solver using receding horizons is applied to reduce the computation burden. The objective function of the detailed monitoring problem is defined as:

$$\max_{\theta_n(\phi)} \mathbb{E}_{\mathscr{S}} \Big(\sum_{\phi \in \Phi} \sum_{c \in \mathscr{C}} \eta_c(\phi) r_{c,s}^{\mathrm{M}}(\phi) \Big) \tag{7.23}$$

where $\eta_c(\phi)$ equals 1 if hexagon c is monitored at monitoring time step ϕ, $r_{c,s}^{\mathrm{M}}(\phi)$ is the reward for monitoring hexagon c in monitoring time step ϕ for scenario s, Φ is the set of monitoring time steps in one prediction horizon of the detailed monitoring problem, and $\mathscr{C}$ is the set of hexagons in the whole distribution and traffic network. The objective of the detailed monitoring problem is to monitor the lines and roads to maximize the total reward. The rewards are modeled in the detailed monitoring problem considering two factors. Firstly, when the transmission lines or roads have been monitored recently by UAVs, the condition, e.g., potential failure, traffic jam, of these transmission lines or roads are less uncertain. Secondly, the longer the time since the transmission lines or roads have been monitored, their conditions are more uncertain. Thus, the reward $r_{c,s}^{\mathrm{M}}(\phi)$ for monitoring hexagon c in monitoring time step ϕ can be defined as:

$$r_{c,s}^{\mathrm{M}}(\phi) = \sum_{(i,j) \in \mathscr{T}_c} r'_{i,j,s}(\phi) + \sum_{(i,j) \in \mathscr{R}_c} r''_{i,j}(\phi), \forall \phi \in \Phi, \forall c \in \mathscr{C}, \forall s \in \mathscr{S} \tag{7.24}$$

where (i, j) represents the transmission line or road between nodes i and j, $\mathscr{T}_c$ and $\mathscr{R}_c$ are the sets of transmission lines and roads included in hexagon c respectively. For

$r'_{i,j,s}(\phi)$ and $r''_{i,j}(\phi)$:

$$
\begin{aligned}
r'_{i,j,s}(\phi) &= \eta_c(\phi) \cdot r^{\mathrm{T}}_{i,j,\min} + (1 - \eta_c(\phi)) \cdot r^{\mathrm{T}}_{i,j,s}, \\
&(i,j) \in \mathcal{T}_c, \ \forall \phi \in \Phi, \ \forall c \in \mathcal{C}, \ \forall s \in \mathcal{S} \\
r''_{i,j}(\phi) &= \eta_c(\phi) \cdot r^{\mathrm{R}}_{i,j,\min} + (1 - \eta_c(\phi)) \cdot r^{\mathrm{R}}_{i,j}, \\
&(i,j) \in \mathcal{R}_c, \ \forall \phi \in \Phi, \ \forall c \in \mathcal{C}, \ \forall s \in \mathcal{S}
\end{aligned}
\tag{7.25}
$$

Note that $r^{\mathrm{T}}_{i,j,s}$ and $r^{\mathrm{R}}_{i,j}$ vary at each inspection time step but not at each monitoring time step, because the loads and the roads preferred by the repair crews are assumed to not change drastically within tens of seconds (one monitoring time step). Then, $\eta_c(\phi)$ can be obtained by:

$$
\eta_c(\phi) = \begin{cases} 0 & \text{if } \chi_n(\phi) = \chi_c \\ 1 & \text{otherwise} \end{cases}, \ \forall n \in \mathcal{N}', \ \forall \phi \in \Phi, \ \forall c \in \mathcal{C} \tag{7.26}
$$

where χ_c represents the geographical position of the center of hexagon c.

The detailed monitoring problem can be solved by firstly transforming the non-linear constraints into mixed-integer form, and then using branch-and-bound method.

7.5. Case study

7.5.1. General settings of the case study

A real-life distribution network and traffic network in the urban and rural area of Zaltbommel and its neighbors, the Netherlands, is considered as shown in Figure 7.3. In this case study, obstacles and a heterogeneous UAV team with multi-rotor UAVs and fixed-wing UAVs are considered. There are 6 multi-rotor UAVs (UAVs 1, 3, 4, 5, 7 and 8) that can be applied for inspection and monitoring and 2 fixed-wing UAVs (UAVs 2 and 6) that can only be used for monitoring.

During the restoration process, some unpredictable events will also be considered in this case study, including changes of damages (i.e. newly emerged damages, and damages inspected by repair crews) and the unpredictable position shifting of the UAVs. We will show that the proposed real-time UAVRS can handle these unpredictable events in time by comparing its performance to the off-line methods, which do not handle these unpredictable events in time. The off-line method used for changes of damages determines the UAVRS plans before implementing the inspection and monitoring tasks and does not change them during implementation. This off-line method is characterized by two aspects. Firstly, when a new damage emerges, the off-line method allocates UAVs to inspect the newly emerged damage after the off-line inspection tasks are all accomplished. Secondly, when a damage is inspected by human repair crews, the off-line method still allocates UAVs to inspect that damage but when the UAVs reach that damage (and find that the damage has been inspected by human repair crews), the UAVs move to another inspection task immediately. While, the off-line method used for position shifting considers that when a position shifting occurs, the UAV first moves back to its original route and then follows the original route.

In addition, the algorithms mentioned in Section 7.3.4 will be compared w.r.t. the

(a) Map for Zaltbommel (*Source: Google map*)

(b) Map for rough monitoring

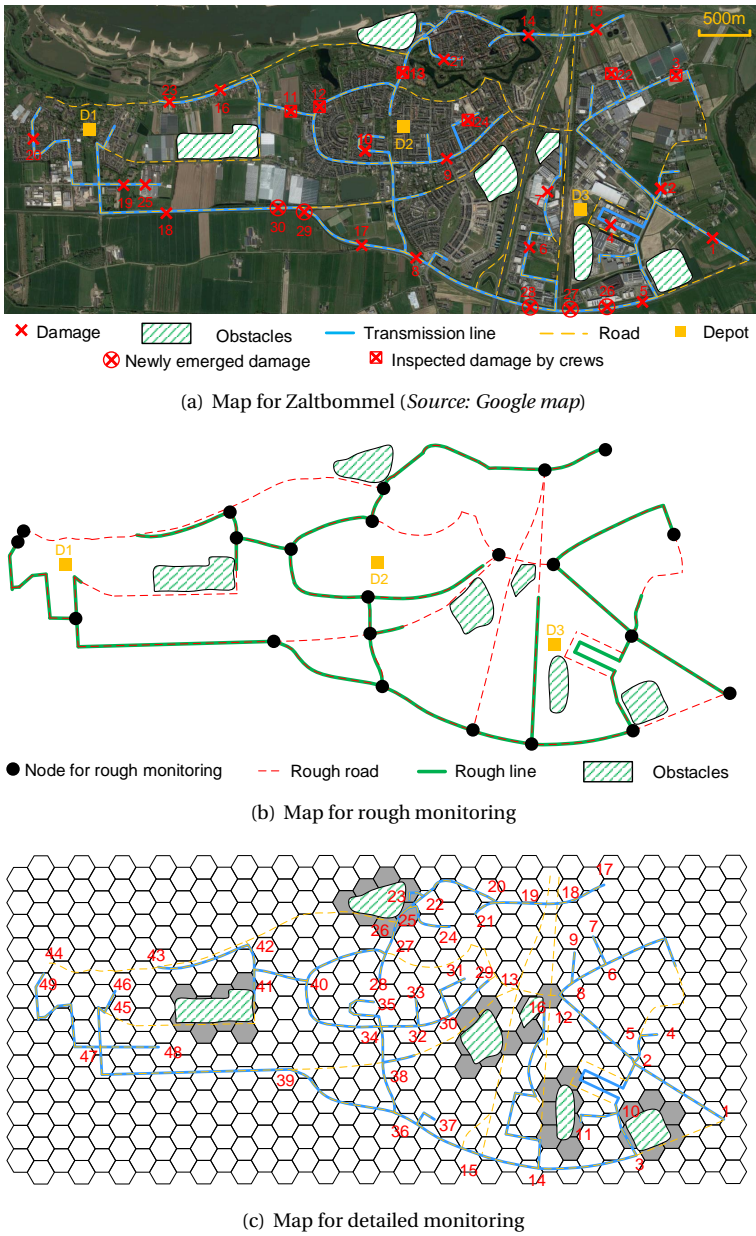(c) Map for detailed monitoring

Figure 7.3: Maps for the case study

optimality and the solving speed.

In this case study, the flying speed of all the UAVs is 0.3 km/min, each inspection time step takes 5 min, and the prediction horizon is 15 min (T_D = 15). In the detailed

monitoring problem, the distance between the center of a hexagon and that of its neighbor hexagon is 300 m. Moreover, there are 5 monitoring time steps in one inspection time step. Furthermore, the prediction horizon of the detailed monitoring is 4 ($|\Phi| = 4$). At the beginning, UAVs 1 and 2 are in Depot 1, UAVs 3 to 6 are in Depot 2, and UAVs 7 and 8 are in Depot 3. The charging times for UAVs are 15 min. The coefficients are $\gamma = 0.5$, $r^{\mathrm{T}}_{i,j,\mathrm{min}} = 1$, and $r^{\mathrm{R}}_{i,j,\mathrm{min}} = 1$ ($\forall i \in \mathscr{I}$, $\forall j \in \mathscr{I}^{\mathrm{N}}_i$).

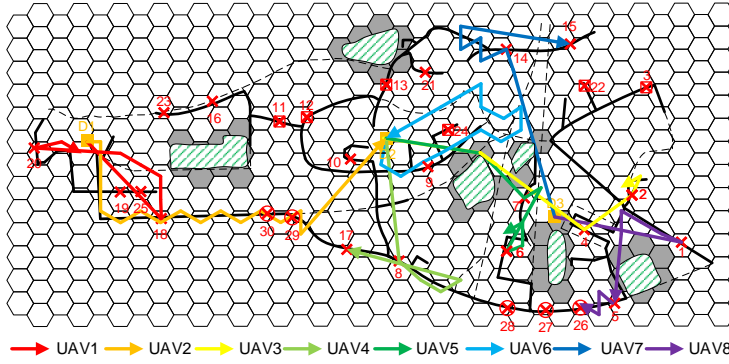### 7.5.2. SETTINGS AND RESULTS FOR CHANGES OF DAMAGES

The following unpredictable events are considered in the case of changes of damages: At $t = 20$ min, Damages 26 to 30 newly emerge. At $t = 25$ min, $t = 30$ min, and $t = 40$ min, Damages 3 and 22, Damages 11 to 13, and Damage 24 have been inspected by the human repair crews respectively. During inspection time steps 1 to 5, the preferred paths of the repair crew are 3-14, 39-47, 29-34, and 8-29-26, while during inspection time steps 6 to 9, the preferred paths are 3-14, 36-39-38, and 34-40 as shown in Figure 7.3(c). All these optimal routes in Figure 7.4 are obtained by the branch-and-bound bi-level solver (Matlab+CPLEX).

Since there are no changes of damages at the first five inspection time steps, the routes for the proposed and the off-line method are the same at inspection time steps 1 to 5 (Figure 7.4(a)). For inspection time steps 6 to 9, the routes obtained with the proposed method are shown in Figure 7.4(b), while the routes of the off-line method used for changes of damages are shown in Figure 7.4(c).

In Figure 7.4(a), UAV 1 is allocated to inspect Damages 18 and 20 and reaches them at $t = 3.54$ min and $t = 17.85$ min. UAV 2 is allocated to monitor paths 45-47-39-36 and then to the charging mode. UAV 3 is allocated to inspect Damages 4 and 2 and reaches them at 9.72 min and 17.1 min. UAV 4 is allocated to Damages 8 and 17 and reaches them at $t = 4.12$ min and $t = 18.77$ min. UAV 5 is allocated to Damages 7 and 6 and reaches them at $t = 8.72$ min and $t = 17.18$ min. UAV 6 is allocated to monitor paths 34-32-30-29-31-27 and then to the charging mode. UAV 7 is allocated to inspect Damages 14 and 15 and reaches them at $t = 5.88$ min and $t = 19.88$ min. UAV 8 is allocated to inspect Damages 1 and 5 and reaches them at $t = 4.32$ min and $t = 17.18$ min.

Then in Figure 7.4(b), UAV 1 is allocated to Damages 19, 25, 23, and 30 and reaches them at $t = 25.9$ min, $t = 30.64$ min, $t = 37.68$ min, and $t = 44.6$ min respectively. UAV 2 is fully charged at $t = 31.5$ min and then start monitoring paths 34-36-38-15. UAV 3 is allocated to inspect Damage 9 and reaches it at $t = 31.34$ min and then monitor paths 30-32 and 38-13. UAV 4 is allocated to Damages 16 and 29 and reaches them at $t = 31.36$ min and $t = 42.98$ min. UAV 5 is allocated to Damages 10 and reaches it at $t = 32.27$ min and then to monitor paths 34-40 and 39-38. UAV 6 is fully charged at $t = 35.5$ min and start to monitor paths 34-35 and 34-40. UAV 7 is allocated to Damage 21 and reaches it at $t = 33.22$ and then to charging mode. UAV 8 is allocated to Damages 27, 28, and 26 and reaches them at $t = 26.16$ min, $t = 31.28$ min, and $t = 37.44$ min respectively. The whole restoration process is accomplished in 9 inspection time steps for the proposed real-time method.
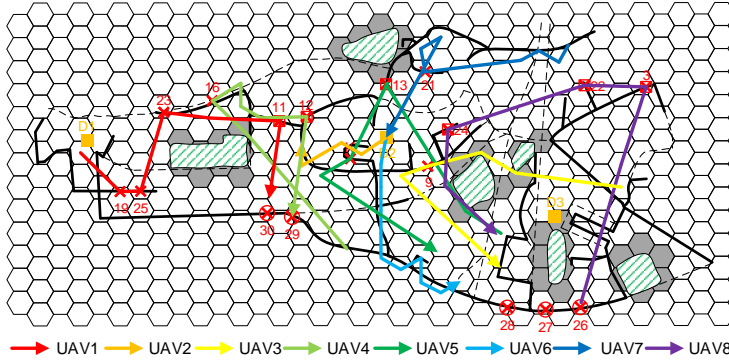
For the off-line method (see Figure 7.4(c)), UAV 1 reaches Damages 19, 25, 23, and 30 at $t = 25.9$ min, $t = 30.64$ min, $t = 37.68$ min, and $t = 45.89$ min respectively. UAV 2 travels the same routes with those of Figure 7.4(b). UAV 3 reaches Damages 9 and 27

(a) Simulation results for steps 1 to 5
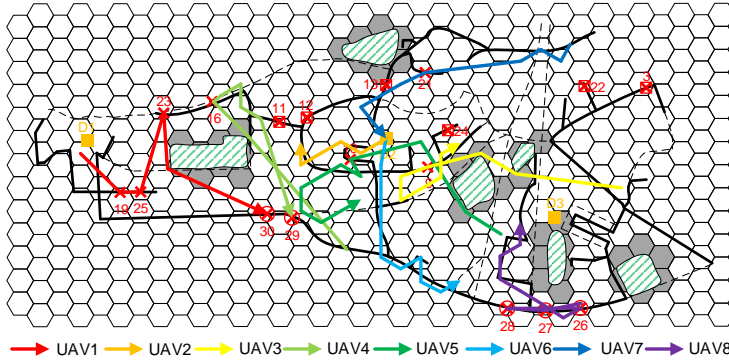
(b) Simulation results of the real-time UAVRS for steps 6 to 9

(c) Simulation results of the off-line UAVRS for steps 6 to 9

Figure 7.4: Routes for changes of damages

at $t = 31.44$ min and $t = 47.1$ min. UAV 4 reaches Damages 16 and 29 at $t = 31.36$ min and $t = 44.92$ min. UAV 5 reaches Damages 10 and 28 at $t = 34.55$ min and $t = 49.5$ min.

(a) Position shifting when monitoring

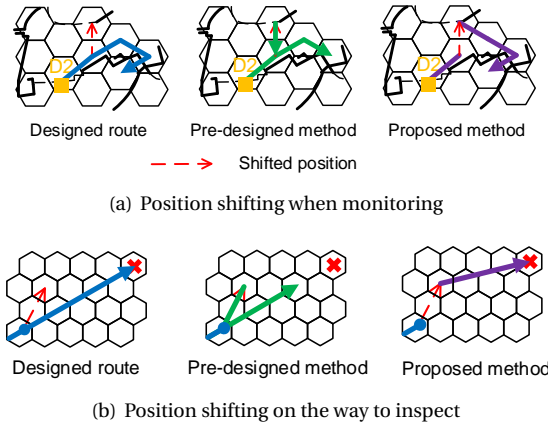(b) Position shifting on the way to inspect

Figure 7.5: Routes for position shifting

UAV 6 travels the same routes with those of Figure 7.4(b). UAV 7 reaches Damage 21 at $t = 33.22$ min. UAV 8 reaches Damage 26 at $t = 51.7$ min. The whole restoration process is not accomplished in 9 inspection time steps (actually 11 inspection time steps) for the off-line method.

The total inspection cost for the real-time method is 3.88 for the whole process, while the inspection cost for the off-line method is 146.07. Thus, to handle the newly emerged damages and adapt to the inspected damages by the human repair crews in time are very important in UAVRS for restoration. The monitoring rewards for the whole process are 378.41 and 313.31 for the real-time method and the off-line method respectively. The objective function value of the whole UAVs routing process for the real-time UAVRS is smaller than that of the off-line UAVRS.

7.5.3. SETTINGS AND RESULTS OF POSITION SHIFTING

In this subsection, unpredictable position shifting on the way to inspect, and when monitoring is considered. The proposed UAVRS is compared with the off-line method used for position shifting as described in Section 7.5.1. The simulation results are shown in Figure 7.5.

In Figure 7.5(a), the designed route for a period of 4 min is shown. However, at t=2 min, the UAV is shifted to a position out of the designed route. The off-line method searches the way back to the trace, while the detailed monitoring routing strategy in the proposed real-time UAVRS architecture determines a better route at t=2 min. By implementing the proposed method, the UAV monitors one more hexagon than the off-line method.

In Figure 7.5(b), when the UAV reaches the blue node, the designed route is determined for the next inspection time step. However, because of position shifting, the UAV reaches the position indicated by red dashed arrow, not the blue node. The off-line method searches the way back to the off-line routes. On the contrary, the proposed real-time UAVRS architecture adjusts to the new position and determines a new direct

Table 7.2: Scales of the programming problem for each inspection time step

	Step 1	Step 2	Step 3	Step 4	Step 5	Step 6	Step 7	Step 8	Step 9
Number of damages	25	22	-	19	-	16	11	5	2
Number of available UAVs	8	5	-	6	-	5	6	3	7

route. In this case, the damage can be inspected earlier than with the off-line method.

7.5.4. COMPARISON OF ALGORITHMS AND SATISFACTION OF REAL-TIME RE-QUIREMENTS

Since for the detailed monitoring problem at the second layer, the solutions can be obtained in several seconds, which is much shorter than one monitoring time step, the real-time requirement is satisfied easily for each time step. This subsection mainly discusses and compares the algorithms mentioned in Section 7.3.4 for the first-layer bi-level programming problem.

The scales of the bi-level programming problem for each inspection time step are listed in Table 7.2. The available UAVs represent the UAVs that are not inspecting or charging. The CPU times and objective function values are shown in Figure 7.6. In Figure 7.6, for inspection time step 3 and 5, there is no UAV available and consequently there is no bi-level programming problem to be solved at these two inspection time steps. Note that the CPU times and objective function values of the GA are obtained by the average value over ten runs. Furthermore, the maximum number of generations to obtain results in one inspection time step is 800, and the number of chromosomes is 601.

From the simulation results, it can be seen that, although the Matlab+ CPLEX and the Matlab+Intlinprog solvers can obtain the optimal solution, the computation time may be larger than one inspection time step if the programming problem involves more than 25 damages and 8 available UAVs, while the Matlab+CPLEX and the Matlab+Intlinprog solvers can only handle cases with up to 19 damages and 6 available UAVs. For the Matlab+GA solver, the computing times can be kept smaller than one inspection time step, and the gaps between the Matlab+GA solutions and the optimal solution are less than 11% for large-scale problems (Step 1, 2, 8, 9), with no gaps at all for small scale problems (Step 6, 7). For the Matlab+Greedy solver, the computation time is quite low, but the optimality fluctuates heavily for different inspection time steps. Therefore, the Matlab+GA solver is more suitable to solve the bi-level programming problem in the first layer of our proposed real-time UAVRS.

7.6. CONCLUSIONS AND FUTURE WORK

This chapter has proposed a real-time UAV routing strategy that can facilitate the fast restoration of distribution networks after disasters. By using UAVs, the road traffic conditions will not influence the inspection and monitoring operations, and the level of safety and efficiency of the human repair crews after the disaster will increase. Then the distribution network operators will obtain updated statuses of the components of the distribution network and of the road infrastructure condition, which benefits the operators

(a) CPU times for the solvers
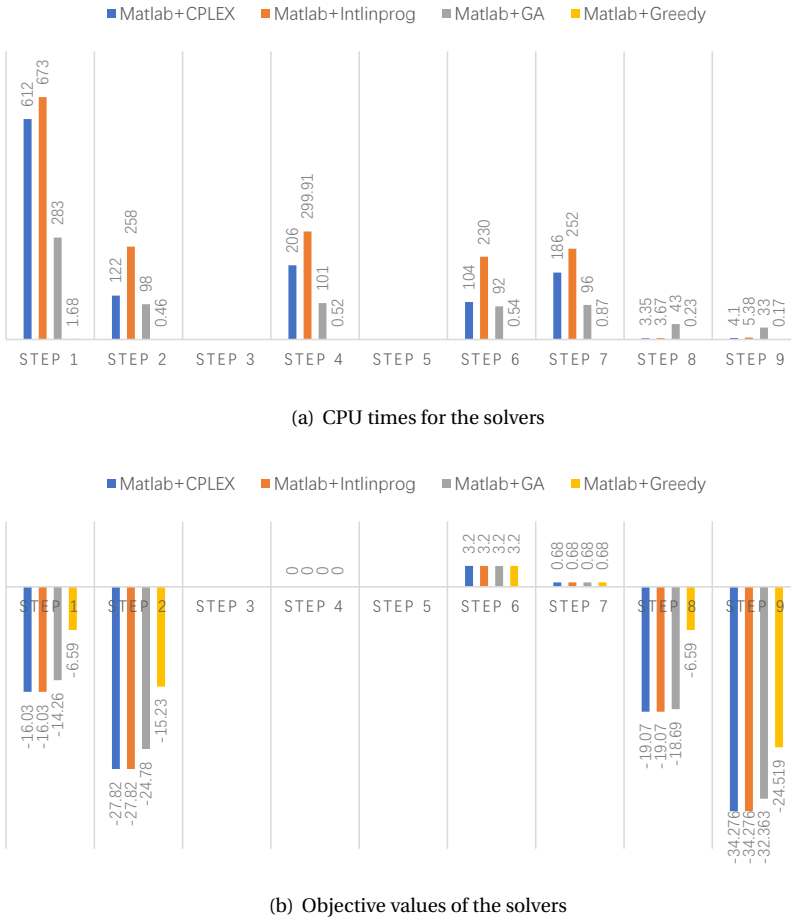

(b) Objective values of the solvers

Figure 7.6: Performance comparison of the solvers

and repair crews to take resilience enhancement measures in time and also guides the way for repair crews to reach the damages considering that some roads might be blocked due to the disasters. In addition, the proposed real-time UAV routing strategy can also adapt to unpredictable events, e.g., newly emerged damages, damages already inspected by human repair crews, and position shift of UAVs. Further research will consider a really larger network, and the multi-level methods will be developed for large-scale instances of the UAVRS problem. Furthermore, although the UAVs can replace human crews to perform risky inspection and monitoring tasks, UAVs may be restricted by no-fly zones [38] and rainy weather [116]. Thus, the effectiveness of using UAVs to inspect and monitor may be influenced. So, another topic for further research is to find alternatives other than UAVs that are not restricted by no-fly zones and weather conditions.

8

CONCLUSIONS AND RECOMMENDATIONS

In this thesis, we have investigated failure prevention, location, and restoration strategies in power systems. These strategies are tools to maintain and restore power systems. In this final chapter, the main conclusions and contributions are summarized, the impacts on the society are analyzed, and recommendations are provided.

8.1. CONCLUSIONS

The main results of this thesis can be summarized as follows:

DEVELOPMENT OF A PREDICTIVE MAINTENANCE APPROACH FOR ACTIVE DISTRIBUTION NETWORKS

We have proposed a short-term preventive scheduling method for active distribution networks systems that are integrated with distributed energy generators. The power supporting potential of distributed generators and batteries when performing maintenance actions in the distribution network can be systematically optimized with the proposed method. This contribution helps the distribution network operators to reduce load loss costs caused by maintenance.

DESIGN OF A MAINTENANCE STRATEGY FOR GENERATION UNITS CONSIDERING INTER-ISO POWER EXCHANGE

We have proposed a bidding mechanism for maintenance of generation units in transmission power systems. In this mechanism, the generation companies (GENCOs) of the host independent system operator (ISO) can bid to change their scheduled maintenance actions and to increase their own benefits. The GENCOs can use their bid price to purchase supportive energy from the GENCOs of the neighbor ISOs, to pay the penalty fee caused by reducing the energy transmitted from the host ISO to the neighbor ISOs

w.r.t. the long-term power exchange transactions, or both. This contribution can provide more flexibility to the GENCOs for maintaining their generation units. Furthermore, the reliability of the power networks can also be improved.

Development of a Truthful platform for maintenance of generation units

We have proposed a truthful platform for the maintenance of generation units and an accelerated Benders decomposition method. The major advantage of the proposed truthful maintenance platform is that it provides a truthful environment for data storage, data sharing, and decision making. This contribution can provide a theoretical design form for truthful maintenance of generation units.

Design of an accelerated Benders decomposition algorithm for maintenance of generation units

Since the solving speeds of maintenance scheduling problems are low, an accelerated Benders decomposition algorithm is proposed by using two specially designed valid inequalities. The proposed valid inequalities can solve the maintenance scheduling problems for generation units with less CPU time.

Design of an EV charging strategy for pre-disaster evacuation situations

We have proposed a PEV charging strategy for pre-disaster evacuation situations. Furthermore, an accelerated Aitken-DMPC algorithm has been proposed to solve the formulated charging problems. The proposed PEV charging control strategy can handle charging planning for pre-disaster evacuation situations by accounting for human evacuation behavior. Furthermore, it can handle the unmet departure demands of the PEVs fairly by adding a penalty mechanism in the formulated charging planning problem. This contribution can provide an accurate load and charging demand prediction method for evacuation situations. Moreover, the proposed Aitken-DMPC approach can reduce the CPU times for solving the charging problems, and consequently, the requirement of CPU times for solving real-time charging problems can be satisfied.

Design of an accurate fault location algorithm considering uncertainty in measurements

We have analyzed the influence of uncertainty in the measurements on the transmission line parameter estimations, which, in turn, influences the results of fault location methods. Then we have used the maximum-likelihood-estimation method to reduce the uncertainty in the measurements. By this means, the cost and duration of the search process for the actual fault location can be reduced.

Development of a UAV routing strategy for post-disaster inspection and monitoring

We have proposed a real-time UAV routing strategy that can facilitate the fast restoration of distribution networks after disasters. By using UAVs, the road traffic conditions will not influence the inspection and monitoring operations, and the level of safety and efficiency of the human repair crews after the disaster will increase. By using the proposed strategy, the failures can be inspected quickly by the UAVs and repaired by the human crews. Furthermore, the traffic situations can be monitored by the UAVs, so that the repair crews can select the best suited ways to reach the damages.

8.2. Impacts of this thesis

8.2.1. Impacts on society

The strategies proposed in this thesis will have several positive impacts on society, which are as follows.

Ensuring the power supply

Sudden failures of the components, e.g., generation units and transmission lines, in power networks may cause large-scale outages. The outages may decrease the quality of life of the residents. Thus, performing maintenance actions on components with bad health conditions can significantly reduce the possibility of sudden outages. Thus, our proposed maintenance strategies can provide tools to schedule maintenance actions on the components in power networks. The power system operators can then perform the maintenance actions according to the scheduling results determined by our proposed strategies to enhance the reliability of power networks.

Dealing with effects of nature disasters on power networks

Nature disasters may damage power networks and result in outages. The pre-disaster evacuation should be well organized, and the post-disaster restoration actions should be performed as soon as possible. Thus, in this thesis, we provide a PEV charging strategy for pre-disaster evacuation situations to optimize the charging decisions. Furthermore, we provide fault location and UAV routing strategies so that the post-disaster restoration actions can be performed as soon as possible.

In summary, the research performed in this thesis has two main positive impacts on society. First, it provides maintenance strategies to ensure power supply in power networks. Second, it provides efficient strategies for the power system operators to counter the effects of nature disasters.

8.2.2. Impacts on science and technology

Real-time control usually requires short computation times so that the control actions can be obtained in time. Thus, in this thesis, we propose an accelerated distributed model predictive control strategy based on the Aitken algorithm to improve the computational efficiency of the real-time PEV charging control. Furthermore, we also provide a hierarchical computing structure and a heuristic algorithm for real-time UAV routing control. By using these proposed algorithms, the CPU times required for solving the real-time control problems can be reduced significantly. Then, the control actions can be obtained in time for the implementation of the real-time control. The algorithms proposed in this thesis can also be leveraged to other real-time control systems in other fields, e.g., real-time control for railway or urban traffic transportation.

8.3. Topics for future works

In this section, we present several directions for future research, categorized as short-term and long-term future topics, respectively.

8.3.1. SHORT-TERM FUTURE TOPICS

EXTENDED TRUTHFUL PLATFORM FOR MAINTENANCE

The contents of the truthful maintenance platform require to be further extended. For example, the profits and costs of using the truthful platform for maintenance should be evaluated via real-life cases. Furthermore, to improve the effectiveness of the planning of maintenance operations, it is of interest to develop mechanisms to ensure that participants are encouraged to share more data so that they can be seen and used by the target entities, while at the same time guaranteeing that sensitive shared data cannot be seen by the competitors.

ACCELERATED DISTRIBUTED MODEL PREDICTIVE CONTROL

Other acceleration approaches, e.g., Anderson [204] and Steffensen [107] acceleration approaches, may be developed for distributed model predictive control. Furthermore, the rates of convergence for distributed model predictive control approaches should be studied for distributed control architectures with more than three blocks.

PREDICTIVE MAINTENANCE STRATEGIES FOR POWER CONVERTERS

The key innovation of this topic is to associate the reliability of power electronics devices with the power system operations. Predictive maintenance and the power converter control strategies can be studied. Specifically, the predictive maintenance strategy for converters considering the mission profiles, e.g., temperature and load profiles, should be developed. Furthermore, power converter control strategies for enhancing the reliability of the power systems should be developed.

8.3.2. LONG-TERM FUTURE TOPIC

FULLY AUTONOMOUS CONTROL PLATFORM TO COUNTER EXTREME NATURE DISASTERS

This topic is to develop an autonomous control platform for power systems to counter the effects of nature disasters. The target of this platform would be to facilitate human power system operators to make decisions. Consequently, the efficiency for decision making can be improved and the visualization and be increased. A variety of tools that can support decision-making based on data will be developed.

MIGRATION OF THE PROPOSED APPROACHES TO OTHER APPLICATIONS

This topic is to extend the approaches developed in this thesis to other applications where maintenance plays an important role, e.g., railway transportation, energy networks, water systems, etc. The physical mechanisms of the maintenance of these networks may be different. However, the formulated maintenance scheduling problems may have the same form, e.g., mixed-integer programming problems. Thus, the accelerated algorithms proposed in this paper, e.g., Aitken-based distributed model predictive control and valid inequalities of the Benders decomposition, may be adapted for these other applications.

INCLUSION OF HUMAN FACTORS IN THE MAINTENANCE AND OPERATION OF POWER NETWORKS

This topic is to include analysis of and models for human factors of the customers, operators, maintenance and repair crews, and prosumers, into the approaches developed in

this thesis. Moreover, such analysis results and models can also be included in the operation of power networks, and be used to design the charging controller of the household batteries, the energy controller of smart buildings, the campus power system controller, etc.

8

BIBLIOGRAPHY

[1] Y. Abbas, A. Martinetti, J.-J. Moerman, T. Hamberg, and L. A. van Dongen, "Do you have confidence in how your rolling stock has been maintained? A blockchain-led knowledge-sharing platform for building trust between stakeholders," *Int. J. Inf. Manage.*, vol. 55, p. 228, 2020.

[2] A. Abiri-Jahromi, M. Fotuhi-Firuzabad, and E. Abbasi, "An efficient mixed-integer linear formulation for long-term overhead lines maintenance scheduling in power distribution systems," *IEEE Trans. Power Deliv.*, vol. 24, no. 4, pp. 2043–2053, 2009.

[3] A. Abiri-Jahromi, M. Fotuhi-Firuzabad, and M. Parvania, "Optimized midterm preventive maintenance outage scheduling of thermal generating units," *IEEE Trans. Power Syst.*, vol. 27, no. 3, pp. 1354–1365, 2012.

[4] M. Adibi, *IEEE 300-bus system*, https://site.ieee.org/pes-tccwg/links-to-test-cases/ Accessed April 4, 2010.

[5] J. I. Aizpurua, S. D. McArthur, B. G. Stewart, B. Lambert, J. G. Cross, and V. M. Catterson, "Adaptive power transformer lifetime predictions through machine learning and uncertainty modeling in nuclear power plants," *IEEE Trans. Ind. Electron.*, vol. 66, no. 6, pp. 4726–4737, 2018.

[6] F. Alavi, E. P. Lee, N. van de Wouw, B. De Schutter, and Z. Lukszo, "Fuel cell cars in a microgrid for synergies between hydrogen and electricity networks," *Appl. Energy*, vol. 192, pp. 296–304, 2017.

[7] A. Aleshi, R. Seker, and R. F. Babiceanu, "Blockchain model for enhancing aircraft maintenance records security," in *2019 IEEE International Symposium on Technologies for Homeland Security*, 2019, pp. 1–7.

[8] A. Ali, D. Raisz, and K. Mahmoud, "Voltage fluctuation smoothing in distribution systems with RES considering degradation and charging plan of EV batteries," *Electr. Power Syst. Res.*, vol. 176, p. 105 933, 2019.

[9] A. Alizadeh, A. Fereidunian, M. Moghimi, and H. Lesani, "Reliability-centered maintenance scheduling considering failure rates uncertainty: A two-stage robust model," *IEEE Trans. Power Deliv.*, 2021, DOI:10.1109/TPWRD.2021.3101458.

[10] M. S. Alvarez-Alvarad and D. Jayaweera, "Bathtub curve as a Markovian process to describe the reliability of repairable components," *IET Gener. Transm. Distrib.*, vol. 12, no. 21, pp. 5683–5689, 2018.

[11] M. S. Alvarez-Alvarado and D. Jayaweer, "Reliability-based smart-maintenance model for power system generators," *IET Gener. Transm. Distrib.*, vol. 14, no. 9, pp. 1770–1780, 2020.

[12] M. S. Alvarez-Alvarado and D. Jayaweera, "Operational risk assessment with smart maintenance of power generators," *Int. J. Electr. Power Energy Syst.*, vol. 117, p. 105, 2020.

[13] S. An, N. Cui, and J. Wang, "Modeling and simulating household evacuation behaviors for evacuation time estimates," in *International Conference on Transportation Engineering 2009*, 2009, pp. 4134–4140.

[14] S. Androutsellis-Theotokis and D. Spinellis, "A survey of peer-to-peer content distribution technologies," *ACM Comput. Surv.*, vol. 36, no. 4, pp. 335–371, 2004.

[15] C. Antal, T. Cioara, M. Antal, *et al.*, "Blockchain based decentralized local energy flexibility market," *Energy Rep.*, vol. 7, pp. 5269–5288, 2021.

[16] J. M. Argüelles, M. Z. Arrieta, J. L. Dominguez, B. L. Jaurrieta, and M. S. Benito, "A new method for decaying DC offset removal for digital protective relays," *Electr. Power Syst. Res.*, vol. 76, no. 4, pp. 194–199, 2006.

[17] A. Arif, S. Ma, Z. Wang, J. Wang, S. M. Ryan, and C. Chen, "Optimizing service restoration in distribution systems with uncertain repair time and demand," *IEEE Trans. Power Syst.*, vol. 33, no. 6, pp. 6828–6838, Nov. 2018.

[18] A. Arif, Z. Wang, J. Wang, and C. Chen, "Power distribution system outage management with co-optimization of repairs, reconfiguration, and DG dispatch," *IEEE Trans. Smart Grid*, vol. 9, no. 5, pp. 4109–4118, 2017.

[19] M. Asprou, E. Kyriakides, and M. M. Albu, "Uncertainty bounds of transmission line parameters estimated from synchronized measurements," *IEEE Trans. Instrum. Meas.*, vol. 68, no. 8, pp. 2808–2818, 2018.

[20] B. Awerbuch, "A new distributed depth-first-search algorithm," *Inf. Process. Lett.*, vol. 20, no. 3, pp. 147–150,

[21] H. R. Baghaee, M. Mirsalim, and G. B. Gharehpetian, "Performance improvement of multi-der microgrid for small- and large-signal disturbances and nonlinear loads: Novel complementary control loop and fuzzy controller in a hierarchical droop-based control scheme," *IEEE Systems Journal*, vol. 12, no. 1, pp. 444–451, 2018.

[22] H. R. Baghaee, M. Mirsalim, G. B. Gharehpetian, and A. K. Kaviani, "Security/cost-based optimal allocation of multi-type facts devices using multi-objective particle swarm optimization," *Simulation*, vol. 88, no. 8, pp. 999–1010, 2012.

[23] H. R. Baghaee, M. Mirsalim, G. B. Gharehpetian, and H. A. Talebi, "MOPSO/FDMT-based pareto-optimal solution for coordination of overcurrent relays in interconnected networks and multi-DER microgrids," *IET Gener. Transm. Distrib.*, vol. 12, no. 12, pp. 2871–2886, 2018.

[24] H. Baghaee, M. Mirsalim, G. Gharehpetian, and H. Talebi, "Reliability/cost-based multi-objective pareto optimal design of stand-alone wind/PV/FC generation microgrid system," *Energy*, vol. 115, pp. 1022–1041, 2016.

[25] B. Bagheri, N. Amjady, and S. Dehghan, "Multiscale multiresolution generation maintenance scheduling: A stochastic affinely adjustable robust approach," *IEEE Syst. J.*, 2020.

8

[26] P. Bangalore and L. B. Tjernberg, "An artificial neural network approach for early fault detection of gearbox bearings," *IEEE Trans. Smart Grid*, vol. 6, no. 2, pp. 980–987, 2015.

[27] R. Barth, P. Meibom, and C. Weber, "Simulation of short-term forecasts of wind and load for a stochastic scheduling model," in *Power and Energy Society General Meeting 2011 IEEE*, IEEE, 2011, pp. 1–8.

[28] S. Behzadirafi and H. Salehfar, "Preventive maintenance scheduling based on short circuit and overload currents," *IEEE Trans. Smart Grid*, vol. 6, no. 4, pp. 1740–1747, 2015.

[29] A. Bemporad and M. Morari, "Control of systems integrating logic, dynamics, and constraints," *Automatica*, vol. 35, no. 3, pp. 407–427, 1999.

[30] D. Bernardon, A. Mello, and L. Pfitscher, *Real-time Reconfiguration of Distribution Network with Distributed Generation*. 2016. [Online]. Available: https://app.dimensions.ai/details/publication/pub.1087204916%20and%20https://www.intechopen.com/citation-pdf-url/50636.

[31] T. Bi, H. Liu, D. Zhang, and Q. Yang, "The PMU dynamic performance evaluation and the comparison of PMU standards," in *2012 IEEE Power and Energy Society General Meeting*, 2012, pp. 1–5.

[32] Z. Bie, Y. Lin, G. Li, and F. Li, "Battling the extreme: A study on the power system resilience," *Proc. IEEE*, vol. 105, no. 7, pp. 1253–1266, 2017.

[33] C. Bordons, F. Garcia-Torres, and M. A. Ridao, *Model Predictive Control of Microgrids*. Springer, 2020, vol. 358.

[34] N. Brinkel, W. Schram, T. AlSkaif, I. Lampropoulos, and W. van Sark, "Should we reinforce the grid? Cost and emission optimization of electric vehicle charging under different transformer limits," *Appl. Energy*, vol. 276, p. 115 285, 2020.

[35] D. Bumblauskas, D. Gemmill, A. Igou, and J. Anzengruber, "Smart maintenance decision support systems (SMDSS) based on corporate big data analytics," *Expert Syst. Appl.*, vol. 90, pp. 303–317, 2017.

[36] G. Q. Butt, T. A. Sayed, R. Riaz, S. S. Rizvi, and A. Paul, "Secure healthcare record sharing mechanism with blockchain," *Appl. Sci.-Basel*, vol. 12, no. 5, p. 2307, 2022.

[37] R. N. Calheiros, E. Masoumi, R. Ranjan, and R. Buyya, "Workload prediction using arima model and its impact on cloud applications' QoS," *IEEE Trans. on Cloud Comput.*, vol. 3, no. 4, pp. 449–458, 2014.

[38] R. Carli, G. Cavone, N. Epicoco, M. D. Ferdinando, P. Scarabaggio, and M. Dotoli, "Consensus-based algorithms for controlling swarms of unmanned aerial vehicles," in *International Conference on Ad-Hoc Networks and Wireless*, Springer, 2020, pp. 84–99.

[39] D. Carrión, J. W. González, I. A. Issac, and G. J. López, "Optimal fault location in transmission lines using hybrid method," in *2017 IEEE PES Innovative Smart Grid Technologies Conference-Latin America (ISGT Latin America)*, 2017, pp. 1–6.

8

[40]   A. E. Carter and C. T. Ragsdale, "A new approach to solving the multiple traveling salesperson problem using genetic algorithms," *Eur. J. Oper. Res.*, vol. 175, no. 1, pp. 246–257, 2006.

[41]   S. Chakrabarti, E. Kyriakides, and M. Albu, "Uncertainty in power system state variables obtained through synchronized measurements," *IEEE Trans. Instrum. Meas.*, vol. 58, no. 8, pp. 2452–2458, 2009.

[42]   F. Chang, G. Zhou, C. Zhang, K. Ding, W. Cheng, and F. Chang, "A maintenance decision-making oriented collaborative cross-organization knowledge sharing block chain network for complex multi-component systems," *J. Clean Prod.*, vol. 282, p. 124 541, 2021.

[43]   R. Chatterjee and R. Chatterjee, "An overview of the emerging technology: Blockchain," in *2017 3rd International Conference on Computational Intelligence and Networks*, IEEE, 2017, pp. 126–127.

[44]   C. Chen, B. He, Y. Ye, and X. Yuan, "The direct extension of ADMM for multi-block convex minimization problems is not necessarily convergent," *Math. Program.*, vol. 155, no. 1-2, pp. 57–79, 2016.

[45]   K. Chen, W. Wu, B. Zhang, and H. Sun, "Robust restoration decision-making model for distribution networks based on information gap decision theory," *IEEE Trans. Smart Grid*, vol. 6, no. 2, pp. 587–597, Mar. 2015.

[46]   Y. Q. Chen, O. Fink, and G. Sansavini, "Combined fault location and classification for power transmission lines fault diagnosis with integrated feature extraction," *IEEE Trans. Ind. Electron.*, vol. 65, no. 1, pp. 561–569, 2017.

[47]   W.-C. Chiang, Y. Li, J. Shang, and T. L. Urban, "Impact of drone delivery on sustainability and cost: Realizing the UAV potential through vehicle routing optimization," *Appl. energy*, vol. 242, pp. 64–75, 2019.

[48]   H. Chung, S. Maharjan, Y. Zhang, F. Eliassen, and K. Strunz, "Placement and routing optimization for automated inspection with UAVs: A study in offshore wind farm," *IEEE Trans. Ind. Inform.*, pp. 1–1, 2020. DOI: 10.1109/TII.2020.3004816.

[49]   B. N. Coelho, V. N. Coelho, I. M. Coelho, *et al.*, "A multi-objective green uav routing problem," *Comput. Oper. Res.*, vol. 88, pp. 306–315, 2017.

[50]   A. J. Conejo, R. Garcia-Bertrand, and M. Diaz-Salazar, "Generation maintenance scheduling in restructured power systems," *IEEE Trans. Power Syst.*, vol. 20, no. 2, pp. 984–992, 2005.

[51]   Z. Cong, B. De Schutter, M. Burger, and R. Babuška, "Monitoring of traffic networks using mobile sensors," in *17th International IEEE Conference on Intelligent Transportation Systems*, 2014, pp. 92–97.

[52]   G. Corbetta, A. Mbistrova, A. Ho, I. Pineda, and K. Ruby, "Wind in power: 2015 European statistics," European Wind Energy Association, Brussels, 2016.

[53]   M. Crosby, P. Pattanayak, S. Verma, V. Kalyanaraman, *et al.*, "Blockchain technology: Beyond bitcoin," *Appl. Innov.*, vol. 2, no. 6-10, p. 71, 2016.

8

[54] P. Crossley, M. Davidson, and P. Gale, "Fault location using travelling waves," in *IEE Colloquium on Instrumentation in the Electrical Supply Industry*, 1993, pp. 6–1.

[55] P. Dash, S. Samantaray, G. Panda, and B. Panigrahi, "Time–frequency transform approach for protection of parallel transmission lines," *IET Gener. Transm. Distrib.*, vol. 1, no. 1, pp. 30–38, 2007.

[56] P. Dehghanian, M. Fotuhi-Firuzabad, F. Aminifar, and R. Billinton, "A comprehensive scheme for reliability centered maintenance in power distribution systems—Part I: Methodology," *IEEE Trans. Power Deliv.*, vol. 28, no. 2, pp. 761–770, 2013.

[57] S. Y. Derakhshandeh, Z. Mobini, M. Mohammadi, and M. Nikbakht, "UAV-assisted fault location in power distribution systems:An optimization approach," *IEEE Trans. Smart Grid*, vol. 10, pp. 628–636, 2018.

[58] A. S. Dobakhshari, "Fast accurate fault location on transmission system utilizing wide-area unsynchronized measurements," *Int. J. Electr. Power Energy Syst.*, vol. 101, pp. 234–242, 2018.

[59] G. Dong, J. Ma, R. Wei, and J. Haycox, "Electric vehicle charging point placement optimisation by exploiting spatial statistics and maximal coverage location models," *Transport. Res. Part D-Transport. Environ.*, vol. 67, pp. 77–88, 2019.

[60] J. Doss-Gollin, D. J. Farnham, U. Lall, and V. Modi, "How unprecedented was the february 2021 texas cold snap?" *Environ. Res. Lett.*, vol. 16, no. 6, p. 064 056, 2021.

[61] Y. S. Duarte, J. Szpytko, and A. M. del Castillo Serpa, "Monte Carlo simulation model to coordinate the preventive maintenance scheduling of generating units in isolated distributed power systems," *Electr. Power Syst. Res.*, vol. 182, p. 106 237, 2020.

[62] A. Esmat, M. de Vos, Y. Ghiassi-Farrokhfal, P. Palensky, and D. Epema, "A novel decentralized platform for peer-to-peer energy trading market with blockchain technology," *Appl. Energy*, vol. 282, p. 116 123, 2021.

[63] "Evaluation of measurement data—guide to the expression of uncertainty in measurement," *International Organization for Standardization*, vol. 50, p. 134, 2008.

[64] F. Fallahi, M. Yildirim, J. Lin, and C. Wang, "Predictive multi-microgrid generation maintenance: Formulation and impact on operations & resilience," *IEEE Trans. Power Syst.*, 2021, DOI:10.1109/TPWRS.2021.3066462.

[65] X. Fang, H. Cui, E. Du, F. Li, and C. Kang, "Characteristics of locational uncertainty marginal price for correlated uncertainties of variable renewable generation and demands," *Appl. Energy*, vol. 282, p. 116 064, 2021.

[66] S. Farí, X. Wang, S. Roy, and S. Baldi, "Addressing unmodeled path-following dynamics via adaptive vector field: A UAV test case," *IEEE Trans. Aerosp. Electron. Syst.*, vol. 56, no. 2, pp. 1613–1622, 2020.

[67] C. Feng and X. Wang, "A competitive mechanism of unit maintenance scheduling in a deregulated environment," *IEEE Trans. Power Syst.*, vol. 25, no. 1, pp. 351–359, 2009.

8

[68] R. Fletcher, "Stable reduced hessian updates for indefinite quadratic programming," *Math. Program.*, vol. 87, no. 2, pp. 251–264, 2000.

[69] R. Fletcher and S. Leyffer, "User manual for filterSQP," Department of Mathematics, University of Dundee, Tech. Rep., 1998.

[70] C. Floudas, A. Aggarwal, and A. Ciric, "Global optimum search for nonconvex nlp and minlp problems," *Comput. Chem. Eng.*, vol. 13, no. 10, pp. 1117–1132, 1989.

[71] J. Fu, A. Nunez, and B. De Schutter, "A short-term preventive maintenance scheduling method for distribution networks with distributed generators and batteries," *IEEE Trans. Power Syst.*, vol. 36, no. 3, pp. 2516–2531, 2020.

[72] J. Fu, A. Nunez, and B. De Schutter, "A real-time accelerated distributed PEV charging control strategy for pre-disaster evacuation situations," Submitted.

[73] J. Fu, A. Nunez, and B. De Schutter, "A bidding mechanism for maintenance of generation units considering inter-iso power exchange," Submitted.

[74] J. Fu, A. Nunez, and B. De Schutter, "Accelerated optimal maintenance scheduling for generation units on a truthful platform," Submitted.

[75] J. Fu, A. Núñez, and B. De Schutter, "Real-time UAV routing strategy for monitoring and inspection for postdisaster restoration of distribution networks," *IEEE Trans. Ind. Inform.*, vol. 18, no. 4, pp. 2582–2592, 2022.

[76] J. Fu, G. Song, and B. De Schutter, "Influence of measurement uncertainty on parameter estimation and fault location for transmission lines," *IEEE Trans. Autom. Sci. Eng.*, pp. 1–9, 2020.

[77] J. Fu, G. Song, and Y. Gong, "Exploration of a DC wind farm integrated by variable-speed squirrel cage induction generator (SCIGs)," *J. Eng.*, vol. 2017, no. 13, pp. 1488–1493, 2017.

[78] Y. Fu, M. Ding, C. Zhou, and H. Hu, "Route planning for unmanned aerial vehicle (UAV) on the sea using hybrid differential evolution and quantum-behaved particle swarm optimization," *IEEE Trans. Syst. Man Cybern. Syst.*, vol. 43, no. 6, pp. 1451–1465, 2013.

[79] N. Ganganath, J. V. Wang, X. Xu, C.-T. Cheng, and C. K. Tse, "Agglomerative clustering-based network partitioning for parallel power system restoration," *IEEE Trans. Ind. Inform.*, vol. 14, no. 8, pp. 325–333, 2018.

[80] H. Gao and P. A. Crossley, "Design and evaluation of a directional algorithm for transmission-line protection based on positive-sequence fault components," *IEE Proceedings-Generation, Transmission and Distribution*, vol. 153, no. 6, pp. 711–718, 2006.

[81] M. F. Ghazvini, H. Morais, and Z. Vale, "Coordination between mid-term maintenance outage decisions and short-term security-constrained scheduling in smart distribution systems," *Appl. Energy*, vol. 96, pp. 281–291, 2012.

[82] M. A. F. Ghazvini, B. Canizes, Z. Vale, and H. Morais, "Stochastic short-term maintenance scheduling of GENCOs in an oligopolistic electricity market," *Appl. Energy*, vol. 101, pp. 667–677, 2013.

8

[83] H. Golmohamadi, M. Ramezani, A. Bashian, and H. Falaghi, "Risk-based maintenance scheduling of generating units in the deregulated environment considering transmission network congestion," *J. Mod. Power Syst. Clean Energy*, vol. 2, no. 2, pp. 150–162, 2014.

[84] J. S. Gómez, D. Sáez, J. W. Simpson-Porco, and R. Cárdenas, "Distributed predictive control for frequency and voltage regulation in microgrids," *IEEE Trans. Smart Grid*, vol. 11, no. 2, pp. 1319–1329, 2020.

[85] J. Gondzio, "Interior point methods 25 years later," *Eur. J. Oper. Res.*, vol. 218, no. 3, pp. 587–601, 2012.

[86] V. Gupta, S. R. Konda, R. Kumar, and B. K. Panigrahi, "Electric vehicle driver response evaluation in multiaggregator charging management with EV routing," *IEEE Trans. Ind. Appl.*, vol. 56, no. 6, pp. 6914–6924, 2020.

[87] Z. M. Haider, K. K. Mehmood, M. K. Rafique, S. U. Khan, S.-J. Lee, and C.-H. Kim, "Water-filling algorithm based approach for management of responsive residential loads," *J. Mod. Power Syst. Clean Energy*, vol. 6, no. 1, pp. 118–131, 2018.

[88] N. Hashemnia, A. Abu-Siada, and S. Islam, "Detection of power transformer bushing faults and oil degradation using frequency response analysis," *IEEE Trans. Dielect. Elect. Insulation*, vol. 23, no. 1, pp. 222–229, 2016.

[89] T. He, Y. Zeng, and Z. Hu, "Research of multi-rotor UAVs detailed autonomous inspection technology of transmission lines based on route planning," *IEEE Access*, vol. 7, pp. 955–965, 2019.

[90] A. M. Helmi, R. Carli, M. Dotoli, and H. S. Ramadan, "Efficient and sustainable reconfiguration of distribution networks via metaheuristic optimization," *IEEE Trans. Autom. Sci. Eng.*, vol. 19, no. 1, pp. 82–98, 2021.

[91] A. Helseth, M. Fodstad, and B. Mo, "Optimal hydropower maintenance scheduling in liberalized markets," *IEEE Trans. Power Syst.*, vol. 33, no. 6, pp. 6989–6998, 2018.

[92] V. T. Hoang, M. D. Phung, T. H. Dinh, and Q. P. Ha, "System architecture for real-time surface inspection using multiple UAVs," *IEEE Syst. J.*, vol. PP, no. 99, 2019.

[93] J. C. Hodgson, S. M. Baylis, R. Mott, A. Herrod, and R. H. Clarke, "Precision wildlife monitoring using unmanned aerial vehicles," *Sci Rep*, vol. 6, p. 22 574, 2016.

[94] M. M. Hosseini, A. Umunnakwe, M. Parvania, and T. Tasdizen, "Intelligent damage classification and estimation in power distribution poles using unmanned aerial vehicles and convolutional neural networks," *IEEE Trans. Smart Grid*, vol. 11, pp. 3325–3333, 2020.

[95] S. M. Hosseini, R. Carli, and M. Dotoli, "Robust optimal energy management of a residential microgrid under uncertainties on demand and renewable power generation," *IEEE Trans. Autom. Sci. Eng.*, vol. 18, no. 2, pp. 618–637, 2021.

[96] D. F. Howard, T. G. Habetler, and R. G. Harley, "Improved sequence network model of wind turbine generators for short-circuit studies," *IEEE Trans. Energy Convers.*, vol. 27, no. 4, pp. 968–977, 2012.

8

[97]   J.-Y. Hsu, Y.-F. Wang, K.-C. Lin, M.-Y. Chen, and J. H.-Y. Hsu, "Wind turbine fault diagnosis and predictive maintenance through statistical process control and machine learning," *IEEE Access*, vol. 8, pp. 23 427–23 439, 2020.

[98]   J. Hu and P. Chen, "Predictive maintenance of systems subject to hard failure based on proportional hazards model," *Reliab. Eng. Syst. Saf.*, vol. 196, p. 106 707, 2020.

[99]   H. Huang and A. V. Savkin, "An algorithm of reactive collision free 3-D deployment of networked unmanned aerial vehicles for surveillance and monitoring," *IEEE Trans. Ind. Inform.*, vol. 16, no. 1, pp. 32–40, 2020.

[100] Y. Huang and K. M. Kockelman, "Electric vehicle charging station locations: Elastic demand, station congestion, and network equilibrium," *Transport. Res. Part D-Transport. Environ.*, vol. 78, p. 102 179, 2020.

[101] "IEEE guide for determining fault location on AC transmission and distribution lines - Redline," *IEEE Std C37.114-2014 (Revision of IEEE Std C37.114-2004) - Redline*, pp. 1–128, Jan. 2015.

[102] IEEE PES Power System Analysis, Computing, and Economics Committee, *IEEE 34 node test feeder*. (Sep. 2010), http://ewh.ieee.org/soc/pes/dsacom/testfeeders/feeder34.zip.

[103] Illinois Center for a Smarter Electric Grid, *IEEE 118-bus system*, [Online], http://motor.ece.iit.edu/data/coop.

[104] E. İlseven and M. Göl, "Incorporation of generator maintenance scheduling with long-term power sector forecasting and planning studies," *IET Gener. Transm. Distrib.*, vol. 14, no. 13, pp. 2581–2591, 2020.

[105] S. Izadkhast, P. Garcia-Gonzalez, P. Frías, L. Ramírez-Elizondo, and P. Bauer, "An aggregate model of plug-in electric vehicles including distribution network characteristics for primary frequency control," *IEEE Trans. Power Syst.*, vol. 31, no. 4, pp. 2987–2998, 2015.

[106] M. Jacob, C. Neves, and D. Vukadinović Greetham, "Short term load forecasting," in *Forecasting and Assessing Risk of Individual Electricity Peaks*. Cham: Springer International Publishing, 2020, pp. 15–37, ISBN: 978-3-030-28669-9.

[107] P. Jain, "Steffensen type methods for solving non-linear equations," *Applied Mathematics and Computation*, vol. 194, no. 2, pp. 527–533, 2007.

[108] G. Ji, W. Wu, B. Zhang, and H. Sun, "Transient outage model considering corrective and preventive maintenance," *J. Mod. Power Syst. Clean Energy*, vol. 4, no. 4, pp. 680–689, 2016.

[109] J.-A. Jiang, J.-Z. Yang, Y.-H. Lin, C.-W. Liu, and J.-C. Ma, "An adaptive PMU based fault detection/location technique for transmission lines. I. Theory and algorithms," *IEEE Trans. Power Deliv.*, vol. 15, no. 2, pp. 486–493, 2000.

[110] Q. Jiang, X. Li, B. Wang, and H. Wang, "PMU-based fault location using voltage measurements in large transmission networks," *IEEE Trans. Power Deliv.*, vol. 27, no. 3, pp. 1644–1652, 2012.

8

[111] S. Jiang, J. Cao, H. Wu, and Y. Yang, "Fairness-based packing of industrial iot data in permissioned blockchains," *IEEE Trans. Ind. Inform.*, vol. 17, no. 11, pp. 7639–7649, 2021.

[112] Y. Jiang, K. Zhou, X. Lu, and S. Yang, "Electricity trading pricing among prosumers with game theory-based model in energy blockchain environment," *Appl. Energy*, vol. 271, p. 115 239, 2020.

[113] X. Jin, F. Wang, and W. Zanji, "Research on fault location based on dynamic synchronous phasor measurement by PMU," *Power System Technology*, vol. 37, no. 10, pp. 2932–2937, 2013.

[114] I. M. Karmacharya and R. Gokaraju, "Fault location in ungrounded photovoltaic system using wavelets and ANN," *IEEE Trans. Power Deliv.*, vol. 33, no. 2, pp. 549–559, 2017.

[115] A. K. Kaviani, H. R. Baghaee, and G. H. Riahy, "Optimal sizing of a stand-alone wind/photovoltaic generation unit using particle swarm optimization," *Simulation*, vol. 85, no. 2, pp. 89–99, 2009.

[116] B. M. Keneni, D. Kaur, A. Al Bataineh, *et al.*, "Evolving rule-based explainable artificial intelligence for unmanned aerial vehicles," *IEEE Access*, vol. 7, pp. 17 001–17 016, 2019.

[117] K. V. Khandeparkar, S. A. Soman, and G. Gajjar, "Detection and correction of systematic errors in instrument transformers along with line parameter estimation using PMU data," *IEEE Trans. Power Syst.*, vol. 32, no. 4, pp. 3089–3098, 2016.

[118] B. H. Kim and R. Baldick, "Coarse-grained distributed optimal power flow," *IEEE Trans. Power Syst.*, vol. 12, no. 2, pp. 932–939, 1997.

[119] S. Kim, D. Kim, S. Jeong, J. W. Ham, J. K. Lee, and K. Y. Oh, "Fault diagnosis of power transmission lines using a UAV-mounted smart inspection system," *IEEE Access*, vol. 8, pp. 99–109, 2020.

[120] M. C. Kisacikoglu, F. Erden, and N. Erdogan, "Distributed control of PEV charging based on energy demand forecast," *IEEE Trans. Ind. Inform.*, vol. 14, no. 1, pp. 332–341, 2018.

[121] M. Kozlov, "Hurricane Ida forces Louisiana researchers to rethink their future," *Nature*, 2021.

[122] K. Krishnanand, P. Dash, and M. Naeem, "Detection, classification, and location of faults in power transmission lines," *Int. J. Electr. Power Energy Syst.*, vol. 67, pp. 76–86, 2015.

[123] I. Kuzle, H. Pandžić, and M. Brezovec, "Hydro generating units maintenance scheduling using Benders decomposition," *Tehnički vjesnik*, vol. 17, no. 2, pp. 145–152, 2010.

[124] M. Latifi, A. Khalili, A. Rastegarnia, and S. Sanei, "A Bayesian real-time electric vehicle charging strategy for mitigating renewable energy fluctuations," *IEEE Trans. Ind. Inform.*, vol. 15, no. 5, pp. 2555–2568, 2019.

8

[125] J. Lázaro, J. Minambres, and M. Zorrozua, "Selective estimation of harmonic components in noisy electrical signals for protective relaying purposes," *Int. J. Electr. Power Energy Syst.*, vol. 56, pp. 140–146, 2014.

[126] S. Lee, N. Chatzipanagiotis, and M. M. Zavlanos, "Complexity certification of a distributed augmented lagrangian method," *IEEE Trans. Autom. Control*, vol. 63, no. 3, pp. 827–834, 2017.

[127] C. Li, Y. Zhang, H. Zhang, Q. Wu, and V. Terzija, "Measurement-based transmission line parameter estimation with adaptive data selection scheme," *IEEE Trans. Smart Grid*, vol. 9, no. 6, pp. 5764–5773, 2017.

[128] H. Li, Z. Wan, and H. He, "Constrained EV charging scheduling based on safe deep reinforcement learning," *IEEE Trans. Smart Grid*, vol. 11, no. 3, pp. 2427–2439, 2020.

[129] P. Li, X. Huang, J. Qi, H. Wei, and X. Bai, "A connectivity constrained MILP model for optimal transmission switching," *IEEE Trans. Power Syst.*, vol. 36, no. 5, pp. 4820–4823, 2021.

[130] Y. Li, X. Liu, F. Wen, X. Zhang, L. Wang, and Y. Xue, "Dynamic charging scheduling for electric vehicles considering real-time traffic flow," in *2018 IEEE Power & Energy Society General Meeting (PESGM)*, IEEE, 2018, pp. 1–5.

[131] G. J. Lim, S. Kim, J. Cho, Y. Gong, and A. Khodaei, "Multi-UAV pre-positioning and routing for power network damage assessment," *IEEE Trans. Smart Grid*, vol. 9, pp. 3643–3651, 2016.

[132] X. Ling, J. Wang, T. Bouchoucha, B. C. Levy, and Z. Ding, "Blockchain radio access network (B-RAN): Towards decentralized secure radio access paradigm," *IEEE Access*, vol. 7, pp. 9714–9723, 2019.

[133] J. P. Lopes, C. Moreira, and A. Madureira, "Defining control strategies for microgrids islanded operation," *IEEE Trans. Power Syst.*, vol. 21, no. 2, pp. 916–924, 2006.

[134] X. Lou, C. Feng, W. Chen, and C. Guo, "Risk-based coordination of maintenance scheduling and unit commitment in power systems," *IEEE Access*, vol. 8, pp. 58 788–58 799, 2020.

[135] S. Lv, Z. Wei, G. Sun, S. Chen, and H. Zang, "Optimal power and semi-dynamic traffic flow in urban electrified transportation networks," *IEEE Trans. Smart Grid*, vol. 11, no. 3, pp. 1854–1865, 2020.

[136] H. Lycklama à Nijeholt, J. Oudejans, and Z. Erkin, "Decreg: A framework for preventing double-financing using blockchain technology," in *Proceedings of the ACM Workshop on Blockchain, Cryptocurrencies and Contracts*, 2017, pp. 29–34.

[137] C. N. Macqueen and M. R. Irving, "An algorithm for the allocation of distribution system demand and energy losses," *IEEE Trans. Power Syst.*, vol. 11, no. 1, pp. 338–343, 1996.

[138] M. Mahdavi, H. Monsef, and R. Romero, "Reliability effects of maintenance on TNEP considering preventive and corrective repairs," *IEEE Trans. Power Syst.*, vol. 32, no. 5, pp. 3768–3781, 2016.

8

[139]   M. Mahzarnia, M. P. Moghaddam, P. T. Baboli, and P. Siano, "A review of the measures to enhance power systems resilience," *IEEE Syst. J.*, vol. 14, no. 3, pp. 4059–4070, 2020.

[140]   N. M. Manousakis, G. N. Korres, and P. S. Georgilakis, "Taxonomy of PMU placement methodologies," *IEEE Trans. Power Syst.*, vol. 27, no. 2, pp. 1070–1077, 2012.

[141]   R. Medjoudj, H. Bediaf, and D. Aissani, "Power system reliability: Mathematical models and applications," *System Reliability*, vol. 279, 2017.

[142]   M. Migliore, V. Martorana, and F. Sciortino, "An algorithm to find all paths between two nodes in a graph," *J. Comput. Phys.*, vol. 87, no. 1, pp. 231–236, 1990.

[143]   V. Milojević, S. Čalija, G. Rietveld, M. V. Ačanski, and D. Colangelo, "Utilization of PMU measurements for three-phase line parameter estimation in power systems," *IEEE Trans. Instrum. Meas.*, vol. 67, no. 10, pp. 2453–2462, 2018.

[144]   H. Mirsaeedi, A. Fereidunian, S. M. Mohammadi-Hosseininejad, P. Dehghanian, and H. Lesani, "Long-term maintenance scheduling and budgeting in electricity distribution systems equipped with automatic switches," *IEEE Trans. Ind. Inform.*, vol. 14, no. 5, pp. 1909–1919, 2017.

[145]   *Model 1133 GPS-synchronized power quality/revenue standard operation manual*, https://www.arbiter.com/files/product-attachments/1133a_manual.pdf, Arbiter Systems, INC., Paso Robles, CA, USA, 2006.

[146]   Z. Moghaddam, I. Ahmad, D. Habibi, and Q. V. Phung, "Smart charging strategy for electric vehicle charging stations," *IEEE Trans. Transp. Electrif.*, vol. 4, no. 1, pp. 76–88, 2018.

[147]   F. Mohammadi and M. Sahraei-Ardakani, "Multidimensional scenario selection for power systems with stochastic failures," *IEEE Trans. Power Syst.*, vol. 35, no. 6, pp. 4528–4538, 2020.

[148]   F. Moinian and M.-T. Ameli, "An ISO-based security constrained generation maintenance coordination considering long-term SCOPF," *Electr. Power Syst. Res.*, vol. 189, p. 106 538, 2020.

[149]   M. Mollahassani-Pour, M. Rashidinejad, and M. Pourakbari-Kasmaei, "Environmentally constrained reliability-based generation maintenance scheduling considering demand-side management," *IET Gener. Transm. Distrib.*, vol. 13, no. 7, pp. 1153–1163, 2018.

[150]   J. T. Moore and J. F. Bard, "The mixed integer linear bilevel programming problem," *Oper. Res.*, vol. 38, pp. 911–921, 1990.

[151]   J. Mora-Florez, J. Melendez, and G. Carrillo-Caicedo, "Comparison of impedance based fault location methods for power distribution systems," *Electr. Power Syst. Res.*, vol. 78, no. 4, pp. 657–666, 2008.

[152]   M. Mrissa, A. Tošić, N. Hrovatin, *et al.*, "Privacy-aware and secure decentralized air quality monitoring," *Appl. Sci.-Basel*, vol. 12, no. 4, p. 2147, 2022.

[153]   R. Negenborn, P. J. Overloop, T. Keviczky, and B. De Schutter, "Distributed model predictive control of irrigation canals.," *Netw. Heterog. Media*, vol. 4, no. 2, pp. 359–380, 2017.

8

[154] R. R. Negenborn, B. De Schutter, and J. Hellendoorn, "Multi-agent model predictive control for transportation networks: Serial versus parallel schemes," *Eng. Appl. Artif. Intell.*, vol. 21, pp. 53–66, 2008.

[155] D. Niu, L. Guo, X. Bi, and D. Wen, "Preventive maintenance period decision for elevator parts based on multi-objective optimization method," *J. Build. Eng.*, vol. 44, p. 102 984, 2021.

[156] I. Nowak, *Relaxation and Decomposition Methods for Mixed Integer Nonlinear Programming*. Springer Science & Business Media, 2005.

[157] F. Ogieva, A. Ike, and C. Anyaeji, "Egbin power station generator availability and unit performance studies," *Int. J. Phys. Sci.*, vol. 10, no. 4, pp. 155–172, 2015.

[158] K. Pan, A. Teixeira, M. Cvetkovic, and P. Palensky, "Cyber risk analysis of combined data attacks against power system state estimation," *IEEE Trans. Smart Grid*, vol. 10, no. 3, pp. 3044–3056, 2018.

[159] H. Pandzic, A. J. Conejo, and I. Kuzle, "An EPEC approach to the yearly maintenance scheduling of generating units," *IEEE Trans. Power Syst.*, vol. 28, no. 2, pp. 922–930, 2012.

[160] A. Parizad and K. Hatziadoniu, "Security/stability-based pareto optimal solution for distribution networks planning implementing NSGAII/FDMT," *Energy*, vol. 192, p. 116 644, 2020.

[161] S. Park, Q. Xu, and B. F. Hobbs, "Comparing scenario reduction methods for stochastic transmission planning," *IET Gener. Transm. Distrib.*, vol. 13, no. 7, pp. 1005–1013, 2019.

[162] I. Pavić, H. Pandžić, and T. Capuder, "Electric vehicle based smart e-mobility system–definition and comparison to the existing concept," *Appl. Energy*, vol. 272, p. 115 153, 2020.

[163] S. Pei-feng, M. Rui, C. Xing-ying, *et al.*, "Research on maintenance schedule optimization of distribution network including distributed generation," in *2016 China International Conference on Electricity Distribution (CICED)*, IEEE, 2016, pp. 1–5.

[164] A. J. Pel, M. C. Bliemer, and S. P. Hoogendoorn, "A review on travel behaviour modelling in dynamic traffic simulation models for evacuations," *Transportation*, vol. 39, no. 1, pp. 97–123, 2012.

[165] X. Peng and X. Tao, "Cooperative game of electricity retailers in China's spot electricity market," *Energy*, vol. 145, pp. 152–170, 2018.

[166] A. Petcu and B. Faltings, "Distributed generator maintenance scheduling," in *Proceedings of the First International ICSC Symposium on Artificial Intelligence in Energy Systems and Power: AIESP'06*, 2006.

[167] M. Picallo, A. Anta, and B. De Schutter, "Comparison of bounds for optimal PMU placement for state estimation in distribution grids," *IEEE Trans. Power Syst.*, vol. 34, pp. 4837–4846, 2019.

[168] Production technology department of State Grid Corporation of China, *The guide of condition-based maintenance for distribution network equipment*. China Electric Power Press, 2011, ISBN: 155123.563.

[169] P. Prukpanit, P. Kaewprapha, and N. Leeprechanon, "Optimal generation maintenance scheduling considering financial return and unexpected failure of distributed generation," *IET Gener. Transm. Distrib.*, vol. 15, no. 12, pp. 1787–1797, 2021.

[170] R. G. Ribeiro, J. R. C. Júnior, L. P. Cota, T. A. M. Euzébio, and F. G. Guimarães, "Unmanned aerial vehicle location routing problem with charging stations for belt conveyor inspection system in the mining industry," *IEEE Trans. Intell. Transp. Syst.*, vol. 21, no. 10, pp. 4186–4195, 2020.

[171] D. Ritzmann, P. S. Wright, W. Holderbaum, and B. Potter, "A method for accurate transmission line impedance parameter estimation," *IEEE Trans. Instrum. Meas.*, vol. 65, no. 10, pp. 2204–2213, 2016.

[172] J. A. Rodriguez, M. F. Anjos, P. Côté, and G. Desaulniers, "MILP formulations for generator maintenance scheduling in hydropower systems," *IEEE Trans. Power Syst.*, vol. 33, no. 6, pp. 6171–6180, 2018.

[173] J. A. Rodrıguez, M. F. Anjos, P. Côté, and G. Desaulniers, "Accelerating benders decomposition for short-term hydropower maintenance scheduling," *Eur. J. Oper. Res.*, vol. 289, no. 1, pp. 240–253, 2021.

[174] P. Rokhforoz, B. Gjorgiev, G. Sansavini, and O. Fink, "Multi-agent maintenance scheduling based on the coordination between central operator and decentralized producers in an electricity market," *Reliab. Eng. Syst. Saf.*, vol. 210, p. 107 495, 2021.

[175] T. Rui, C. Hu, G. Li, J. Tao, and W. Shen, "A distributed charging strategy based on day ahead price model for PV-powered electric vehicle charging station," *Appl. Soft Comput.*, vol. 76, pp. 638–648, 2019.

[176] M. Sachdev and R. Agarwal, "A technique for estimating transmission line fault locations from digital impedance relay measurements," *IEEE Trans. Power Deliv.*, vol. 3, no. 1, pp. 121–129, 1988.

[177] O. Sadeghian, A. Oshnoei, S. Nikkhah, and B. Mohammadi-Ivatloo, "Multi-objective optimisation of generation maintenance scheduling in restructured power systems based on global criterion method," *IET Smart Grid*, vol. 2, no. 2, pp. 203–213, 2019.

[178] O. Sadeghian, A. M. Shotorbani, and B. Mohammadi-Ivatloo, "Generation maintenance scheduling in virtual power plants," *IET Gener. Transm. Distrib.*, vol. 13, no. 12, pp. 2584–2596, 2019.

[179] M. T. Sarwar, P. C. Anastasopoulos, S. V. Ukkusuri, P. Murray-Tuite, and F. L. Mannering, "A statistical analysis of the dynamics of household hurricane-evacuation decisions," *Transportation*, vol. 45, no. 1, pp. 51–70, 2018.

[180] K. P. Schneider, B. Mather, B. Pal, *et al.*, "Analytic considerations and design basis for the IEEE distribution test feeders," *IEEE Trans. Power Syst.*, vol. 33, no. 3, pp. 3181–3188, 2017.

8

[181]   Z. A. Shaikh, A. A. Khan, L. Baitenova, *et al.*, "Blockchain hyperledger with non-linear machine learning: A novel and secure educational accreditation registration and distributed ledger preservation architecture," *Appl. Sci.-Basel*, vol. 12, no. 5, p. 2534, 2022.

[182]   C. Shao, X. Wang, M. Shahidehpour, X. Wang, and B. Wang, "Partial decomposition for distributed electric vehicle charging control considering electric power grid congestion," *IEEE Trans. Smart Grid*, vol. 8, no. 1, pp. 75–83, 2016.

[183]   K. K. Sharma, "New algorithms for removal of DC offset and sub synchronous resonance terms in the current and voltage signals under fault conditions," *WSEAS Transactions on Power Systems*, vol. 9, pp. 103–110, 2014.

[184]   P. K. Sharma, N. Kumar, and J. H. Park, "Blockchain-based distributed framework for automotive industry in a smart city," *IEEE Trans. Ind. Inform.*, vol. 15, no. 7, pp. 4197–4205, 2019.

[185]   M. Shin, D.-H. Choi, and J. Kim, "Cooperative management for PV/ESS-enabled electric vehicle charging stations: A multiagent deep reinforcement learning approach," *IEEE Trans. Ind. Inform.*, vol. 16, no. 5, pp. 3493–3503, 2019.

[186]   M. Šíra, S. Mašláň, V. N. Zachovalová, G. Crotti, and D. Giordano, "Modelling of PMU uncertainty by means of Monte Carlo method," in *2016 Conference on Precision Electromagnetic Measurements (CPEM 2016)*, 2016, pp. 1–2.

[187]   G. Sivanagaraju, S. Chakrabarti, and S. C. Srivastava, "Uncertainty in transmission line parameters: Estimation and impact on line current differential protection," *IEEE Trans. Instrum. Meas.*, vol. 63, no. 6, pp. 1496–1504, 2013.

[188]   W. Smolinski, "An algorithm for digital impedance calculation using a single pi section transmission line model," *IEEE Trans. Power Appar. Syst.*, no. 5, pp. 1546–1551, 1979.

[189]   S. Soliman, R. Alammari, and M. El-Hawary, "A new digital transformation for harmonics and DC offset removal for the distance fault locator algorithm," *Int. J. Electr. Power Energy Syst.*, vol. 26, no. 5, pp. 389–395, 2004.

[190]   D. Song, "Research on generating power forecasting of grid-connected PV power plant," M.S. thesis, Liaoning University of Technology, 2016.

[191]   G. Song, J. Suonan, Q. Xu, P. Chen, and Y. Ge, "Parallel transmission lines fault location algorithm based on differential component net," *IEEE Trans. Power Deliv.*, vol. 20, no. 4, pp. 2396–2406, 2005.

[192]   P. de Sousa Oliveira, M. T. B. de Oliveira, E. Oliveira, *et al.*, "Maintenance schedule optimization applied to large hydroelectric plants: Towards a methodology encompassing regulatory aspects," *IEEE Access*, vol. 9, pp. 29 883–29 894, 2021.

[193]   D. Strepparava, L. Nespoli, E. Kapassa, M. Touloupou, L. Katelaris, and V. Medici, "Deployment and analysis of a blockchain-based local energy market," *Energy Rep.*, vol. 8, pp. 99–113, 2022.

8

[194] Z. Su, A. Jamshidi, A. Núñez, S. Baldi, and B. De Schutter, "Multi-level condition-based maintenance planning for railway infrastructures–a scenario-based chance-constrained approach," *Transp. Res. Pt. C-Emerg. Technol.*, vol. 84, pp. 92–123, 2017.

[195] S. Sugiarto, M. Isya, M. Haiqal, *et al.*, "Characterizing mode choice behaviors of the evacuees during emergency evacuation using a logistic regression model," in *IOP Conference Series: Materials Science and Engineering*, IOP Publishing, vol. 523, 2019, p. 012 032.

[196] J. Suonan, S. Gao, G. Song, Z. Jiao, and X. Kang, "A novel fault-location method for HVDC transmission lines," *IEEE Trans. Power Deliv.*, vol. 25, no. 2, pp. 1203–1209, 2009.

[197] M. Tajdinian, M. Z. Jahromi, K. Mohseni, and S. M. Kouhsari, "An analytical approach for removal of decaying DC component considering frequency deviation," *Electr. Power Syst. Res.*, vol. 130, pp. 208–219, 2016.

[198] L. Tang, X. Dong, S. Luo, S. Shi, and B. Wang, "A new differential protection of transmission line based on equivalent travelling wave," *IEEE Trans. Power Deliv.*, vol. 32, no. 3, pp. 1359–1369, 2016.

[199] Y. Tang, "Research on condition maintenance decision of distribution network," M.S. thesis, North China Electric Power University, 2014.

[200] Y. Tang, Q. Liu, J. Jing, Y. Yang, and Z. Zou, "A framework for identification of maintenance significant items in reliability centered maintenance," *Energy*, vol. 118, pp. 1295–1303, 2017.

[201] R. Tarjan, "Depth-first search and linear graph algorithms," *SIAM J. Comput.*, vol. 1, no. 2, pp. 146–160, 1972.

[202] V. Terzija, G. Preston, V. Stanojević, N. I. Elkalashy, and M. Popov, "Synchronized measurements-based algorithm for short transmission line fault analysis," *IEEE Trans. Smart Grid*, vol. 6, no. 6, pp. 2639–2648, 2015.

[203] O. Tor and M. Shahidehpour, "Power distribution asset management," in *Power and Energy Society General Meeting 2006 IEEE*, Jun. 2006, pp. 1–6.

[204] A. Toth and C. T. Kelley, "Convergence analysis for Anderson acceleration," *SIAM Journal on Numerical Analysis*, vol. 53, no. 2, pp. 805–819, 2015.

[205] J.-F. Toubeau, L. Pardoen, L. Hubert, *et al.*, "Machine learning-assisted outage planning for maintenance activities in power systems with renewables," *Energy*, p. 121 993, 2021.

[206] R. Van Katwijk, B. De Schutter, and J. Hellendoorn, "Traffic adaptive control of a single intersection: A taxonomy of approaches," in *Proc. 11th IFAC Symposium on Control in Transportation Systems*, Citeseer, 2006, pp. 227–232.

[207] K. Verbert, B. De Schutter, and R. Babuška, "Timely condition-based maintenance planning for multi-component systems," *Reliab. Eng. Syst. Saf.*, vol. 159, pp. 310–321, 2017.

8

[208] Y. Wan, J. Qin, F. Li, X. Yu, and Y. Kang, "Game theoretic-based distributed charging strategy for PEVs in a smart charging station," *IEEE Trans. Smart Grid*, vol. 12, no. 1, pp. 538–547, 2021.

[209] B. Wang, X. Wang, Z. Bie, P. D. Judge, X. Wang, and T. C. Green, "Reliability model of MMC considering periodic preventive maintenance," *IEEE Trans. Power Deliv.*, vol. 32, no. 3, pp. 1535–1544, 2017.

[210] C. Wang, Q.-Q. Jia, X.-B. Li, and C.-X. Dou, "Fault location using synchronized sequence measurements," *Int. J. Electr. Power Energy Syst.*, vol. 30, no. 2, pp. 134–139, 2008.

[211] G. Wang, M. Ciobotaru, and V. G. Agelidis, "Power smoothing of large solar PV plant using hybrid energy storage," *IEEE Trans. Sustain. Energy*, vol. 5, no. 3, pp. 34–42, 2014.

[212] Y. Wang, D. S. Kirschen, H. Zhong, Q. Xia, and C. Kang, "Coordination of generation maintenance scheduling in electricity markets," *IEEE Trans. Power Syst.*, vol. 31, no. 6, pp. 4565–4574, 2016.

[213] Y. Wang, H. Zhong, Q. Xia, D. S. Kirschen, and C. Kang, "An approach for integrated generation and transmission maintenance scheduling considering N-1 contingencies," *IEEE Trans. Power Syst.*, vol. 31, no. 3, pp. 2225–2233, 2015.

[214] Y. Wang, C. Chen, J. Wang, and R. Baldick, "Research on resilience of power systems under natural disasters—A review," *IEEE Trans. Power Syst.*, vol. 31, pp. 1604–1613, 2015.

[215] W. Wei, F. Liu, and S. Mei, "Charging strategies of EV aggregator under renewable generation and congestion: A normalized nash equilibrium approach," *IEEE Trans. Smart Grid*, vol. 7, no. 3, pp. 1630–1641, 2015.

[216] W. Wei, L. Wu, J. Wang, and S. Mei, "Expansion planning of urban electrified transportation networks: A mixed-integer convex programming approach," *IEEE Trans. Transp. Electrification*, vol. 3, no. 1, pp. 210–224, 2017.

[217] E. Wong, *Active-set methods for quadratic programming*. University of California, San Diego, 2011.

[218] Y. Wu, G. Zhao, J. Hu, *et al.*, "Overhead transmission line parameter reconstruction for UAV inspection based on tunneling magnetoresistive sensors and inverse models," *IEEE Trans. Power Deliv.*, vol. 34, pp. 819–827, 2019.

[219] J. Xia, X. Zhang, X. Huang, X. Kang, W. Shao, and Y. Liu, "Fault locating based on longitudinal impedance according to dual-terminal variables," *Electric Power Automation Equipment*, vol. 35, no. 10, pp. 133–139, 2015.

[220] S. Xia, S. Bu, X. Luo, K. W. Chan, and X. Lu, "An autonomous real-time charging strategy for plug-in electric vehicles to regulate frequency of distribution system with fluctuating wind generation," *IEEE Trans. Sustain. Energy*, vol. 9, no. 2, pp. 511–524, 2017.

[221] Y.-s. Xie, X.-q. Chang, X. Yin, H. Zheng, *et al.*, "Research on the transaction mode and mechanism of grid-side shared energy storage market based on blockchain," *Energy Rep.*, vol. 8, pp. 224–229, 2022.

[222] Y. Xu, X. Han, M. Yang, M. Wang, X. Zhu, and Y. Zhang, "Condition-based midterm maintenance scheduling with rescheduling strategy," *Int. J. Electr. Power Energy Syst.*, vol. 118, p. 105 796, 2020.

[223] Z. Xu, W. Su, Z. Hu, Y. Song, and H. Zhang, "A hierarchical framework for coordinated charging of plug-in electric vehicles in China," *IEEE Trans. Smart Grid*, vol. 7, no. 1, pp. 428–438, 2016.

[224] T. Yabe and S. V. Ukkusuri, "Effects of income inequality on evacuation, reentry and segregation after disasters," *Transport. Res. Part D-Transport. Environ.*, vol. 82, p. 102 260, 2020.

[225] L. Yao, W. H. Lim, and T. S. Tsai, "A real-time charging scheme for demand response in electric vehicle parking station," *IEEE Trans. Smart Grid*, vol. 8, no. 1, pp. 52–62, 2016.

[226] C. Yapa, C. de Alwis, M. Liyanage, and J. Ekanayake, "Survey on blockchain for future smart grids: Technical aspects, applications, integration challenges and future research," *Energy Rep.*, vol. 7, pp. 6530–6564, 2021.

[227] Z. Ye, C. Chen, B. Chen, and K. Wu, "Resilient service restoration for unbalanced distribution systems with distributed energy resources by leveraging mobile generators," *IEEE Trans. Ind. Inform.*, vol. 17, no. 2, pp. 1386–1396, 2021.

[228] M. Yildirim, X. A. Sun, and N. Z. Gebraeel, "Sensor-driven condition-based generator maintenance scheduling—Part I: Maintenance problem," *IEEE Trans. Power Syst.*, vol. 31, no. 6, pp. 4253–4262, 2016.

[229] X. Yu, C. Tang, P. Palensky, and A. Colombo, "Blockchain: What does it mean to industrial electronics? Technologies, challenges, and opportunities," *IEEE Ind. Electron. Mag.*, 2021, DOI: 10.1109/MIE.2021.3066332.

[230] L. Yuansheng, W. Gang, and L. Haifeng, "Time-domain fault-location method on HVDC transmission lines under unsynchronized two-end measurement and uncertain line parameters," *IEEE Trans. Power Deliv.*, vol. 30, no. 3, pp. 1031–1038, 2015.

[231] T. Zeng, H. Zhang, and S. Moura, "Solving overstay and stochasticity in PEV charging station planning with real data," *IEEE Trans. Ind. Inform.*, vol. 16, no. 5, pp. 3504–3514, 2019.

[232] D. Zhang, W. Li, and X. Xiong, "Overhead line preventive maintenance strategy based on condition monitoring and system reliability assessment," *IEEE Trans. Power Syst.*, vol. 29, no. 4, pp. 1839–1846, 2014.

[233] G. Zhang, S. T. Tan, and G. G. Wang, "Real-time smart charging of electric vehicles for demand charge reduction at non-residential sites," *IEEE Trans. Smart Grid*, vol. 9, no. 5, pp. 4027–4037, 2017.

[234] J. Zhang, J. Yan, M. Lv, X. Kong, and P. Zhang, "UAV formation flight cooperative tracking controller design," in *2018 15th International Conference on Control, Automation, Robotics and Vision (ICARCV)*, IEEE, 2018, pp. 856–861.

8

[235] J. Zhang and C. Wang, "Application of arma model in ultra-short term prediction of wind power," in *2013 International Conference on Computer Sciences and Applications*, IEEE, 2013, pp. 361–364.

[236] Y. Zhang, Y. Zhou, C. Jiang, Y. Wang, R. Zhang, and G. Chen, "Plug-in electric vehicle charging with multiple charging options: A systematic analysis of service providers' pricing strategies," *IEEE Trans. Smart Grid*, vol. 12, no. 1, pp. 524–537, 2021.

[237] Y. Zhang, D. Liu, J. Wu, and Y. Yin, "A modified algorithm for the simulation of charge behavior in water tree aged cross-linked polyethylene cable," *IEEE Access*, vol. 6, pp. 23 929–23 938, 2018.

[238] J. Zhao, S. Si, and Z. Cai, "A multi-objective reliability optimization for reconfigurable systems considering components degradation," *Reliab. Eng. Syst. Saf.*, vol. 183, pp. 104–115, 2019.

[239] Y. Zhao, X. He, Y. Yao, and J. Huang, "Plug-in electric vehicle charging management via a distributed neurodynamic algorithm," *Appl. Soft Comput.*, vol. 80, pp. 557–566, 2019.

[240] Y. J. Zheng, Y. C. Du, Z. L. Su, H. F. Ling, M. X. Zhang, and S. Y. Chen, "Evolutionary human-UAV cooperation for transmission network restoration," *IEEE Trans. Ind. Inform.*, vol. 17, no. 3, pp. 648–657, 2021.

[241] Y. Zheng, Y. Song, D. J. Hill, and K. Meng, "Online distributed MPC-based optimal scheduling for EV charging stations in distribution systems," *IEEE Trans. Ind. Inform.*, vol. 15, no. 2, pp. 638–649, 2018.

[242] Y. Zhong, X. Kang, Z. Jiao, Z. Wang, and J. Suonan, "A novel distance protection algorithm for the phase-ground fault," *IEEE Trans. Power Deliv.*, vol. 29, no. 4, pp. 1718–1725, 2013.

[243] K. Zhou, Q. Xiong, W. Zhao, W. Wen, and W. Tao, "Electrical properties and microstructures of water-tree aged XLPE cables after siloxane fluid injection," *High Volt.*, vol. 41, no. 8, pp. 2657–2664, 2015.

[244] Y. Zhou, R. Kumar, and S. Tang, "Incentive-based distributed scheduling of electric vehicle charging under uncertainty," *IEEE Trans. Power Syst.*, vol. 34, no. 1, pp. 3–11, 2018.

[245] Z. Zhou, C. Zhang, C. Xu, F. Xiong, Y. Zhang, and T. Umer, "Energy-efficient industrial internet of UAVs for power line inspection in smart grid," *IEEE Trans. Ind. Inform.*, vol. 14, no. 6, pp. 2705–2714, 2018.

[246] L. Ziegler, E. Gonzalez, T. Rubert, U. Smolka, and J. J. Melero, "Lifetime extension of onshore wind turbines: A review covering Germany, Spain, Denmark, and the UK," *Renew. Sustain. Energy Rev.*, vol. 82, pp. 1261–1271, 2018.

CURRICULUM VITÆ

Jianfeng Fu was born in Dalian city, Liaoning Province, China. He obtained his bachelor's and master's degrees from Northeast Electric Power University and Xi'an Jiaotong University in 2015 and 2018, respectively. He is now working towards his Ph.D. degree in Delft Center for Systems and Control, Delft University of Technology, under the supervision of Prof. De Schutter (Bart) and Prof. Núñez (Alfredo). He has been to Aalborg University for a research visit hosted by Prof. Peyghami (Saeed) and Prof. Blaabjerg (Frede) in the section of Applied Power Electronic Systems on March, 2022.

In his Ph.D. period, he has published in prestigious journals, such as IEEE Trans on Industrial Informatics (Impact factor 10.215) and IEEE Trans on Power Systems (impact factor 6.663), and he has various journal papers under review and in the process to be submitted. He has won a Best Student Paper Award at IEEE International Conference on Automation Science and Engineering (CASE). He has also attended several conferences and meetings, e.g., Benelux meeting.

His research topics include power system maintenance, infrastructure resilience, distributed model predictive control in power system reliability and resilience.

LIST OF PUBLICATIONS

8. **J. Fu, A. Núñez and B. De Schutter,** *A Short-Term Preventive Maintenance Scheduling Method for Distribution Networks With Distributed Generators and Batteries,* IEEE Transactions on Power Systems, vol. 36, no. 3, pp. 2516-2531, May 2021.

7. **J. Fu, G. Song and B. De Schutter,** *Influence of Measurement Uncertainty on Parameter Estimation and Fault Location for Transmission Lines,* IEEE Transactions on Automation Science and Engineering, vol. 18, no. 1, pp. 337-345, Jan. 2021.

6. **J. Fu, A. Núñez and B. De Schutter,** *Real-time UAV routing strategy for monitoring and inspection for post-disaster restoration of distribution networks,* IEEE Transactions on Industrial Informatics, vol. 18, no. 4, pp. 2582-2592, April 2022.

5. **J. Fu, G. Song and B. De Schutter,** *A pilot protection method based on energy balance for half-wavelength transmission lines,* 2019 IEEE 15th International Conference on Automation Science and Engineering (CASE), 2019, pp. 18-23.

4. **J. Fu, A. Núñez and B. De Schutter,** *A real-time accelerated distributed PEV charging control strategy for pre-disaster evacuation situations,* Submitted.

3. **J. Fu, A. Núñez and B. De Schutter,** *A bidding mechanism for maintenance of generation units considering inter-ISO power exchange,* Submitted.

2. **J. Fu, A. Núñez and B. De Schutter,** *Accelerated optimal maintenance scheduling for generation units on a truthful platform,* Submitted.

1. **J. Fu, S. Peyghami, A. Núñez, F. Blaabjerg, and B. De Schutter,** *A tractable failure probability prediction model for predictive maintenance scheduling of large-scale modular-multilevel-converters,* Submitted.